Interaction networks of small GTPases in human diseases

Inaugural-Dissertation

zur Erlangung des Doktorgrades

der Mathematisch-Naturwissenschaftlichen Fakultät

der Heinrich-Heine-Universität Düsseldorf

vorgelegt von

Oliver Krumbach

aus Osnabrück

Düsseldorf, Mai 2020

aus dem Institut für Biochemie & Molekularbiologie II
der Medizinischen Fakultät der Heinrich-Heine-Universität Düsseldorf

Gedruckt mit der Genehmigung der Mathematisch-Naturwissenschaftlichen
Fakultät der Heinrich-Heine-Universität Düsseldorf

Berichterstatter:

1. Prof. Dr. Reza Ahmadian

2. Prof. Dr. Lutz Schmitt

Tag der mündlichen Prüfung: 08.09.2020

“The significant problems we have cannot be solved at the same level of thinking with which we created them.”

– Albert Einstein

Summary

Small GTPases of the RAS superfamily are signaling nodes that control various cellular functions, including proliferation, differentiation, and actin dynamics by acting as molecular switches. This switch mechanism is tightly regulated by GEFs and GAPs which accelerate the slow intrinsic nucleotide exchange and stimulate GTP hydrolysis, respectively. RHO GTPases are additionally regulated by GDIs which shuttle prenylated RHO GTPases between cytoplasm and the plasma membrane. In their GTP-bound state GTPases transduce signals by physically interacting with effector proteins. Dysfunction of small GTPases has been frequently reported as a cause for cancer and developmental disorders. We identified several missense mutations in *CDC42, RRAS2*, and *MRAS* in patients with Noonan syndrome, an autosomal dominant disorder caused by germline mutations in genes encoding components of the MAPK cascade. To understand disease progression mediated by RAS and RHO family members comprehensive study of the interaction networks of small GTPases is required. Biochemical and structural analyses provided valuable insights into molecular mechanisms underlying Noonan syndrome. CDC42 variants perturb the function by dysregulated GTPase cycle or impaired binding to effectors, such as WASP, PAK1, and IQGAP1. We divided the CDC42 variants into three groups illustrating the functional impact of the missense mutations. Characterization of RRAS2 mutations demonstrated an accumulation in its active state due to GAP insensitivity and accelerated nucleotide exchange. Moreover, loss of interaction with RASSF5 suggests multiple signaling pathways may contribute to pathogenesis of Noonan syndrome. MRAS variants were found to additionally increase AKT phosphorylation, supporting the notion that several pathways contribute to disease progression. Furthermore, we identified a novel disorder characterized by a Golgi restricted mislocalization of CDC42 mediated by impaired binding to RHOGDI1 and IQGAP1, controlling membrane-cytoplasm shuttling and translocation from Golgi to the plasma membrane, respectively. Spatial and temporal organization of protein interaction networks is crucial for strength, efficiency, and specificity of signal transduction. Scaffold proteins, such as IQGAPs, modulate the assembly of large protein complexes by binding two or more molecules simultaneously. Characterization of RHO GTPase-IQGAP interaction revealed selectivity determinants promoting the knowledge regarding regulation of scaffold proteins. Finally, we discovered and characterized a small molecule inhibitor against the RACGEF VAV3, significantly reducing RAC activation and inducing apoptosis in a BCR-ABL leukemia model, suggesting a potential therapeutic strategy for B-cell acute lymphoblastic leukemia.

Zusammenfassung

Kleine GTPasen der RAS-Superfamilie sind Signalknoten, die als molekulare Schalter verschiedene zelluläre Funktionen wie Proliferation, Differenzierung und Aktindynamik kontrollieren. Dieser Schaltmechanismus wird durch GEFs und GAPs streng reguliert, die den langsamen, intrinsischen Nukleotidaustausch beschleunigen bzw. die GTP-Hydrolyse stimulieren. RHO GTPasen werden zusätzlich durch GDIs reguliert, die prenylierte RHO GTPasen zwischen Zytoplasma und Plasmamembran hin- und herbewegen. In ihrem GTP-gebundenen Zustand übertragen GTPasen Signale durch physikalische Interaktion mit Effektorproteinen. Eine häufige Ursache für Krebs und Krankheiten mit Entwicklungsstörungen sind Funktionsstörungen von kleinen GTPasen. Wir haben mehrere Mutationen in *CDC42*, *RRAS2* und *MRAS* bei Noonan-Syndrom Patienten identifiziert. Noonan-Syndrom ist eine autosomal-dominante Erkrankung, die durch Keimbahnmutationen in Genen verursacht wird, die Komponenten der MAPK-Kaskade kodieren. Um den durch Mitglieder der RAS und RHO-Familie vermittelten Krankheitsverlauf zu verstehen, ist eine umfassende Untersuchung der Interaktionsnetzwerke der kleinen GTPasen erforderlich. Biochemische und strukturelle Analysen lieferten wertvolle Einblicke in die molekularen Mechanismen, die dem Noonan-Syndrom zugrunde liegen. CDC42-Varianten stören die Funktion durch einen dysregulierten GTPase-Zyklus oder eine gestörte Bindung an Effektoren wie WASP, PAK1 und IQGAP1. Die CDC42-Varianten wurden in drei Gruppen, die die funktionellen Auswirkungen der Mutationen veranschaulichen, unterteilt. Die Charakterisierung der RRAS2-Mutationen zeigte eine Akkumulation in ihrem aktiven Zustand aufgrund von GAP-Unempfindlichkeit und beschleunigtem Nukleotidaustausch. Darüber hinaus deutet der Verlust der Interaktion mit RASSF5 darauf hin, dass mehrere Signalwege zur Pathogenese des Noonan-Syndroms beitragen könnten. Es wurde festgestellt, dass MRAS-Varianten zusätzlich die AKT-Phosphorylierung erhöhen, was die Annahme unterstützt, dass mehrere Signalwege zum Fortschreiten der Krankheit beitragen. Darüber hinaus identifizierten wir eine neue Krankheit, die durch eine Golgi-beschränkte Fehllokalisierung von CDC42 gekennzeichnet ist. Auslöser dafür sind eine gestörte Bindung an RHOGDI1 und IQGAP1, welche die Membran-Zytoplasma–Bewegung bzw. die Translokation vom Golgi zur Plasmamembran kontrollieren. Die räumliche und zeitliche Organisation von Proteininteraktionsnetzwerken ist entscheidend für die Stärke, Effizienz und Spezifität der Signaltransduktion. Gerüstproteine, wie IQGAPs, modulieren den Aufbau großer Proteinkomplexe, indem sie zwei oder mehr Moleküle gleichzeitig binden. Die Charakterisierung der RHO GTPasen-IQGAP-Interaktion ergab Selektivitätsdeterminanten, die das Wissen über die Regulation von Gerüstproteinen fördern. Zuletzt entdeckten wir einen Inhibitor gegen das RACGEF VAV3, der die RAC-Aktivierung signifikant reduziert und Apoptose in einem BCR-ABL-Leukämie-Modell induziert, was auf eine mögliche therapeutische Strategie für akute lymphoblastische B-Zell-Leukämie hindeutet.

Table of Content

I. List of abbreviations

aa	Amino acid
AID	Autoinhibitory domain
AP1	Activator protein 1
ARF	ADP ribosylation factor
ARP2/3	Actin-related proteins 2/3
BAD	Bcl-2 Antagonist of cell death
C-terminus	Carboxy-terminus
CDC42	Cell division cycle protein 42 homolog
CFC	Cardio-facio-cutaneous syndrome
CHD	Calponine homology domain
CRIB	CDC42/RAC1 interactive binding
CS	Costello syndrome
DH	Dbl homology
EGFR	Epidermal growth factor receptor
ERK	Extracellular regulated kinase
F-actin	Filamentous-actin
FGFR	Fibroblast growth factor receptor
FMNL2	Formin Like 2
FTase	Farnesyltransferase
FPT	Farnesyl protein transferase
GAP	GTPase-activating protein
GBD	GTPase binding domain
GDI	Guanine nucleotide dissociation inhibitor
GDP	Guanosine diphosphate
GEF	Guanine-nucleotide-exchange factor
GGTase	Geranylgeranyltransferase
GPCR	G-protein coupled receptor
GRB2	Growth factor receptor-bound protein 2
GRD	GAP-related domain
GTP	Guanosine triphosphate
GTPases	Guanosine triphosphatases
HCM	Hypertrophic cardiomyopathy
HLH	Hemophagocytic lymphohistiocytosis
HVR	Hypervariable region
IL-18	Interleukin-18
IODVA1	Inhibitor of oncogene driven VAV3 activation 1
IQGAP	IQ motif containing GTPase activating protein
ITSN1	Intersectin1
JNK	c-Jun N-terminal kinase

kDa	Kilo Dalton
KSR	Kinase suppressor of Ras
MAPK	Mitogen-activated protein kinase
MEK	MAPK/ERK kinase
MRAS	Muscle RAS
N-terminus	Amino-terminus
NOCARH	Neonatal onset of pancytopenia, autoinflammation, rash, HLH
NS	Noonan syndrome
NSML	Noonan syndrome with multiple lentigines
PAK	p21 activated kinase
PH	Pleckstrin homology
PI3K	Phosphoinositide 3-kinase
P-loop	Phosphate binding-loop
RA	RAS association
RAB	RAS-related in brain
RAC	RAS-related C3 botulinum toxin substrate
RAF	Rapidly accelerated fibrosarcoma
RAN	RAS-related nuclear protein
RAS	Rat sarcoma
RASSF5	RAS association domain family member 5
RBD	RAS binding domain
RGCT	RASGAP C-terminal domain
RHO	RAS homologue
RRAS2	RAS-related 2
RTK	Receptor tyrosine kinase
SARAH	Salvador-Rassf-Hippo
SH2	Src homology 2
SH3	Src homology 3
SOS1	Son of Sevenless1
SPR	Surface plasmon resonance
WASP	Wiskott-Aldrich-syndrome protein
WT	Wild type

II. Amino acid abbreviation

Amino Acid	Three letter code	One letter code
Alanine	Ala	A
Arginine	Arg	R
Asparagine	Asn	N
Aspartic acid	Asp	D
Cysteine	Cys	C
Glutamine	Gln	Q
Glutamic acid	Glu	E
Glycine	Gly	G
Histidine	His	H
Isoleucine	Ile	I
Leucine	Leu	L
Lysine	Lys	K
Methionine	Met	M
Phenylalanine	Phe	F
Proline	Pro	P
Serine	Ser	S
Threonine	Thr	T
Tryptophan	Trp	W
Tyrosine	Tyr	Y
Valine	Val	V

III. List of tables

IV. List of figures

Chapter I

General introduction

1 The RAS/mitogen-activated protein kinase (MAPK) pathway

The RAS/mitogen-activated protein kinase (MAPK) pathway plays a key role in many biological and cellular processes which are crucial for development, such as proliferation, differentiation, apoptosis, survival, and senescence [1, 2]. This signaling cascade gets activated by binding of several extracellular stimuli, like growth factors, hormones, or cytokines to their respective membrane receptors. Stimulated and activated cell surface receptors, like for example the epidermal growth factor receptors (EGFRs) and fibroblast growth factor receptors (FGFRs) are transautophosphorylated after ligand binding and cause recruitment of various proteins to the cytosolic leaflet of the plasma membrane [3, 4].

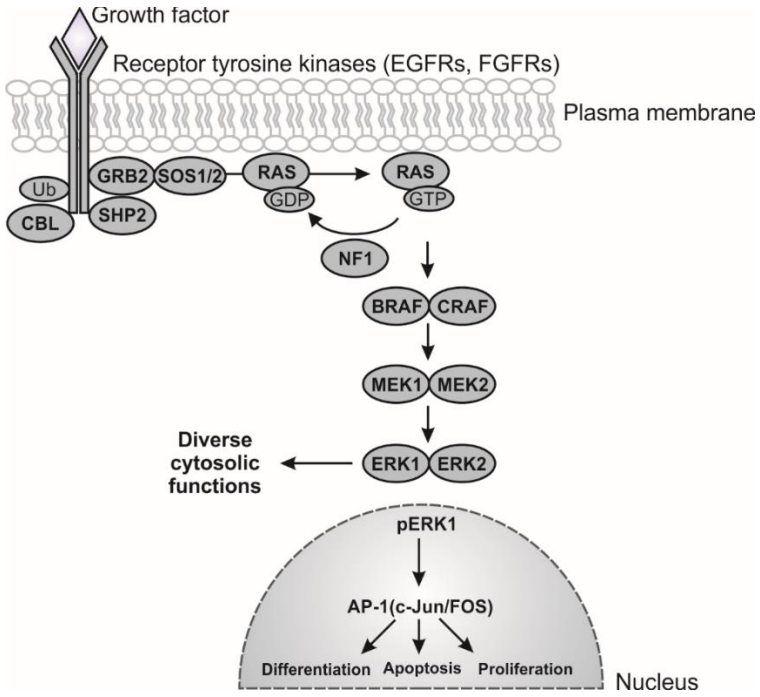

Figure 1. Schematic view of the canonical RAS/MAPK pathway. Growth factors bind to their specific receptors at the plasma membrane, resulting in transphosphorylation. GRB2 in complex with SOS1 consequently translocates to the membrane and activates RAS by accelerating the nucleotide exchange from GDP to GTP. Active, GTP-bound RAS in turn activates the kinase cascade RAF-MEK-ERK. Nuclear translocation of phosphorylated ERK leads to the activation of the transcription factor AP-1, controlling many cellular functions, such as differentiation, apoptosis, and proliferation.

Recruitment of the adaptor protein GRB2 to the plasma membrane leads to a complex formation with guanine nucleotide exchange factors (GEFs), like SOS1, that convert RAS proteins, such as KRAS, NRAS, and HRAS from their inactive, guanosine diphosphate (GDP)-bound form to their active, guanosine triphosphate (GTP)-bound form [1, 5, 6]. Activated RAS proteins in turn activate the RAF-MEK-ERK phosphorylation cascade, resulting in translocation

of phosphorylated ERK proteins, such as ERK1 and ERK2, into the nucleus which on their part activate several transcription factors [7-10]. The activator protein-1 (AP-1) is one of the transcription factors that is known to be activated by the RAS-MAPK signal transduction. AP-1 is a heterodimeric protein complex composed of JUN and FOS. Its activation results in various biological responses, such as differentiation, apoptosis and cell cycle progression [11].

1.1 RAS/MAPK pathway syndromes (RASopathies)

The RASopathies are groups of phenotypically overlapping developmental disorders caused by germline mutations in genes that encode components or regulators of the RAS/MAPK pathway [2, 12, 13]. The RAS/MAPK pathway is one of the best studied signal transduction pathways and plays a key role in regulating many cellular functions, such as cell cycle, proliferation, and differentiation [1].

Table 1. RASopathy genes and related syndromes.

	RASopathies (Syndromes)						
Gene	Cardio-facio-cutaneous	Costello	Legius	Neurofibromatosis type 1	Noonan	NSML (LEOPARD)	NSLAH (MAZZANTI)
BRAF	X				X		
CBL					X		
CDC42					X		
HRAS		X					
KRAS	X				X		
MRAS					X		
NRAS					X		
MAP2K1 (MEK1)	X				X		
MAP2K2 (MEK2)	X						
NF1				X			
PTPN11					X	X	
RAF1					X	X	
RIT1					X		
RRAS2					X		
SHOC2	X				X		X
SOS1					X		
SOS2					X		
SPRED1			X				

Hence, it is not surprising that dysregulation within this pathway leads to severe consequences in development. These disorders include neurofibromatosis type I, Legius syndrome, Noonan syndrome, Noonan syndrome with multiple lentigines (LEOPARD syndrome), Costello syndrome, cardiofaciocutaneous (CFC) syndrome, Mazzanti syndrome, hereditary gingival fibromatosis and capillary malformation-arteriovenous malformation, affecting around 1 in 1000 individuals [12]. They all exhibit unique phenotypes but share many overlapping characteristics as well, such as craniofacial dysmorphology, growth delays, cardiac defects, cutaneous and ocular abnormalities, neurocognitive impairment, and an increased risk of cancer. Mutations in more than 15 genes, such as *NF1*, *PTPN11*, *SOS1*, *SOS2*, *SPRED1*, *RAF1*, *BRAF*, *HRAS*, *KRAS*, *NRAS MRAS*, *RRAS2*, *RIT1*, *SHOC2*, *CBL*, *MEK1*, and *MEK2* have been reported to be associated with RASopathies [14-17].

Figure 2. Clinical images of patients with RASopathies. A is showing a young boy diagnosed with neurofibromatosis type 1. **B** PTPN11 mutation in a young girl resulted in Noonan syndrome. **C** A young adult woman with Costello syndrome due to a p.G12S mutation in HRAS. **D** A young boy with CFC syndrome caused by a mutation in MEK2 (pictures taken from [2]).

1.2 Noonan syndrome

Noonan syndrome (NS) is an autosomal dominant developmental disease which is in general caused by germline mutations in components or regulators of the RAS/MAPK pathway affecting approximately 1 in 2000 newborns [9]. NS is mainly characterized by distinctive craniofacial features, including a broad forehead, hypertelorism, down-slanting palpebral fissures, and low-set, posteriorly rotated ears. Furthermore, they show several other phenotypic features, such as cardiac defects, reduced growth, and a neurocognitive delay [14]. Like for other RASopathies, individuals with NS show an overall increased cancer risk. The syndrome has been associated with mutations in more than 10 genes and is genetically heterogeneous. While mutations in *PTPN11*, *SOS1*, *RAF1*, and *RIT1* have been documented to

occur most frequently, a smaller proportion of cases has been ascribed to mutations in other functionally related genes, including *NRAS*, *KRAS*, *BRAF*, *CDC42*, *MAP2K1*, *SOS2*, *SHOC2*, *MRAS*, and *RRAS2* [18-31]. *PTPN11* is with a prevalence of about 50% the most common gene associated with NS which encodes a nonreceptor protein tyrosine phosphatase, called SHP2.

2 RAS superfamily at a glance

The RAS (Rat sarcoma) superfamily of small guanosine triphosphatases (GTPases) comprises 167 human members which are monomeric G-proteins of around 20-30 kDa with conserved structure and functions related to the α subunit of heterotrimeric G-proteins [32, 33]. The *RAS* proto-oncogenes, including *KRAS* and *HRAS*, are the founding members of the RAS superfamily which is structurally classified into five major subfamilies, such as RAS, RHO, RAB, RAN, and ARF [34-36].

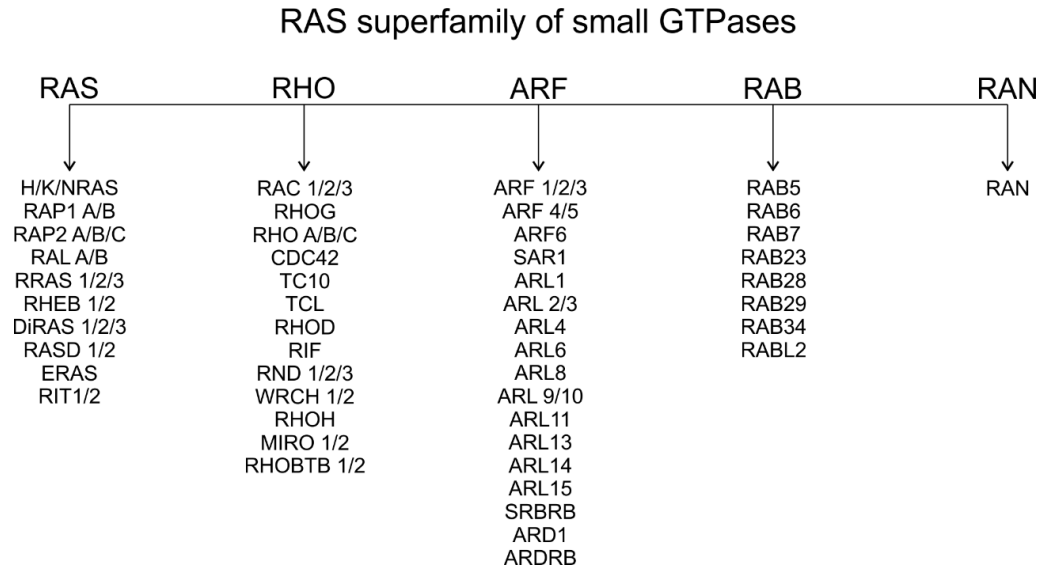

Figure 3. The RAS superfamily of small GTPases. The RAS superfamily consists of 167 human members which can be divided into five subfamilies, such as RAS, RHO, ARF, RAB, and RAN.

Small GTPases bind guanine nucleotides and act as molecular switches cycling between a GDP-bound (inactive) and GTP-bound (active) state. Since the intrinsic GTP hydrolysis and nucleotide exchange reaction are slow, two main classes of regulators are needed for a fast on/off cycle. GEFs stimulate the activation of small GTPases by increasing the rate of GDP release and subsequent GTP binding, while GAPs catalyze the slow intrinsic GTP hydrolysis [37, 38]. In their active state, small GTPases form a surface which is capable of effector binding and thus signal transduction [39, 40]. Proteins of the RAS superfamily control a wide range of

cellular functions, including differentiation, proliferation, actin reorganization, cell-cell contact, exocytosis, polarity, and cell migration.

2.1 RAS GTPases

The RAS family comprises 23 genes that encode for at least 25 proteins which can be divided into eight different paralog groups based on their sequence identity, structural properties, and functional aspects: RAS, RAL, RRAS, RIT, RAP, RHEB, RASD, and DIRAS [33, 41]. KRAS, HRAS, and NRAS are among the most studied proteins. These genes were first identified as viral oncogenes found in Harvey and Kirsten murine sarcoma viruses (Ha-MSV and Ki-MVS) by Jennifer Harvey and Werner Kirsten [42, 43]. *HRAS* and *KRAS* oncogenes are, together with the neuroblastoma RAS (*NRAS*) homolog, hyperactivated versions of their genes encoding a 21 kDa phosphoprotein. RAS proteins share a common regulatory mechanism cycling between a GDP-bound and GTP-bound state. This cycle is controlled by two classes of regulators, called GEFs and GAPs. Moreover, RAS proteins get posttranslationally modified at a specific conserved cysteine at the very C-terminus of the proteins by addition of a 15-carbon farsenyl isoprenoid moiety *via* a farsenyl protein transferase (FPT) [44, 45]. This prenylation enables the RAS proteins to be translocated and connected to the plasma membrane which is proposed to be essential for the function. Once activated, RAS family proteins transduce signals in response to extracellular stimuli to downstream signaling proteins, called effectors.

RRAS2 (RAS related 2, also known as TC21, teratocarcinoma 21) belongs to the RAS family of GTPases, described for the first time in 1990 [46]. TC21 which shares 55% amino acid sequence homology to the classical RAS proteins HRAS, KRAS, and NRAS, is a member of the RRAS subfamily consisting of RRAS1, TC21, and RRAS3/MRAS. Considering just the region between amino acid 5 to 120, excluding the hypervariable region, it reaches about 80% sequence homology [41, 47]. The RRAS proteins have been shown to be involved in multiple cellular processes like proliferation, survival, mitogenesis and control of the actin cytoskeleton. Activating mutations of TC21 have been documented to contribute to oncogenesis in a variety of solid tumors, such as G23V, A70T, and Q72L [47-49].

MRAS shares about 50% sequence homology with the classical RAS proteins. Crystal structures has been solved for the GDP-and GTP-bound state, showing that in both states an “open” conformation can be found. Usually, in the GTP-bound conformation Thr35 and Gly60 of the

switch I and switch II region are in contact with the γ-phosphate of the GTP, resulting in a so called “closed” conformation [50, 51]. The sequence of switch I of MRAS shows high similarities compared to HRAS except for the two residues Asp30 and Glu31 (HRAS numbering) which are proline and aspartic acid in MRAS, respectively. Mutational analysis showed that replacement of proline and aspartic acid by aspartate and glutamate increased the “closed” conformation of MRAS to about 30%, indicating that these two residues are also critical for the molecular switch mechanism of RAS GTPases [52].

2.1.1 Structural properties of RAS GTPases

All RAS GTPases share a conserved GDP/GTP-binding domain, G-domain (aa 1-169 in HRAS), that changes its conformation based on the nucleotide that is bound to the GTPase [35]. The G-domain consists of five conserved motifs, called G1-G5, that are essential for nucleotide and magnesium binding, as well as the molecular switch mechanism [32, 53]. The G1 motif which is also known as phosphate binding loop (P-loop) or “Walker A motif” with the consensus sequence GX4GKS/T (aa 10-17 HRAS numbering), is responsible for the high-affinity binding of the phosphate groups of GDP and GTP. The P-loop is a glycine rich region followed by a lysine and serine or threonine which are responsible for the formation of a ring-like structure to stabilize the binding to the β-and γ-phosphate oxygen and to coordinate the magnesium ion, respectively [54, 55]. Gly12 and Gly13 are the most frequently mutated RAS codons causing human tumors due to an impairment of the GTPase reaction [56]. Most of the GTPases contain a glycine at residue 12, except ERAS, RASD1/2, and DIRAS3. These exceptions do not cycle between an on and off state since they are GAP insensitive and accumulate in its active GTP-bound state [57, 58]. The G2 motif, also known as the switch I region (aa 32-40 HRAS numbering), contains two highly conserved residues, such as Tyr32 and Thr35 (HRAS numbering), which are essential for the conformational changes upon nucleotide exchange [59, 60]. For this reason, the G2 motif is crucial for the interactions with effector proteins. G3 or the “Walker B motif” (aa 53-62 HRAS numbering) is part of the switch II region (aa 59-67) with the sequence DXXG. Asp57 is close to but does not bind the magnesium ion directly. Gly60 coordinates the γ-phosphate by a main chain hydrogen bond which is crucial for the conformational change of the switch II region [61]. G4 contains the N/TKXD motif (aa 112-119 HRAS numbering) which is important for the specificity of the guanidine base. Asp119 binds the nitrogen atoms of the base, while Asn116 can contact the oxygen of the purine [36]. G5 is

the SAK motif which interacts with the G4 *via* Ser145 and Asp119 for stabilization of the structure and the nucleotide binding. Furthermore, Ala146 is able to bind the guanine base showing the complex implication of RAS proteins for guanine nucleotide binding [35, 36, 60]. RAS GTPases contain at their carboxy (C)-terminus a highly variable sequence, called hypervariable region (HVR), which has been shown to be involved in membrane binding as well as contributing to effector selectivity [44, 45, 62]. The HVR is a highly unstructured region and is therefore often truncated for structural studies. A conserved cysteine in the CAAX motif at the very C-terminus of RAS proteins gets posttranslationally modified by farnesyl isoprenoid lipids [63, 64]. This modification serves as an important component for membrane binding.

2.1.2 RAS effector proteins

RAS GTPases in their active, GTP-bound form are capable of interacting with a multitude of signaling molecules, called effector proteins. RAS proteins get activated by signals through different transmembrane receptors, such as receptor tyrosine kinases (RTKs), G-protein coupled receptors (GPCRs), ion channel receptors, and adhesion receptors. Once activated, RAS proteins transduce these extracellular signals *via* different downstream effector proteins to distinct pathways [65-68]. These RAS effector proteins have been shown to carry either a RAS binding domain (RBD) or a RAS association (RA) domain [40, 69, 70]. More than 60 effector proteins have been identified for all RAS proteins which are able to activate about 49 signaling pathways. However, the RAF kinases, PI3Ks, and RASSFs are the most studied effector proteins in RAS signaling.

Rapidly accelerated fibrosarcoma (RAF) proteins are Ser/Thr kinases which are key components of the canonical RAS/MAPK pathway and regulate many cellular functions, such as proliferation, differentiation, development, survival, and apoptosis [71-74]. Three RAF paralogs have been identified in humans, including ARAF, BRAF, and CRAF. All paralogs consist of an N-terminal RBD and a C-terminal Ser/Thr kinase domain. RAF kinases are proposed to be in an inactive conformation due to autoinhibitory interactions between the N-and C-terminus. GTP-bound RAS proteins have been shown to bind to the RBD of RAF leading to membrane localization, displacement of 14-3-3, and release of its autoinhibited, closed conformation [75-77]. Further activating modifications, such as dephosphorylation and phosphorylation are required for RAF dimerization. This dimerization has been proposed to stabilize the active

conformation of RAF [78]. Activated RAF homo- and heterodimers have been shown to phosphorylate and activate MEK1 and MEK2 which in turn phosphorylate ERK [79, 80].

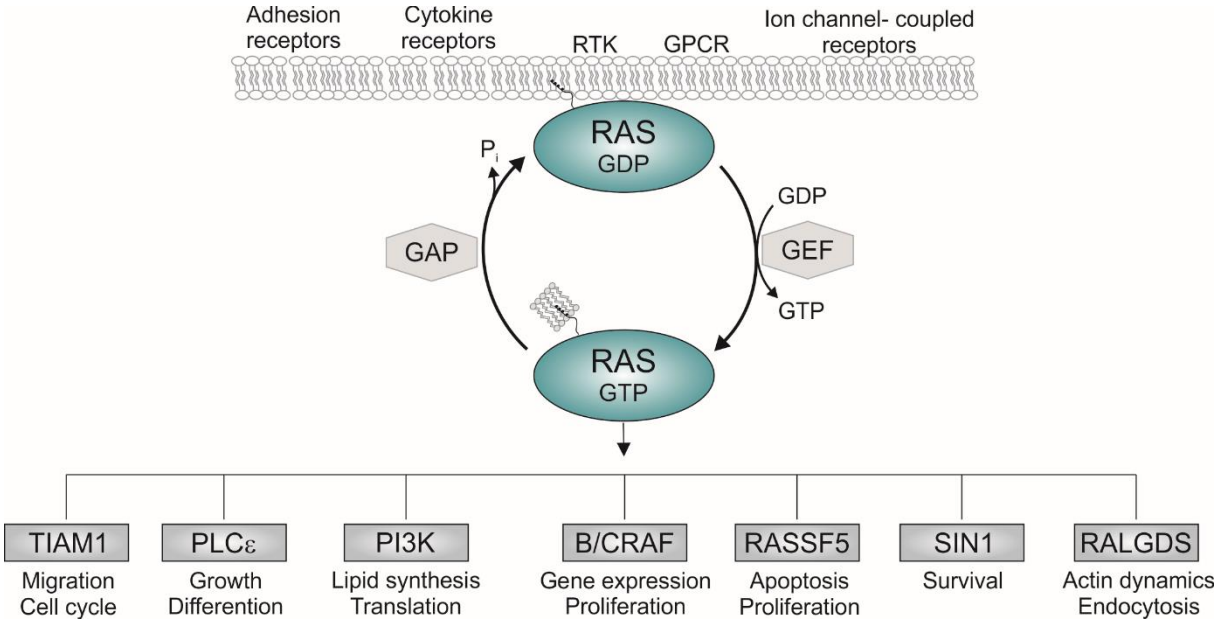

Figure 4. The RAS GTPase cycle and downstream effector proteins. RAS GTPases can be activated by diverse extracellular stimuli through several membrane receptors, such as receptor tyrosine kinases (RTK) or G-protein-coupled receptors (GPCR). Once activated by GEFs, RAS proteins transduce this information *via* several effector proteins through the cell controlling various cellular functions, including differentiation, gene expression, and apoptosis. GAPs are required to inactivate the RAS proteins within milliseconds.

Phosphatidylisonitol 3-kinases (PI3Ks) are a family of lipid kinases that phosphorylate phosphoinositides on the 3` position of the inositol head group to generate the second messengers PI-3,4-P_2 and PIP3, using PI-4-P and PI-4,5-P_2 as substrates, respectively [81, 82]. They are divided into three classes with several 85 kDa regulatory and 110 kDa catalytic subunits. Upon receptor activation PI3Ks are translocated to the plasma membrane and interact *via* the SH2 domain with phosphotyrosine residues of the receptor [83]. Class I PI3Ks have been shown to interact with RAS proteins. Four isoforms of the class I p110 subunits exist, such as p110α, p110β, p110γ, and p110δ. RAS proteins interact directly with the N-terminal RBD of p110α, p110γ, and p110δ [84-86]. However, RAS proteins are not able to bind p110β, while the RHO GTPases CDC42 and RAC1 have been shown to bind and activate the p110β subunit [87]. Following activation and membrane translocation PI3Ks have been reported to target for example AKT, PDK1, GEFs, GAPs, and adaptor proteins [88].

The RAS association domain family (RASSF) represents a group of ten members with several splice variants acting as tumor suppressor proteins [89, 90]. All of them contain a RAS association (RA) domain either at their N-terminus or C-terminus. RAS proteins are capable of binding to this RA domain controlling various cellular functions, such as proliferation, apoptosis, and membrane trafficking [89-93]. Only RASSF2, 4, 5A, 6, and 9 have been shown to directly interact with KRAS [94, 95]. Two additional domains, such as a C1 domain in RASSF1A, RASSF5A, and RASSF5B and a Salvador-Rassf-Hippo (SARAH) domain in RASSF1-6 can be found [96]. Since RASSF proteins do not show any enzymatic activity they are proposed to function as scaffold proteins assembling larger protein complexes. RASSF proteins have been shown to interact with a multitude of proteins including MST1/2, 14-3-3, Aurora A, and several RAS proteins [97-102].

2.2 RHO GTPases

RHO (RAS homologous) GTPases belong to the RAS superfamily and can be divided into six groups based on their sequence homology: RHO (RHOA, RHOB, RHOC), RAC (RAC1, RAC2, RAC3, RHOG), CDC42 (CDC42, TC10, TCL, CHP/WRCH-2, WRCH-1), RND (RND1, RND2, RND3/RHOE), RHOBTB (RHOBTB1 and RHOBTB2) and MIRO (MIRO-1 and MIRO-2) [103-107]. They are involved in multiple cellular processes, including cell cycle progression, reorganization of the cytoskeleton, transcription, and polarity. Like RAS proteins, most of the RHO GTPases act as molecular switches cycling between an “on” and “off” state which is tightly regulated by GAPs and GEFs [108]. RHO GTPases are additionally regulated by a third class of regulators, called guanine nucleotide dissociation inhibitors (GDIs), which shuttle prenylated RHO GTPases between cytoplasm and the plasma membrane [109].

Cell division cycle 42 (CDC42) is a member of the RHO GTPase family functioning as a signaling node controlling several cellular processes, including cell cycle, migration, adhesion, endocytosis, and polarity. CDC42 stimulates the formation of actin-rich membrane protrusions, called filopodia, formed by bundles of filamentous (F)-actin [105, 110]. There are two isoforms that arise from alternative exon splicing of the same gene. Both isoforms consist of 191 amino acids that differ at residue 163 and in their last 10 residues at the very C-terminus: 163 K (isoform 1) → R (isoform 2) and PKKSRRCVLL (isoform 1) → TQPKRKCCIF (isoform 2) [111, 112]. Isoform 1 is ubiquitously expressed, while isoform 2 is mainly found in

brain. CDC42 function is also controlled by three classes of regulators. One of the regulatory proteins which converts CDC42 in its active, GTP-bound state is intersectin-1 (ITSN-1). More than 60 interaction partners for ITSN-1 have been identified, however one of the functions is the stimulation of the nucleotide exchange reaction of CDC42 with its C-terminal DH-PH domains [113]. The inactivation of CDC42 is regulated by p50GAP that is known to be specific for CDC42 and accelerate the slow intrinsic GTP hydrolysis [114]. The GTPase primarily acts by spatiotemporal interactions with effector proteins, such as WASP, FMNL-2, and PAK. The localization of CDC42 at the plasma membrane and the shuttling to other intracellular membranes is regulated by RHOGDI1 and IQGAP1, respectively [115-117]. The function of CDC42 requires a posttranslational modification at the Cys188, including prenylation (geranyl-geranylation) followed by proteolytic cleavage of the last three residues and carboxyl-methylation [118].

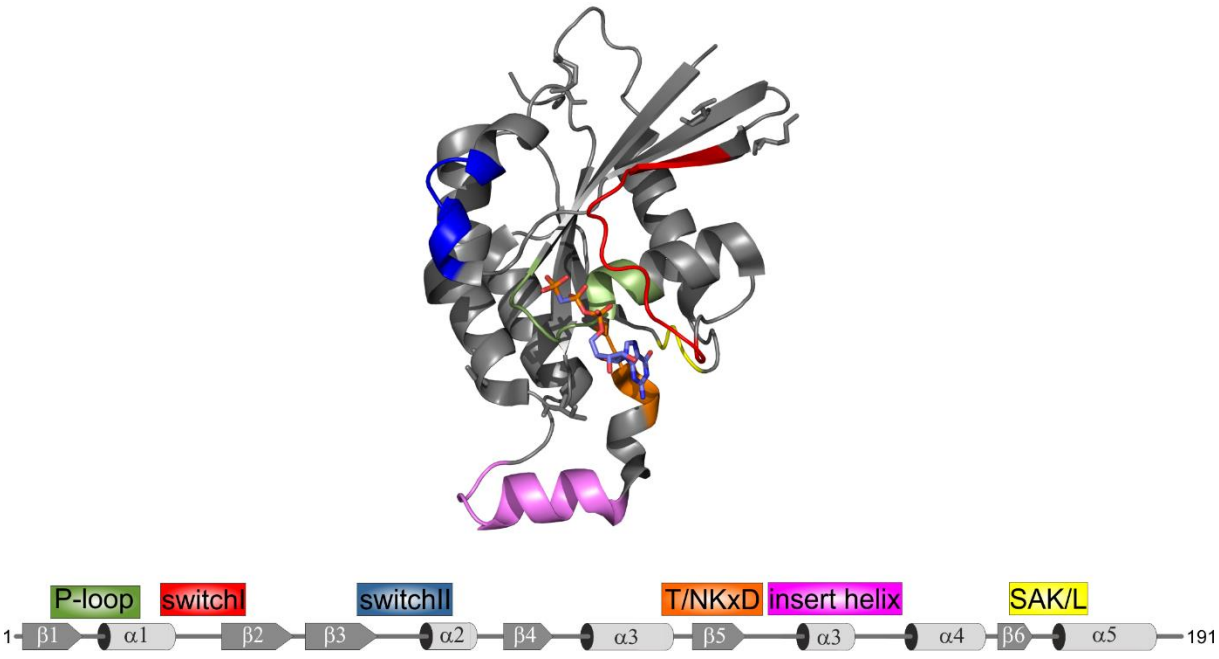

Figure 5. Crystal structure and corresponding secondary structure of CDC42. The highlighted regions in the structure are conserved motifs within all small GTPases which are critical for nucleotide binding and the molecular switch mechanism (Structure of CDC42 bound to GMP-PCP. PDB: 2QRZ [119]).

TC10 and TCL belong to the CDC42-related protein subfamily and show highly similar functions compared to CDC42. The induced filopodia by TC10 and TCL are longer in comparison to those induced by CDC42. They share most effectors, however differences exist [114, 120].

Furthermore, TC10 is additionally modified by palmitate which prevents RHOGDI1 binding and function [121].

The RAC-related proteins stimulate the formation of lamellipodia and membrane ruffles [122]. RAC1, RAC2, and RAC3 share about 88% sequence homology, while RHOG is about 72% identical to RAC1. There is a splicing variant of RAC1, called RAC1b that is generated by alternative exon splicing and contains a 19 amino acid insertion C-terminal to the switch II region. RAC1b is expressed in breast and colon cancers and shows an increased nucleotide exchange reaction rate and a decreased GTP hydrolysis [123, 124]. Moreover, RAC1b does not interact with RHOGDI1 resulting in an enhanced association to the plasma membrane and consequently in a constitutively active protein [125]. RAC1 is ubiquitously expressed, while RAC2 expression is restricted to hematopoietic cells and RAC3 is highly expressed in brain [126, 127]. RHOG has been described as a late-response gene induced after serum stimulation of fibroblasts, suggesting its regulation by transcription and involvement in the regulation of the cell cycle [128].

The RHO-related proteins RHOA, RHOB, and RHOC share about 85% sequence identity with the highest variations within the C-terminal 15 amino acids which is proposed to be important for the distinct subcellular localizations of the different RHO proteins. They are a key factor for the assembly of contractile actin-myosin filaments (stress fibers) and contribute to cellular processes, such as migration, exocytosis, endocytosis, cell cycle, and proliferation [121, 129, 130].

2.2.1 Structural properties of RHO GTPases

The structural properties of RHO GTPases show many similarities to those of RAS GTPases. They comprise the five conserved G1-G5 motifs (G domain) which are responsible for the nucleotide binding as well as the interaction with regulatory proteins and effectors [131]. G domains are highly conserved through all RHO GTPases. However, differences determine selectivity towards regulators and effector proteins. The C-terminus of RHO GTPases also consists of the HVR with the CAAX box which gets posttranslationally modified and allows RHO binding to membranes [36, 132]. The lipid anchor at the C-terminus is not the only posttranslational modification of RHO GTPases. They undergo several further modifications, such as ubiquitination, phosphorylation, and acetylation [103, 133]. The hallmark of all RHO

GTPases is an additional 12 aa “insert region” which is located between β5 and α4 of the G domain [134]. This “insert region” has been shown to be involved in the binding and activation of several proteins, such as GEFs, p67phox, IQGAP1, ROCK, and mDia [135-138].

2.2.2 RHO effector proteins

RHO GTPases also interact physically with a multitude of effector proteins leading to the control of many cellular processes [39]. Different RHO GTPases have been observed to show specificity towards different effector proteins. Proteins of the RHO subfamily like RHOA are able to interact with ROCK, PKN, and Rhotekin, while RAC1 and CDC42 show interaction with WASP, PAK1, and IQGAP1. Basically, effectors for RHO proteins could be kinases, regulators, and scaffold proteins as well.

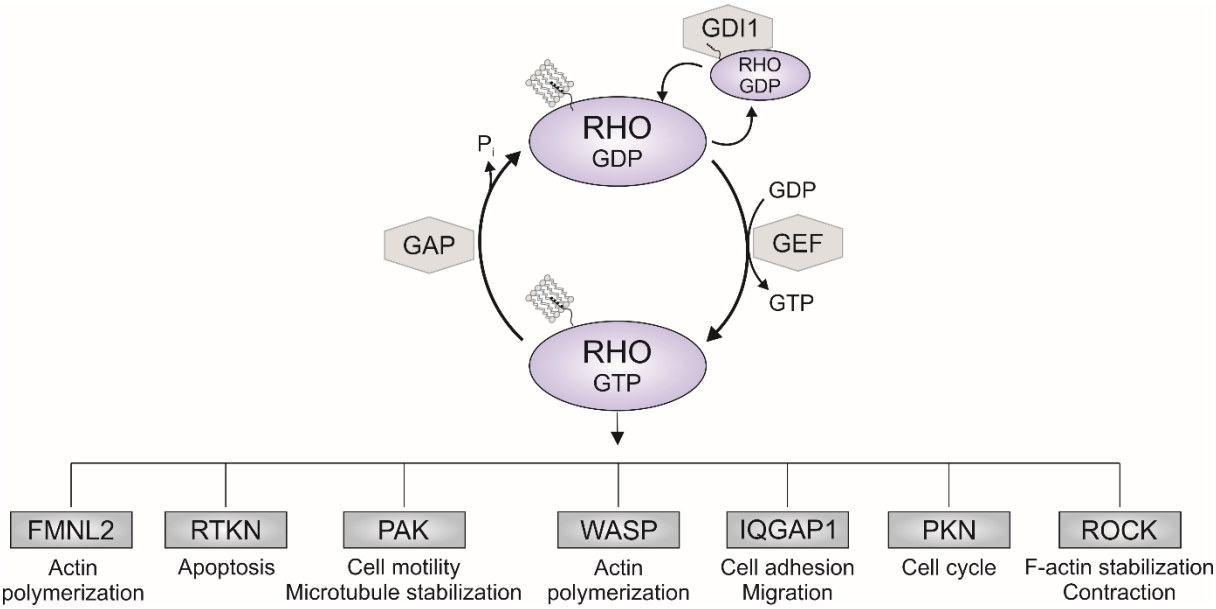

Figure 6. The RHO GTPase cycle and downstream effector proteins. RHO GTPases are tightly controlled by three classes of regulators. GEFs stimulate the activation by increasing the slow intrinsic nucleotide exchange reaction. GAPs accelerate the GTP hydrolysis leading to an inactive GDP-bound form. GDIs are able to bind the isoprenyl group of RHO GTPases preventing them from proteasomal degradation and shuttle them between cytoplasm and different membranes. RHO GTPases in their GTP-bound conformation are able to physically interact with various proteins leading to signal transduction and regulation of various cellular functions. FMNL2 (Formin-like protein 2), RTKN (Rhotekin), PKN (protein kinase novel), ROCK (RHO-associating coiled-coil kinase).

The Wiskott Aldrich syndrome protein (WASP) participates in processes which are dependent on the regulation of the actin cytoskeleton, such as migration, cell signaling, phagocytosis, and cytotoxicity [139]. Since the *WAS* gene was identified more than 20 years ago, over 300 different mutations have been described, resulting in a high variation of phenotypes, such as

immunodeficiency, inflammatory symptoms, and autoimmunity [140, 141]. WASP has been described as a cytosolic protein with 502 amino acids consisting of several domains including Ena-VASP homology domain (EVH1), short basic domain (B), GBD, polyproline domain (PP), and verprolin homology/ central/ acidic (VCA) domain. In resting cells WASP has been shown to be in an autoinhibited state, where the VCA domain binds the hydrophobic pocket of the GBD [142]. Binding of RHO GTPases like CDC42 and phosphorylation of Tyr291 have been proposed to destabilize the autoinhibited conformation, leading to an open, active conformation [143, 144]. As a consequence, the VCA region is then able to bind actin related protein (ARP) 2/3, resulting in actin nucleation and formation of actin branches [145]. Furthermore, phosphorylation of two serines in the VCA domain results in an enhanced binding affinity towards the ARP 2/3 complex [146]. Interaction of the WASP interacting protein (WIP) with the EVH1 domain protects WASP from proteasomal degradation, as well as translocation to areas of actin polymerization [147, 148].

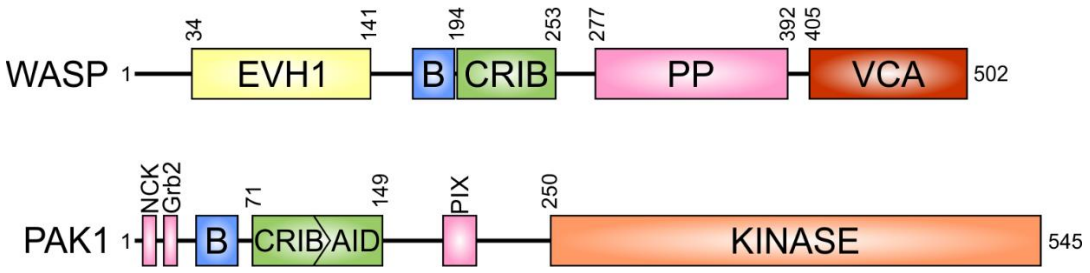

Figure 7. Domain organization of the RHO effector proteins WASP and PAK1. EVH1= Ena-VASP homology domain; B= basic region; CRIB= CDC42/RAC1 interactive binding motif; AID= autoinhibitory domain; PP= polyproline domain; VCA= verprolin homology/ central/ acidic domain.

The p21-activated kinases (PAKs) comprise a family of six (PAK1-6) Ser/Thr protein kinases acting as downstream effectors of the RHO GTPases RAC1 and CDC42 [149]. PAKs have been shown to stabilize the active form of CDC42 and RAC1 by inhibiting the intrinsic GTP hydrolysis [149]. All members of the family consist, in addition to a conserved catalytic kinase domain, an N-terminal CDC42/RAC1 interactive binding (CRIB) motif [150]. However, they have been classified into two groups consisting of three members each. Group I PAKs (PAK1-3) are characterized by an N-terminal CRIB motif which overlaps with an autoinhibitory domain (AID), and a conserved catalytic domain at the C-terminus. Furthermore, the group I PAKs comprise two SH3 binding motifs at the very N-terminus which are capable of binding NCK and Grb2, as well as a non-classical SH3-binding site for a GEF, called PAK-interacting exchange

factor (PIX) [151-153]. These interactions suggest group I PAKs to be recruited and activated at the plasma membrane [154]. The group II PAKs (PAK4-6) have never been shown to interact with SH3-domain-containing proteins. On top of that, they are structurally different compared to group I PAKs. They show neither the N-terminal SH3-binding motifs, nor the PIX binding site and they lack the AID as well [155]. The most studied substrates of PAK1 and PAK2 are MLCK, BAD, RAF, MEK1, LIMK, and Merlin linking them to be involved in cellular processes, such as cytoskeletal organization, cell motility, proliferation, apoptosis, transcriptional regulation, and cell-cycle progression [156-160].

2.3 Regulation of small GTPases

2.3.1 GAPs

The GTP hydrolysis is a key mechanism in intracellular signal transduction and important for the regulation of small GTPases. It is the timing reaction that converts GTPases from their active, GTP-bound state into their inactive, GDP-bound state [161, 162]. This process is intrinsically very slow but can be accelerated by several orders of magnitude by GTPase activating proteins (GAPs). GAPs actively participate in the process of GTP hydrolysis by providing a catalytic residue, called “arginine finger”, which stabilizes the transition state of this reaction [163]. The arginine residue interacts with the P-loop and the switch regions of the GTPases. It forms a hydrogen bond with Gln61 for stabilization of the switch regions and for optimizing the orientation of the catalytic GAP domain. Gln61 is then able to activate a water molecule for a nucleophilic attack of the γ-phosphate of GTP. Moreover, the positively charged arginine stabilizes the transition state by neutralizing the generated negative charges by the transferred phosphoryl group or the leaving group oxygen [163-165]. Mutations in Gly12 or Gln61 are commonly found in human diseases since changes in these residues lead to steric conflicts with the side chains of the catalytic arginine residue and as a consequence to constitutively active variants due to their GAP insensitivity [166-168].

2.3.2 GEFs

Cell-surface receptors transduce signals in response to extracellular stimuli, such as cytokines, hormones, and growth factors by activation of guanine nucleotide exchange factors (GEFs) which are capable of catalyzing the slow intrinsic nucleotide exchange reaction of small GTPases by several orders of magnitude [35]. GEFs that are responsible for the activation of

RAS proteins, like SOS1 or RASGRF contain a CDC25 homology domain and a RAS exchange motif (REM), while RHO specific GEFs contain a DH-PH tandem domain or an unrelated domain identified in DOCK proteins [169]. GEFs are usually multidomain proteins that are able to bind to different proteins or lipids, suggesting their role as a scaffold protein by forming large protein complexes. Due to the high affinity of small GTPases for GDP and GTP which is in the range of picomolar, the intrinsic nucleotide dissociation may take several hours [107]. Therefore, GEFs are required for accelerating this process. They strongly reduce the affinity of the GTPase towards the bound GDP, leading to its subsequent association with GTP [169]. During this reaction, GEFs form a complex with the nucleotide-free GTPase in an intermediate state. This complex does not accumulate in the cell due to the much higher affinity of GTP towards the GTPase compared to GEFs, resulting in a rapid dissociation [35].

2.3.3 GDIs

RHO GTPases are proposed to be membrane-bound due to posttranslational modifications which seems critical for their biological functions. However, only a small fraction of RHO GTPases is associated with the membrane, while more than 90 % are in an inactive cytosolic complex with RHOGDIs [109]. Three different RHOGDIs exist in humans, including RHOGDI1, RHOGDI2, and RHOGDI3 [170]. The best-characterized member of the family is RHOGDI1 which has been shown to be ubiquitously expressed and is able to interact with several RHO GTPases including RHOA, RHOC, RAC1, RAC2, and CDC42 [171, 172]. RHOGDI2 is highly expressed in hematopoietic cells and associates with several RHO GTPases, as well [173-175]. However, the binding affinities observed for RHOGDI2 and the RHO GTPases are significantly lower compared to RHOGDI1 and many of these interactions have not been proofed *in vivo* [176]. The most divergent member of the family is RHOGDI3 which has been shown to target the Golgi complex and other cellular membranes due to a unique N-terminal extension [177]. RHOGDIs bind with their N-terminal domain to the switch regions of RHO proteins and stabilize their flexibility. Structural studies showed that RHOGDIs are in contact with numerous key residues for the switch mechanism of RHO proteins, such as Thr35, Tyr64, Arg66, His103, and His104 (RAC1 numbering) [119, 178-180]. The isoprenoid moiety of RHO GTPases have been shown to impair the ability of proper folding in the absence of membranes. Without RHOGDIs the cytosolic pool of RHO proteins would be rapidly degraded in a proteasome-dependent manner [181]. RHOGDIs are capable of binding this isoprenyl group by inserting it

into a hydrophobic pocket of the C-terminus and thus, stabilize the RHO GTPases [182]. Furthermore, RHOGDIs shuttle prenylated RHO proteins between cytoplasm and different membranes, suggesting that RHOGDIs play a key role in the subcellular localization and spatiotemporal activation of RHO GTPases [109].

2.3.4 Posttranslational modification

Small GTPases of the RAS superfamily undergo several post translational modifications. One of them is the modification by three enzymes of the C-terminal CAAX motif, where C is cysteine, A an aliphatic amino acid and X any amino acid [183]. RAS and RHO proteins are immediately post translationally targeted by cytosolic prenyltransferases, such as farnesyltransferase (FTase) or geranylgeranyltransferase (GGTase I) which attach a 15- or 20 carbon polyisoprene lipid to the cysteine of the CAAX motif, respectively [184]. Proteins that contain a serine or a methionine at the end of the CAAX motif are primary substrates for FTase, while proteins ending with leucine are usually targeted by GGTase I [63, 185]. The prenylation of RAS proteins is followed by a proteolytic cleavage of the last three residues AAX *via* an endoprotease called RAS Converting enzyme 1 (RCE1) [186-188]. Afterwards, the new C-terminus with the prenylated cysteine undergoes a carboxymethylation by isoprenylcysteine carboxymethyltransferase (ICMT) to neutralize the negative charge at the C-terminus [189-193]. This CAAX processing enables RAS proteins to associate with membranes due to the remodeling of a hydrophilic to hydrophobic C-terminus. This modification of the HVR is constitutive, while G-domain modifications, such as mono-diubiquitination, sumoylation, acetylation, nitroslyation, and phosphorylation are reversible. For many of these modifications the physiological roles in RAS signaling are still unknown [194].

3 Scaffold proteins

The tight regulation of signal transduction processes is crucial for many cellular functions. Multidomain proteins, called scaffold or adaptor proteins, modulate protein-protein interactions and the assembly of protein complexes by binding two or more signaling molecules simultaneously [195, 196]. These scaffold proteins do not show any enzymatic activity but have critical roles in cellular signaling pathways [197, 198]. They serve as a docking site for multiple protein partners and efficiently enhance signaling cascades by bringing proteins in close vicinity. Several additional functions have been proposed for scaffolding

proteins, such as activation of kinases, inhibition of phosphatases, and subcellular localization of protein complexes [199, 200]. Not all extracellular stimuli result in the same cellular response. The different scaffold proteins form complexes at various subcellular sites by linking the kinases with different substrates or reaction partners. Many scaffold proteins for the MAPK pathway have been described, such as Kinase suppressor of RAS (KSR), β-arrestin, CNK1/2, MEK partner 1 (MP1), MAP Kinase Organizer 1 (MORG1), flotillin-1, and IQGAP1 [201, 202]. However, in most cases it is unknown how the scaffold proteins are regulated themselves. Oligomerization, conformational activation, nucleocytoplasmic shuttling, and phosphorylation have been proposed as main mechanisms for this regulation [203].

3.1 IQGAPs

The IQ motif containing GTPase activating proteins (IQGAPs) belong to the class of multidomain proteins which play a central role in the assembly of protein complexes by pooling proteins in distinct signaling networks [204-208]. Three IQGAPs have been described in humans sharing a similar domain organization and high sequence homology. The best characterized ubiquitously expressed IQGAP1 is overexpressed in many human tumors, including pancreatic adenocarcinoma, colon cancers, ovarian carcinomas, and glioma. Furthermore, IQGAP1 contributes tumor progression by scaffolding for example the main components of the RAS/MAPK pathway [209]. Less is known about the other two paralogs of the IQGAP family. IQGAP2 has been shown to be expressed in liver, prostate, kidney, thyroid, stomach, testis, and platelets, while IQGAP3 is found in brain, lung, testis, intestine, and colon [209]. The IQGAPs modulate many cellular processes, such as adhesion, directional migration, and cancer progression [204-208, 210, 211].

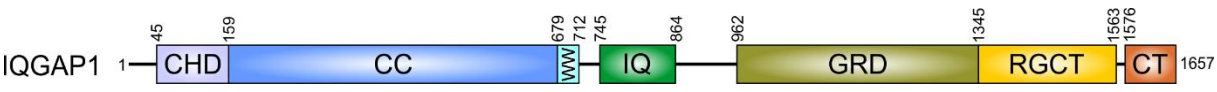

Figure 8. Domain organization of IQGAP1. CHD= calponin homology domain; CC= coiled-coil; WW= polyproline binding domain; IQ= Isoleucine/Glutamine motif; GRD= GAP-related domain; RGCT= RASGAP C-terminal domain; CT= very C-terminal domain.

Multiple domains enable IQGAPs to interact with the large number of proteins to achieve their scaffolding function. Through the N-terminal calponin homology domain (CHD) IQGAPs are able to bind F-actin [212]. The polyproline-binding region (WW) has been shown to interact with ERK1/2, while the IQ motif (IQ) binds to HER1/2, KRAS, B/CRAF, MEK1/2, and calmodulin

[207, 213]. The RASGAP-related domain (GRD) and the RASGAP C-terminal domain (RGCT) bind to the RHO GTPases CDC42 and RAC1 [214-218]. GRD of IQGAPs show high sequence homology to the GAP domain of RASGAPs. However, due to a conserved threonine instead of a catalytic arginine which is essential for the GAP stimulated GTP hydrolysis, IQGAPs are not able to accelerate the GTP hydrolysis reaction of small GTPases [215]. The very C-terminal domain (CT) binds E-cadherin, β-catenin, APC, and CLIP-170 [206].

4 Aims

The small GTPases of the RAS and RHO family are known to play a key role in many cellular processes, such as differentiation, proliferation, polarity, adhesion, migration, and cell cycle. Hence, it is not surprising that dysfunction of these proteins may result in different diseases, including developmental disorders and cancer. Most of the small GTPases act as molecular switches cycling between an active, GTP-bound and an inactive, GDP-bound conformation. This cycle is tightly regulated by GEFs and GAPs which accelerate the slow intrinsic nucleotide exchange from GDP-bound to GTP-bound form and stimulate the intrinsic hydrolysis activity, respectively. Several missense mutations in *CDC42*, *RRAS2*, and *MRAS* were identified in patients with Noonan syndrome, an autosomal dominant developmental syndrome caused by germline mutations in genes encoding components of the RAS/MAPK pathway. Furthermore, we identified a novel disorder, termed NOCARH syndrome, due to a specific amino acid change in CDC42 which is characterized by neonatal onset of pancytopenia, autoinflammation, rash, and episodes of HLH. The ubiquitously expressed scaffold protein IQGAP1 has been shown, among more than 100 interaction partners, to physically interact with the RHO GTPases RAC1 and CDC42. Binding of RHO GTPases to IQGAP1 and/or phosphorylation of Ser1441 and Ser1443 have been proposed to release IQGAP1 from an autoinhibited state. However, the interaction between IQGAP1 and IQGAP2 with a large number of RHO GTPases has not been analyzed so far. Understanding how IQGAPs get activated and how they achieve their scaffolding function to orchestrate many signaling pathways is of major interest. Therefore, this thesis aimed to: (i) characterize the missense mutations biochemically and structurally to better understand the pathogenesis of developmental disorders, like Noonan syndrome, (ii) investigate the molecular mechanism underlying the new disease, called NOCARH syndrome, (iii) identify how RHO GTPases interact with IQGAPs in detail and if there are selectivity determinants for this bimolecular interaction.

Chapter II

Functional Dysregulation of CDC42 Causes Diverse Developmental Phenotypes

Graphical abstract

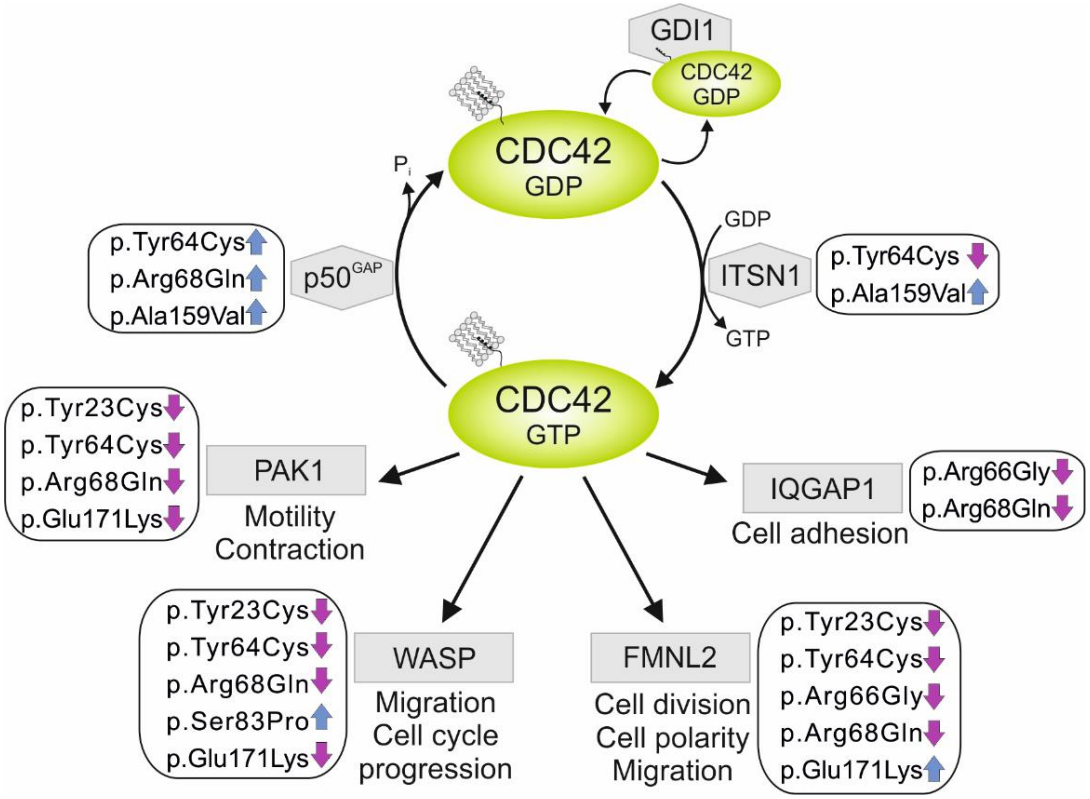

Status: Published in The American Journal of Human Genetics, January 25th 2018

Impact factor: 9.924

Own proportion: 35 %

Expression and purification of CDC42 variants, effectors and regulators, structural analyses, GTP hydrolysis assay, nucleotide exchange assay, interaction studies, figure preparation, writing the manuscript, discussion.

REPORT

Functional Dysregulation of CDC42 Causes Diverse Developmental Phenotypes

Simone Martinelli,[1] Oliver H.F. Krumbach,[2,30] Francesca Pantaleoni,[3,30] Simona Coppola,[4,30] Ehsan Amin,[2,31] Luca Pannone,[3] Kazem Nouri,[2,32] Luciapia Farina,[4] Radovan Dvorsky,[2] Francesca Lepri,[3] Marcel Buchholzer,[2] Raphael Konopatzki,[2] Laurence Walsh,[5] Katelyn Payne,[5] Mary Ella Pierpont,[6,7] Samantha Schrier Vergano,[8] Katherine G. Langley,[9] Douglas Larsen,[10] Kelly D. Farwell,[11] Sha Tang,[11] Cameron Mroske,[11] Ivan Gallotta,[12] Elia Di Schiavi,[12] Matteo della Monica,[13] Licia Lugli,[14] Cesare Rossi,[15] Marco Seri,[16] Guido Cocchi,[16] Lindsay Henderson,[9] Berivan Baskin,[9] Mariëlle Alders,[17] Roberto Mendoza-Londono,[18,19,20] Lucie Dupuis,[18] Deborah A. Nickerson,[21] Jessica X. Chong,[22] The University of Washington Center for Mendelian Genomics, Naomi Meeks,[23] Kathleen Brown,[23] Tahnee Causey,[24] Megan T. Cho,[9] Stephanie Demuth,[25] Maria Cristina Digilio,[3] Bruce D. Gelb,[26] Michael J. Bamshad,[21,22] Martin Zenker,[27] Mohammad Reza Ahmadian,[2,33] Raoul C. Hennekam,[28,33] Marco Tartaglia,[3,33,*] and Ghayda M. Mirzaa[22,29,33,*]

Exome sequencing has markedly enhanced the discovery of genes implicated in Mendelian disorders, particularly for individuals in whom a known clinical entity could not be assigned. This has led to the recognition that phenotypic heterogeneity resulting from allelic mutations occurs more commonly than previously appreciated. Here, we report that missense variants in *CDC42*, a gene encoding a small GTPase functioning as an intracellular signaling node, underlie a clinically heterogeneous group of phenotypes characterized by variable growth dysregulation, facial dysmorphism, and neurodevelopmental, immunological, and hematological anomalies, including a phenotype resembling Noonan syndrome, a developmental disorder caused by dysregulated RAS signaling. *In silico*, *in vitro*, and *in vivo* analyses demonstrate that mutations variably perturb CDC42 function by altering the switch between the active and inactive states of the GTPase and/or affecting CDC42 interaction with effectors, and differentially disturb cellular and developmental processes. These findings reveal the remarkably variable impact that dominantly acting *CDC42* mutations have on cell function and development, creating challenges in syndrome definition, and exemplify the importance of functional profiling for syndrome recognition and delineation.

The rate of identification of genes implicated in human disorders has dramatically increased with the use of second-generation sequencing technologies. In particular, exome sequencing has emerged as a feasible and efficient strategy to uncover the molecular basis of Mendelian disorders, particularly for individuals with a rare clinical presentation or for whom a unifying clinical diagnosis is not discerned.[1] Mutations affecting the same gene but resulting in substantial phenotypic differences is a very well-known phenomenon, but the wide use of exome sequencing has led to the recognition that this event occurs much more commonly than previously appreciated.[2–4] In the last few years, it has been recognized that the variable clinical manifestation of allelic mutations can often result from their differential impact on protein function, although the consequences of specific variants

[1]Department of Oncology and Molecular Medicine, Istituto Superiore di Sanità, Rome 00161, Italy; [2]Institute of Biochemistry and Molecular Biology II, Medical Faculty of the Heinrich-Heine University, Düsseldorf 40225, Germany; [3]Genetics and Rare Diseases Research Division, Ospedale Pediatrico Bambino Gesù, IRCCS, Rome 00146, Italy; [4]National Center for Rare Diseases, Istituto Superiore di Sanità, Rome 00161, Italy; [5]Riley Hospital for Children, Indianapolis, IN 46202, USA; [6]Department of Pediatrics, University of Minnesota, Minneapolis, MN 55454, USA; [7]Children's Hospital of Minnesota, Minneapolis, MN 55454, USA; [8]Division of Medical Genetics and Metabolism, Children's Hospital of The King's Daughters, Norfolk, VA 23507, USA; [9]GeneDX, Gaithersburg, MD 20877, USA; [10]Department of Neurology, Washington University, St. Louis, MO 63130, USA; [11]Ambry Genetics, Department of Clinical Genomics, Aliso Viejo, CA 92656, USA; [12]Institute of Biosciences and Bioresources, National Research Council, 80131 Naples, Italy; [13]Genetica Medica, Azienda Ospedaliera Universitaria Meyer, 50139 Florence, Italy; [14]Struttura Complessa di Neonatologia, Policlinico di Modena, 41124 Modena, Italy; [15]Genetica Medica, Policlinico S.Orsola-Malpighi, 40138 Bologna, Italy; [16]Department of Medical and Surgical Sciences, University of Bologna, 40138 Bologna, Italy; [17]Department of Clinical Genetics, Academic Medical Centre, University of Amsterdam, Amsterdam 1105-AZ, the Netherlands; [18]Division of Clinical and Metabolic Genetics, The Hospital for Sick Children, Toronto, ON M5G 1X8, Canada; [19]Genetics and Genome Biology, The Hospital for Sick Children, Toronto, ON M5G 1X8, Canada; [20]Department of Pediatrics, University of Toronto, Toronto, ON M5G 1X8, Canada; [21]Department of Genome Sciences, University of Washington, Seattle, WA 98195, USA; [22]Department of Pediatrics, University of Washington, Seattle, WA 98195, USA; [23]Children's Hospital Colorado, Aurora, CO 80045, USA; [24]Department of Human and Molecular Genetics, Virginia Commonwealth University, Richmond, VA 23284, USA; [25]Praxis für Humangenetik Erfurt, Erfurt 99084, Germany; [26]Mindich Child Health and Development Institute and Departments of Pediatrics, and Genetics and Genomic Sciences, Icahn School of Medicine at Mount Sinai, New York, NY 10029, USA; [27]Institute of Human Genetics, University Hospital Magdeburg, Magdeburg 39120, Germany; [28]Department of Pediatrics, Academic Medical Center, University of Amsterdam, Amsterdam 1105-AZ, the Netherlands; [29]Center for Integrative Brain Research, Seattle Children's Research Institute, Seattle, WA 98101, USA
[30]These authors contributed equally to this work
[31]Present address: Institute of Neural and Sensory Physiology, Medical Faculty of the Heinrich-Heine University, Düsseldorf, Germany
[32]Present address: Department of Pathology and Molecular Medicine, Richardson Laboratory, Queen's University, Kingston, ON K7L 3N6, Canada
[33]These authors contributed equally to this work
*Correspondence: marco.tartaglia@opbg.net (M.T.), gmirzaa@u.washington.edu (G.M.M.)
https://doi.org/10.1016/j.ajhg.2017.12.015.

can be difficult to predict and may require substantial efforts to be fully understood.[5–7] Here, we report that missense mutations in *cell division cycle 42* (*CDC42* [MIM: 116952]), a gene encoding a member of the RAS superfamily of low-molecular-weight GTP/GDP-binding proteins functioning as a major node in intracellular signaling, underlie a clinically heterogeneous group of developmental phenotypes. Our *in silico*, *in vitro*, and *in vivo* dissection of the structural and functional impact of disease-causing mutations documents that they variably perturb CDC42 biochemical behavior and differentially affect cellular and developmental processes, highlighting the variable impact of the functional dysregulation of this GTPase in cell physiology and development. Our findings also exemplify the importance of functional profiling for syndrome recognition and delineation.

A total of 15 subjects from 13 unrelated families were included in the study. Clinical data and DNA samples were collected from the participating families (after written informed consent was obtained) and stored and used under research projects approved by the Review Boards of the participating institutions. Investigators studying the affected individuals described here were connected via the MatchMaker Exchange (MME) network of web-based tools[8] GeneMatcher and MyGene2.[9,10] Nine affected individuals (subjects 1 to 5 and 8 to 11), who exhibited a molecularly unexplained and clinically unrecognized multi-systemic disorder, were investigated by whole-exome sequencing (WES) using DNA samples obtained from either leukocytes or saliva specimens, and a child-parent trio-based strategy. Exome capture was carried out using the SureSelect Clinical Research Exome (Agilent) (subjects 1 and 8), SureSelect Human All Exon v.1, v.3, and v.5 (Agilent) (subjects 2, 10, and 5, respectively), Nextera Exome Enrichment Kit (Illumina) (subject 3), SeqCap EZ VCRome 2.0 (Roche) (subject 4), and SeqCap EZ MedExome v2 (Roche) (subjects 9 and 11) target enrichment kits, and sequencing was performed on a HiSeq 2000 platform (Illumina), using paired-end. WES data processing, sequence alignment to GRCh37, and variant filtering and prioritization by allele frequency, predicted functional impact, and inheritance models were performed as previously described.[11–13] Mean coverage of target regions and average reads depth for individual samples are provided in Table S1. Subjects 12 (simplex case subject) and 13 to 15 (affected members of family 30153) (Figure S1) belonged to a cohort of 235 unrelated individuals with clinical features fitting Noonan syndrome (MIM: 163950) or overlapping with this disorder, followed at three participating genetic centers (Rome, Bologna, and Magdeburg),[14,15] who did not harbor mutations in previously identified genes implicated in RASopathies. Based on the hypothesis that mutations in *CDC42* might be linked causally to Noonan syndrome (or a clinically related RASopathy), the entire *CDC42* coding sequence was analyzed by targeted resequencing, using genomic DNA from blood, skin fibroblasts, hair bulbs, and/or epithelial cells from the oral mucosa. Target enrichment was performed using the Nextera Rapid Capture kit (Illumina), and sequencing was carried out on a NextSeq550 (Illumina) with a 2 × 150 bp paired-end read protocol. Alignment and variant calling were performed with the BWA Enrichment BaseSpace App (Illumina), and VCF output files were annotated using Variant Studio v.2.2 (Illumina). Finally, Sanger sequencing was used to screen the *CDC42* coding exons in subjects 6 and 7, who showed clinical features suggestive for the condition associated with *CDC42* group I mutations (see below).

Overall, nine different missense mutations distributed across the entire *CDC42* coding sequence were identified (Table 1). Two amino acid substitutions affected the N-terminal α helix (residues Ile21 and Tyr23), three involved adjacent residues within the switch II motif (Tyr64, Arg66, and Arg68), two mapped to the fourth β strand (Cys81 and Ser83), and the remaining two were located close to the C terminus (Ala159 and Glu171) (Figure 1A). Four variants were recurrent, and all occurred as a *de novo* event in at least one family. Of note, the c.511G>A substitution (p.Glu171Lys) was shared by the four affected subjects with clinical features resembling Noonan syndrome, occurring *de novo* in subject 12, and co-segregating with the phenotype in family 30153 (subjects 13 to 15), consistent with dominant inheritance. None of these variants had been reported in ExAC/gnomAD, and all were predicted to be pathogenic and met the American College of Medical Genetics (ACMG) criteria to be considered disease causing (Table S2).[19] One variant, c.191A>G (p.Tyr64Cys), had previously been reported in two subjects with syndromic thrombocytopenia (MIM: 616737).[20,21]

CDC42 encodes a small GTPase of the RHO family modulating multiple signaling pathways controlling cell polarity and migration, endocytosis, and cell cycle progression, by cycling between an active (GTP-bound) and an inactive (GDP-bound) state.[22,23] It is characterized by five major highly conserved motifs, G1 to G5, which mediate GTP binding and hydrolysis (G4 and G5), phosphate binding (G1 and G3), and effector binding (G2) (Figure 1A).[24,25] Based on clinical heterogeneity (see below) and location of affected residues, we predicted that the mutations would have a variable functional impact. The structural consequences of the identified disease-causing mutations on CDC42 structure and function were assessed by Pymol molecular viewer (see Web Resources), using available PDB structures. This allowed us to inspect CDC42 interactions with ARHGAP1 ($p50^{GAP}$/CDC42GAP; PDB: 1grn), ARHGAP18 (MacGAP; PDB: 5c2j), and ITSN1 (PDB: 1ki1) and WAS (WASP; PDB: 1cee), as representatives for CDC42's GTPase activating proteins (GAPs), guanine nucleotide exchange factors (GEFs), and effectors, respectively, and to classify them structurally and functionally into three different groups. A first group of mutations affected the switch II region (p.Tyr64Cys, p.Arg66Gly, and p.Arg68Gln; group I), which mediates CDC42 binding to effectors and regulators (Figures 1B–1D).[25] Tyr64 and

Table 1. List of the Germline *CDC42* Missense Mutations Identified in This Study

Exon	Nucleotide Change	Amino Acid Change	Domain	Mutation Group	Subjects	Origin	MetaSVM[a]	CADD phred[a]	REVEL[a]	ACMG
1	c.62T>C	p.Ile21Thr	α1	III	1	*de novo*	0.3729	27.1	0.901	pathogenic
1	c.68A>G	p.Tyr23Cys	α1	III	2	*de novo*	0.7752	27.1	0.937	pathogenic
3	c.191A>G	p.Tyr64Cys	switch II	I	3	*de novo*	0.7976	23.4	0.834	pathogenic
3	c.196A>G	p.Arg66Gly	switch II	I	4, 5	*de novo*	0.5326	26.9	0.836	pathogenic
3	c.203G>A	p.Arg68Gln	switch II	I	6, 7	*de novo*	0.6586	26.3	0.827	pathogenic
3	c.242G>T	p.Cys81Phe	β4	II	8	*de novo*	0.6280	30.0	0.840	pathogenic
3	c.247T>C	p.Ser83Pro	β4	II	9, 10	*de novo*	0.8283	27.8	0.853	pathogenic
4	c.476C>T	p.Ala159Val	NBP	II	11	*de novo*	1.0179	34.0	0.916	pathogenic
5	c.511G>A[b]	p.Glu171Lys	CBR	III	12, 13–15	1 *de novo*, 1 familial	0.0158	24.7	0.768	pathogenic

Nucleotide numbering reflects cDNA numbering with 1 corresponding to the A of the ATG translation initiation codon in the *CDC42* reference sequence (GenBank: NM_001791.3). No variants were reported in the public databases ExAC and GnomAD. All variants were predicted to be "deleterious" by Combined Annotation Dependent Depletion (CADD) v.1.3, Database for Nonsynonymous SNPs' Functional Predictions (dbNSFP) Support Vector Machine (SVM) v.3.0, and REVEL algorithms.[16–18] All changes satisfied the necessary criteria to be classified as pathogenic according to the American College of Medical Genetics guidelines.[19] Abbreviations: NBP, nucleotide binding pocket; CBR, CRIB motif binding region.

[a]Scores > 0 (MetaSVM), > 15 (CADDphred) or > 0.5 (REVEL) predict that the sequence change has a significant impact on protein structure and function.

[b]This change affects transcript variant 1 (GenBank: NM_001791.3) and isoform 1 (GenBank: NP_001782.1), while it does not affect transcript variant 2 (GenBank: NM_044472.2) and isoform 2 (GenBank: NP_426359.1). The two isoforms have the same amino acid length but are characterized by a different C terminus.

Arg66 are located on the surface of CDC42 and directly participate in interactions with regulatory proteins and effectors. These changes were predicted to affect these interactions and, as a consequence, the catalytic activity of the GTPase and/or its capability to transduce signaling. Similarly, Arg68 is embedded in the protein interior and stabilizes the conformation of the switch II region via intramolecular interactions with multiple residues (Ala59, Gln61, and Glu100). The Arg-to-Gln change was assumed to strongly destabilize the switch II loop and the interaction with signaling partners. Group II included substitutions involving residues located within (Ala159) or close to (Cys81 and Ser83) the nucleotide-binding pocket (Figures 1B, 1C, and 1E). Ala159 faces the guanine base and replacement by valine was predicted to promote fast GDP/GTP cycling, favoring a GEF-independent active, GTP-bound state of the protein. A similar hyperactive behavior has been reported in RAS proteins.[26–28] Similarly, Ser83 binds to Gln116, which interacts with the guanine base, predicting indirect perturbation of nucleotide binding properties of CDC42. Cys81 is an invariant residue among RHO GTPases located in proximity of the phosphate-binding loop, and its substitution to phenylalanine was expected to cause favorable hydrophobic interactions with this loop, dislocation of Gly12, and consequently defective GTP hydrolysis. Finally, group III (CRIB mutations) included variants at Ile21, Tyr23, and Glu171, which are exposed residues predicted to affect interactions with effectors containing a CDC42/RAC-interacting binding (CRIB) motif (Figures 1B, 1C, and 1F).[29] Glu171 binds to Lys235 of WAS (WASP, hereafter) and plays a major role in the electrostatic binding network stabilizing the WASP-CDC42 association,[30,31] which was predicted to be disrupted by the Glu-to-Lys change. Tyr23 lies at the CDC42 surface implicated in PAK1 binding and stabilizes proper orientation of helix α5 mediating WASP binding.[32,33] Ile21 is located near the switch I region contributing to the hydrophobic pocket of helix α1 participating in WASP binding.[30] The Ile-to-Thr substitution was predicted to perturb CDC42 binding to signaling partners.

We assessed the effects of the disease-causing mutations on CDC42 GTPase activity, GDP/GTP exchange, and binding to effectors *in vitro*, using recombinant proteins. The p.Tyr23Cys, p.Tyr64Cys, p.Arg66Gly, p.Arg68Gln, p.Ser83Pro, p.Ala159Val, and p.Glu171Lys amino acid substitutions were selected as representative of the three mutation groups that were predicted to perturb differentially CDC42 function. pGEX vectors were used for bacterial overexpression of GST-tagged wild-type and mutant CDC42 proteins, and the GTPase-binding domains (GBD) of WASP (residues 154–321), PAK1 (residues 57–141), FMNL2 (residues 1–379), and IQGAP1 (residues 863–1657) in *E. coli* BL21 (DE3). Proteins were purified after cleavage of the GST tag (Superdex 75 or 200, GE Healthcare).[31] Nucleotide-free and fluorescent nucleotide-bound CDC42 variants were prepared using alkaline phosphatase

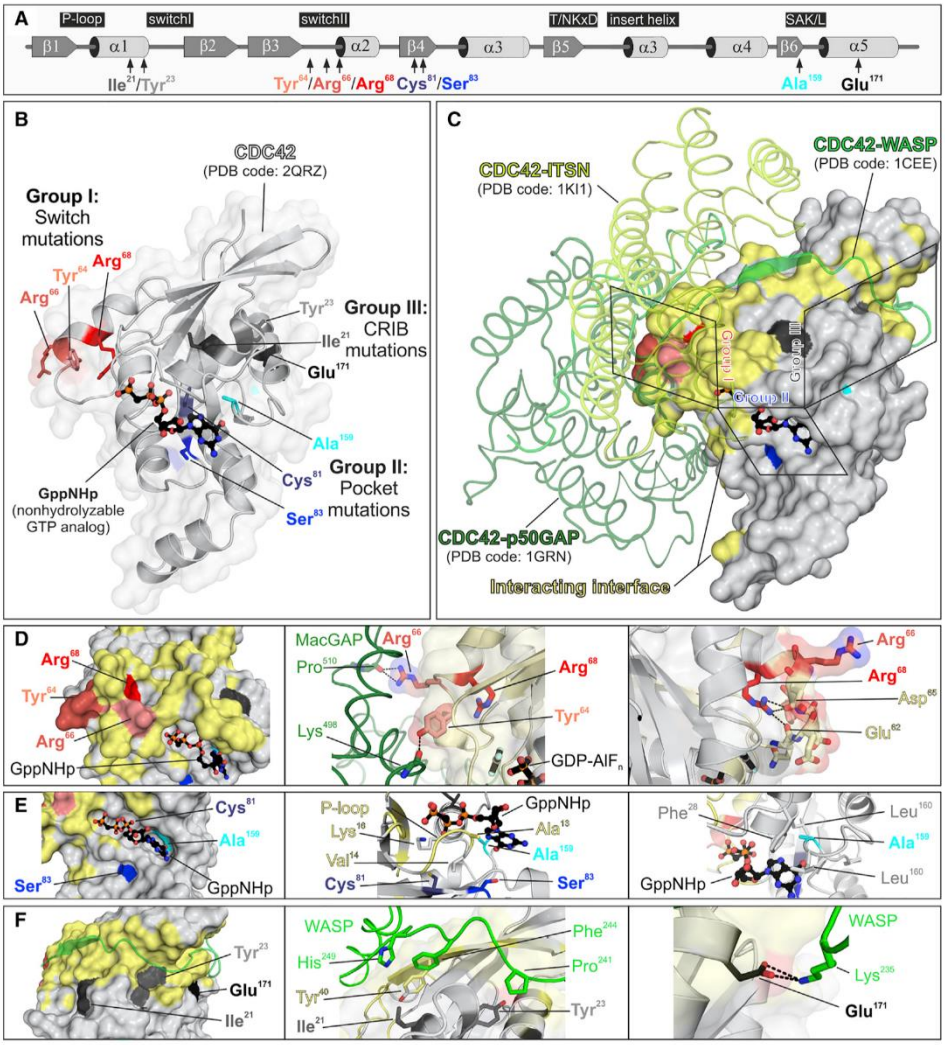

Figure 1. Location of Disease-Causing *CDC42* Mutations and Their Structural Impact

(A) Secondary structure elements (α helices and β strands), conserved motifs critical for tight guanine nucleotide binding and hydrolysis (G1–G5), and position of the identified disease-causing *CDC42* mutations are illustrated.

(B) Variant residues are assigned to three groups according to their position in the context of CDC42 structure (PDB: 2QRZ): group I or switch mutations (Tyr64, Arg66, and Arg68) are part of the switch II loop; group II or pocket mutations (Cys81, Ser83, and Ala159) are located in the vicinity of nucleotide binding pocket; and group III or CRIB mutations (Ile21, Tyr23, and Glu171) are far outside of the major interaction sites of CDC42 with GTP/GDP and involve exposed residues located in or close to regions of the protein mediating binding to effectors containing a CRIB motif.

(C) The position of the mutant residues relative to CDC42 interactions is illustrated by overlaying three different crystal structures of CDC42 in complex with ARHGAP1 ($p50^{GAP}$) (PDB: 1GRN), ITSN (PDB: 1KI1), and WAS (WASP) (PDB: 1CEE). Residues in reciprocal vicinity up to 4 Å were considered as part of binding interface. Residues of CDC42 mediating these interactions are shown in yellow.

(D) Group I mutations. Tyr64 and Arg66 are solvent-exposed residues and contribute to interactions with regulatory proteins and effectors (left). Interaction of both residues with ARHGAP18 (PDB: 5c2j) is shown as a representative for other interactions such as GEFs and effectors (middle). The disease-causing amino acid changes are predicted to affect this interaction. Arg68 participates in stabilizing the conformation of the switch II region via intramolecular interactions with Glu62 and Asp65 (right). The Arg-to-Gln change is predicted to destabilizes the switch II loop that is crucial for the interaction with signaling partners.

(E) Group II mutations. Cys81, Ser83, and Ala159 are in close vicinity of the phosphates (G1) and guanine base (G5) of bound GTP/GDP. Their substitutions are predicted to directly or indirectly affect the nucleotide binding affinity and to shift the balance between inactive and active CDC42 toward the latter.

(F) Group III mutations. Ile21, Tyr23, and Glu171 are part of a cavity on the CDC42 surface that accommodates the CRIB motif of bound effector proteins (e.g., WASP) (left). Ile21 and Tyr23 are critical for hydrophobic interactions (middle) with these type of proteins, while Glu171 contribute to binding mediating an electrostatic interaction (right).

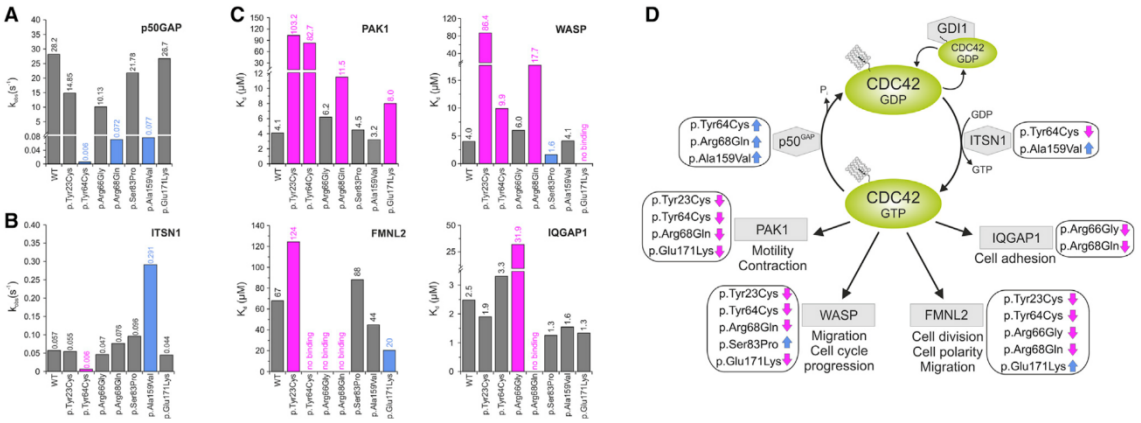

Figure 2. Assessment of the GTPase Activity, Nucleotide Exchange, and Binding to Effectors of Disease-Causing CDC42 Mutants
(A) Mean rate constants (k_{obs} values) of $p50^{GAP}$-stimulated GTP hydrolysis. Grey bars indicate non-significant differences compared to wild-type CDC42; blue bars indicate abolished/impaired GTP hydrolysis, which in turn results in an increased amount of active, GTP-bound CDC42 and thus enhanced signal flow. Data were obtained from >4 independent experiments.
(B) Mean rate constants (k_{obs} values) of the GEF-catalyzed release of labeled GDP (mantGDP). Grey bars indicate non-significant differences compared to wild-type CDC42; blue and magenta bars indicate increased or abolished nucleotide exchange, respectively. The former is predicted to promote enhanced signaling, while the latter blocks CDC42 in its inactive state. Data were obtained from >4 independent experiments.
(C) CDC42 mutants variably affect binding to effectors. Dissociation constants (K_d) obtained for the interaction of CDC42 proteins with PAK1, WASP, IQGAP1, and FMNL2 determined by fluorescence polarization. Data were collected from titration of increasing concentrations of the respective effectors. They were obtained from >4 independent experiments and are illustrated as bar charts. Grey bars indicate non-significant differences compared to wild-type CDC42; blue and magenta bars indicate increased or decreased binding affinity, respectively.
(D) Scheme summarizing the functional dysregulation of disease-causing mutants on downstream signaling pathways and cellular processes. ITSN1 is a specific GEF for CDC42 promoting the active state of the GTPase by catalyzing GDP release. $p50^{GAP}$ negatively controls CDC42 function by stimulating the GTP hydrolysis reaction. CDC42 interaction with PAK1, WASP, FMNL2, and IQGAP1 activates signaling pathways controlling different cellular processes. For each specific function, the blue and magenta arrows indicate the hyperactive or defective behavior, respectively.

(Roche) and phosphodiesterase (Sigma Aldrich) at 4°C.[31,34] First, GTPase activity was measured basally and following ARHGAP1 ($p50^{GAP}$, hereafter) stimulation by fluorescent experiments using tetramethylrhodamine (tamra-) GTP as substrate with a Hi-Tech Scientific (SF-61) stopped-flow instrument (Figures 2A and S2). The assays documented a variably increased basal GTP hydrolysis for $CDC42^{Tyr64Cys}$, $CDC42^{Arg68Gln}$, and $CDC42^{Ala159Val}$. Each of these mutants, however, exhibited robust GAP insensitivity, showing respectively a 4,700-fold ($CDC42^{Tyr64Cys}$), 392-fold ($CDC42^{Arg68Gln}$), and 366-fold ($CDC42^{Ala159Val}$) reduction in GAP-stimulated GTPase activity, compared to wild-type CDC42. A mildly decreased GAP-stimulated GTP hydrolysis was documented for $CDC42^{Tyr23Cys}$ and $CDC42^{Arg66Gly}$. By using the same experimental approach, release of methylanthraniloyl (mant-) GDP was used to assess the basal and GEF-catalyzed nucleotide exchange reactions (Figures 2B and S3). The assays documented an increase of GDP release for $CDC42^{Ala159Val}$ and a slightly increased nucleotide exchange for $CDC42^{Arg68Gln}$ and $CDC42^{Ser83Pro}$. By contrast, p.Tyr64Cys resulted in an almost completely abolished response to GEF. No substantial difference in GDP/GTP exchange behavior was observed for the other mutants. Then, fluorescence experiments were performed by using increasing amounts of the CDC42 interacting domains of WASP, PAK1, FMNL2, and IQGAP1 titrated to CDC42 proteins bound to mant-GppNHp, a non-hydrolyzable GTP analog, to assess the binding of mutants to four major CDC42 effectors and evaluate their ability to transduce signaling (Figures 2C and S4). Experiments were performed using a Fluoromax 4 fluorimeter in polarization mode, and the dissociation constants (K_d) were calculated by fitting the concentration-dependent binding curve using a quadratic ligand binding equation. Interaction with WASP was completely abolished in $CDC42^{Glu171Lys}$ and markedly decreased (21.6-fold) in $CDC42^{Tyr23Cys}$. Decreased binding, albeit to a milder degree, was documented for $CDC42^{Arg68Gln}$ and $CDC42^{Tyr64Cys}$, while $CDC42^{Ser83Pro}$ exhibited a slightly increased binding. Binding to PAK1 was impaired for $CDC42^{Tyr23Cys}$ and $CDC42^{Tyr64Cys}$ and reduced for $CDC42^{Arg68Gln}$ and $CDC42^{Glu171Lys}$. Tyr64 and Arg66 contribute to CDC42 binding to FMNL2;[35] consistently, $CDC42^{Tyr64Cys}$ and $CDC42^{Arg66Gly}$ had impaired FMNL2 binding, with the latter also having defective interaction with IQGAP1. Impaired binding to FMNL2 was also documented for $CDC42^{Tyr23Cys}$ and $CDC42^{Arg68Gln}$, the latter also exhibiting defective IQGAP1 binding. By contrast, $CDC42^{Glu171Lys}$ showed enhanced FMNL2 binding. Overall, biochemical characterization of CDC42

mutants confirmed the heterogeneous clinical and structural impact of variants demonstrating a stabilized GTP-bound conformation but defective interaction with all tested partners for group I mutations, variable hyperactive behavior for group II mutations, and a diversified binding to effectors for group III mutations (Figure 2D).

CDC42 is a master regulator of cell polarization and controls cell migration and growth.[36,37] The impact of CDC42 mutations on polarized migration was assessed by an *in vitro* wound-healing assay on fibronectin-coated wells (Sigma-Aldrich) (Figures 3A and S5). Monolayers of NIH 3T3 cells (American Type Culture Collection) cultured in high-glucose Dulbecco's modified Eagle's medium (DMEM) supplemented with 10% FCS, 2 mM L-glutamine, and 10 U/mL penicillin/streptomycin (Sigma-Aldrich) were transiently transfected using Fugene 6 (Roche) to express wild-type FLAG-tagged CDC42 isoform 1 (GenBank: NP_001782.1) or each of the p.Tyr23Cys, p.Arg68Gln, p.Ser83Pro, p.Ala159Val, and p.Glu171Lys mutants. 24 hr after transfection, cells were scratched and incubated in low serum medium in the presence of thymidine (Sigma-Aldrich) to inhibit cell proliferation. Cells that had migrated in the wounded area were counted 4 and 7 hr after scratch (four fields per well). Comparable transfection efficiency was verified by western blot analysis of the protein lysates. Only cells expressing group II mutants exhibited enhanced wound closure ability compared to cells expressing wild-type CDC42. Other tested mutants failed to increase migration, suggesting loss of function of this CDC42-mediated process, in line with defective binding of these mutants to WASP, a mediator of polarized migration.[38] Mutants also affected cell proliferation differentially (Figure 3A). $CDC42^{Ala159Val}$ and $CDC42^{Ser83Pro}$ variably enhanced cell growth, while $CDC42^{Tyr23Cys}$ and $CDC42^{Arg68Gln}$ significantly impaired proliferation, indicating a dominant-negative effect.

In *Caenorhabditis elegans*, CDC-42 controls early and late developmental programs (see WormBook in Web Resources), including vulval development,[39–41] a process that is regulated by LET-60/RAS-dependent and -independent signals.[42] To explore the impact of the disease-causing *CDC42* mutations *in vivo*, transgenic lines were generated to conditionally express wild-type CDC-42 or a selected subset of mutations for each mutation group (p.Tyr23Cys, p.Arg68Gln, p.Ser83Pro, p.Ala159Val, and p.Glu171Lys) affecting residues conserved in the nematode ortholog (Figure S6).[43] The wild-type *cdc-42* cDNA (ORF clone R07G3.1; ThermoScientific) was subcloned into the pPD49.83 heat shock-inducible vector (gift of A. Fire, Stanford University School of Medicine), and the generated constructs were injected at 100 ng/μL. The pJM67 plasmid (*pelt-2::NLS::GFP*) (gift from J.D. McGhee, University of Calgary), which drives green fluorescent protein (GFP) expression in intestinal cell nuclei, was used as co-injection marker (30 ng/μL). To analyze vulval induction and morphogenesis, synchronized animals from at least three independent lines for each construct were grown at 20°C and heat-shocked (90 min at 33°C followed by 30 min at 30°C) at late L2/early L3 larval stages and scored for vulval induction and morphogenesis from late L3 to mid L4 stages. The presence of a protruding vulva (Pvl phenotype), multiple ectopic pseudovulvae (multivulva [Muv] phenotype), and lack of a vulva (vulvaless [Vul] phenotype) was analyzed at the adult stage. Lines were scored in triplicate experiments using a Nikon Eclipse 80i instrument equipped with Nomarski differential interference contrast optics and used for further analyses and crosses. After each cross, the genotype of individual alleles was confirmed by direct sequencing of the appropriate genomic region. Isogenic animals that had lost the transgene were cloned separately and used as controls in each experiment. Overexpression of wild-type CDC-42 at the L2/L3 stage elicited a low-penetrant Muv phenotype, exacerbated the Muv phenotype associated with a *let-60* gain-of-function allele, *let-60(n1046) IV*, and partially rescued the Vul phenotype of animals carrying a hypomorphic *let-23/EGFR* allele, *let-23(sy1) II*, indicating LET-60/RAS signaling hyperactivation (Figures 3B and S7, Table S3). Compared to wild-type CDC-42, group II mutations induced a more severe Muv phenotype and more efficiently rescued the Vul phenotype of *let-23(sy1)* animals, indicative of enhanced signal flow through LET-60. Overexpression of wild-type CDC-42 also engendered aberrant vulva morphogenesis, generating a Pvl phenotype that was mediated, in part, by WSP-1/WASP (Figures 3B and S7, Tables S3 and S4). The same phenotype had previously been reported in *C. elegans* lines expressing the RASopathy-causing $SHOC2^{S2G}$ and $RRAS^{G39dup}$ mutants.[44,45] Like those animals, a variable proportion of CDC-42 hermaphrodites exhibiting Pvl displayed egg-laying defects (Egl phenotype) and accumulation of larvae inside the mother (Bag-of-worms phenotype) (data not shown). Of note, this phenotype was markedly promoted by group II mutations in a WASP-independent manner, indicating a gain-of-function effect of these changes. By contrast, $CDC\text{-}42^{Tyr23Cys}$, $CDC\text{-}42^{Arg68Gln}$, and $CDC\text{-}42^{Glu171Lys}$ significantly reduced the Pvl phenotype, supporting a selective hypomorphic behavior. Pvl was not modulated by *wsp-1* RNAi in animals expressing $CDC\text{-}42^{Tyr23Cys}$ and $CDC\text{-}42^{Glu171Lys}$ and was only slightly reduced in those expressing $CDC\text{-}42^{Arg68Gln}$, consistent with the biochemical data indicating an abolished or strongly reduced binding to WASP of those mutants, respectively. Nomarski observations of L3 and L4 control larvae showed that only P6.p descendants detached from the cuticle generating a single, symmetric invagination; by contrast, a variable proportion of larvae expressing wild-type and mutant CDC-42 displayed asymmetric and/or multiple invaginations (Figure S7), which represent the earliest signs of the Pvl and Muv phenotypes, respectively. Overall, the data indicate that group II mutations upregulate multiple signaling pathways, including LET-60/RAS, while the other variants behave as hypomorphic mutations on WASP-dependent signaling.

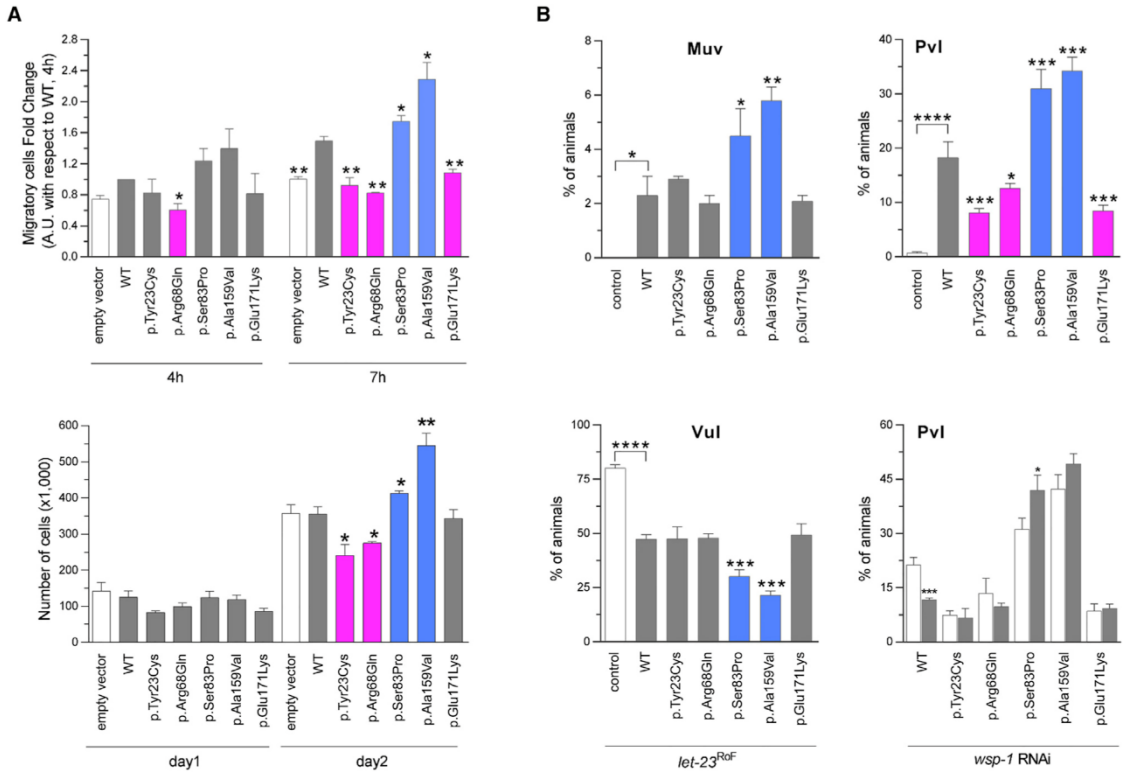

Figure 3. ***In Vitro* and *In Vivo* Functional Characterization of *CDC42* Mutations**

(A) *CDC42* mutations differentially impact polarized migration and cell proliferation. Wound-healing assays (above) and proliferation assays (below) were performed using NIH 3T3 cells transiently transfected to express wild-type CDC42 or each of the indicated mutants. Mean ± SD densitometry values of three independent experiments are shown. The wound was generated 24 hr after transfection, and migration in the wounded area was evaluated after 4 and 7 hr. Cells expressing exogenous wild-type CDC42 migrate more rapidly into the scratched area than cells transfected with the empty vector (EV). Mutants differentially perturb polarized migration, with $CDC42^{Ser83Pro}$ and $CDC42^{Ala159Val}$ overexpression variably enhancing the wound closure ability of transfected cells compared to the wild-type protein, whereas $CDC42^{Tyr23Cys}$, $CDC42^{Arg68Gln}$, and $CDC42^{Glu171Lys}$ fail to do that, supporting a gain-of-function and a loss-of-function effect of these mutants, respectively. Cell proliferation was evaluated in transfected cells at the indicated time points and quantified by manual counting using a Neubauer hemocytometer. The trypan blue dye exclusion test was used to consider viable cells only. While the $CDC42^{Ala159Val}$ and $CDC42^{Ser83Pro}$ mutants variably enhance proliferation compared to cells expressing wild-type CDC42, no effect on proliferation ($CDC42^{Glu171Lys}$) and reduced proliferation ($CDC42^{Tyr23Cys}$ and $CDC42^{Arg68Gln}$) is documented for the other mutants, indicating a loss-of-function and a dominant-negative effect, respectively. Asterisks indicate significant differences compared with wild-type CDC42 (*$p < 0.05$; **$p < 0.01$; Student's t test).

(B) Consequences of *CDC-42* expression on vulval development in *C. elegans*. Ectopic expression of wild-type CDC-42 at the L2/L3 stage elicits a multivulva (Muv) phenotype (left, upper panel), and CDC-42 overexpression in a LET-23/EGFR hypomorphic background reduces the penetrance of the vulvaless (Vul) phenotype (left, lower panel). Compared to animals expressing wild-type CDC-42, those expressing $CDC\text{-}42^{Ser83Pro}$ and $CDC\text{-}42^{Ala159Val}$ show higher prevalence of the Muv phenotype and lower prevalence of the Vul phenotype, indicating a gain-of-function role on LET-60/RAS signaling. Animals expressing the other tested CDC-42 mutants do not significantly differ from those expressing wild-type CDC-42. Ectopic expression of wild-type CDC-42 at the early L3 stage elicits a protruding vulva (Pvl) phenotype (right, upper panel). Animals expressing $CDC\text{-}42^{Ser83Pro}$ and $CDC\text{-}42^{Ala159Val}$ show a higher prevalence of the phenotype compared to worms expressing wild-type CDC-42, while a less penetrant phenotype was scored for animals expressing $CDC\text{-}42^{Tyr23Cys}$, $CDC\text{-}42^{Arg68Gln}$, or $CDC\text{-}42^{Glu171Lys}$ mutants. RNA interference (RNAi) experiments show that the Pvl phenotype associated with overexpression of wild-type CDC-42 is mediated, in part, by WSP-1/WASP (right, lower panel). White and gray bars indicate the penetrance of Pvl in non-interfered and interfered animals, respectively. Error bars indicate SEM of four independent experiments, and asterisks specify significance differences between animals expressing CDC-42 mutants and those expressing wild-type CDC-42 or between interfered and non-interfered nematodes (*$p < 0.05$; **$p < 0.001$; ***$p < 0.0001$; ****$p < 0.00005$; two-tailed Fisher's exact test). Comparisons between worms expressing wild-type CDC-42 and control animals are also shown. RNAi was performed by feeding using HT115 *E. coli* bacteria expressing double stranded *wsp-1* RNA (Ahringer's *C. elegans* RNAi feeding library) and optimized to overcome lethality. As a control of the efficiency of the modified RNAi protocol, *let-60* RNAi experiments were performed on animals carrying the *let-60* gain-of-function allele *n1046* (p.Gly13Glu), and the prevalence of the Muv phenotype was scored at a dissecting microscope (Table S4).

Figure 4. Facial Features of Individuals with Heterozygous *CDC42* Mutations
(A–C) Subject 3 (p.Tyr64Cys) at age 2 years and 6 months (A) and 15 years (B and C) showing upslanted palpebral fissures, smooth philtrum, flaring alae nasi, thin upper vermilion, and wide mouth with widely spaced teeth.
(D) Subject 4 (p.Arg66Gly) at 15 years showing broad forehead and broad nasal bridge with bulbous nasal tip.
(E and F) Subject 6 (p.Arg68Gln) at 24 months (E) and 4 years (F) showing a prominent broad forehead, hypertelorism, long philtrum, and thin upper vermilion.
(G and H) Subject 9 (p.Ser83Pro) at age 2 (G) and 6 (H) years showing prominent forehead, hypertelorism, wide mouth with cupid's bow, thin upper vermilion, and widely spaced teeth.
(I and J) Subject 10 (p.Ser83Pro) at 13 (I) and 32 (J) years showing prominent forehead, wide nasal bridge, ptosis, flared nostrils, and wide mouth with widely spaced teeth.
(K and L) Subject 11 (p.Ala159Val) at 2 years (K) and at 3 years and 7 months (L) showing very broad and prominent forehead, bulbous nasal tip, flared nostrils, cupid's bow, and downturned corners of the mouth.
(M–O) Subject 1 (p.Ile21Thr) at age 3 months (M), 2 years (N), and 10 years (O) showing synophrys, wide palpebral fissures, high and narrow nasal bridge, bulbous nasal tip, wide mouth with downturned corners, and mildly laterally prominent ears.
(P) Subject 2 (p.Tyr23Cys) at 14 years showing wide palpebral fissures, high nasal bridge with elevated nasal tip, short philtrum, and long neck.
(Q) Subject 12 (p.Glu171Lys) at 12 years showing typical facial features of Noonan syndrome, including broad forehead, hypertelorism, low-set ears, bulbous nasal tip, and flared nostrils.
(R) Subject 13 (p.Glu171Lys) showing ptosis, broad neck, and pectus deformity.
Note that individuals fitting the different mutation groups share some facial characteristics, and that intragroup variability is also observed.

The cohort of individuals carrying heterozygous mutations in *CDC42* had an unusually broad spectrum of anomalies. Core clinical features included defective growth, intellectual disability (ID), facial dysmorphism, hearing/vision problems, cardiac malformations, immune, hematologic, and lymphatic abnormalities, and brain malformations (Figures 4 and S8, Tables S5–S7, Supplemental Note). Correlating the functional impact of mutations on clinical phenotypes observed in affected individuals permitted a preliminary analysis of genotype-phenotype relationships (Table 2). Individuals with group I mutations manifested with ID, muscle tone abnormalities, and variable other less common features, including cardiac defects. All individuals within this group had thrombocytopenia, similar to two previously reported individuals.[20,21] Individuals with group II mutations manifested with strikingly dysmorphic facial features: subject 11 (p.Ala159Val) had marked hypertelorism, prominent forehead, bitemporal narrowing, and downslanting palpebral fissures with coarse thick hair, resembling a RASopathy (Figures 4K and 4L). Features within the Noonan syndrome phenotypic spectrum were observed in all affected individuals from two unrelated families carrying the c.511G>A (p.Glu171Lys) change (subjects 12 to 15), with

Table 2. Summary of the Clinical Features of *CDC42* Mutation-Positive Subjects

Mutation group	Group I	Group II	Group III
Number of individuals	5	4	6
Amino acid substitutions	p.Tyr64Cys, p.Arg66Gly, p.Arg68Gln	p.Cys81Phe, p.Ser83Pro, p.Ala159Val	p.Ile21Thr, p.Tyr23Cys, p.Glu171Lys
Growth			
Prenatal – weight at birth ≤ 2 SD	1/4	2/4	1/4
Prenatal – OFC at birth ≤ 2 SD	1/3	1/2	1/2
Postnatal – weight ≤ 2 SD	4/5	2/3	1/4
Postnatal – OFC ≤ 2 SD	3/5	2/4	3/4
Postnatal – growth deficiency	3/5	4/4	4/6
Intellectual disability	5/5	4/4	2/6
Seizures	1/4	2/4	1/6
MRI brain anomalies[a]	4/4	4/4	1/2
Tone anomalies	3/4	2/4	2/6
Optic atrophy	1/4	0/4	2/6
Endocrine anomalies	2/4	1/4	1/5
Facial dysmorphism[b]	4/5	4/4	6/6
Pectus deformity	1/5	0/4	4/5
Scoliosis/vertebral anomalies	2/5	1/4	2/6
Camptodacyly	1/5	2/4	1/5
Cardiac anomalies	3/5	2/4	2/5
GU anomalies	2/5	2/4	1/6
Lymphatic anomalies	1/5	1/4	0/6
Recurrent infections	4/5	3/4	1/6
Platelet anomalies (thrombocytopenia, macrothrombocytes)	4/4	1/3	0/5

Abbreviations: OFC, occipito-frontal circumference; SD, standard deviation; GU, genitourinary. Detailed phenotypic description of subjects is reported in the Supplemental Note and Table S5.
[a]For details regarding brain MRI features, see Figure S8 and Table S7.
[b]For details regarding the facial features, see Table S6.

a particularly striking gestalt of this disorder occurring in subject 12 (Figure 4Q). Notably, brain malformations occurred in all groups, and four individuals manifested with cerebellar-posterior fossa abnormalities. Subjects 8 and 11 (with group II mutations) had a large cerebellum with evidence of posterior fossa crowding and cerebellar tonsillar ectopia, features commonly reported in RASopathies.[46] It should be noted that notwithstanding the occurrence of a clinical overlap within each mutation group, intra-group phenotypic variability was observed, which would suggest a specific impact of individual mutations on developmental processes.

While traditionally CDC42 has been functionally linked to remodeling of the actin cytoskeletal architecture,[47] its role in controlling intracellular signaling has recently been broadened.[48] Such complex modulatory function is accomplished by interactions with a wide array of signaling partners functioning in distinct signal cascades. Cdc42 loss of function is embryonic lethal, and its targeted deletion has been shown to disrupt cell fate decision, differentiation, and function of multiple cell lineages as well as tissue homeostasis.[49] Here, we report that dominantly acting mutations differentially perturb CDC42 function and cause clinically heterogeneous phenotypes affecting development and growth. Group I mutations associated with impaired binding to regulators and effectors cause a syndromic form of thrombocytopenia, while the variably hyperactive group II mutations are associated with a variable developmental disorder characterized by striking dysmorphic features, and one specific amino acid change among the group III mutations, which affects only one of the two CDC42 isoforms and specifically impairs binding to WASP, results in an overall milder clinical phenotype that phenocopies Noonan syndrome.[14]

Noonan syndrome, the most common and clinically variable among the RASopathies, is caused by dysregulated signaling through RAS and the MAPK cascade. This disorder and its clinically related phenotypes result from

heterozygous germline mutations affecting *RAS* genes or genes coding proteins functioning as RAS effectors, regulators of RAS function, or more generally as modulators of RAS-MAPK signaling.[15] More recently, the family of genes implicated in RASopathies has been extended to include *LZTR1* (MIM: 600574), *RIT1* (MIM: 609591), and *RRAS* (MIM: 165090), which encode for signal transducers whose direct link to the RAS and the MAPK cascade had not previously been appreciated.[45,50,51] While it is possible that functional dysregulation of these proteins may impact RAS signaling directly or indirectly, these findings raise also the possibility that other pathways may contribute to disease pathogenesis. The present *in vivo* data provide evidence for enhanced signaling through RAS for group II mutations, indicating that upregulated CDC42 function is able to perturb signal flow through RAS; however, no effect on RAS-mediated signaling was inferred for the p.Glu171Lys change, here identified to be associated with a phenotype resembling Noonan syndrome. While it is possible that the used *in vivo* model failed in providing informative data for the specific effect of $CDC42^{Glu171Lys}$ on RAS signaling, our finding suggests that other processes, including aberrant cytoskeletal rearrangement, may represent a previously unappreciated aspect contributing to disease pathogenesis in Noonan syndrome. Consistent with this possibility, SOS1, SHOC2, and RRAS function has been linked to cell migration and other cellular processes strictly dependent on cytoskeletal rearrangement.[52–54] Further studies are thus required to specifically address the impact of dysregulated CDC42 function on RAS signaling as well as on the cellular and developmental processes that are altered in Noonan syndrome.

Overall, the present work links different classes of dominantly acting mutations of CDC42, a master regulator of actin cytoskeleton and major node in intracellular signaling, to a heterogeneous set of developmental and multi-system phenotypes, demonstrating the critical requirement of proper CDC42 function in a large array of developmental processes. This study also exemplifies current challenges in syndrome delineation in the post-WES era and emphasizes the relevance of functional profiling in syndrome recognition and delineation.

Accession Numbers

ClinVar accession ID for data provided herein are SCV000572034.2 (c.62T>C), SCV000244190.3 (c.68A>G), SCV000577577.2 (c.191A>G), SCV000244118.3 (c.196A>G), SCV000589746.1 (c.242G>T), SCV000678254 (c.203G>A), SCV000678255 (c.247T>C), SCV000678256 (c.476C>T), and SCV000678257 (c.511G>A).

Supplemental Data

Supplemental Data include a supplemental note (clinical data), eight figures, and seven tables and can be found with this article online at https://doi.org/10.1016/j.ajhg.2017.12.015.

Acknowledgments

We thank the families and referring physicians for their participation in this study. We thank Dr. David Wilson (Washington University, St. Louis) for providing clinical expertise and Dr. Serenella Venanzi (Istituto Superiore di Sanità, Rome) for technical assistance. This project was supported by the National Institute of Neurological Disorders and Stroke (NINDS) (K08NS092898 to G.M.M.), the Associazione Italiana per la Ricerca sul Cancro (AIRC) (IG17583 to M.T.), Fondazione Bambino Gesù (Vite Coraggiose to M.T.), Italian Ministry of Health (RF-2011-02349938 and Ricerca Corrente 2017 to M.T.), E-Rare (NSEuroNet to M.Z., M.R.A., and M.T.), International Research Training Group 1902 Intra- and Interorgan Communication of the Cardiovascular System (IRTG 1902 to E.A., M.B., and M.R.A.), and Medical Faculty of the Heinrich-Heine University Duesseldorf (9772617 to K.N., O.H.F.K., R.K., and M.R.A.). Exome sequencing was performed at the University of Washington Center for Mendelian Genomics (UW-CMG) and was funded by the National Human Genome Research Institute and the National Heart, Lung, and Blood Institute grant HG006493 (to D.A.N. and M.J.B.). This work was also supported by grants U01HL131003, UM1HL098147, UM1HL098123, UM1HL128761, UM1HL128711, and UM1HL098162 in support of the Pediatric Cardiac Genomics Consortium from the National Heart, Lung, and Blood Institute and the Eunice Kennedy Shriver National Institute of Child Health and Human Development. *C. elegans* strains were provided by the *Caenorhabditis* Genetics Center, which is funded by NIH Office of Research Infrastructure Programs (P40 OD010440). We also thank WormBase, the contributors to MyGene2, and the University of Washington Center for Mendelian Genomics for use of data.

Received: October 18, 2017
Accepted: December 18, 2017
Published: January 25, 2018

Web Resources

CADD, http://cadd.gs.washington.edu/
ClinVar, https://www.ncbi.nlm.nih.gov/clinvar/
dbNSFP, https://sites.google.com/site/jpopgen/dbNSFP
dbSNP, https://www.ncbi.nlm.nih.gov/projects/SNP/
ExAC Browser, http://exac.broadinstitute.org/
GenBank, https://www.ncbi.nlm.nih.gov/genbank/
gnomAD Browser, http://gnomad.broadinstitute.org/
NCBI Gene, https://www.ncbi.nlm.nih.gov/gene
OMIM, http://www.omim.org/
PyMOL, https://pymol.org/2
RCSB Protein Data Bank, http://www.rcsb.org/pdb/home/home.do
REVEL, https://sites.google.com/site/revelgenomics
WormBase, http://www.wormbase.org/
WormBook, http://www.wormbook.org

References

1. Bamshad, M.J., Ng, S.B., Bigham, A.W., Tabor, H.K., Emond, M.J., Nickerson, D.A., and Shendure, J. (2011). Exome sequencing as a tool for Mendelian disease gene discovery. Nat. Rev. Genet. *12*, 745–755.

2. Chong, J.X., Buckingham, K.J., Jhangiani, S.N., Boehm, C., Sobreira, N., Smith, J.D., Harrell, T.M., McMillin, M.J., Wiszniewski, W., Gambin, T., et al.; Centers for Mendelian Genomics (2015). The genetic basis of Mendelian phenotypes: discoveries, challenges, and opportunities. Am. J. Hum. Genet. *97*, 199–215.
3. Menke, L.A., van Belzen, M.J., Alders, M., Cristofoli, F., Ehmke, N., Fergelot, P., Foster, A., Gerkes, E.H., Hoffer, M.J., Horn, D., et al.; DDD Study (2016). CREBBP mutations in individuals without Rubinstein-Taybi syndrome phenotype. Am. J. Med. Genet. A. *170*, 2681–2693.
4. Lee, C.S., Fu, H., Baratang, N., Rousseau, J., Kumra, H., Sutton, V.R., Niceta, M., Ciolfi, A., Yamamoto, G., Bertola, D., et al.; Baylor-Hopkins Center for Mendelian Genomics (2017). Mutations in fibronectin cause a subtype of spondylometaphyseal dysplasia with "corner fractures". Am. J. Hum. Genet. *101*, 815–823.
5. Niceta, M., Stellacci, E., Gripp, K.W., Zampino, G., Kousi, M., Anselmi, M., Traversa, A., Ciolfi, A., Stabley, D., Bruselles, A., et al. (2015). Mutations impairing GSK3-mediated MAF phosphorylation cause cataract, deafness, intellectual disability, seizures, and a Down syndrome-like facies. Am. J. Hum. Genet. *96*, 816–825.
6. Reijnders, M.R.F., Ansor, N.M., Kousi, M., Yue, W.W., Tan, P.L., Clarkson, K., Clayton-Smith, J., Corning, K., Jones, J.R., Lam, W.W.K., et al.; Deciphering Developmental Disorders Study (2017). RAC1 missense mutations in developmental disorders with diverse phenotypes. Am. J. Hum. Genet. *101*, 466–477.
7. Martinelli, S., Torreri, P., Tinti, M., Stella, L., Bocchinfuso, G., Flex, E., Grottesi, A., Ceccarini, M., Palleschi, A., Cesareni, G., et al. (2008). Diverse driving forces underlie the invariant occurrence of the T42A, E139D, I282V and T468M SHP2 amino acid substitutions causing Noonan and LEOPARD syndromes. Hum. Mol. Genet. *17*, 2018–2029.
8. Philippakis, A.A., Azzariti, D.R., Beltran, S., Brookes, A.J., Brownstein, C.A., Brudno, M., Brunner, H.G., Buske, O.J., Carey, K., Doll, C., et al. (2015). The Matchmaker Exchange: a platform for rare disease gene discovery. Hum. Mutat. *36*, 915–921.
9. Sobreira, N., Schiettecatte, F., Valle, D., and Hamosh, A. (2015). GeneMatcher: a matching tool for connecting investigators with an interest in the same gene. Hum. Mutat. *36*, 928–930.
10. Chong, J.X., Yu, J.H., Lorentzen, P., Park, K.M., Jamal, S.M., Tabor, H.K., Rauch, A., Saenz, M.S., Boltshauser, E., Patterson, K.E., et al. (2016). Gene discovery for Mendelian conditions via social networking: de novo variants in KDM1A cause developmental delay and distinctive facial features. Genet. Med. *18*, 788–795.
11. Homsy, J., Zaidi, S., Shen, Y., Ware, J.S., Samocha, K.E., Karczewski, K.J., DePalma, S.R., McKean, D., Wakimoto, H., Gorham, J., et al. (2015). De novo mutations in congenital heart disease with neurodevelopmental and other congenital anomalies. Science *350*, 1262–1266.
12. Tanaka, A.J., Cho, M.T., Millan, F., Juusola, J., Retterer, K., Joshi, C., Niyazov, D., Garnica, A., Gratz, E., Deardorff, M., et al. (2015). Mutations in SPATA5 are associated with microcephaly, intellectual disability, seizures, and hearing loss. Am. J. Hum. Genet. *97*, 457–464.
13. Farwell Hagman, K.D., Shinde, D.N., Mroske, C., Smith, E., Radtke, K., Shahmirzadi, L., El-Khechen, D., Powis, Z., Chao, E.C., Alcaraz, W.A., et al. (2017). Candidate-gene criteria for clinical reporting: diagnostic exome sequencing identifies altered candidate genes among 8% of patients with undiagnosed diseases. Genet. Med. *19*, 224–235.
14. Roberts, A.E., Allanson, J.E., Tartaglia, M., and Gelb, B.D. (2013). Noonan syndrome. Lancet *381*, 333–342.
15. Tartaglia, M., and Gelb, B.D. (2010). Disorders of dysregulated signal traffic through the RAS-MAPK pathway: phenotypic spectrum and molecular mechanisms. Ann. N Y Acad. Sci. *1214*, 99–121.
16. Kircher, M., Witten, D.M., Jain, P., O'Roak, B.J., Cooper, G.M., and Shendure, J. (2014). A general framework for estimating the relative pathogenicity of human genetic variants. Nat. Genet. *46*, 310–315.
17. Dong, C., Wei, P., Jian, X., Gibbs, R., Boerwinkle, E., Wang, K., and Liu, X. (2015). Comparison and integration of deleteriousness prediction methods for nonsynonymous SNVs in whole exome sequencing studies. Hum. Mol. Genet. *24*, 2125–2137.
18. Ioannidis, N.M., Rothstein, J.H., Pejaver, V., Middha, S., McDonnell, S.K., Baheti, S., Musolf, A., Li, Q., Holzinger, E., Karyadi, D., et al. (2016). REVEL: an ensemble method for predicting the pathogenicity of rare missense variants. Am. J. Hum. Genet. *99*, 877–885.
19. Richards, S., Aziz, N., Bale, S., Bick, D., Das, S., Gastier-Foster, J., Grody, W.W., Hegde, M., Lyon, E., Spector, E., et al.; ACMG Laboratory Quality Assurance Committee (2015). Standards and guidelines for the interpretation of sequence variants: a joint consensus recommendation of the American College of Medical Genetics and Genomics and the Association for Molecular Pathology. Genet. Med. *17*, 405–424.
20. Takenouchi, T., Kosaki, R., Niizuma, T., Hata, K., and Kosaki, K. (2015). Macrothrombocytopenia and developmental delay with a de novo CDC42 mutation: Yet another locus for thrombocytopenia and developmental delay. Am. J. Med. Genet. A. *167A*, 2822–2825.
21. Takenouchi, T., Okamoto, N., Ida, S., Uehara, T., and Kosaki, K. (2016). Further evidence of a mutation in CDC42 as a cause of a recognizable syndromic form of thrombocytopenia. Am. J. Med. Genet. A. *170A*, 852–855.
22. Etienne-Manneville, S. (2004). Cdc42–the centre of polarity. J. Cell Sci. *117*, 1291–1300.
23. Heasman, S.J., and Ridley, A.J. (2008). Mammalian Rho GTPases: new insights into their functions from in vivo studies. Nat. Rev. Mol. Cell Biol. *9*, 690–701.
24. Colicelli, J. (2004). Human RAS superfamily proteins and related GTPases. Sci. STKE *2004*, RE13.
25. Dvorsky, R., and Ahmadian, M.R. (2004). Always look on the bright site of Rho: structural implications for a conserved intermolecular interface. EMBO Rep. *5*, 1130–1136.
26. Janakiraman, M., Vakiani, E., Zeng, Z., Pratilas, C.A., Taylor, B.S., Chitale, D., Halilovic, E., Wilson, M., Huberman, K., Ricarte Filho, J.C., et al. (2010). Genomic and biological characterization of exon 4 KRAS mutations in human cancer. Cancer Res. *70*, 5901–5911.
27. Gremer, L., Merbitz-Zahradnik, T., Dvorsky, R., Cirstea, I.C., Kratz, C.P., Zenker, M., Wittinghofer, A., and Ahmadian, M.R. (2011). Germline KRAS mutations cause aberrant biochemical and physical properties leading to developmental disorders. Hum. Mutat. *32*, 33–43.
28. Chang, M.T., Asthana, S., Gao, S.P., Lee, B.H., Chapman, J.S., Kandoth, C., Gao, J., Socci, N.D., Solit, D.B., Olshen, A.B.,

et al. (2016). Identifying recurrent mutations in cancer reveals widespread lineage diversity and mutational specificity. Nat. Biotechnol. *34*, 155–163.

29. Pirone, D.M., Carter, D.E., and Burbelo, P.D. (2001). Evolutionary expansion of CRIB-containing Cdc42 effector proteins. Trends Genet. *17*, 370–373.
30. Abdul-Manan, N., Aghazadeh, B., Liu, G.A., Majumdar, A., Ouerfelli, O., Siminovitch, K.A., and Rosen, M.K. (1999). Structure of Cdc42 in complex with the GTPase-binding domain of the 'Wiskott-Aldrich syndrome' protein. Nature *399*, 379–383.
31. Hemsath, L., Dvorsky, R., Fiegen, D., Carlier, M.F., and Ahmadian, M.R. (2005). An electrostatic steering mechanism of Cdc42 recognition by Wiskott-Aldrich syndrome proteins. Mol. Cell *20*, 313–324.
32. Morreale, A., Venkatesan, M., Mott, H.R., Owen, D., Nietlispach, D., Lowe, P.N., and Laue, E.D. (2000). Structure of Cdc42 bound to the GTPase binding domain of PAK. Nat. Struct. Biol. *7*, 384–388.
33. Gizachew, D., Guo, W., Chohan, K.K., Sutcliffe, M.J., and Oswald, R.E. (2000). Structure of the complex of Cdc42Hs with a peptide derived from P-21 activated kinase. Biochemistry *39*, 3963–3971.
34. Hemsath, L., and Ahmadian, M.R. (2005). Fluorescence approaches for monitoring interactions of Rho GTPases with nucleotides, regulators, and effectors. Methods *37*, 173–182.
35. Kühn, S., Erdmann, C., Kage, F., Block, J., Schwenkmezger, L., Steffen, A., Rottner, K., and Geyer, M. (2015). The structure of FMNL2-Cdc42 yields insights into the mechanism of lamellipodia and filopodia formation. Nat. Commun. *6*, 7088.
36. Melendez, J., Liu, M., Sampson, L., Akunuru, S., Han, X., Vallance, J., Witte, D., Shroyer, N., and Zheng, Y. (2013). Cdc42 coordinates proliferation, polarity, migration, and differentiation of small intestinal epithelial cells in mice. Gastroenterology *145*, 808–819.
37. Zegers, M.M., and Friedl, P. (2014). Rho GTPases in collective cell migration. Small GTPases *5*, e28997.
38. Beaty, B.T., and Condeelis, J. (2014). Digging a little deeper: the stages of invadopodium formation and maturation. Eur. J. Cell Biol. *93*, 438–444.
39. Welchman, D.P., Mathies, L.D., and Ahringer, J. (2007). Similar requirements for CDC-42 and the PAR-3/PAR-6/PKC-3 complex in diverse cell types. Dev. Biol. *305*, 347–357.
40. Lohmer, L.L., Clay, M.R., Naegeli, K.M., Chi, Q., Ziel, J.W., Hagedorn, E.J., Park, J.E., Jayadev, R., and Sherwood, D.R. (2016). A sensitized screen for genes promoting invadopodia function in vivo: CDC-42 and Rab GDI-1 direct distinct aspects of invadopodia formation. PLoS Genet. *12*, e1005786.
41. Choi, M.S., Yoo, A.S., and Greenwald, I. (2010). sel-11 and cdc-42, two negative modulators of LIN-12/Notch activity in *C. elegans*. PLoS ONE *5*, e11885.
42. Schmid, T., and Hajnal, A. (2015). Signal transduction during *C. elegans* vulval development: a NeverEnding story. Curr. Opin. Genet. Dev. *32*, 1–9.
43. Mello, C.C., Kramer, J.M., Stinchcomb, D., and Ambros, V. (1991). Efficient gene transfer in *C.elegans*: extrachromosomal maintenance and integration of transforming sequences. EMBO J. *10*, 3959–3970.
44. Cordeddu, V., Di Schiavi, E., Pennacchio, L.A., Ma'ayan, A., Sarkozy, A., Fodale, V., Cecchetti, S., Cardinale, A., Martin, J., Schackwitz, W., et al. (2009). Mutation of SHOC2 promotes aberrant protein N-myristoylation and causes Noonan-like syndrome with loose anagen hair. Nat. Genet. *41*, 1022–1026.
45. Flex, E., Jaiswal, M., Pantaleoni, F., Martinelli, S., Strullu, M., Fansa, E.K., Caye, A., De Luca, A., Lepri, F., Dvorsky, R., et al. (2014). Activating mutations in RRAS underlie a phenotype within the RASopathy spectrum and contribute to leukaemogenesis. Hum. Mol. Genet. *23*, 4315–4327.
46. Gripp, K.W., Hopkins, E., Doyle, D., and Dobyns, W.B. (2010). High incidence of progressive postnatal cerebellar enlargement in Costello syndrome: brain overgrowth associated with HRAS mutations as the likely cause of structural brain and spinal cord abnormalities. Am. J. Med. Genet. A. *152A*, 1161–1168.
47. Nobes, C.D., and Hall, A. (1995). Rho, rac and cdc42 GTPases: regulators of actin structures, cell adhesion and motility. Biochem. Soc. Trans. *23*, 456–459.
48. Arias-Romero, L.E., and Chernoff, J. (2013). Targeting Cdc42 in cancer. Expert Opin. Ther. Targets *17*, 1263–1273.
49. Pedersen, E., and Brakebusch, C. (2012). Rho GTPase function in development: how in vivo models change our view. Exp. Cell Res. *318*, 1779–1787.
50. Aoki, Y., Niihori, T., Banjo, T., Okamoto, N., Mizuno, S., Kurosawa, K., Ogata, T., Takada, F., Yano, M., Ando, T., et al. (2013). Gain-of-function mutations in RIT1 cause Noonan syndrome, a RAS/MAPK pathway syndrome. Am. J. Hum. Genet. *93*, 173–180.
51. Yamamoto, G.L., Aguena, M., Gos, M., Hung, C., Pilch, J., Fahiminiya, S., Abramowicz, A., Cristian, I., Buscarilli, M., Naslavsky, M.S., et al. (2015). Rare variants in SOS2 and LZTR1 are associated with Noonan syndrome. J. Med. Genet. *52*, 413–421.
52. Sini, P., Cannas, A., Koleske, A.J., Di Fiore, P.P., and Scita, G. (2004). Abl-dependent tyrosine phosphorylation of Sos-1 mediates growth-factor-induced Rac activation. Nat. Cell Biol. *6*, 268–274.
53. Holly, S.P., Larson, M.K., and Parise, L.V. (2005). The unique N-terminus of R-ras is required for Rac activation and precise regulation of cell migration. Mol. Biol. Cell *16*, 2458–2469.
54. Kaduwal, S., Jeong, W.J., Park, J.C., Lee, K.H., Lee, Y.M., Jeon, S.H., Lim, Y.B., Min, S., and Choi, K.Y. (2015). Sur8/Shoc2 promotes cell motility and metastasis through activation of Ras-PI3K signaling. Oncotarget *6*, 33091–33105.

Chapter III

A novel disorder involving dyshematopoiesis, inflammation, and HLH due to aberrant CDC42 function

Graphical abstract

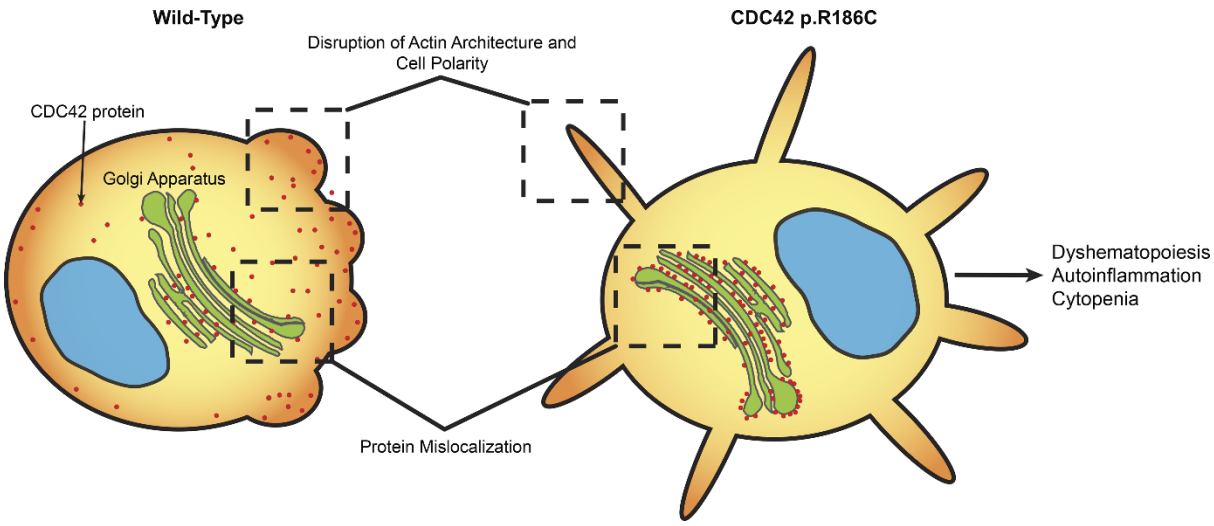

Status: Published in Journal of Experimental Medicine, October 10th 2019

Impact factor: 10.892

Own proportion: 25 %

Expression and purification of CDC42 variants, effectors and regulators, structural modeling, interaction studies, GTP hydrolysis assay, nucleotide exchange assay, pull down assay, figure preparation, writing the manuscript, discussion.

Published Online: 10 October, 2019 | Supp Info: http://doi.org/10.1084/jem.20190147

JEM Journal of Experimental Medicine

ARTICLE

A novel disorder involving dyshematopoiesis, inflammation, and HLH due to aberrant CDC42 function

Michael T. Lam[1,2,32*], Simona Coppola[3*], Oliver H.F. Krumbach[4*], Giusi Prencipe[5*], Antonella Insalaco[5*], Cristina Cifaldi[6,7], Immacolata Brigida[8], Erika Zara[3], Serena Scala[8], Silvia Di Cesare[6,7], Simone Martinelli[9], Martina Di Rocco[9,10], Antonia Pascarella[5], Marcello Niceta[11], Francesca Pantaleoni[11], Andrea Ciolfi[11], Petra Netter[1], Alexandre F. Carisey[1,2], Michael Diehl[12], Mohammad Akbarzadeh[4], Francesca Conti[6], Pietro Merli[13], Anna Pastore[11], Stefano Levi Mortera[11], Serena Camerini[14], Luciapia Farina[3,5], Marcel Buchholzer[4], Luca Pannone[9,11], Tram N. Cao[1], Zeynep H. Coban-Akdemir[15,16], Shalini N. Jhangiani[16,17], Donna M. Muzny[16,17], Richard A. Gibbs[15,16,17], Luca Basso-Ricci[8], Maria Chiriaco[6], Radovan Dvorsky[4], Lorenza Putignani[11], Rita Carsetti[5], Petra Janning[18], Asbjorg Stray-Pedersen[15,19,20], Hans Christian Erichsen[21], AnnaCarin Horne[22,23], Yenan T. Bryceson[24,25], Lamberto Torralba-Raga[24], Kim Ramme[26], Vittorio Rosti[27], Claudia Bracaglia[5], Virginia Messia[5], Paolo Palma[6], Andrea Finocchi[6,7], Franco Locatelli[13,28], Ivan K. Chinn[1,29], James R. Lupski[1,15,16,17], Emily M. Mace[2], Caterina Cancrini[6,7], Alessandro Aiuti[8,30,31], Mohammad R. Ahmadian[4**], Jordan S. Orange[2,32**], Fabrizio De Benedetti[5**], and Marco Tartaglia[11**]

Hemophagocytic lymphohistiocytosis (HLH) is characterized by immune dysregulation due to inadequate restraint of overactivated immune cells and is associated with a variable clinical spectrum having overlap with more common pathophysiologies. HLH is difficult to diagnose and can be part of inflammatory syndromes. Here, we identify a novel hematological/autoinflammatory condition (NOCARH syndrome) in four unrelated patients with superimposable features, including neonatal-onset cytopenia with dyshematopoiesis, autoinflammation, rash, and HLH. Patients shared the same de novo *CDC42* mutation (Chr1:22417990C>T, p.R186C) and altered hematopoietic compartment, immune dysregulation, and inflammation. *CDC42* mutations had been associated with syndromic neurodevelopmental disorders. In vitro and in vivo assays documented unique effects of p.R186C on CDC42 localization and function, correlating with the distinctiveness of the trait. Emapalumab was critical to the survival of one patient, who underwent successful bone marrow transplantation. Early recognition of the disorder and establishment of treatment followed by bone marrow transplant are important to survival.

[1]Department of Pediatrics, Baylor College of Medicine, Houston, TX; [2]Department of Pediatrics, Columbia University, Irving Medical Center, New York, NY; [3]National Center for Rare Diseases, Istituto Superiore di Sanità, Rome, Italy; [4]Institute of Biochemistry and Molecular Biology II, Medical Faculty of the Heinrich-Heine University, Düsseldorf, Germany; [5]Immunology Research Division, Ospedale Pediatrico Bambino Gesù, Istituto di Ricovero e Cura a Carattere Scientifico, Rome, Italy; [6]Academic Department of Pediatrics, Ospedale Pediatrico Bambino Gesù, Istituto di Ricovero e Cura a Carattere Scientifico, Rome, Italy; [7]Department of Systems Medicine, University of Rome Tor Vergata, Rome, Italy; [8]San Raffaele Telethon Institute for Gene Therapy, Istituto di Ricovero e Cura a Carattere Scientifico San Raffaele Scientific Institute, Milan, Italy; [9]Department of Oncology and Molecular Medicine, Istituto Superiore di Sanità, Rome, Italy; [10]Department of Cellular Biotechnology and Haematology, Sapienza University of Rome, Rome, Italy; [11]Genetics and Rare Diseases Research Division, Ospedale Pediatrico Bambino Gesù, Istituto di Ricovero e Cura a Carattere Scientifico, Rome, Italy; [12]Department of Bioengineering, Rice University, Houston, TX; [13]Department of Pediatric Hematology and Oncology, Ospedale Pediatrico Bambino Gesù, Istituto di Ricovero e Cura a Carattere Scientifico, Rome, Italy; [14]Core Facilities, Italian National Institute of Health, Rome, Italy; [15]Baylor-Hopkins Center for Mendelian Genomics, Houston, TX; [16]Department of Molecular and Human Genetics, Baylor College of Medicine, Houston, TX; [17]Human Genome Sequencing Center of Baylor College of Medicine, Houston, TX; [18]Department of Chemical Biology, Max-Planck Institute of Molecular Physiology, Dortmund, Germany; [19]Norwegian National Unit for Newborn Screening, Department of Pediatric and Adolescent Medicine, Oslo University Hospital, Oslo, Norway; [20]Institute of Clinical Medicine, University of Oslo, Oslo, Norway; [21]Department of Pediatric and Adolescent Medicine, Oslo University Hospital, Oslo, Norway; [22]Pediatric Rheumatology, Astrid Lindgren Children's Hospital, Karolinska University Hospital, Stockholm, Sweden; [23]Department of Women's and Children's Health, Karolinska Institutet, Karolinska University Hospital Solna, Stockholm, Sweden; [24]Department of Medicine, Karolinska Institutet, Karolinska University Hospital Huddinge, Stockholm, Sweden; [25]Broegelmann Research Laboratory, Institute of Clinical Sciences, University of Bergen, Bergen, Norway.; [26]Pediatric Hematology, Immunology and HCT Section, Astrid Lindgren Children's Hospital, Karolinska University Hospital, Stockholm, Sweden; [27]Center for Myelofibrosis, Fondazione Istituto di Ricovero e Cura a Carattere Scientifico Policlinico San Matteo, Pavia, Italy; [28]Department of Pediatrics, Sapienza University of Rome, Italy; [29]Division of Pediatric Immunology, Allergy, Rheumatology, Department of Pediatrics, Baylor College of Medicine, Houston, TX; [30]Pediatric Immunohematology, San Raffaele Scientific Institute, Milan, Italy; [31]Vita Salute San Raffaele University, Milan, Italy; [32]Medical Scientist Training Program and Translational Biology and Molecular Medicine Graduate Program, Baylor College of Medicine, Houston, TX.

*M.T. Lam, S. Coppola, O.H.F. Krumbach, G. Prencipe, and A. Insalaco contributed equally to this paper; **M.R. Ahmadian, J.S. Orange, F. De Benedetti, and M. Tartaglia contributed equally to this paper; Correspondence to Marco Tartaglia: marco.tartaglia@opbg.net; Mohammad R. Ahmadian: reza.ahmadian@hhu.de; Jordan S. Orange: jso2121@cumc.columbia.edu; Fabrizio De Benedetti: fabrizio.debenedetti@opbg.net.

JEM

Introduction

The diagnosis and delineation of novel genetic syndromes is often difficult given the limited availability of patients, genetic heterogeneity, and clinical variability. Hemophagocytic lymphohistiocytosis (HLH) has recently been characterized as a clinical syndrome with hyperinflammation driven by excessive activation and expansion of macrophages and $CD8^+$ T lymphocytes (Jordan et al., 2011; Rosado and Kim, 2013). Typical features include persistent high fever, liver involvement, splenomegaly, intravascular activation of coagulation associated with pancytopenia, and usually an increase in ferritin. Although this syndrome is clinically unique, the mechanisms underlying this disorder are diverse (Sepulveda and de Saint Basile, 2017; Chinn et al., 2018). Mutations leading to defective cytotoxicity by natural killer (NK) and $CD8^+$ T lymphocytes are the typical cause of monogenic HLH, typically termed primary HLH. However, a markedly higher number of patients present with HLH in the absence of genetically defective cytotoxicity in the context of infections, rheumatic inflammatory diseases and malignancy. HLH in its various forms, both in children and adults, is invariably fatal if untreated.

Cell division cycle 42 (CDC42) is a member of the Ras-homologous (Rho) GTPase family functioning as a signaling node controlling a number of cellular processes, including adhesion, migration, polarity, cell cycle, and proliferation (Zhou et al., 2013; Baschieri et al., 2014). CDC42 functions as a molecular switch by cycling between a guanosine 5′-triphosphate (GTP)–bound (active) and a guanosine diphosphate (GDP)–bound (inactive) state. Two CDC42 isoforms have been characterized. While isoform 1 is ubiquitously expressed, isoform 2 is primarily found in the brain. CDC42 function is controlled by three different classes of regulators: guanine nucleotide exchange factors (GEFs), GTPase-activating proteins (GAPs), and guanine nucleotide dissociation inhibitors (Dvorsky and Ahmadian, 2004). The GTPase primarily acts through its spatial and temporal localized interaction with multiple downstream effectors, such as IQGAP1, p21-activated kinase (PAK), and Wiskott–Aldrich syndrome protein (WASP). Reversible localization of CDC42 at the cytoplasmic leaflet of the plasma membrane and other intracellular membranes is regulated by Rho GDP-dissociation inhibitor (RhoGDI) and IQGAP1. The former controls the dynamic membrane–cytoplasm shuttling of the GTPase (Gibson and Wilson-Delfosse, 2001; Gibson et al., 2004), while the latter promotes CDC42 translocation from the Golgi apparatus to the plasma membrane (Swart-Mataraza et al., 2002). These regulatory events play a crucial role in controlling CDC42 function, cytoskeletal rearrangement, cell polarity, and migration. Notably, altered binding of CDC42 to IQGAP1 induces multiple leading edge formation and aberrant multipolarized morphology (Fukata et al., 2002). Actin rearrangements and cell migration are also promoted by CDC42 interaction with its effector, WASP, a critical actin regulator and mediator of NK cell cytotoxicity (Orange et al., 2002; Ridley et al., 2003). Finally, CDC42 function requires posttranslational processing at the C-terminus, including prenylation at Cys^{188} (geranylgeranylation, most commonly) followed by proteolytic cleavage of the last three residues and carboxyl-methylation (Aicart-Ramos et al., 2011).

We and others recently identified germline heterozygous mutations in *CDC42* as the event underlying a remarkably heterogeneous collection of neurodevelopmental phenotypes (Takenouchi et al., 2015; Martinelli et al., 2018). Core clinical features of these traits include variable growth dysregulation; facial dysmorphism; intellectual disability; cardiac defects; immunological, hematological, and lymphatic abnormalities; and brain malformations. Mutations were found to variably disrupt CDC42 function by altering the switch between the active and inactive states of the GTPase and/or affecting its interaction with effectors (Martinelli et al., 2018). As a result, multiple cellular and developmental processes were differentially perturbed. Remarkably, the biochemical and functional characterization of mutations allowed the identification of genotype–phenotype relationships, suggesting a link between the specific impact of individual mutation class and its phenotypic expression (Martinelli et al., 2018). Mutations were documented to behave either as activating or inactivating, with the latter specifically associated with thrombocytopenia. Multisystem/organ involvement occurred in all groups.

Using whole-exome sequencing/whole-genome sequencing (WES/WGS) coupled to biochemical and functional validation, we describe a novel hematological and autoinflammatory phenotype in four unrelated patients caused by the same de novo missense mutation of *CDC42* (NM_001791, c.556C>T, p.R186C). The disease differs considerably from those previously associated with *CDC42* mutations and is characterized by neonatal onset of pancytopenia, autoinflammation, rash, and episodes of HLH (NOCARH). Through in silico, in vitro, and in vivo analyses, we describe the mechanism by which this specific amino acid change affects CDC42 function, intracellular signaling, and cellular and developmental processes. Finally, we provide a clinical delineation of this disorder and document the clinical response to IFN-γ and IL-1β neutralization and hematopoietic stem cell transplantation (HSCT).

Results

Clinical features of patients

The four unrelated patients included in the study showed a superimposable previously unrecognized multisystem disease characterized by neonatal onset of pancytopenia, persistent fever, skin rash, hepatosplenomegaly, and persistently elevated inflammatory markers in the absence of any evidence of neurodevelopmental involvement (Tables 1, S1, and S2; and Fig. 1 A). A suspicion of neonatal-onset multisystem inflammatory disease in three of the four patients led to treatment with IL-1 inhibitors with incomplete improvement of fever and rash, but not cytopenia. In all cases, high chronic doses of glucocorticoids were required to treat inflammation. All patients developed HLH, which was fatal in three subjects. Based on the shared features, we propose the term of NOCARH syndrome for this trait. A detailed description of the patients' clinical history is provided in the Materials and methods.

JEM

Table 1. **Features of patients sharing the de novo missense *CDC42* c.556C>T (p.R186C) mutation**

	Pt 1	Pt 2	Pt 3	Pt 4
Outcome and status	Alive, 6 yr	Dead, 6 mo	Dead, 1.5 yr	Dead, 4.5 mo
Fever	+	+	+	+
Skin rash	+	+	+	+
Facial dysmorphism	–	–	–	–
Failure to thrive	+	+	+	+
Hepatomegaly	+	+	+	+
Splenomegaly	+	+	+	–
CNS inflammatory disease[a]	+	–	–	–
Gastrointestinal symptoms[b]	+	+	+	+
Cardiac abnormalities	–	–	–	–
HLH[c]	+	+	+	+
Anemia[d]	+	+	+	+
Thrombocytopenia[d]	+	+	+	+
Neutropenia[e]	+	+	+	+
Monocytopenia	+	+	N/A	N/A
Acute-phase response	+	+	+	+
BM dysplasia	+	+	+	+
Other notable features	+[f]	–	–	+[g]

CNS, central nervous system; N/A, not applicable.
[a]Pt 1, three episodes at age 2 yr with generalized seizures and white and gray matter lesions in MRI; Pt 3, increased CSF protein and MRI with leptomeningitis.
[b]Pt 1, diarrhea, intestinal bleeding at age 11 mo, and intestinal infarction at age 5 yr; Pt 2, chronic diarrhea; Pt 3, small intestine inflammation; Pt 4, severe, unremitting enterocolitis from birth and diarrhea with intestinal bleedings and infarctions.
[c]Pt 1, four episodes; Pt 2, a single episode leading to death; Pt 3, died of secondary HLH after transplant; Pt 4, four episodes.
[d]Pt 1, constant transfusion requirement until age 2 yr; Pt 2, intermittent transfusion requirement during flares; Pt 3, transfusion dependent; Pt 4, transfusion dependent.
[e]Pt 1, Pt 2, and Pt 3, profound neutropenia; Pt 4, mild neutropenia.
[f]Suspected trigonocephaly.
[g]Very small thymus; arthritis.

Genetic studies

Two patients (patient 1 [Pt 1] and Pt 3) were enrolled in the Undiagnosed Disease Programs at the Ospedale Pediatrico Bambino Gesù and Baylor-Hopkins Center for Mendelian Genomics (CMG) at Baylor College of Medicine and the NK cell Evaluation and Research Program at Baylor and Columbia University. Using a trio-based WES strategy, a de novo missense *CDC42* change (NM_001791, Chr1:22417990, c.556C>T, p.R186C) affecting an isoform 1–specific exon was identified as the only candidate variant underlying the disorder in both subjects (Table S3). Occurrence of mutations in genes known to be associated with HLH or other immunological and hematologic disorders was excluded. Similarly, there was no other rare substantively damaging variant shared by the two patients. The missense mutation had not previously been reported in the Exome Aggregation Consortium/Genome Aggregation Database (gnomAD) and was predicted to be damaging by in silico tools (Combined Annotation-Dependent Depletion [CADD] v1.3: 24.5, and Mendelian clinically applicable pathogenicity [M-CAP] v1.3: 0.0531). Based on this finding, a third patient (Pt 2) having clinical features resembling those of the two previously studied subjects underwent Sanger sequencing for the relevant *CDC42* coding portion, revealing heterozygosity for the same c.556C>T transition, which was validated to occur as a de novo event. Finally, through networking, a fourth patient (Pt 4) sharing a similar clinical phenotype, and the same de novo *CDC42* mutation was identified. In this case, the mutation was revealed by WGS using a trio-based strategy (Table S3), which excluded the occurrence of functionally and clinically relevant variants in HLH- and autoinflammation-related genes.

Biochemical and functional studies

To explore the functional consequence of the identified missense change, we initially assessed CDC42 levels in primary fibroblasts (Pt 1 and Pt 2) and HEK-293T cells transiently expressing the FLAG-tagged CDC42 mutant. In primary fibroblasts, the protein was expressed to similar levels without any apparent accelerated degradation (Fig. 1 B). Similarly, no reduction in the level of the mutant was observed in transfected cells. These data suggested that the disease-associated missense change does not significantly decrease CDC42 synthesis/stability, pointing to a specific perturbing effect on protein function.

Compared with the previously identified variants of CDC42 underlying neurodevelopmental disorders (Takenouchi et al., 2015; Martinelli et al., 2018), the p.R186C amino acid substitution occurs in a unique region at the C-terminus, within the hypervariable region (Fig. 1 C). Specifically, Arg^{186} lies in proximity of Cys^{188}, which serves as substrate site for CDC42 prenylation. This irreversible posttranslational modification is required for proper CDC42 subcellular localization and function. To assess a possible effect of the p.R186C substitution on CDC42 prenylation, mass spectrometry (MS) analysis of the purified CDC42 mutant was performed, revealing proper C-terminal processing and lipid incorporation (Fig. 1 D), excluding the possibility of a defective or aberrant CDC42 posttranslational processing. Structural studies indicate that Arg^{186} is located far from the GDP/GTP-binding pocket and major regions controlling CDC42 interaction with positive and negative regulators (switch regions I and II; Phillips et al., 2008). Consistently, fluorescence-based cell-free assays showed that replacement of Arg^{186} by cysteine did not have a significant impact on either CDC42 basal and GEF-catalyzed GDP/GTP exchange activity or basal and GAP-stimulated GTPase activity of the protein (Fig. 1 E).

Arg^{186} is a solvent-exposed residue located at the surface of CDC42 in one of the two major sites of binding to RhoGDI (Hoffman et al., 2000; Fig. 2 A). The residue stabilizes the geranylgeranyl-mediated CDC42–RhoGDI interaction. This interaction has a key role in the control of CDC42 function, as it

JEM

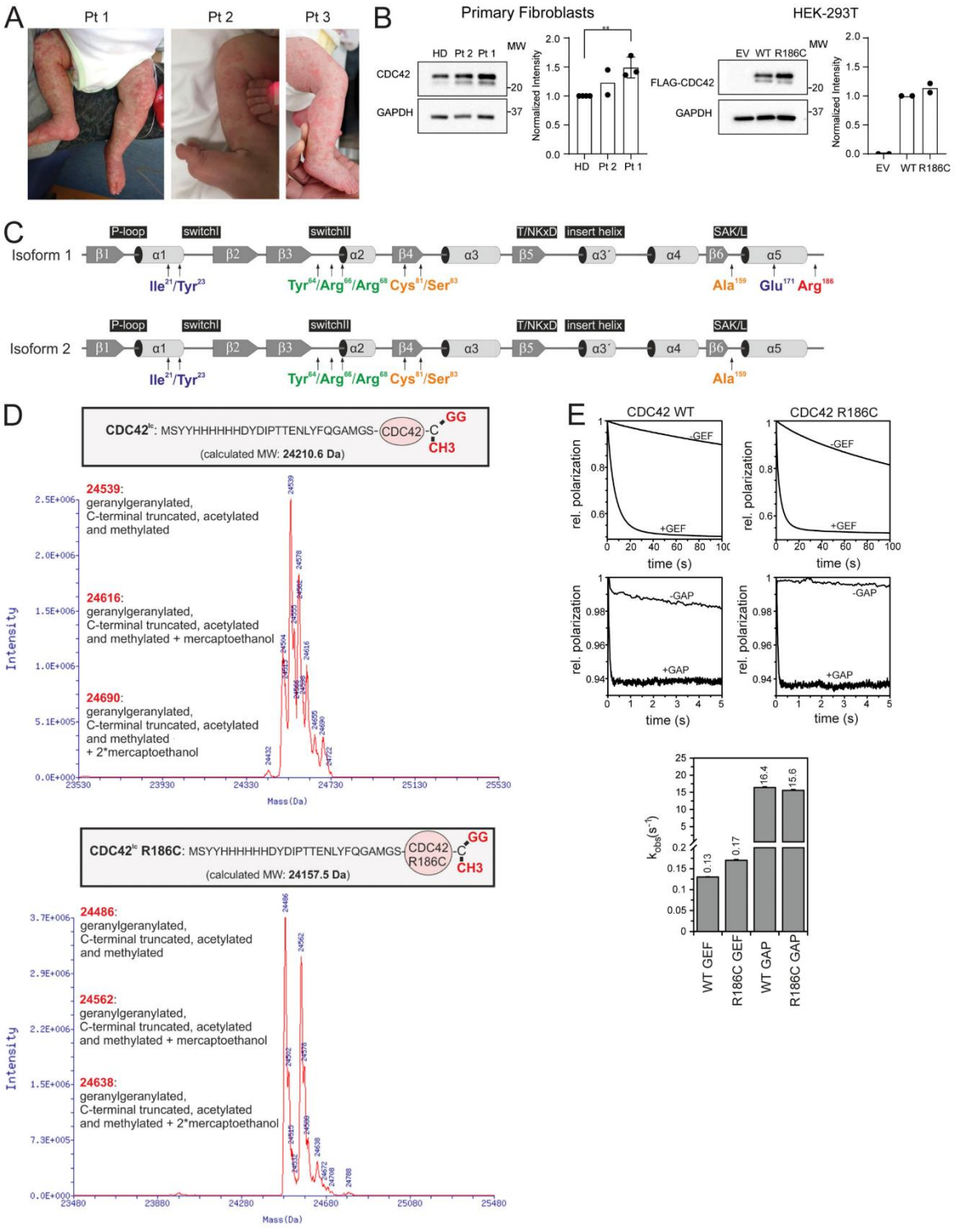
A
Pt 1
Pt 2
Pt 3
B
Primary Fibroblasts
HD Pt 2 Pt 1
MW
CDC42
GAPDH
20
37
Normalized Intensity
HD Pt 2 Pt 1
HEK-293T
EV WT R186C
FLAG-CDC42
EV WT R186C
C
Isoform 1
Isoform 2
P-loop
switchI
switchII
T/NKxD
insert helix
SAK/L
β1 α1 β2 β3 α2 β4 α3 β5 α3´ α4 β6 α5
Ile21/Tyr23
Tyr64/Arg66/Arg68 Cys81/Ser83
Ala159
Glu171 Arg186
D
CDC42lc: MSYYHHHHHHDYDIPTTENLYFQGAMGS-(CDC42)-C-GG CH3
(calculated MW: 24210.6 Da)
24539:
geranylgeranylated,
C-terminal truncated, acetylated
and methylated
24616:
geranylgeranylated,
C-terminal truncated, acetylated
and methylated + mercaptoethanol
24690:
geranylgeranylated,
C-terminal truncated, acetylated
and methylated
+ 2*mercaptoethanol
Intensity
Mass (Da)
CDC42lc R186C: MSYYHHHHHHDYDIPTTENLYFQGAMGS-(CDC42 R186C)-C-GG CH3
(calculated MW: 24157.5 Da)
24486:
geranylgeranylated,
C-terminal truncated, acetylated
and methylated
24562:
geranylgeranylated,
C-terminal truncated, acetylated
and methylated + mercaptoethanol
24638:
geranylgeranylated,
C-terminal truncated, acetylated
and methylated + 2*mercaptoethanol
E
CDC42 WT
CDC42 R186C
rel. polarization
-GEF
+GEF
-GAP
+GAP
time (s)
kobs(s-1)
0.13
0.17
16.4
15.6
WT GEF
R186C GEF
WT GAP
R186C GAP

JEM

Figure 1. **Clinical features of patients carrying the c.556C>T change (p.R186C) in *CDC42*, and biochemical profiling of the disease-causing mutant. (A)** Skin findings of the affected subjects. **(B)** CDC42 levels in Pt 1 (n = 3, normalized intensity relative to HDs; **, P < 0.01, unpaired t test) and Pt 2 (n = 2) primary fibroblasts and HEK-293T cells (n = 2) expressing FLAG-tagged WT and mutant CDC42 or an empty vector (EV). **(C)** CDC42 domain organization indicating key functional regions and locations of residues affected by disease-causing variants. The two CDC42 isoforms are shown. Isoform 1 is ubiquitously expressed, while isoform 2 is brain restricted. The missense variants affecting E171 and R186 only affect isoform 1, while mutations affecting the other residues involve both isoforms. **(D)** p.R186C does not affect CDC42 posttranslational processing. MS analysis of WT and R186C CDC42 proteins shows a strong peak at 24,539 daltons and 24,486 daltons, respectively, indicating that $CDC42^{R186C}$ is properly processed at the C-terminus. Da, daltons. **(E)** p.R186C does not affect CDC42 GTPase activity and nucleotide exchange behavior. GTPase activity and nucleotide exchange reaction in $CDC42^{R186C}$ (right) are compared with WT CDC42 (left). k_{obs} values (observed dissociation constant) are reported (bottom). Representative polarization curves are shown (n = 4–6). MW, molecular weight; SAK/L, serine-alanine-lysine/leucine motif.

negatively regulates stable binding of the GTPase to the cytoplasmic leaflet of membranes and modulates CDC42 trafficking (Gibson and Wilson-Delfosse, 2001; Gibson et al., 2004). Based on the predicted disruptive effect of the Arg-to-Cys substitution on RhoGDI binding (Fig. 2 A), pull-down assays were performed to confirm defective interaction between the CDC42 mutant and RhoGDI (Fig. 2 B). The impaired binding of prenylated $CDC42^{R186C}$ protein to RhoGDI was also demonstrated by surface plasmon resonance (SPR) analysis (Fig. 2 C). These data strongly suggest a perturbation of proper subcellular localization and trafficking of CDC42 as a major event contributing to pathogenesis. Notably, since other residues previously reported to be mutated in CDC42-related neurodevelopmental disorders are located at the interacting surface of the second major site of the GTPase mediating binding to RhoGDI, with a subset of them directly involved in RhoGDI binding (Fig. 2 A), the defective binding of CDC42 to RhoGDI likely does not represent a distinctive impairment of the $CDC42^{R186C}$ mutant. This was confirmed by pull-down assays using a panel of bacterially expressed mutants to assess the impact of amino acid substitutions in regions far from the C-terminal tail on RhoGDI binding, which consistently with the structural data suggest that other missense changes variably impact CDC42 binding to RhoGDI (data not shown).

GTP-bound CDC42 activates multiple downstream signaling pathways by interacting with a variety of effectors (Dvorsky and Ahmadian, 2004; Nouri et al., 2017). We assessed the capability of the $CDC42^{R186C}$ mutant to transduce signals by measuring its direct binding to major effectors, including WASP, PAK1, and IQGAP1. Glutathione S-transferase (GST) pull-down assays coupled to immunoblotting demonstrated a decreased effector binding of the mutant protein compared with WT CDC42, with a significantly diminished binding to WASP and a dramatically reduced interaction with IQGAP1 (Fig. 2 D). Given the established role of RhoGDI and IQGAP1 in the control of the dynamic redistribution of CDC42 within cells, we analyzed the possible disruption of the subcellular localization of the $CDC42^{R186C}$ protein by using complementary cellular models. Depending on the cellular context and stimuli, CDC42 localizes to the cytoplasmic leaflet of multiple compartments, vesicles, and plasma membrane and partly the cytoplasm (Valdés-Mora and Lacal, 2011). Surprisingly, a constitutive cis/medial-Golgi–restricted localization of $CDC42^{R186C}$ was observed in the totality of COS-1 cells ectopically expressing the mutant protein (Fig. 3 A). On the other hand, a similar Golgi-specific targeting was not observed for a representative panel of previously identified disease-associated CDC42 mutants (e.g., p.Y23C, p.R68Q, p.S83P, p.A159V, and p.E171K; Martinelli et al., 2018), supporting the unique consequence of the p.R186C change on CDC42 subcellular distribution. This distinctive localization was observed in a disease-relevant cellular model, the YTS NK cell line, generated by CRISPR/Cas9 technology to express the mutant allele in the homozygous state (Fig. 3 B). Consistent with these findings, an enriched Golgi localization was also observed in the heterozygous primary fibroblasts obtained from Pt 1 (Fig. 3 C).

We investigated the consequences of altered CDC42 localization and function on major cellular processes controlled by CDC42, including proliferation, polarized migration, and cytoskeletal rearrangement. In vitro proliferation of $CD34^+$ cells from Pt 1 assessed in response to KIT ligand (KITLG) or a growth factor mixture (KITLG, FLT3L, thrombopoietin, and IL3) revealed a specific unresponsiveness to KITLG, suggesting a selective hematopoietic proliferation signaling defect (Fig. 4 A). Defective proliferation was also observed in fibroblasts derived from Pt 1 and Pt 2, and NIH-3T3 cells transiently transfected to overexpress the CDC42 mutant (Fig. 4 B). Notably, Pt 1 fibroblasts and NIH-3T3 cells overexpressing the mutant protein also showed reduced polarized migration (Fig. 4 C). Consistently, defective chemotaxis toward C-X-C motif chemokine 12 (CXCL12) was observed in Pt 1 purified bone marrow (BM) $CD34^+$ cells, peripheral blood mononuclear cells (PBMCs), as well as in the homozygous $CDC42^{R186C}$ YTS NK cell line (Fig. 4 C). CDC42 is critical for cytoskeletal rearrangement primarily through the formation of filopodia, an F-actin–based structure contributing to cell adhesion, polarization, and migration (Etienne-Manneville, 2004; Mattila and Lappalainen, 2008; Jacquemet et al., 2015). Thus, imaging of filopodial pattern and cell polarization was performed in serum-stimulated fibroblasts from Pt 1. A higher number of cells with filopodia and an aberrantly polarized morphology compared with control cells was observed. In particular, aberrant polarization consisted of multiple lateral F-actin flat protruding edges (multipolar cells), in contrast with the front-rear canonical polarization (Fig. 4 D). Interestingly, in a cytolytic immunological synapse model on glass surface utilizing higher resolution imaging, a lower number of filopodia was detected in the mutant YTS cells, with a higher proportion of these cells retracting when activated on a CD18/28 surface (Fig. 4 E). Together, these data documented a variable perturbation of diverse cell-specific processes mediated by remodeling of the actin architecture, including cell polarity and migration.

JEM

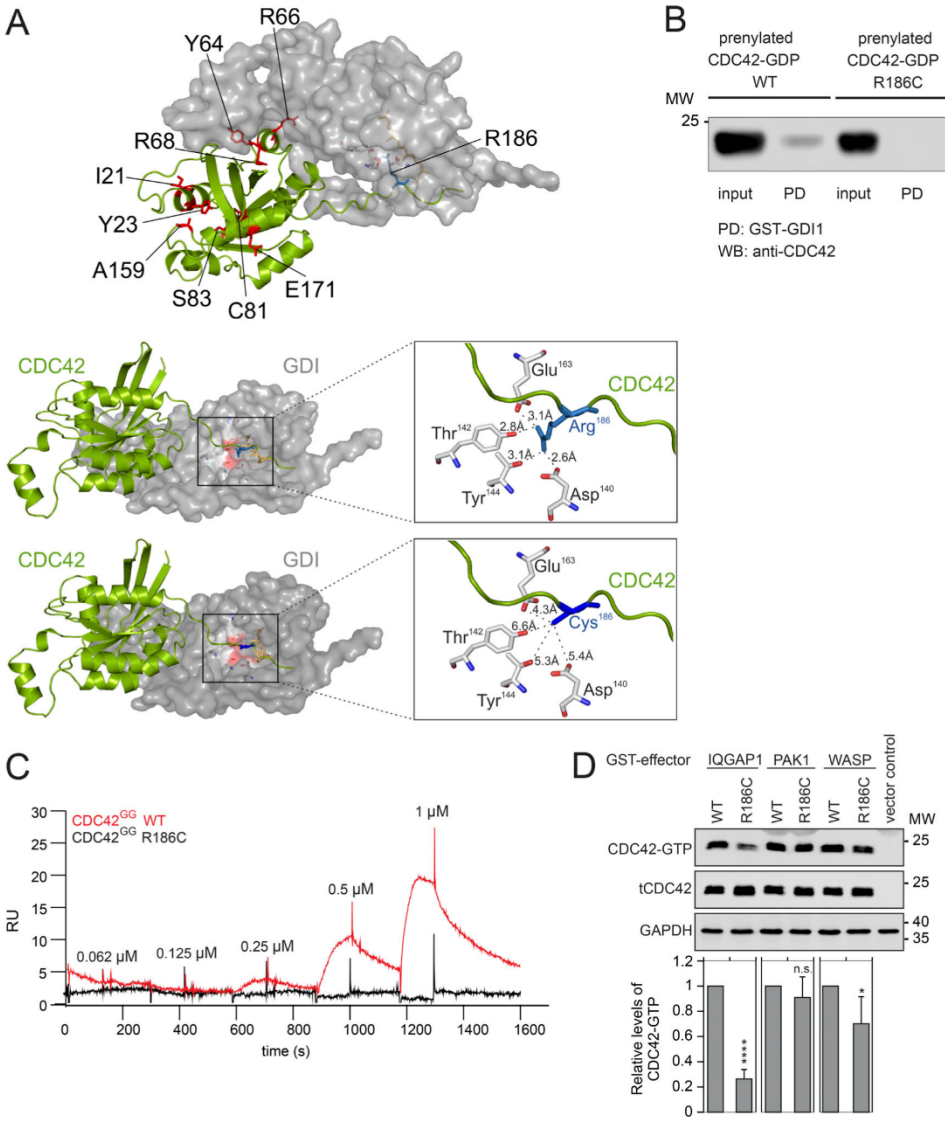

Figure 2. **p.R186C affects CDC42 binding to RhoGDI, IQGAP1, and WASP. (A)** Structure of CDC42 complexed with RhoGDI. Visualization of residues affected in human disease (left). Arg^{186} has a unique localization within the hypervariable region. Arg^{186} is surrounded by Asp^{140}, Thr^{142}, Tyr^{144}, and Glu^{163} of RhoGDI (within 4 Å; right middle panel). p.R186C is predicted to disrupt the interaction between the hypervariable region of CDC42 and RhoGDI (right lower panel). **(B)** Pull-down (PD) assays showing RhoGDI interaction of prenylated WT and mutant CDC42. Binding of GST-fused RhoGDI to CDC42 proteins was analyzed by WB documenting defective $CDC42^{R186C}$ binding. A representative image is shown (n = 2). **(C)** SPR analysis of the RhoGDI–CDC42 interaction. Immobilized GST-tagged RhoGDI was titrated with increasing concentrations of WT (red) and R186C (black) $CDC42^{GG}$ proteins. No binding for the mutant protein was observed. RU, response unit (n = 1). **(D)** Representative WB visualizing pull-down of overexpressed FLAG-tagged WT and R186C CDC42 from COS-7 cell lysates by GST-fused effector proteins IQGAP1, PAK1, and WASP. The same amount of cell lysate was used as a loading control (tCDC42). Bar charts indicate the relative levels of GTP-bound WT and R186C CDC42 normalized to the levels of total CDC42. A strongly reduced and decreased binding of $CDC42^{R186C}$ to IQGAP1 and WASP was documented, respectively (mean ± SD, n = 3 independent experiments; *, P < 0.05; ****, P < 0.0001, one-way ANOVA with Sidak's multiple comparison test). n.s., not significant; MW, molecular weight.

HLH occurring in infants and young children is generally associated with defects in immune regulation, including function of NK cells (Henter et al., 2007). We observed a slightly to markedly reduced NK cell activity in Pt 2 and Pt 3 through clinical assessments of immune cell function (Fig. 5 A). The homozygous $CDC42^{R186C}$ YTS cell line was used as an immune cell model to directly study the impact of the mutant on NK cytotoxicity. Chromium release assay against MHC class

JEM

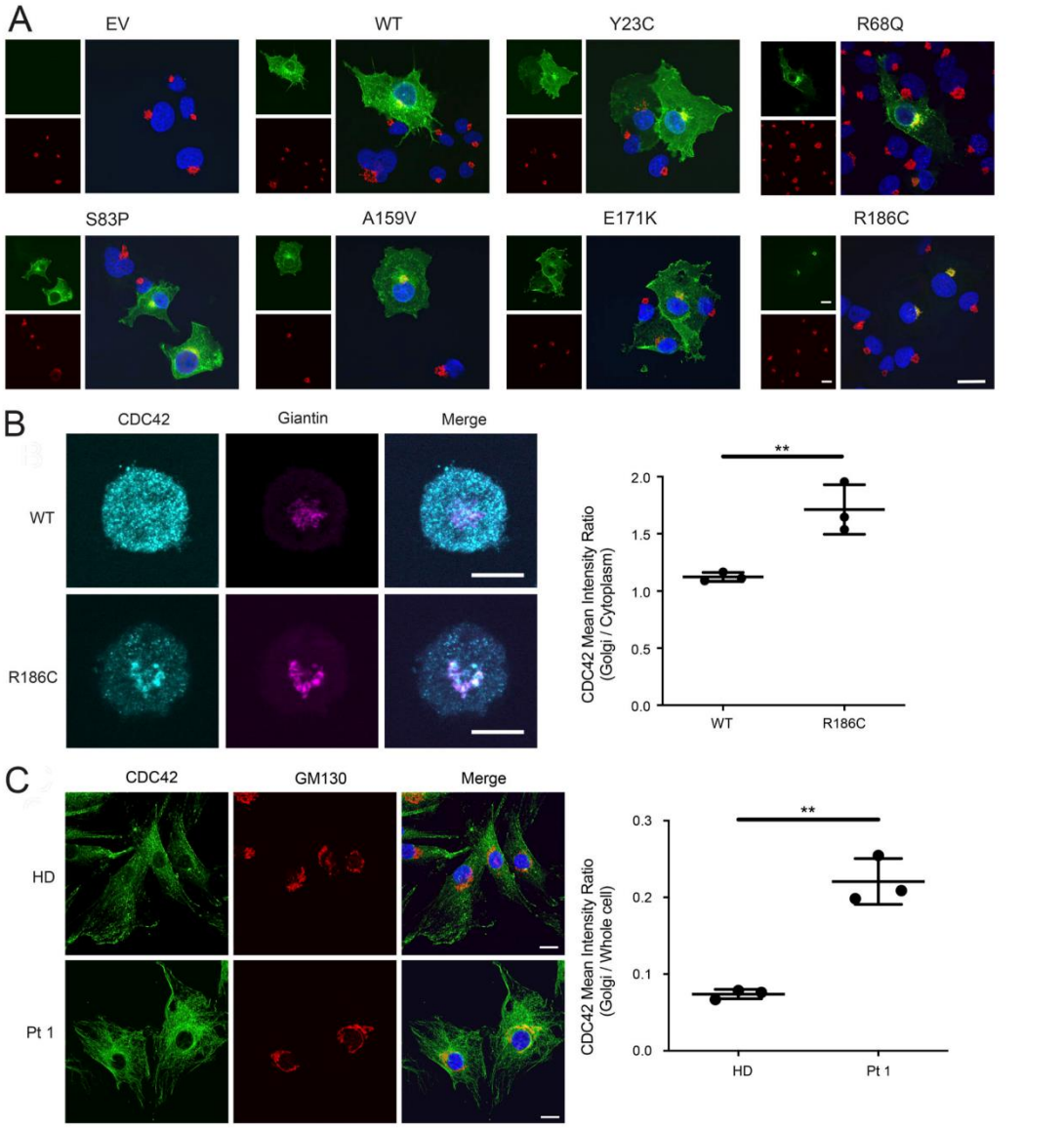

Figure 3. **p.R186C leads to aberrant subcellular localization of CDC42. (A)** $CDC42^{R186C}$ shows a Golgi apparatus–restricted localization. Immunofluorescence staining of FLAG-tagged CDC42 proteins (green) and GM130 (red), a marker of cis/medial-Golgi apparatus, in COS1 cells transiently transfected with mock DNA (empty vector [EV]), WT CDC42, or mutant alleles carrying different disease-causing mutations (Y23C, R68Q, S83P, A159V, E171K, and R186C). Composite colocalization images are shown in the right panels with nuclei in blue. At least 200 FLAG-tagged CDC42-expressing cells were analyzed for each sample. Representative image of three independent repeats. Scale bar, 20 µm (applicable to all other images shown). **(B)** Subcellular localization of CDC42 in YTS NK cell lines homozygous for the p.R186C mutation. $CDC42^{R186C}$ was found to be predominantly localized to the Golgi apparatus with reduced cytoplasmic signal. CDC42 signal intensity within the Golgi apparatus was quantified using giantin as a Golgi-specific marker relative to the cytoplasm and presented as a ratio. Representative images of three independent repeats are shown. The graph shows the mean + SD of three independent experiments with $n = 38$ cells for WT and $n = 35$ cells for R186C; **, $P \leq 0.01$, unpaired two-tailed t test. Scale bar, 10 µm (applicable to all images shown). **(C)** Immunofluorescence staining of CDC42 (green), GM130 (red), and nuclei (blue) in primary fibroblasts expressing WT CDC42 (HD) or heterozygous for p.R186C (Pt 1). Visual composite colocalization images are shown in the merge panels. Colocalization (orange/yellow overlay) of CDC42 and cis-Golgi is detected in mutant CDC42–expressing cells. Images refer to representative pictures of three independent experiments. Using GM130 as a mask for cis/medial-Golgi, CDC42 fluorescence intensity was quantified as the ratio of Golgi to whole-cell staining using ImageJ software (mean ± SD, $n = 3$; **, $P < 0.01$, unpaired two-tailed t test). Scale bar, 20 µm (applicable to all images shown).

JEM

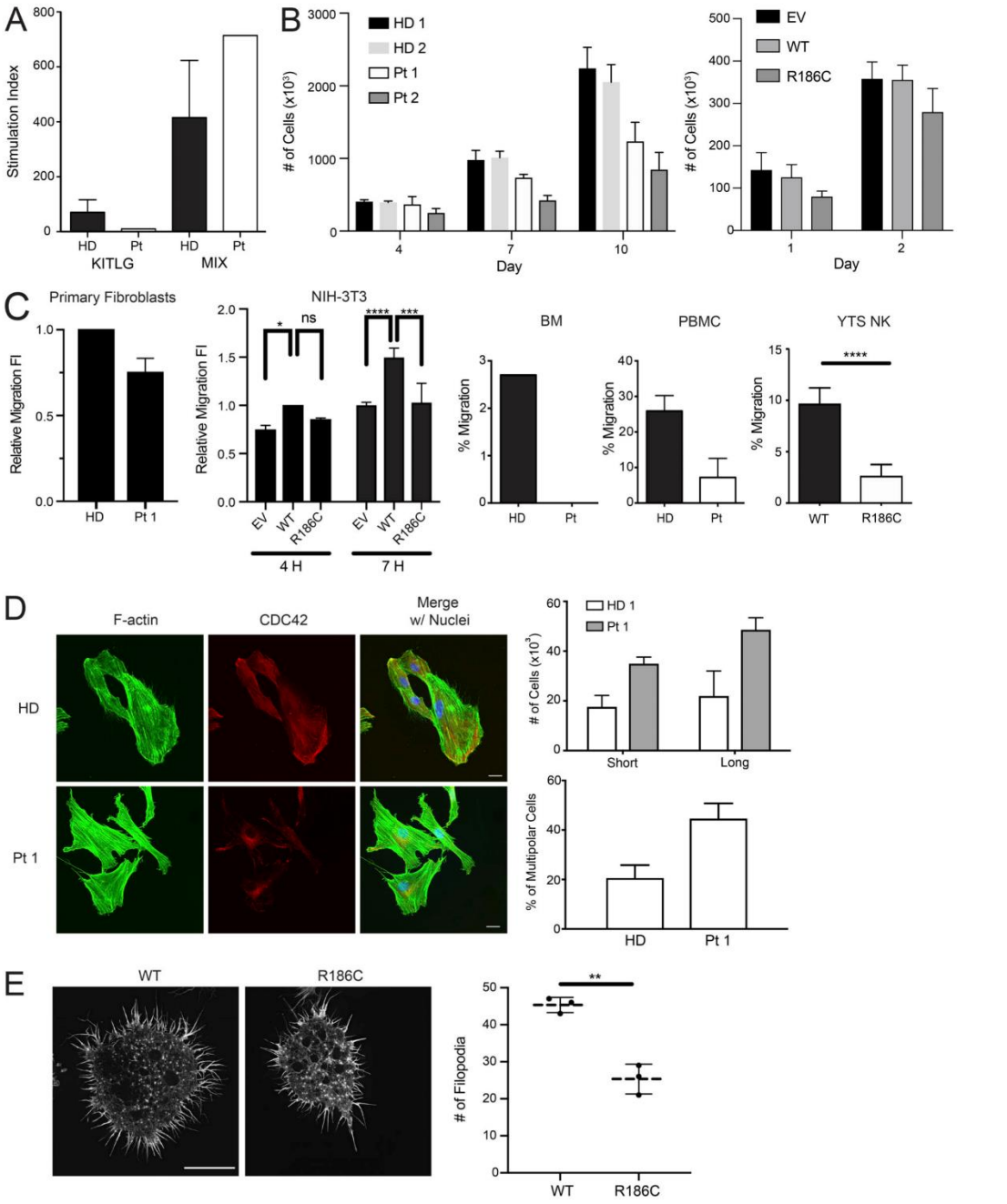

Figure 4. **p.R186C is associated with defects in proliferation, migration, and formation of actin-based structures. (A)** Proliferation of BM CD34⁺ cells from Pt 1 in response to stem cell factor (SCF/KITLG) or a cytokine mixture (MIX; $n = 1$). **(B)** Proliferation of primary fibroblasts from Pt 1 ($n = 3$) and Pt 2 ($n = 3$) at indicated time points of culture, and NIH-3T3 cells transiently expressing WT or mutant CDC42 or an empty vector (EV). **(C)** Migration assays of primary fibroblasts from Pt 1 ($n = 3$), transfected NIH-3T3 cells ($n = 3$; *, $P < 0.05$; **, $P < 0.01$; ****, $P < 0.0001$, two-way ANOVA with Sidak's multiple comparisons), purified BM CD34⁺ sorted cells ($n = 1$), PBMCs ($n = 2$), and a YTS CRISPR/Cas9-modified cell line ($n = 3$; ****, $P < 0.0001$, unpaired two-tailed t test; mean ± SEM for CD34⁺/PBMCs and mean ± SD for NK cells, NIH-3T3 cell line, and primary fibroblasts). Migration was assayed using a wound-healing assay on primary fibroblasts and transfected NIH-3T3 cells and directed migration toward chemoattractant CXCL12 in BM CD34⁺ cells, PBMCs, and YTS NK cells. Decreased directed migration of all tested cell types was observed. FI, fold increase of migratory cells. **(D)** Cytoskeletal rearrangements of cells expressing $CDC42^{R186C}$. Multipolarization and filopodia in primary fibroblasts from Pt 1 ($n = 3$) compared with fibroblasts from an HD. Immunofluorescence staining of CDC42 (red),

JEM

F-actin (green), and nuclei (blue) in cells stimulated 3 h with 20% serum. In HD fibroblasts, CDC42 localizes to the front leading edge, whereas in Pt 1 fibroblasts, the protein mostly localizes to the perinuclear area. On the right of the panel, quantification of multipolar cells and number of cells with short and long filopodia length are shown. Cells bearing multiple F-actin flat protruding edges (butterfly shaped) were considered multipolar. While HD fibroblasts polarize showing a front (leading edge), a large proportion of Pt 1 fibroblasts show multiple protruding edges. Filopodia twofold longer than nuclei diameter were considered long filopodia. Filopodial length and number were notably increased in fibroblasts, suggesting a disruption of CDC42-dependent actin architecture. Scale bar, 20 µm (applicable to all images shown). **(E)** Filopodia dynamics of the YTS cells on an activating CD18/CD28 surface. Filopodia were imaged using SIM-TIRF microscopy with representative images showing decreased filopodia count (mean ± SD, $n = 3$; **, $P < 0.01$, unpaired two-tailed t test with Welch's correction) in cells expressing $CDC42^{R186C}$. Scale bar, 10 µm (applicable to all images shown). n.s., not significant.

I-negative 721.221 target cells demonstrated reduced cytotoxic function in the mutant cell line through a cell-intrinsic defect (Fig. 5 B). The reduction in cytotoxic function was in part due to a reduction in the ability to form conjugates with target cells (Fig. 5 C) and impaired migration (Fig. 4 C). Consistent with the observed altered filopodia structure and number, these findings suggest that immune dysfunction in the patients is likely linked to actin dysregulation (Sinai et al., 2010).

The unique behavior of the $CDC42^{R186C}$ mutant was also validated in vivo. In *Caenorhabditis elegans*, CDC-42 controls a number of developmental programs, including vulval development (Reiner and Lundquist, 2018). Our previous studies documented that *CDC42* mutations differentially perturb vulval induction and morphogenesis, with some amino acid changes up-regulating multiple signaling pathways, including those mediated by LET-60/rat sarcoma (RAS), and others behaving as hypomorphic mutations on WSP-1/WASP-dependent signaling (Martinelli et al., 2018). In particular, overexpression of WT *cdc-42* at early/mid larval stage 3 (L3) was shown to induce the formation of a single protrusion at the site of the vulva (protruding vulva [Pvl] phenotype) in a WSP-1–dependent manner. Ectopic expression of the WT protein also elicited a low penetrant multivulva (Muv) phenotype and partially rescued the vulvaless (Vul) phenotype of nematodes carrying a hypomorphic *let-23/EGFR* allele, demonstrating hyperactivation of signal flow through LET-60 and the MAPK cascade. Compared with WT CDC-42, the K186C (homologue of R186C) mutant induced a less penetrant Pvl phenotype and less efficiently rescued the Vul phenotype, indicating a hypomorphic effect of this mutation on both LET-60/RAS and WSP-1/WASP signaling pathways (Fig. 6, A and B; and Table S4).

Collectively, the in vitro and in vivo biochemical and functional data consistently indicate a unique impact of the identified disease-causing p.R186C change on CDC42 subcellular

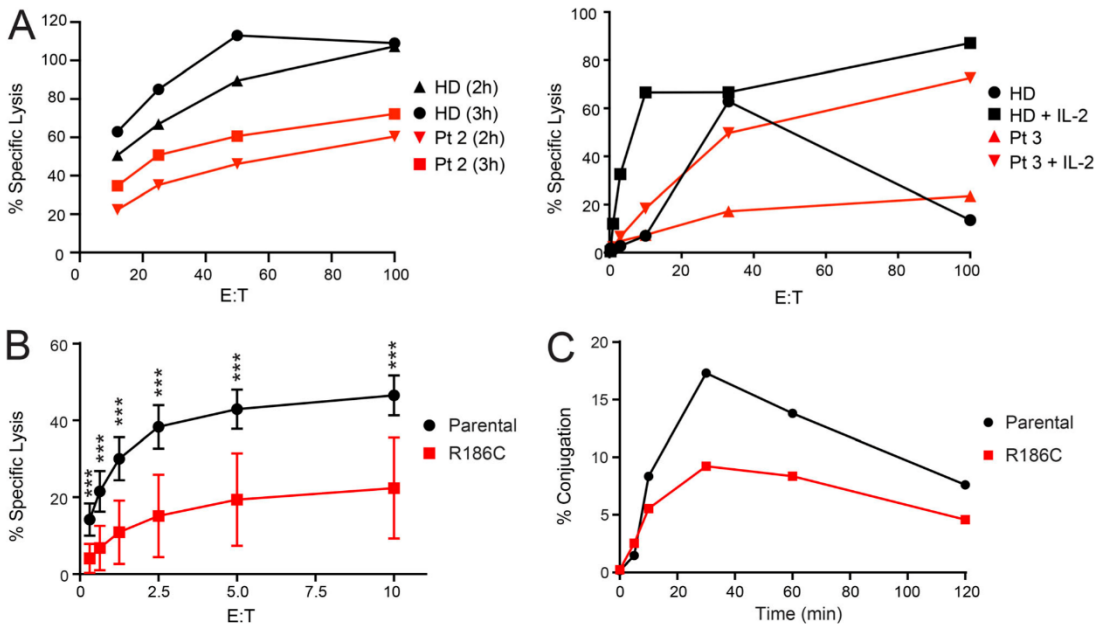

Figure 5. **p.R186C is associated with impaired NK cell cytotoxic function. (A)** Assessment of NK cell cytotoxicity in Pt 2 and 3. Using NK cell cytotoxicity assays, Pt 2 at diagnosis had a decreased cytotoxic function compared with an HD at the shown E/T ratios at time points 2 h and 3 h. For Pt 3 at diagnosis, NK cells were stimulated with IL-2, and cytotoxicity was also decreased. **(B)** Functional characterization of YTS NK cell model. Standard Cr-51 release assay of YTS NK cell lines against 721.221 target cells. The mutant cell line showed a significant decrease in cytotoxicity (pooled mean ± SD, $n = 3$ independent repeats each with triplicates; ***, $P < 0.001$, Mann–Whitney U test). **(C)** Co-culture conjugation assay of YTS NK cell lines against 721.221 target cells. Compared with parental YTS NK cells, a reduced ability of the YTS NK cells expressing the mutant allele to form conjugates with 721.221 target cells was also observed. A representative figure is shown ($n = 4$).

JEM

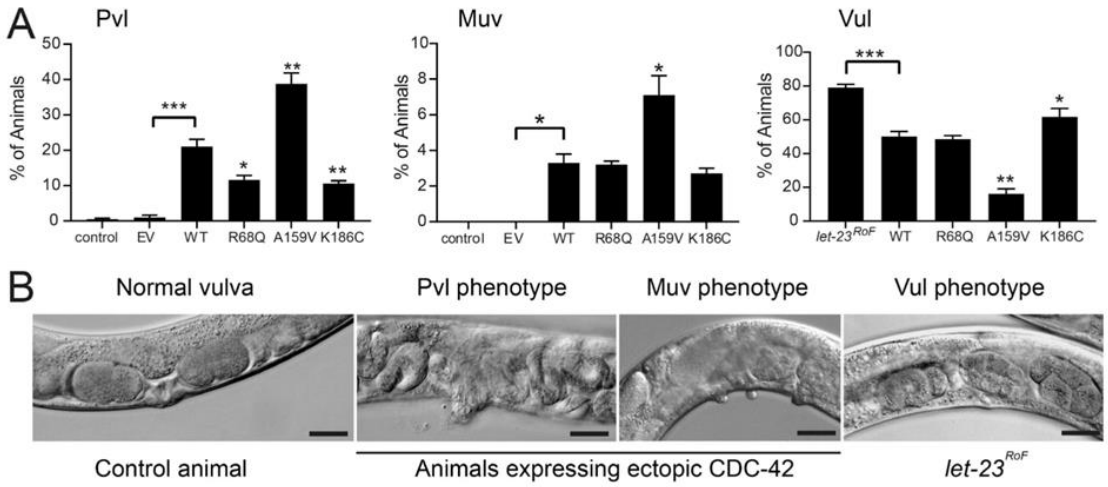

Figure 6. **p.R186C affects *C. elegans* vulval development. (A)** Hypomorphic effect of the mutation on pathways controlling *C. elegans* vulval development. Compared with WT CDC-42, the K186C mutant induces a less penetrant Pvl phenotype and less efficiently rescues the Vul phenotype of animals carrying a hypomorphic *let-23/EGFR* allele, indicating a hypomorphic behavior on multiple signaling pathways. The R68Q and A159V mutants, representative of group I (substitutions characterized by impaired binding to regulators and effectors) and group II (gain-of-function changes) mutations, respectively, are shown for comparison. Error bars indicate SEM of three independent experiments. Asterisks specify significant differences between animals expressing WT CDC-42 and those expressing the empty vector (EV) or the *let-23(sy1)* allele (*, P < 0.05; ***, P < 1.2e-6; two-tailed Fisher's exact test), and between animals expressing WT and mutant CDC-42 (*, P < 0.05 [Muv] or P < 0.005 [Pvl and Vul]; **, P < 0.00002 [Pvl] or P < 3.2e-6 [Vul]). Number of animals are reported in Table S4. **(B)** Representative images of *C. elegans* phenotypes. Scale bars, 20 µm.

localization and function, which likely underlies the distinctiveness of the trait.

Clinical profiling of NOCARH syndrome

The four unrelated patients sharing the same de novo missense *CDC42* mutation (p.R186C) showed a similar multisystem inflammatory disease characterized by pancytopenia, fever, skin rash, hepatosplenomegaly, and persistently elevated inflammatory markers. Differently from what had previously been reported for other *CDC42* mutations (Martinelli et al., 2018), no neurodevelopmental involvement was observed. In these patients, Wiskott–Aldrich syndrome, idiopathic myelofibrosis, dyskeratosis congenita, and classical immunodeficiency were rapidly excluded based on established clinical, biochemical, and genetic diagnostic criteria. Treatment with IL-1 inhibitors partially improved fever and rash, and high chronic doses of glucocorticoids were required to treat inflammation. Fatal HLH developed in three cases.

Trilineage dyshematopoiesis was observed in BM with prevalence of early differentiation elements, and decreased clonogenic progenitor content having altered clonogenicity was documented (Fig. 7 and Table S5). This indicates that the p.R186C substitution in CDC42 affects hematopoiesis, ultimately altering BM composition.

Since typical autoinflammatory features were present, we investigated IL-1β production. Increased IL-1β secretion was measured via ex vivo spontaneous IL-1β release from unstimulated BM mononuclear cells as well as high levels of IL-1β in BM supernatants and plasma (Fig. 8, A and B). This finding demonstrates that IL-1β overproduction is likely responsible for part of the phenotype, particularly the observed features typically associated with IL-1β–driven inflammasopathies (i.e., fever, rash and elevated acute phase proteins; Harapas et al., 2018). Remarkably, patients showed strikingly increased production of IL-18. This was demonstrated by a 300-fold higher ex vivo spontaneous IL-18 release from unstimulated BM mononuclear cells and by levels of IL-18 in BM supernatant and plasma that were ∼1,000-fold higher than those of healthy donors (HDs; Fig. 8, A and B). Stimulation of BM mononuclear cells with LPS or LPS plus ATP did not increase further IL-18 production as compared with unstimulated cells, suggesting the presence of constitutive maximal activation of IL-18 processing and release in the patient's marrow. In contrast, no ex vivo spontaneous IL-6 release from unstimulated BM mononuclear cells was observed (Fig. 8 A), and circulating IL-6 levels in Pt 1 and Pt 2 were comparable to those observed in healthy subjects (data not shown). Importantly, IL-18 is a potent costimulator of IFN-γ production (Okamura et al., 1995), and IFN-γ appears to be a common mediator of all forms of HLH (Grom et al., 2016). Consistently, IFN-γ levels were increased in patients, particularly during HLH episodes. In multiple samples available from Pt 1, we observed that elevated IFN-γ levels were strictly correlated (r = 0.82) with elevated levels of CXCL9 (Fig. 8 C), a chemokine specifically induced by IFN-γ that has been proposed as biomarker of HLH (Bracaglia et al., 2017). CXCL9 levels were strictly correlated with levels of ferritin (r = 0.82), which is the most typical marker of HLH activity. In line with the finding that IL-18 alone is not sufficient to induce IFN-γ, we did not find a significant correlation between IL-18 and IFN-γ or ferritin levels (Fig. 8 C). Accordingly, in Pt 2, high IFN-γ levels were also

JEM

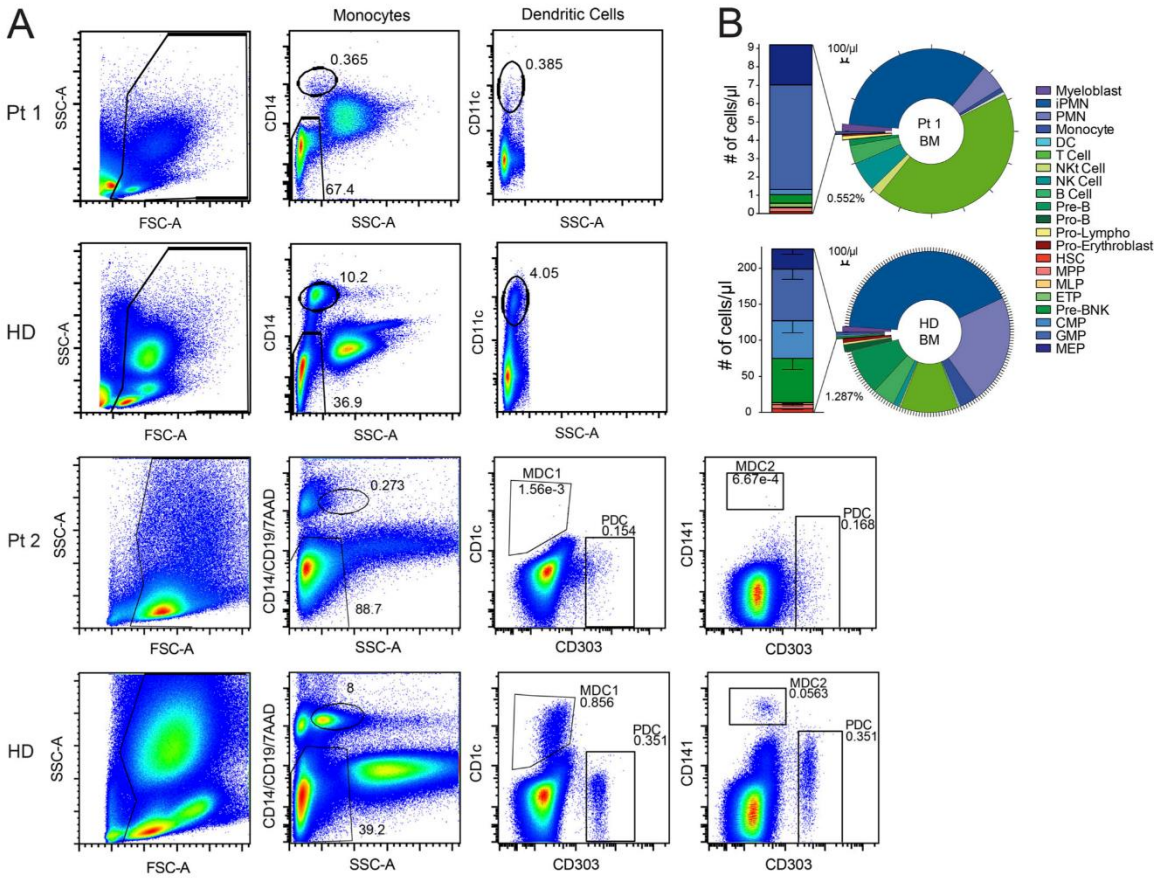

Figure 7. **p.R186C leads to disruption of certain hematopoietic compartments. (A)** Flow cytometric analysis of monocyte and dendritic cell (DC) immunophenotype on whole lysed peripheral blood of Pt 1 (n = 1) and Pt 2 (n = 1) showing a severe reduction of monocytes and myeloid dendritic cells. Upper plots (Pt 1 and Pt 2) from left to right: after elimination of debris, we gated on CD14 or CD14, CD19, 7AAD SSC^{low} cells to identify monocytes. In the $CD14^{-}$ SSC^{low} population, we gated on $CD11c^{+}$ cells for dendritic cell identification in Pt 1. In the $CD14^{-}CD19^{-}7AAD^{-}$ SSC^{low} population, we gated on CD1c, CD141, or CD303 to distinct the dendritic cell major subtypes (MDC1, type 1 myeloid dendritic cell; MDC2, type 2 myeloid dendritic cell; PDC, plasmacytoid dendritic cell) in Pt 2. Numbers within the plots show the frequency of monocytes and dendritic cells in the total events displayed. SSC-A, SSC-area; FSC-A, FSC-area. **(B)** The ring chart shows absolute counts of distinct hematopoietic subpopulations on total $CD45^{+}$ cells (indicated in the legend) in BM of pediatric HDs (n = 6) and Pt 1. The stacked bar graph on the left is a zoom on the absolute count of hematopoietic stem and progenitor cell subtypes within the $LIN^{-}CD34^{+}$ compartment. PreB/NK, B and NK cell progenitor; CMP, common myeloid progenitor; ETP, early T progenitor; GMP, granulocyte/monocyte progenitor; iPMN, immature polymorphonucleated cell; MEP, megakaryocyte/erythrocyte progenitor; MLP multi-lymphoid progenitor; MPP, multi-potent progenitor; NKt, NK T cell; PMN, polymorphonucleated cell.

associated with high CXCL9 and ferritin levels (Table S1). In addition, serum IL-6 levels were measured, and persistent elevation was not detected (Fig. 8 A). Notably, in Pt 1, the last severe HLH episode not responding to repeated glucocorticoid pulses, cyclosporine A, and high-dose anakinra (10 mg/kg/d) was successfully treated with emapalumab, a monoclonal antibody targeting IFN-γ. Altogether, these data show that the R186C change in CDC42 leads eventually to activation of the IFN-γ pathway through overproduction of IL-18, which has been demonstrated to be associated with secondary HLH development in the context of autoinflammatory diseases (Canna et al., 2014; Weiss et al., 2018).

The surviving patient (Pt 1) underwent allogeneic HSCT from his HLA-haploidentical father after selective depletion of αβ T cells and $CD19^{+}$ cells from the graft for preventing occurrence of graft-versus-host disease and Epstein-barr virus–related posttransplant lymphoproliferative disease, respectively (Locatelli et al., 2017). The conditioning regimen used treosulfan, thiotepa, and fludarabine. To avoid HLH flares, the patient was given emapalumab and anakinra until days +28 and +100 after HSCT, respectively. Neutrophil and platelet recovery occurred on days +18 and +12 after HSCT; successful engraftment of donor hematopoiesis was associated with normalization of IL-1β and IL-18 production (Fig. 8 B). No inflammatory or HLH flare has been observed up to day +210.

JEM

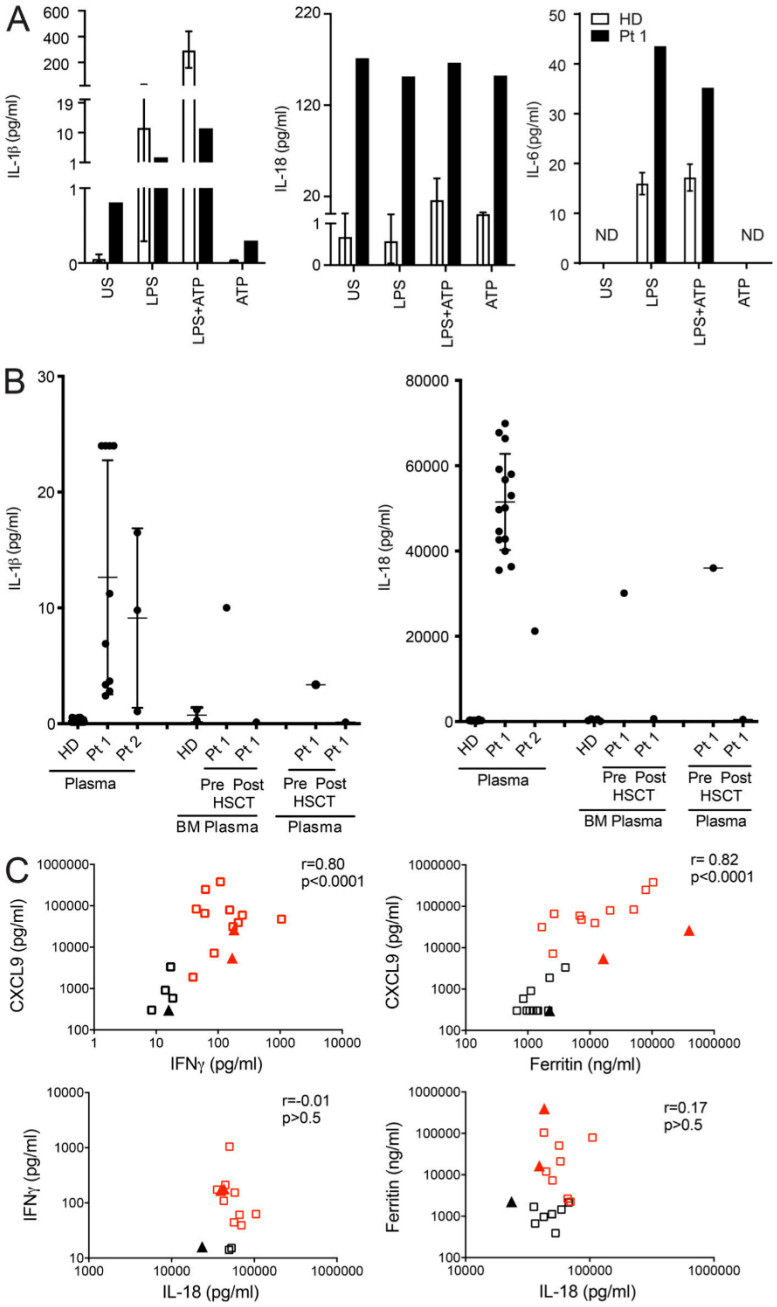

Figure 8. **p.R186C is associated with high production of inflammasome-related cytokines IL-1β and IL-18 in vivo and ex vivo. (A)** HD (n = 3) and Pt 1 BM mononuclear cells were left unstimulated (US) or stimulated with LPS (10 µg/ml) for 5 h, with or without ATP (1 mM) for an additional 1 h. Compared with unstimulated HD cells, unstimulated Pt 1 cells release high levels of IL-1β and IL-18. In LPS-primed HD cells, ATP addition caused a marked increase in IL-1β and IL-18 release, while this is not observed in LPS-primed Pt 1 cells. IL-6 levels released in supernatants were also measured; no spontaneous release was observed. ND, not detectable. Secreted cytokines were measured by ELISA, and results obtained were normalized by the absolute number of monocytes per milliliter BM. **(B)** IL-1β and IL-18 levels were measured in plasma samples collected from Pt 1 and Pt 2 at different time points over the course of the disease. IL-1β and IL-18 levels were also measured in BM, and plasma samples were obtained from Pt 1 30 d before and after HSCT. For HDs, plasma n = 24 and BM n = 5. For Pt 1 and Pt 2, n = 1. Mean ± SD is indicated. **(C)** Plasma levels of IFN-γ, CXCL9, and IL-18 were measured in Pt 1 (squares) and Pt 2 (triangles) and correlated with ferritin levels, a typical marker of HLH activity. IFN-γ and CXCL9 levels, but not IL-18 levels, are significantly correlated with ferritin levels. Red squares and triangles indicate samples collected when Pt 1 and Pt 2 fulfilled at least five criteria required for HLH diagnosis.

Discussion

Here, we characterize a previously unrecognized and distinctive hematological/autoinflammatory disorder due to a specific missense mutation of *CDC42* (p.R186C). By using complementary biochemical and functional analyses, we provide evidence that the disease-causing amino acid substitution has unique consequences on CDC42 function, leading to a perturbation of hematopoiesis, immune function, and inflammatory response. We also provide a first characterization of the clinical profile of the associated phenotype and propose the acronym of NOCARH syndrome to highlight the major features of the condition, including neonatal onset of cytopenia, autoinflammation, rash, and episodes of HLH.

JEM

CDC42 codes for a small GTPase of the Rho family controlling multiple signaling pathways regulating cell polarity and migration, endocytosis, and cell cycle progression by cycling between an active (GTP-bound) and an inactive (GDP-bound) state (Etienne-Manneville and Hall, 2002; Etienne-Manneville, 2004). Recently, a number of missense mutations in this gene have been associated with developmental traits characterized by an unusually broad spectrum of anomalies, with core clinical features including defective growth, intellectual disability, brain malformations, facial dysmorphism, hearing/vision problems, cardiac malformations, and immune and hematologic and lymphatic defects (Takenouchi et al., 2015; Martinelli et al., 2018). Genotype–phenotype correlations were identified and linked to a variable functional impact of mutations, suggesting specific consequences of individual mutations on cellular processes controlling development. In contrast to those phenotypes, NOCARH syndrome is a hematological and autoinflammatory condition with no major involvement of other systems, which is in line with the documented peculiar functional consequences of the p.R186C change on protein function.

Our immunophenotype and clonogenic data are consistent with previous findings showing that controlled inactivation of CDC42 in BM cells results in altered frequency and distribution of hematopoietic stem cells, decreased abundance of long-term hematopoietic stem cells, and occurrence of myeloid and erythroid developmental defects, as well as functional defects in engraftment, migration, and BM retention (Yang et al., 2007a,b). Notably, present findings confirm the key role of the GTPase in controlling processes implicated in hematopoietic stem and progenitor cell fate and behavior.

Based on structural modeling and biochemical and cellular testing, we predicted and confirmed the mutated protein to have impaired interaction with known regulators and effectors, including RhoGDI, IQGAP1, and WASP, leading to aberrant subcellular localization, actin cytoskeleton rearrangement, and reduced migration. CDC42 mislocalization data are consistent with the physiological role played by RhoGDI and IQGAP1, key mediators of membrane cycling of CDC42 (Gibson and Wilson-Delfosse, 2001; Swart-Mataraza et al., 2002; Gibson et al., 2004). The observation that cells expressing the p.R186C variant undergo deep cytoskeletal rearrangements leading to multiple leading edges is congruous to findings by Fukata et al. (2002) showing that cells expressing IQGAP1 mutants defective in CDC42 binding display aberrant multipolar morphology. This supports the notion that the IQGAP1–CDC42 interaction is crucial to cell polarization and migration. Notably, the finding that CDC42 aberrant localization and trafficking is coupled to altered polarization and migration is in line with the relevant role played by CDC42 at the Golgi and the leading edge in the control of cell polarity (Baschieri et al., 2014). Compositional and functional assessment revealed impaired proliferation and polarized migration, further emphasizing the requirement of proper CDC42 function in these processes (Martinelli et al., 2018). Notably, although we were unable to identify a specific CDC42 functional perturbation associated with the p.R186C change as causally linked to the complex phenotype of NOCARH syndrome, this mutant seems unique in its mislocalization, which suggests this is a key factor in the pathogenesis for this uniquely presenting disease.

Our findings indicate that aberrant CDC42 function can involve components of hyperinflammation and immune impairment in NK cells, contributing to the HLH phenotype observed in NOCARH. The underlying pathogenetic mechanism of the p.R186C mutation in the context of anemia and thrombocytopenia has yet to be determined, suggesting a context-dependent effect on specific blood cell compartments. Future studies involving murine models carrying the heterozygous mutation would be needed to assess the effect on hematopoiesis in a similar context to that of our patients.

Several mutations in genes with a role in actin cytoskeleton remodeling of immune cells have been demonstrated to be involved in the pathogenesis of hematological/autoinflammatory diseases, underlining the importance of the actin cytoskeleton in modulating inflammatory responses. Indeed, mutations in the actin-binding protein cofilin (CFL1; Seeland et al., 2018), WAS (Li et al., 2017), DOCK8 (Dasouki et al., 2011), and ARPC1B (Brigida et al., 2018), as well as in RAC2, a Rho GTPase structurally and functionally related to CDC42 (Caye et al., 2015; Hsu et al., 2019), cause abnormal migration, proliferation, and/or differentiation of lymphoid and/or myeloid cells and are associated with features of autoinflammation. Moreover, aberrant actin depolymerization due to an inactivating mutation of the actin-depolymerizing cofactor Wdr1 has been demonstrated to cause in mice an autoinflammatory disease characterized by spontaneous autoinflammation, thrombocytopenia, and neutrophilia (Kim et al., 2015). In these mice, the autoinflammatory phenotype is IL-18, but not IL-1β, dependent and is driven by activation of the pyrin inflammasome. In our study, we could not investigate the exact molecular mechanism involved in the overproduction of IL-18 and the role of CDC42 in inflammasome regulation. However, the spontaneous release of IL-18 by BM mononuclear cells, associated with high IL-18 circulating levels, has been exclusively described in patients carrying mutations in the NLRC4 protein (Canna et al., 2014) who present with recurrent episodes of HLH. Moreover, it is well known that inactivation of RhoA GTPases by many bacterial toxins is sensed by the inflammasome (Jamilloux et al., 2018). Interestingly, IQGAP1 has also been described as a novel regulator of caspase-1 in macrophages infected with *Yersinia pestis* (Chung et al., 2014). Based on the above-mentioned observations regarding the connection between the actin cytoskeleton and inflammation, we propose the term "inflammatory actinopathies" to group these diseases, including NOCARH, differently from actinopathies with neurological and myologic features.

In conclusion, NOCARH is an autoinflammatory disease at high risk for HLH, similarly to what has been observed for the disorder caused by NLRC4 gain-of-function mutations (Canna et al., 2014; Romberg et al., 2014). Given the observed autoinflammation associated with markedly elevated IL-18 levels, the mechanism is most likely associated with the role of IL-18 as a costimulus for IFN-γ production. The characteristic inflammation in two patients in conjunction with elevated IL-18 levels support IL-18 as a disease biomarker for diagnosing NOCARH and potentially related syndromes of dysregulated CDC42

JEM

function that involve inflammation. One patient survived severe HLH, and this appears to have been dependent on timely therapeutic neutralization of IL-1 and IFN-γ. Early recognition and establishment of treatment for NOCARH, based on the unique association of early-onset trilinear cytopenia and autoinflammation, are crucial to prevent multiorgan failure and subsequent death.

Materials and methods

Detailed clinical history of patients

Pt 1

Pt 1 is a 6-yr-old Caucasian girl born from healthy unrelated parents with no family history of genetic disease. At birth, she presented with persistent high fever; erythematous skin lesions of the face, trunk, and limbs; a large abdomen because of hepatosplenomegaly (spleen diameter, 6.4 cm); and suspected trigonocephaly (Table 1). Laboratory tests showed an increase in inflammatory markers and a severe trilinear cytopenia requiring frequent red blood cell and platelet transfusions during the first year of life. BM biopsy at disease onset revealed fibrosis with trilineage dyshematopoiesis (prevalence of early differentiation elements in erythroid and myeloid lineage, dysmorphic and reduced megakaryocytes, increased lymphocytes, and abundant $CD68^+$ histiocytes with focal or absent phagocytosis; Tables S1 and S2). Given the partial clinical overlap with chronic infantile neurological cutaneous articular syndrome–neonatal-onset multisystem inflammatory disease (CINCA-NOMID), she was started on glucocorticoids and daily therapy with anakinra, with improvement of fever and rash, but no effect on cytopenia. Failure to thrive was present. Treatment with G-CSF was started with partial response. Recurrence of inflammatory symptoms following tapering and/or discontinuation of glucocorticoids was observed. At age of 11 mo, she presented with recurrent episodes of intestinal bleeding, associated with persistent/chronic diarrhea. Meckel's diverticulum was excluded. At 2 yr and 6 mo, she presented with three episodes of generalized seizures followed by hypotonia, hypersomnia, and transient hemiparesis requiring in one case admission to an intensive care unit. Magnetic resonance imaging (MRI) performed during the first episode showed lesions suggestive of inflammatory central nervous system involvement; during the third episode, the MRI showed one additional lesion of the brainstem. CSF was sterile, CSF white blood cells were 18/mmc, and no hemophagocytic cells were detected. All the episodes were treated with a high dose of i.v. glucocorticoid with good response; therapy with levetiracetam was started. At the age of 5 yr, because of incomplete control of the inflammatory state, anakinra was switched to canakinumab. Starting from 5 yr of age, she developed four episodes of full-blown HLH, fulfilling the HLH-2004 diagnostic criteria. All episodes were treated with high dose of i.v. glucocorticoids and cyclosporine-A with resolution in all cases except one. The last episode was severe and associated with massive intestinal ischemia and necrosis requiring surgical resection and consequent ileocolostomy. This episode was unresponsive to high-dose glucocorticoids and IL-1 inhibition. Treatment with emapalumab, an anti–IFN-γ antibody, was added with rapid resolution of the episode. At age of 6 yr, the patient underwent allogeneic HSCT from her HLA-haploidentical father after a selective depletion of αβ T cells and $CD19^+$ cells from the graft. The conditioning regimen consisted of a combination of treosulfan, thiotepa, and fludarabine. To avoid flares of HLH, the patient was given emapalumab and anakinra until days +28 and +100 after the allograft, respectively. Neutrophil and platelet recovery occurred on days +18 and +12 after HSCT. Normalization of the acute phase response and no inflammatory or HLH flare have been observed up to day +210.

Pt 2

Pt 2 was a male born from Caucasian healthy unrelated parents. Since the first day of life, he presented with persistent fever, skin rash, mild hepatosplenomegaly, failure to thrive, increase in inflammatory markers, and trilinear pancytopenia that required red blood cell and platelet transfusions. Extensive microbiological screening revealed a positive IgM titer for parvovirus B19, with B19 parvovirus PCR negative on whole blood. At age 57 d, he was first seen at one of our centers transferred from another hospital. He presented with failure to thrive (height and weight below the fifth percentile), persistent fever, skin rash, mild hepatosplenomegaly, and chronic diarrhea and positive blood stool. Inflammatory bowel disease was suspected, and temporary parenteral nutrition started. Laboratory tests showed elevated acute-phase reactants and severe trilinear cytopenia requiring recurrent red blood cells and platelet transfusions. BM biopsy revealed dyshematopoiesis and some lymphohistiocytic aggregates without significant hemophagocytosis. The disease course was characterized by a persistent inflammatory state despite several treatment attempts with glucocorticoids, antibiotics, high doses of i.v. immunoglobulins, and cyclosporine-A. Suspecting an autoinflammatory condition, treatment with anakinra was also started with only partial improvement of the clinical and laboratory parameters. At age 7 mo, he developed severe HLH with multiorgan failure that rapidly progressed to death. Extensive immunological workup showed severe monocytopenia and reduction of plasmacytoid, myeloid dendritic cells, neutropenia, increased central memory $CD4^+$ cells with reduced naive and recent thymic emigrant $CD31^+$ cells, increased regulatory T cells with high memory phenotype, and increased switched B cell memory cells, plasma cells, and autoreactive B cells associated with reduced transitional B cells (Table S2).

Pt 3

Pt 3 was a female born from nonconsanguineous Caucasian parents with no family history of inherited diseases. At birth, she presented with generalized rash, intermittent cytopenia (leukopenia, thrombocytopenia, and anemia requiring transfusions), and generalized lymphadenopathy. Hepatosplenomegaly, nutritional problems, and stagnant growth were also noted within the first few months after birth. The anemia was profound and required several red blood cell transfusions. At age 3 mo, the condition was thought to be CINCA-NOMID, and treatment with anakinra was started, which was temporarily

JEM

effective for rash and overall inflammation, but not cytopenia. Treatment was stopped due to respiratory infections and no clear effect of the treatment. 6 mo later, she started treatment per modified HLH-2004 protocol with steroids and weekly etoposide-phosphate over 8 wk. No neurological deficits were noted, but the patient declined over time, requiring increasing erythrocyte and thrombocyte transfusions. She was then transferred to another hospital, and for the first few weeks, she was stable, but she developed signs of an HLH relapse with increased hepatosplenomegaly, high ferritin, high triglycerides, bicytopenia, and a florid rash. Histologically, hemophagocytosis was not detected. She also developed breathing difficulties of unknown origin. She was commenced on a modified HLH-2004 protocol with the addition of antithymocyte globulin, infliximab, and anakinra. There was some clinical response on this treatment and a decision to opt for a stem cell transplant was made. While she was being investigated and prepared for transplant, she continuously deteriorated; she was treated with two courses of alemtuzumab in this time period. She received a CD3/CD19-depleted haploidentical transplant and died 4 d later.

Pt 4

Pt 4 was a boy born in week 34 to nonconsanguineous parents from a Christian minority originating from the Middle East with a history of thalassemia minor and familial cardiomyopathy. The patient was small for gestational age and presented at birth with bloody diarrhea, cholestasis, ascites, and a generalized rash. He had an unusually small thymus for his age. The patient also rapidly developed additional symptoms, including stiff/contracted joints, high fever, highly elevated inflammatory markers, intermittent cytopenia (thrombocytopenia and anemia requiring transfusions), hepatomegaly, and diatheses (bleeding from the mucosas; Table 1). At 2 wk of age, an extensive workup was initiated. Investigations excluded known gut, liver, and metabolic diseases. Immunological investigations slightly lowered number of T cells with prevalence of naive T cells. Results of functional tests of NK/T cells and degranulation ability were normal. Serum IL-6 and IL-18 was remarkably high on repeated occasions. An autoinflammatory condition in combination with a primary immunodeficiency was suspected. The patient was treated with high dose glucocorticoids and anakinra. Because of insufficient response tocilizumab was also added. This intensive antiinflammatory treatment was effective for some of the rash, ascites, cholestasis, as well as intermittently for overall inflammation and cytopenia. The patient needed supportive treatment in the intensive care unit on six separate occasions, four of which were due to macrophage activation syndrome–HLH episodes, likely triggered by infection.

Severe gastrointestinal symptoms and unexplained mucosal bleedings persisted. The patient continued to have watery diarrhea. Gastroduodenal endoscopy showed severe inflammation with ongoing bleeding. Biopsies of the duodenum showed acute and chronic inflammation with ulcers. In connection with colonoscopy, the patient suffered a perforation and needed surgery. Since no matched related SCT donor was available, a search for an unrelated matched donor was initiated; however, his conditions were too unstable with no signs of remission, and HSCT was considered too risky. Because of the symptoms of agonizing pain and high levels of anxiety, and in the presence of no response to treatments, the antiinflammatory therapies were gradually stopped, and the patient was transferred to another hospital for palliative care, where he died at 4.5 mo of age.

Mutation analyses

This study was approved by the Ospedale Pediatrico Bambino Gesù and Baylor College of Medicine Ethical Committees. Clinical data and DNA specimens from the subjects included in the study were collected following procedures in accordance with the ethical standards of the declaration of Helsinki protocols and approved by the review boards of all involved institutions, with signed informed consents from the participating subjects/families (study protocol for Pt 1 and 3: "Genome Sequencing to Elucidate the Causes and Mechanisms of Mendelian Genetic Disorders" [H-29697] of Baylor College of Medicine; study protocol for Pt 1 and 2: 1702_OPBG_2018).

Pt 1

Exome capture was performed using SureSelect AllExon v5+UTR (Agilent) and sequenced on a HiSeq platform (Illumina). WES data were processed and analyzed using an in-house–implemented pipeline as previously described (Flex et al., 2016; Stray-Pedersen et al., 2017; Bauer et al., 2018). Briefly, reads were aligned to human genome build GRCh37/UCSC hg19, and variants were quality filtered according to the Genome Analysis Toolkit's 2016 best practices, annotated, and filtered against public (dbSNP150 and gnomAD V.2.0.1) and in-house (>1,300 population-matched exomes) databases to retain private and rare (unknown frequency or minor allele frequency <0.1%) variants located in exons with any effect on the coding sequence (CDS) and within splice site regions. Functional annotation of variants was performed using SnpEff v.4.3 and dbNSFP V.2.9, and functional impact was analyzed by CADD v.1.3 and M-CAP v.1.0.(Cingolani et al., 2012; Liu et al., 2013; Kircher et al., 2014; Jagadeesh et al., 2016). Average coverage was 91× and 20× for ≥86% of the target. Among 127,405 high-quality variants, 14,224 affect either the CDS or splice sites, while 338 have low or unknown frequencies according to the aforementioned frequency thresholds. For sequencing statistics, see Table S3. Relevant variants and the de novo origin of the c.556C>T change were validated by Sanger sequencing.

Pt 2

Mutation analysis was performed by Sanger sequencing using DNA obtained from circulating leukocytes. Primer pairs are available upon request.

Pt 3

Initial mutation analysis was performed by Sanger sequencing (and Baylor College of Medicine CMA v9.1), which was negative for *NLRP3*, *IL1RN*, *LPIN2*, *NOD2*, *MEFV*, *TNFRSF1A*, *PSTPIP1*, *MVK*, and *PSMB8*. The patient was identified in a shared CMG database at Baylor College of Medicine by searching for rare, likely damaging variants (using the Exome Aggregation Consortium and CADD) in *CDC42* in a cohort of unsolved immunodeficiency

probands. On further study, patient had underwent trio-based WES in Norway, revealing the presence of the de novo c.556C>T change in *CDC42*, and proband-only WES was repeated at Baylor College of Medicine. Sanger sequencing of proband and parents was then performed, confirming the presence of a de novo variant (Table S3).

Pt 4

Blood samples from the patient and his parents were obtained with informed consent according to the Declaration of Helsinki. The study was approved by the Regional Ethics Review Board in Stockholm, Sweden. DNA samples were subjected to trio-based WGS with a TruSeq DNA PCR-free protocol followed by sequencing on an Illumina HiSeq X machine with an average coverage of 34×. Sequencing reads were analyzed with the pipeline SpeedSeq. In brief, reads were mapped to the human genome build GRCh37 with Burrows–Wheeler aligner, while calling of single-nucleotide and structural variants was performed, respectively, with FreeBayes and Lumpy. No mutations were identified in HLH/autoinflammation–related genes. The genomic region spanning *CDC42* was visualized with the Integrative Genomics Viewer, indicating a de novo c.556C>T mutation, which was validated by Sanger sequencing (Table S3).

MS

WT CDC42 from TNAO38 insect cells were dissolved in 50% (vol/vol) acetonitrile and 0.2% (vol/vol) formic acid at a final concentration of 2 mg/ml. Proteins were subjected to a C4 HPLC column (MassPrep Online Desalting Cartridge, dimensions 2.1 × 10 mm; Waters) equilibrated with 20% (vol/vol) acetonitrile and 0.1% (vol/vol) formic acid. For HPLC separation, the following conditions were used: HPLC-system U300 series (Agilent Technology), a flow rate of 500 µl/min; eluent A, 0.1% (vol/vol) formic acid in water; eluent B, 0.1% (vol/vol) formic acid in acetonitrile; gradient conditions, 20% B for 0.5 min, linear gradient up to 60% B in 1.5 min, linear gradient up to 90% B in 0.5 min, 90% B for 0.5 min, and reequilibration of the column. The HPLC system was coupled on-line to an ion trap mass spectrometer (VelosPro; ThermoFisher Scientific) equipped with an electrospray ionization source. Full spectra were acquired using a mass-to-charge range of 700–2,000. Obtained spectra were deconvoluted using the program package Promass (ThermoFisher Scientific). Masses obtained from the respective spectra are described with respect to calculated molecular weights (CH3, methyl group; Ic, insect cells; GG, geranylgeranyl moiety).

Constructs and proteins for biochemical analysis

pGEX vectors were used for bacterial overexpression of $CDC42^{WT}$, $CDC42^{R186C}$, RhoGDI-1, p50GAP, ITSN1, WASP (GTPase-binding domain), PAK1 (GTPase-binding domain), and IQGAP1 (863–1,657). All proteins were isolated as GST fusion proteins in *Escherichia coli* BL21 (DE3) purified after cleavage of the GST tag via gel filtration (Superdex 75 or 200; Pharmacia). Nucleotide-free and fluorescent nucleotide-bound CDC42 were prepared using alkaline phosphatase (Roche) and phosphodiesterase (Sigma-Aldrich) at 4°C as described. Fluorescent nucleotide was methylanthraniloyl (mant-) GppNHp (guanosine 5′-β,γ-imidotriphosphate), a nonhydrolysable GTP analogue. All proteins were analyzed by SDS-PAGE and stored at −80°C. The GTPase assay and nucleotide exchange reaction were performed with a Hi-Tech Scientific (SF-61) stopped-flow instrument. The release of fluorescently labeled GDP (mantGDP) was measured basally and with the catalytic GEF domain of ITSN1. Hydrolysis of tamraGTP was measured basally and following stimulation with the catalytic GAP domain of ARHGAP1 (p50GAP). The excitation wavelengths were 543 nm and 362 nm for tamraGTP and mantGDP, respectively. Fluorescence experiments were performed in a Fluoromax 4 fluorimeter in polarization mode. Human WT and mutant *CDC42* were subcloned into pFastBacHTB vector (Invitrogen) and fused with an N-terminal hexa-histidine (6xHis) tag and transformed into DH10BAC strain for insect cell purification.

Fluorescence assays

The GTPase assay and nucleotide exchange reaction were performed with a Hi-Tech Scientific (SF-61) stopped-flow instrument. The excitation wavelengths were 543 nm and 362 nm for tamraGTP (Jena Bioscience) and mantGDP (Jena Bioscience), respectively. For the GTPase assay, equal volumes (600 µl) of 0.2 µM CDC42-tamraGTP and 10 µM of p50GAP in 30 mM Tris/HCl, pH 7.5, 10 mM K_2HPO_4/KH_2PO_4, 5 mM $MgCl_2$, and 3 mM dithiothreitol at 25°C were rapidly mixed and transferred to a fluorescence detection cell within seconds. For the nucleotide exchange reaction, 0.2 µM CDC42-mantGDP and 40 µM GDP + 10 µM ITSN1 were used.

Structural analysis

To elucidate the impact of substituted arginine to cysteine at residue 186, the protein–protein interaction between CDC42 and RhoGDI-1 (PDB: 1DOA) was analyzed. Residues in vicinity ≤4 Å were considered as part of binding interface of Arg^{186}. Analysis and illustrations were made using the PyMOL molecular viewer.

SPR

A Biacore X100 instrument (GE Healthcare) was used in a single-cycle mode to analyze the kinetics of interaction between WT or R186C $CDC42^{GG}$ with RhoGDI. SPR experiments were performed at 25°C in HBS-P+ running buffer (10 mM HEPES pH 7.4, 0.15 M NaCl, 0.05% [vol/vol] surfactant P20; GE Healthcare). GST capturing method was used to immobilized GST antibody on the surface of CM5 chip. 4 µM GST-GDI (5 µl/min) in HBS-P buffer injects for the period of 180 s in order to immobilized GST-GDI over the chip surface. Regeneration of the chip performed using 10 mM glycine, pH 3.0, at the end of each experiment. WT and R186C $CDC42^{GG}$ were injected in 0.06–1 µM concentrations with twofold increase in each injection step. Final curve was fitted in a 1:1 binding model.

Cell lines and cultures

Dermal mutant fibroblasts were obtained from patients, and HEK-293T, COS-1, and NIH-3T3 cell lines and primary control dermal fibroblasts were obtained from American Type Culture Collection and grown in high-glucose DMEM supplemented

JEM

with 10% FCS, 2 mM L-glutamine, and 10 U/ml penicillin/streptomycin (all from Sigma-Aldrich). YTS cells, a subclone of the YT cell line, were cultured in R10 composed of RPMI-1640 supplemented with 10% FBS (Premium; Atlanta Biologicals), 2 mM L-glutamine (ThermoFisher Scientific), 1 mM sodium pyruvate (ThermoFisher Scientific), 1% MEM nonessential amino acid (100×; ThermoFisher Scientific), 10 mM Hepes (ThermoFisher Scientific), and 1% penicillin/streptomycin (ThermoFisher Scientific).

Plasmids for CDC42 expression in HEK-293T, COS-1, and NIH-3T3 cell lines

WT human CDC42 isoform 1 (NP_001782.1) was cloned into a pcDNA3-FLAG backbone using PCR and standard cloning methods via BamHI and EcoRI digestion. Mutant constructs carrying the R186C change were generated by site-directed mutagenesis using the QuikChange XL kit (Agilent Technologies) and verified by direct sequencing. Each of the FLAG-tagged CDC42 protein expression constructs or the empty vector was transfected using Fugene 6 (Roche). 24 h after transfection, cells were assayed for cell growth or processed for wound healing assays, immunofluorescence, or immunoprecipitation analysis. Transfection efficiency was verified by Western blot (WB) analysis of the protein lysate.

Pull-down of CDC42 variants from COS-7 cell lysates

COS-7 cells were transfected with pcDNA3.1-Flag plasmids containing WT and R186C CDC42 and transiently overexpressed for 48 h. 10 µg of each plasmid was used for transfection of the COS-7 cells (900,000 cells per 10-cm Petri dish). Empty vector was used as control. 20 µl TurboFect transfection reagent (ThermoFisher Scientific) was added to the plasmids and incubated for 20 min at room temperature before adding it to the cells. Medium was changed after 4 h, and cells were incubated for 48 h. Cells were lysed in an ice-cold buffer containing 50 mM Tris/HCl, pH 7.4, 100 mM NaCl, 2 mM $MgCl_2$, 1% Igepal Ca-630, 10% glycerol, 20 mM β-glycerolphosphate, 1 mM Na_3VO_4, and one tablet EDTA-free protease inhibitor (Roche). Cell lysates were incubated with glutathione beads coupled to GST-effector proteins for 30 min at 4°C. Beads were washed five times, heated in 1× Laemmli buffer at 95°C for 10 min, and subjected to SDS-PAGE for immunoblot analysis. WB was performed using an anti-FLAG antibody (F3165, M2; Sigma-Aldrich) and anti-GAPDH antibody (21185, clone 14C10; Cell Signaling Technology).

Polarized migration

Polarized migration of primary fibroblasts and NIH-3T3 cells on fibronectin-coated wells (10 µg/ml; Sigma-Aldrich) were evaluated by wound-healing assays. Monolayers of cells were scratched with a 200-µl micropipette tip and incubated in low-serum medium (2% FBS in DMEM high glucose without Phenol red, 2 mM L-glutamine, and 1% penicillin/streptomycin; all purchased from Sigma-Aldrich) in the presence of thymidine (10 mM, T1895; Sigma-Aldrich) to inhibit cell proliferation. Images were acquired at different time points using a Nikon Eclipse TS100 microscope, a Nikon Plan Fluor 10×/0.13 objective, and a Nikon Coolpix 990 digital camera. Cells that had migrated in the wounded area were counted in four fields per well, and the fold increase of migratory cells was evaluated after scratch at the time points indicated.

Proliferation and viability

Proliferation and viability of transiently transfected NIH-3T3 cells and primary fibroblasts were quantified by manual counting using a Neubauer hemocytometer. Cell viability was detected by the exclusion of trypan blue dye (5 mg/ml in PBS, ECB4004L; Euroclone). Cells were counted at different time points by phase contrast using a Leitz Ortholux II microscope and a Leitz 10×/0.13 objective.

Immunofluorescence analysis of primary fibroblasts and COS-1 cells

Cells were washed in PBS, fixed (4% paraformaldehyde [PFA], 20 min, room temperature), washed twice, treated for free aldehydes quenching (50 mM NH_4Cl, 10 min at room temperature), and washed again. After 5-min permeabilization with 0.5% Triton X-100 in PBS, cells were blocked for 30 min with 2% FBS and 1% BSA in PBS. Then, cells were sequentially incubated with primary and secondary antibodies 1.5 h at 37°C, 1:500 mouse anti-FLAG (F-1804; Sigma-Aldrich) or 1:50 mouse anti-CDC42 (SC8401; Santa Cruz); 30 min at room temperature, 1:100 goat anti mouse Alexa Fluor 488 (A11017; ThermoFisher Scientific); 30 min room temperature, 1:50 rabbit anti-GM130 (PA1-077; ThermoFisher Scientific); and 30 min at room temperature, 1:100 goat anti-rabbit Alexa Fluor 568 (A11011; ThermoFisher Scientific). All antibodies were diluted in 0.5% BSA and 0.1% saponin in PBS. Unbound antibodies were removed after each incubation by three washes with washing buffer (0.2% BSA in PBS). After a 30-min incubation with phalloidin-Alexa Fluor 647 (Life Technologies), coverslips were washed and then mounted on glass slides with 5 µg/ml Hoechst33342 (Life Technologies) nuclear dye in antifade reagent (ThermoFisher Scientific) and analyzed. Imaging was performed on an Olympus FV1000 using excitation spectral laser lines at 405, 488, and 633 nm. Signals from different fluorescent probes were taken in sequential scanning mode. Images were captured using Olympus FluoView Viewer Software. Golgi localization of CDC42 in primary fibroblasts was quantitated using GM130 as a mask for cis/medial-Golgi, and CDC42 fluorescence intensity was quantified as the ratio of Golgi to whole-cell staining by using ImageJ software. Multipolar and filopodia-bearing cells were determined (blinded to sample information) by manually counting in FluoView Viewer ≥200 cells from ≥10 randomly chosen images. Cells having multiple F-actin flat protruding edges (butterfly shaped) were considered multipolar, while cells showing a front (leading edge) and a rear were considered unipolar. To calculate the average filopodial length, the distance from the cell base to the tip was determined. Actin protrusions <1 µm were not considered as filopodia. Filopodia measured as twofold longer than nuclei diameter were considered long filopodia, while the remaining filopodia were considered short.

JEM

CRISPR cell line production

The immortalized YTS human NK cell line was used as the model for immune function. In collaboration with the Cell Based Assay Screening Service at Baylor College of Medicine, a homozygous knock-in of the c.556C>T/p.R186C mutation was placed into chromosome 1, isoform 1 of *CDC42*. Briefly, guide RNAs were screened in 293T cells for editing efficiency. Each guide RNA was incorporated into an all-in-one vector encoding Cas9 and eGFP.

A single-stranded donor oligonucleotide template (antisense; 5′-GAATGTATTTGACGAAGCAATATTGGCTGCCCTGGAGCC TCCAGAACCGAAAAAGTCCTGCAGGTGTGTGCTGCTATGAAC ATCTCTCCAGAGCCCTTTCTGCACAGCTGGTGTCGGC-3′) was synthesized incorporating the desired mutation, a silent mutation encoding for the SbfI restriction site, and another mutation to reduce Cas9 recutting. Constructs were transfected into the parental YTS cell line (Neon electroporator, 1,400 V/10 ms/three pulses, 2.5e6 YTS cells). Cells were sorted based on eGFP 48 h later and plated by limiting dilution. Clones were screened based on genomic extraction and SbfI digestion and then sequenced using Sanger sequencing of the targeted region for verification. Clones were expanded in R10 medium and then underwent repeat Sanger sequencing for the presence of the *CDC42* mutation and for the lack of off-site mutagenesis at *GBA3*, a known pseudogene of *CDC42*. A single clone was used for all YTS experiments presented.

YTS fixed-cell immunofluorescence confocal microscopy

YTS cells were washed once with complete R10 and resuspended to a final concentration of 1e6/ml in complete R10. 200,000 cells were plated onto a poly-lysine–coated slide and incubated at 37°C for 20 min for adherence. After incubation, cells were gently washed three times with PBS and fixed and permeabilized with BD cytofix/cytoperm (554655; BD Biosciences) for 20 min at room temperature. All subsequent washes and antibody incubations are done with PBS-S (PBS + 1% BSA + 0.1% saponin). Cells were incubated with anti-CDC42 (1:300, 187643; Abcam) for 1 h at room temperature followed by goat anti-rabbit Alexa Fluor 568 (1:300, A11011; ThermoFisher Scientific) for 1 h. Lastly, cells were incubated with phalloidin-Alexa Fluor 647 (1:100, A22287; ThermoFisher Scientific) and anti-giantin Alexa Fluor 488 (1:200, #908701/Poly19087; BioLegend) for 1 h. After washing, cells were mounted with Prolong Diamond (P36970; ThermoFisher Scientific) to a #1.5 coverslip and allowed to cure for 24 h before sealing with nail varnish. Imaging was done using Metamorph on a Zeiss Axio Observer CSU-X confocal microscope with a 63×/1.4 NA objective. Colocalization was conducted in ImageJ software where a segmentation mask was created around the Golgi apparatus (using giantin thresholding) and cell membrane (using CDC42 thresholding) and average intensity signal within the Golgi and the cytoplasm were measured. The ratios between the signal within the Golgi and the cytoplasm were calculated.

SIM-TIRF microscopy and filopodial analysis

A Lab-Tek II 8-well chambered #1.5 coverglass (#155409; Nunc) was coated with 5 µg/ml anti-CD18 (IB4, single batch) and 5 µg/ml anti-CD28.2 (LEAF anti-CD28.2, 302923; BioLegend) and incubated for ≥30 min at 37°C. YTS cells were resuspended in R10 without FBS and phenol red (imaging media) and resuspended in imaging media at ∼50,000 cells/150 µl (0.33e6/ml). 50,000 YTS cells plated in 150 µl imaging media and incubated at 37°C for exactly 20 min. After, cells were immediately fixed with 4% PFA for 20 min at room temperature. Cell were then washed once with PBS and permeabilized with 0.1% Triton X-100 in PBS for 10 min at room temperature. After three additional PBS washes, cells were stained with phalloidin-Alexa Fluor 568 (1:50, A12380; ThermoFisher Scientific) for ≥1 h and cells were imaged thereafter without buffer exchange. Imaging was done on a GE DeltaVision OMX-SR microscope under structured illumination microscopy–total internal reflection fluorescence (SIM-TIRF) mode using a 60×/1.42 PlanApoN objective and a pco.edge 4.2 camera. Images were then reconstructed in GE Softworx using experimentally measured OTF files. Filopodia were manually counted for cells that spread onto the surface on ImageJ. Cells with retraction fibers and not filopodia were omitted from calculation.

Immune cytotoxicity assay for NK cell lines and Pt 2 and Pt 3

For the NK cell line, a chromium-based assay was used. For Pt 2, the DELFIA cytotoxicity assay was used as described below. For Pt 3, a flow cytometric–based cytotoxicity assay was performed similarly to that previously described (Bryceson et al., 2009; Valiathan et al., 2012). Target cells (721.221) were incubated with 100 µCi of ^{51}Cr (sodium chromate in normal saline, NEZ030005MC; PerkinElmer) for 1 h at 37°C, washed three times in complete R10, and resuspended in complete R10 at a final concentration of 10^5 cells/ml. Unlabeled effector YTS cells were washed once in complete R10 and resuspended to a final concentration of 10^6/ml. 10^5 (200 µl) effector cells were plated into the first well of a 96-well, round-bottomed polystyrene tissue culture–treated plate and serially diluted 1:2, except for the spontaneous and total lysis control wells, which contain only target cells. 10^4 ^{51}Cr signal from the LumaPlate was read using a TopCount NXT (PerkinElmer) at the conditions indicated by the manufacturer. Percent lysis is calculated as: [(TopCount measured cpm − spontaneously released cpm)/(total cpm − spontaneously released cpm)] × 100. Total cpm was derived from a target containing well that was lysed with 1% IGEPAL (I3021; Sigma-Aldrich) in water.

The DELFIA cytotoxicity assay is based on loading cells with an acetoxymethyl ester of a fluorescence enhancing ligand. After the ligand has penetrated the cell membrane the ester bonds are hydrolyzed within the cell to form a hydrophilic ligand, which no longer passes through the membrane. After cytolysis, the released ligand is introduced to a europium solution to form a fluorescent chelate. The measured signal correlates directly with the amount of lysed cells. 100 µl of loaded target cells (5,000 cells) is pipetted into a round-bottomed sterile plate, and 100 µl effector cells of varying cell concentration is added. An E/T ratio from 6:1 to 100:1 is commonly used for NK cells. Additional wells containing only target cells are plated for detection of background, spontaneous release, and maximum release. Cells are then incubated 2 and 3 h in a humidified 5% CO_2 atmosphere at

JEM

37°C. After incubation, the plate is centrifuged for 5 min at 500 ×*g*. 20 µl the supernatant is transferred to a flat-bottomed plate with 200 µl Eu solution, the plate is shaken at 250 rpm for 15 min, and fluorescence is measured. Percent lysis is calculated as: [(TopCount measured cpm − spontaneously released cpm)/(total cpm − spontaneously released cpm)] × 100. To measure spontaneous release, incubate the target cells (100 µl) with 100 µl of medium instead of effector cells. After centrifugation, transfer 20 µl of the supernatant to the flat-bottomed plate and add 200 µl Eu solution. Shake for 15 min and measure. To measure maximum release, incubate the target cells (100 µl) with 100 µl of medium supplemented with 10 µl of lysis buffer. After centrifugation, transfer 20 µl of the supernatant to the flat-bottomed plate and add 200 µl Eu solution. Shake for 15 min and measure.

Transwell migration assay for immune cells

A standard Boyden chamber assay was used. Corning transwell polycarbonate membrane cell culture inserts (6.5 mm, 5-µm pore polycarbonate, 3421; Corning) were coated overnight with 10 µg/ml fibronectin in PBS at 4°C. YTS cells were washed once using complete R10 and resuspended to a final concentration of 2–4e6 cells/ml. 600 µl of complete R10 supplemented with 100 ng/ml SDF1a/CXCL12 (300-28A; Peprotech) chemoattractant was plated into a 24-well tissue culture–treated plate. Fibronectin was removed from the transwell, and the transwell was placed into the wells containing CXCL12-supplemented media. 100 µl (200,000–400,000 cells) YTS cells were plated onto the upper chamber of the transwell. The cells were incubated at 37°C for 4 h. After incubation, the cells were counted by measuring the volume in the lower chamber and counting the number of events at medium speed for 1 min on an LSR Fortessa Flow Cytometer. The live events were gated for based on forward scatter (FSC) and side scatter (SSC) and used for the migration measurement. The percent migration was calculated as the number of cells that migrated into the lower chamber divided by the number of cells in a control well (input cell count) containing the same number of cells but no transwell.

Immune conjugation assay

YTS NK cells and 721.221 target cells were washed once with complete R10. YTS cells were then resuspended in PBS at 1e6/ml and incubated with efluor 450 (#65-0842-85; 1:1,000, 10 min, and 37°C; eBioscience). 721.221 cells were resuspended in PBS at 1e6/ml and incubated with Cell Trace CFSE (#C34554; 1:2,000, 10 min, and 37°C). Both labeled cells were then washed once with complete R10 and counted. Labeled YTS cells were resuspended to 1e6/ml and labeled 721.221 cells resuspended to 2e6/ml in complete R10. Cells were then combined at an E/T ratio of 1:2 (100,000 YTS cells:200,000 721.221 cells) and incubated at 37°C for 0, 5, 10, 30, and 60 min. The conjugation reaction was stopped by vortexing for 3 s and fixed with 4% PFA in PBS for ≥10 min before acquisition. Cells were then counted on a BD LSR Fortessa flow cytometer and gated based on negative and single-positive control cells. At least 20,000 live cells were counted based on FSC/SSC gating. Percent conjugation was calculated as: (double-positive cells)/(single-positive eFluor 450/YTS cells + double-positive cells) × 100.

Peripheral blood immunophenotype

All flow cytometric analyses were performed on EDTA blood samples within 24 h of venipuncture. After red blood cell lysis with ammonium chloride, lymphocytes were washed, resuspended in PBS, and stained with the following mouse anti-human antibodies to identify T and B cell subsets: CD45RA APC-H7 (clone T6D11; Miltenyi Biotec), CD3 PerCP (clone BW264/56; Miltenyi Biotec), CCR7 PE (clone 3D12; eBioscience), CD4 APC (clone OKT4; Becton Dickinson), CD8 PE-Cy7 (clone RPA-T8; Becton Dickinson), CD19 PE-CY7 (clone SJ25C1; Becton Dickinson), CD16 PE (clone 3G8), CD56 PE, CD27 FITC (clone M-T271, Becton Dickinson), TCR α-beta APC (clone T10B9; Becton Dickinson), TCR gamma-delta FITC (11F3; Miltenyi Biotec), CD21 PE (clone B-ly4; Becton Dickinson), CD24 PE (clone ML5; Becton Dickinson), IgD FITC (clone IA6-2; Becton Dickinson), Goat F(ab) 2 anti-Human IgM (µ)-Alexa Fluor 647 (Jackson ImmunoResearch), and CD38 FITC (clone HIT2; Becton Dickinson). Cells were incubated with the appropriate antibody cocktail for 30 min at 4°C and then washed with PBS and resuspended in PBS for flow cytometric acquisition. At least 50,000 events were acquired within the lymphogate. Data were acquired on a FACSCanto II (Becton Dickinson) and analyzed with FlowJo software (Tree Star).

Dendritic cell flow cytometric analysis

Dendritic cell analysis was performed with the Blood Dendritic cell enumeration kit (#130-091-086; Miltenyi Biotec). This assay is based on dendritic cell–specific surface antigens CD303 (BDCA-2), CD141 (BDCA-3), and CD1c (BDCA-1). Three distinct dendritic cell subsets were identified in whole blood: plasmacytoid dendritic cells as $CD303^+$ (FITC clone: AC144, BDCA-2), type 1 myeloid dendritic cells (MDC1s) as $CD1c^+$ (PE clone: AD5-8E7, BDCA-1), and type 2 myeloid dendritic cells (MDC2s) as $CD141^+$ (APC clone: Ad4-14H12, BDCA-3) surface expression. Gate exclusion for CD19, CD14, and dead cells was performed. After 10 min of incubation in ice with the mix of antibodies, red blood cells were lysed. Cells were washed with PBS, fixed with 1% PFA for 10 min, acquired with a FACSCanto II (Becton Dickinson), and analyzed with FlowJo software (Tree Star Inc.; version 8.8.6). At least 10^6 total events were acquired.

Clinical flow cytometry for BM analysis/composition

The detailed protocol for whole BM staining has been previously reported (Basso-Ricci et al., 2017). In brief, Precision Count beads (BioLegend) were added to 100 µl of P1 BM sample to allow absolute quantification of hematopoietic cell subsets, and red blood cell lysis was performed. The lysed sample was labeled with fluorescent antibodies for CD3-BV605, CD56-PE-Cy5, CD14-BV510, CD61/41-PE-Cy7, CD135-PE, CD34-BV421, CD45RA-APC-Cy7 (BioLegend), CD33-BB515, CD66b-BB515, CD38-BUV737, CD45-BUV395, CD90-APC, CD10-BV786, CD11c-BV650, CD19-APCR700, CD7-PE-Cy5.5, and CD71-BV711 (BD Biosciences). Titration assays were performed to assess the best antibody concentration. After surface marking, the cells were incubated

JEM

with PI (BioLegend) to stain dead cells. All samples were acquired using a BD LSR Fortessa (BD Bioscience) flow cytometer after calibration with SPHERO rainbow calibration particles (Spherotech), and raw data were collected using BD FACSDIVA software. The data were subsequently analyzed with FlowJo software, and the graphical output was automatically generated using GraphPad Prism.

Functional characterization of proliferation and migration of CD34⁺ cells

Purification of CD34⁺ cells was performed by two steps of immunomagnetic selection (CD34⁺ microbeads, 130-097-047; Miltenyi Biotec). For proliferation, 10^4 BM CD34⁺ cells were stimulated with stem cell factor (SCF; 100 ng/ml) or a growth factor mixture (SCF 300 ng/ml, thrombopoietin 100 ng/ml, IL3 60 ng/ml). Proliferation was evaluated at day 5 of stimulation by 16 h liquid scintillation counting of ^{3}H-thymidine (Amersham Biosciences). The stimulation index was calculated as the ratio between stimulated and nonstimulated cells. For the transwell migration assay, 0.5×10^6 peripheral blood lymphocytes or 0.5×10^4 BM CD34⁺ cells were seeded on a transwell chambers in presence of SDF1-α/CXCL12 (100 ng/ml; Peprotech). Migration was assessed after 3 h. To evaluate clonogenic potential of CDC42⁻ cells, 2×10^5 BM mononuclear cells as well as 10^3 BM CD34⁺ cells were plated in Methocult medium (H4434; Stemcell Technologies), and the number of colony-forming units per cell was scored at day 14 to determine number and type of colonies.

BM mononuclear cells stimulation and cytokine measurements

BM mononuclear cells were isolated from HD (n = 3) and Pt BM and were left unstimulated or stimulated with LPS (10 µg/ml) for 5 h, with or without the addition of ATP (1 mM) for an additional hour. Secreted cytokines were measured by in conditioned media. Plasma and supernatant levels of IFNγ, CXCL9, and IL-6 were assessed using enzyme-linked immunosorbent assays with human Duoset ELISA kits, and IL-1β plasma levels were measured using the high-sensitivity quantikine ELISA kit (all purchased from R&D Systems). Plasma IL-18 levels were measured using an ELISA kit obtained from MBL.

C. elegans studies

WT *cdc-42* cDNA (open reading frame clone R07G3.1; ThermoFisher Scientific) was cloned into the pPD49.83 heat shock–inducible vector (a kind gift of Andrew Fire, Stanford University, Stanford, CA). The c.556_558AAG>TGT trinucleotide substitution (p.K186C corresponding to human p.R186C) was introduced by site-directed mutagenesis (Stratagene). Germline transformation and genetic crosses were performed using standard techniques. Constructs were injected at a concentration of 100 ng/ml. The pJM67 plasmid (p*elt-2*::NLS::GFP; 30 ng/ml) was used as coinjection marker. To explore vulval defects, synchronized animals from three independent lines for each construct were grown at 20°C and heat shocked (33°C, 90 min followed by 30°C, 30 min) in parallel at the early (Muv and Vul) or mid (Pvl) L3 larval stages. Adults were scored blindly at a Leica MZ10F dissecting microscope to check for the presence of Pvl phenotype, multiple ectopic pseudovulvae (Muv phenotype) and lack of a vulva (Vul phenotype). After each cross, the genotype was confirmed by Sanger sequencing. Isogenic worms that had lost the transgene were cloned separately and used as controls. Microscopy observations were performed with a Nikon Eclipse 80i instrument equipped with Nomarski differential interference contrast optics on live animals mounted on 2% agarose pads containing 10 mM sodium azide as anesthetic. The N2 (Bristol) and PS21 (*let-23*(*syl*), *let-23/EGFR* hypomorphic allele) strains were provided by the *Caenorhabditis* Genetics Center, which is funded by the National Institutes of Health Office of Research Infrastructure Programs (P40 OD010440).

Statistical analyses

Data are represented as means ± SD or SEM where indicated. Statistical analyses were conducted in GraphPad Prism. WB of patient CDC42 expression intensity measurements and protein localization intensity measurements were analyzed with the Student's t test. GTPase function assays were analyzed using a Student's t test. For variance analysis in pull-down assays, an ordinary one-way ANOVA was performed using the Sidak's multiple comparison test. Proliferation assays were analyzed using either a two-way ANOVA with Dunnett's multiple comparisons for patient fibroblasts. Migration assays were assessed using a Student's t test (for YTS NK cell and primary fibroblasts) or a two-way ANOVA with Tukey's multiple comparisons (for NIH-3T3 cells). Multipolarity cell counts, filopodia number, and filopodia length were assessed using a Welch's t test. NK cell cytotoxicity was assessed using the Mann–Whitney U test of three pooled replicates. NK cell conjugation was assessed using a Welch's t test. For *C. elegans* studies, P values were calculated using two-tailed Fisher's exact test. All remaining assays were performed with n of ≤2. Statistical significance is indicated with asterisks (*, $P < 0.05$; **, $P < 0.01$; ***, $P < 0.001$; ****, $P < 0.0001$) for all tests except two-tailed Fisher's exact test (*, $P < 0.005$; **, $P < 0.00002$, ***, $P < 1.2e^{-6}$).

Online supplemental material

Table S1 reports clinical laboratory data for Pt 1 and Pt 2. Table S2 shows the hematological and immunological profiles of Pt 1–3. Table S3 provide WES/WGS metrics and data output. Table S4 reports on the vulval phenotypes in transgenic *C. elegans* expressing WT CDC-42 or the K186C, R68Q, and A159V disease-causing mutants. Table S5 reports on the clonogenic assay of BM cells from Pt 1.

Acknowledgments

We would like to thank the Baylor College of Medicine Medical Scientist Training Program for training support.

This work was supported by grants from Fondazione Bambino Gesù (Vite Coraggiose to M. Tartaglia), Italian Ministry of Health (Ricerca Corrente to F. Locatelli, C. Cancrini, F. De Benedetti and M. Tartaglia; Ricerca Finalizzata NET-2011-02350069 to C. Cancrini and A. Aiuti), Associazione Italiana per la Ricerca sul Cancro (IG21614 to M. Tartaglia), National Institutes of Health (R01AI120989-05 and R01AI067946 to J.S. Orange),

JEM

National Human Genome Research Institute/National Heart, Lung, and Blood Institute (grant UM1HG006542 to the Baylor-Hopkins Center for Mendelian Genomics), German Research Foundation (AH 92/8-1 to M.R. Ahmadian), German Federal Ministry of Education and Research (01GM1902C to M.R. Ahmadian), German Research Foundation (International Research Training Group 1902 Intra- and Interorgan Communication of the Cardiovascular System, IRTG 1902-P6, to M.R. Ahmadian), and E-Rare (NSEuroNet to M.R. Ahmadian and M. Tartaglia; and EUROCID to C. Cancrini and A. Aiuti).

The authors declare no competing financial interests.

Author contributions: M.T. Lam and S. Coppola performed the in vitro studies and contributed to manuscript drafting; O.H.F. Krumbach, M. Akbarzadeh, A. Pastore, S. Levi Mortera, S. Camerini, L. Farina, M. Buchholzer, R. Dvorsky, L. Pannone, and P. Janning performed the in silico, biochemical, and MS analyses; G. Prencipe, C. Cifaldi, I. Brigida, S. Scala, S. Di Cesare, A. Pascarella, F. Conti, P. Merli, L. Farina, L. Basso-Ricci, M. Chiriaco, R. Carsetti, Y.T. Bryceson, L. Torralba-Raga, K. Ramme, V. Rosti, C. Bracaglia, and V. Messia performed the hematological and immunological studies; E. Zara, P. Netter, A.F. Carisey, M. Diehl, and E.M. Mace performed the in vitro studies and assisted with experimental design and data analysis; A. Insalaco, A. Stray-Pedersen, H.C. Erichsen, A.C. Horne, K. Ramme, P. Palma, A. Finocchi, F. Locatelli, C. Cancrini, and A. Aiuti provided the clinical data and biological material; S. Martinelli, L. Pannone, and M. Di Rocco performed the *C. elegans* studies; M. Niceta, F. Pantaleoni, A. Ciolfi, T.N. Cao, Z.H. Coban-Akdemir, S.N. Jhangiani, D.M. Muzny, R.A. Gibbs, A.C. Horne, Y.T. Bryceson, L. Torralba-Raga, I.K. Chinn, J.R. Lupski, and E.M. Mace contributed to the genomic analyses; and M.R. Ahmadian, J.S. Orange, F. De Benedetti, and M. Tartaglia coordinated the study, conceived and designed the experiments, analyzed the data, and contributed to manuscript drafting.

Submitted: 23 January 2019
Revised: 19 April 2019
Accepted: 6 August 2019

References

Aicart-Ramos, C., R.A. Valero, and I. Rodriguez-Crespo. 2011. Protein palmitoylation and subcellular trafficking. *Biochimica et Biophysica Acta (BBA) -. Biomembranes*. 1808:2981–2994. https://doi.org/10.1016/j.bbamem.2011.07.009

Baschieri, F., S. Confalonieri, G. Bertalot, P.P. Di Fiore, W. Dietmaier, M. Leist, P. Crespo, I.G. Macara, and H. Farhan. 2014. Spatial control of Cdc42 signalling by a GM130-RasGRF complex regulates polarity and tumorigenesis. *Nat. Commun.* 5:4839. https://doi.org/10.1038/ncomms5839

Basso-Ricci, L., S. Scala, R. Milani, M. Migliavacca, A. Rovelli, M.E. Bernardo, F. Ciceri, A. Aiuti, and L. Biasco. 2017. Multiparametric Whole Blood Dissection: A one-shot comprehensive picture of the human hematopoietic system. *Cytometry A.* 91:952–965. https://doi.org/10.1002/cyto.a.23148

Bauer, C.K., P. Calligari, F.C. Radio, V. Caputo, M.L. Dentici, N. Falah, F. High, F. Pantaleoni, S. Barresi, A. Ciolfi, et al. 2018. Mutations in KCNK4 that Affect Gating Cause a Recognizable Neurodevelopmental Syndrome. *Am. J. Hum. Genet.* 103:621–630. https://doi.org/10.1016/j.ajhg.2018.09.001

Bracaglia, C., K. de Graaf, D. Pires Marafon, F. Guilhot, W. Ferlin, G. Prencipe, I. Caiello, S. Davì, G. Schulert, A. Ravelli, et al. 2017. Elevated circulating levels of interferon-γ and interferon-γ-induced chemokines characterise patients with macrophage activation syndrome complicating systemic juvenile idiopathic arthritis. *Ann. Rheum. Dis.* 76:166–172. https://doi.org/10.1136/annrheumdis-2015-209020

Brigida, I., M. Zoccolillo, M.P. Cicalese, L. Pfajfer, F. Barzaghi, S. Scala, C. Oleaga-Quintas, J.A. Álvarez-Álvarez, L. Sereni, S. Giannelli, et al. 2018. T-cell defects in patients with *ARPC1B* germline mutations account for combined immunodeficiency. *Blood.* 132:2362–2374.

Bryceson, Y.T., C. Fauriat, J.M. Nunes, S.M. Wood, N.K. Björkström, E.O. Long, and H.-G. Ljunggren. 2009. Natural Killer Cell Protocols, Cellular and Molecular Methods. *Methods Mol. Biol.* 612:335–352. https://doi.org/10.1007/978-1-60761-362-6_23

Canna, S.W., A.A. de Jesus, S. Gouni, S.R. Brooks, B. Marrero, Y. Liu, M.A. DiMattia, K.J.M. Zaal, G.A.M. Sanchez, H. Kim, et al. 2014. An activating NLRC4 inflammasome mutation causes autoinflammation with recurrent macrophage activation syndrome. *Nat. Genet.* 46:1140–1146. https://doi.org/10.1038/ng.3089

Caye, A., M. Strullu, F. Guidez, B. Cassinat, S. Gazal, O. Fenneteau, E. Lainey, K. Nouri, S. Nakhaei-Rad, R. Dvorsky, et al. 2015. Juvenile myelomonocytic leukemia displays mutations in components of the RAS pathway and the PRC2 network. *Nat. Genet.* 47:1334–1340. https://doi.org/10.1038/ng.3420

Chinn, I.K., O.S. Eckstein, E.C. Peckham-Gregory, B.R. Goldberg, L.R. Forbes, S.K. Nicholas, E.M. Mace, T.P. Vogel, H.A. Abhyankar, M.I. Diaz, et al. 2018. Genetic and mechanistic diversity in pediatric hemophagocytic lymphohistiocytosis. *Blood.* 132:89–100. https://doi.org/10.1182/blood-2017-11-814244

Chung, L.K., N.H. Philip, V.A. Schmidt, A. Koller, T. Strowig, R.A. Flavell, I.E. Brodsky, and J.B. Bliska. 2014. IQGAP1 is important for activation of caspase-1 in macrophages and is targeted by Yersinia pestis type III effector YopM. *MBio.* 5:e01402–e01414. https://doi.org/10.1128/mBio.01402-14

Cingolani, P., A. Platts, L. Wang, M. Coon, T. Nguyen, L. Wang, S.J. Land, X. Lu, and D.M. Ruden. 2012. A program for annotating and predicting the effects of single nucleotide polymorphisms, SnpEff: SNPs in the genome of Drosophila melanogaster strain w1118; iso-2; iso-3. *Fly (Austin).* 6:80–92. https://doi.org/10.4161/fly.19695

Dasouki, M., K.C. Okonkwo, A. Ray, C.K. Folmsbeel, D. Gozales, S. Keles, J.M. Puck, and T. Chatila. 2011. Deficient T Cell Receptor Excision Circles (TRECs) in autosomal recessive hyper IgE syndrome caused by DOCK8 mutation: implications for pathogenesis and potential detection by newborn screening. *Clin. Immunol.* 141:128–132. https://doi.org/10.1016/j.clim.2011.06.003

Dvorsky, R., and M.R. Ahmadian. 2004. Always look on the bright site of Rho: structural implications for a conserved intermolecular interface. *EMBO Rep.* 5:1130–1136. https://doi.org/10.1038/sj.embor.7400293

Etienne-Manneville, S. 2004. Cdc42--the centre of polarity. *J. Cell Sci.* 117:1291–1300. https://doi.org/10.1242/jcs.01115

Etienne-Manneville, S., and A. Hall. 2002. Rho GTPases in cell biology. *Nature*. 420:629–635. https://doi.org/10.1038/nature01148

Flex, E., M. Niceta, S. Cecchetti, I. Thiffault, M.G. Au, A. Capuano, E. Piermarini, A.A. Ivanova, J.W. Francis, G. Chillemi, et al. 2016. Biallelic Mutations in TBCD, Encoding the Tubulin Folding Cofactor D, Perturb Microtubule Dynamics and Cause Early-Onset Encephalopathy. *Am. J. Hum. Genet.* 99:962–973. https://doi.org/10.1016/j.ajhg.2016.08.003

Fukata, M., T. Watanabe, J. Noritake, M. Nakagawa, M. Yamaga, S. Kuroda, Y. Matsuura, A. Iwamatsu, F. Perez, and K. Kaibuchi. 2002. Rac1 and Cdc42 capture microtubules through IQGAP1 and CLIP-170. *Cell.* 109:873–885. https://doi.org/10.1016/S0092-8674(02)00800-0

Gibson, R.M., and A.L. Wilson-Delfosse. 2001. RhoGDI-binding-defective mutant of Cdc42Hs targets to membranes and activates filopodia formation but does not cycle with the cytosol of mammalian cells. *Biochem. J.* 359:285–294. https://doi.org/10.1042/bj3590285

Gibson, R.M., P.N. Gandhi, X. Tong, J. Miyoshi, Y. Takai, M. Konieczkowski, J.R. Sedor, and A.L. Wilson-Delfosse. 2004. An activating mutant of Cdc42 that fails to interact with Rho GDP-dissociation inhibitor localizes to the plasma membrane and mediates actin reorganization. *Exp. Cell Res.* 301:211–222. https://doi.org/10.1016/j.yexcr.2004.07.033

Grom, A.A., A. Horne, and F. De Benedetti. 2016. Macrophage activation syndrome in the era of biologic therapy. *Nat. Rev. Rheumatol.* 12:259–268. https://doi.org/10.1038/nrrheum.2015.179

Harapas, C.R., A. Steiner, S. Davidson, and S.L. Masters. 2018. An Update on Autoinflammatory Diseases: Inflammasomopathies. *Curr. Rheumatol. Rep.* 20:40. https://doi.org/10.1007/s11926-018-0750-4

Henter, J.I., A. Horne, M. Aricó, R.M. Egeler, A.H. Filipovich, S. Imashuku, S. Ladisch, K. McClain, D. Webb, J. Winiarski, and G. Janka. 2007. HLH-

2004: Diagnostic and therapeutic guidelines for hemophagocytic lymphohistiocytosis. *Pediatr. Blood Cancer.* 48:124–131. https://doi.org/10.1002/pbc.21039

Hoffman, G.R., N. Nassar, and R.A. Cerione. 2000. Structure of the Rho family GTP-binding protein Cdc42 in complex with the multifunctional regulator RhoGDI. *Cell.* 100:345–356. https://doi.org/10.1016/S0092-8674(00)80670-4

Hsu, A.P., A. Donkó, M.E. Arrington, M. Swamydas, D. Fink, A. Das, O. Escobedo, V. Bonagura, P. Szabolcs, H.N. Steinberg, et al. 2019. Dominant activating RAC2 mutation with lymphopenia, immunodeficiency, and cytoskeletal defects. *Blood.* 133:1977–1988. https://doi.org/10.1182/blood-2018-11-886028

Jacquemet, G., H. Hamidi, and J. Ivaska. 2015. Filopodia in cell adhesion, 3D migration and cancer cell invasion. *Curr. Opin. Cell Biol.* 36:23–31. https://doi.org/10.1016/j.ceb.2015.06.007

Jagadeesh, K.A., A.M. Wenger, M.J. Berger, H. Guturu, P.D. Stenson, D.N. Cooper, J.A. Bernstein, and G. Bejerano. 2016. M-CAP eliminates a majority of variants of uncertain significance in clinical exomes at high sensitivity. *Nat. Genet.* 48:1581–1586. https://doi.org/10.1038/ng.3703

Jamilloux, Y., F. Magnotti, A. Belot, and T. Henry. 2018. The pyrin inflammasome: from sensing RhoA GTPases-inhibiting toxins to triggering autoinflammatory syndromes. *Pathog. Dis.* 76:fty020. https://doi.org/10.1093/femspd/fty020

Jordan, M.B., C.E. Allen, S. Weitzman, A.H. Filipovich, and K.L. McClain. 2011. How I treat hemophagocytic lymphohistiocytosis. *Blood.* 118:4041–4052. https://doi.org/10.1182/blood-2011-03-278127

Kim, M.L., J.J. Chae, Y.H. Park, D. De Nardo, R.A. Stirzaker, H.-J. Ko, H. Tye, L. Cengia, L. DiRago, D. Metcalf, et al. 2015. Aberrant actin depolymerization triggers the pyrin inflammasome and autoinflammatory disease that is dependent on IL-18, not IL-1β. *J. Exp. Med.* 212:927–938. https://doi.org/10.1084/jem.20142384

Kircher, M., D.M. Witten, P. Jain, B.J. O'Roak, G.M. Cooper, and J. Shendure. 2014. A general framework for estimating the relative pathogenicity of human genetic variants. *Nat. Genet.* 46:310–315. https://doi.org/10.1038/ng.2892

Li, W., X. Sun, J. Wang, Q. Zhao, R. Dai, Y. Wang, L. Zhou, L. Westerberg, Y. Ding, X. Zhao, and C. Liu. 2017. Defective thymic output in WAS patients is associated with abnormal actin organization. *Sci. Rep.* 7:11978. https://doi.org/10.1038/s41598-017-12345-z

Liu, X., X. Jian, and E. Boerwinkle. 2013. dbNSFP v2.0: a database of human non-synonymous SNVs and their functional predictions and annotations. *Hum. Mutat.* 34:E2393–E2402. https://doi.org/10.1002/humu.22376

Locatelli, F., P. Merli, D. Pagliara, G. Li Pira, M. Falco, D. Pende, R. Rondelli, B. Lucarelli, L.P. Brescia, R. Masetti, et al. 2017. Outcome of children with acute leukemia given HLA-haploidentical HSCT after αβ T-cell and B-cell depletion. *Blood.* 130:677–685. https://doi.org/10.1182/blood-2017-04-779769

Martinelli, S., O.H.F. Krumbach, F. Pantaleoni, S. Coppola, E. Amin, L. Pannone, K. Nouri, L. Farina, R. Dvorsky, F. Lepri, et al. University of Washington Center for Mendelian Genomics. 2018. Functional Dysregulation of CDC42 Causes Diverse Developmental Phenotypes. *Am. J. Hum. Genet.* 102:309–320. https://doi.org/10.1016/j.ajhg.2017.12.015

Mattila, P.K., and P. Lappalainen. 2008. Filopodia: molecular architecture and cellular functions. *Nat. Rev. Mol. Cell Biol.* 9:446–454. https://doi.org/10.1038/nrm2406

Nouri, K., D.J. Timson, and M.R. Ahmadian. 2017. New model for the interaction of IQGAP1 with CDC42 and RAC1. *Small GTPases.*:1–7. https://doi.org/10.1080/21541248.2017.1321169

Okamura, H., H. Tsutsi, T. Komatsu, M. Yutsudo, A. Hakura, T. Tanimoto, K. Torigoe, T. Okura, Y. Nukada, K. Hattori, et al. 1995. Cloning of a new cytokine that induces IFN-γ production by T cells. *Nature.* 378:88–91. https://doi.org/10.1038/378088a0

Orange, J.S., N. Ramesh, E. Remold-O'Donnell, Y. Sasahara, L. Koopman, M. Byrne, F.A. Bonilla, F.S. Rosen, R.S. Geha, and J.L. Strominger. 2002. Wiskott-Aldrich syndrome protein is required for NK cell cytotoxicity and colocalizes with actin to NK cell-activating immunologic synapses. *Proc. Natl. Acad. Sci. USA.* 99:11351–11356. https://doi.org/10.1073/pnas.162376099

Phillips, M.J., G. Calero, B. Chan, S. Ramachandran, and R.A. Cerione. 2008. Effector proteins exert an important influence on the signaling-active state of the small GTPase Cdc42. *J. Biol. Chem.* 283:14153–14164. https://doi.org/10.1074/jbc.M706271200

Reiner, D.J., and E.A. Lundquist. 2018. Small GTPases. *WormBook.* 2018:1–65. https://doi.org/10.1895/wormbook.1.67.2

Ridley, A.J., M.A. Schwartz, K. Burridge, R.A. Firtel, M.H. Ginsberg, G. Borisy, J.T. Parsons, and A.R. Horwitz. 2003. Cell migration: integrating signals from front to back. *Science.* 302:1704–1709. https://doi.org/10.1126/science.1092053

Romberg, N., K. Al Moussawi, C. Nelson-Williams, A.L. Stiegler, E. Loring, M. Choi, J. Overton, E. Meffre, M.K. Khokha, A.J. Huttner, et al. 2014. Mutation of NLRC4 causes a syndrome of enterocolitis and autoinflammation. *Nat. Genet.* 46:1135–1139. https://doi.org/10.1038/ng.3066

Rosado, F.G.N., and A.S. Kim. 2013. Hemophagocytic lymphohistiocytosis: an update on diagnosis and pathogenesis. *Am. J. Clin. Pathol.* 139:713–727. https://doi.org/10.1309/AJCP4ZDKJ4ICOUAT

Seeland, I., Y. Xiong, C. Orlik, D. Deibel, S. Prokosch, G. Küblbeck, B. Jahraus, D. De Stefano, S. Moos, F.C. Kurschus, et al. 2018. The actin remodeling protein cofilin is crucial for thymic αβ but not γδ T-cell development. *PLoS Biol.* 16:e2005380. https://doi.org/10.1371/journal.pbio.2005380

Sepulveda, F.E., and G. de Saint Basile. 2017. Hemophagocytic syndrome: primary forms and predisposing conditions. *Curr. Opin. Immunol.* 49:20–26. https://doi.org/10.1016/j.coi.2017.08.004

Sinai, P., C. Nguyen, J.D. Schatzle, and C. Wülfing. 2010. Transience in polarization of cytolytic effectors is required for efficient killing and controlled by Cdc42. *Proc. Natl. Acad. Sci. USA.* 107:11912–11917. https://doi.org/10.1073/pnas.0913422107

Stray-Pedersen, A., H.S. Sorte, P. Samarakoon, T. Gambin, I.K. Chinn, Z.H. Coban Akdemir, H.C. Erichsen, L.R. Forbes, S. Gu, B. Yuan, et al. 2017. Primary immunodeficiency diseases: Genomic approaches delineate heterogeneous Mendelian disorders. *J. Allergy Clin. Immunol.* 139:232–245. https://doi.org/10.1016/j.jaci.2016.05.042

Swart-Mataraza, J.M., Z. Li, and D.B. Sacks. 2002. IQGAP1 is a component of Cdc42 signaling to the cytoskeleton. *J. Biol. Chem.* 277:24753–24763. https://doi.org/10.1074/jbc.M111165200

Takenouchi, T., R. Kosaki, T. Niizuma, K. Hata, and K. Kosaki. 2015. Macrothrombocytopenia and developmental delay with a de novo CDC42 mutation: Yet another locus for thrombocytopenia and developmental delay. *Am. J. Med. Genet. A.* 167A:2822–2825. https://doi.org/10.1002/ajmg.a.37275

Valdés-Mora, F., and J.C. Lacal. 2011. CDC42 (cell division cycle 42 (GTP binding protein, 25kDa)). *Atlas Genet. Cytogenet. Oncol. Haematol.* (11). https://doi.org/10.4267/2042/44606

Valiathan, R., J.E. Lewis, A.B. Melillo, S. Leonard, K.H. Ali, and D. Asthana. 2012. Evaluation of a flow cytometry-based assay for natural killer cell activity in clinical settings. *Scand. J. Immunol.* 75:455–462. https://doi.org/10.1111/j.1365-3083.2011.02667.x

Weiss, E.S., C. Girard-Guyonvarc'h, D. Holzinger, A.A. de Jesus, Z. Tariq, J. Picarsic, E.J. Schiffrin, D. Foell, A.A. Grom, S. Ammann, et al. 2018. Interleukin-18 diagnostically distinguishes and pathogenically promotes human and murine macrophage activation syndrome. *Blood.* 131:1442–1455. https://doi.org/10.1182/blood-2017-12-820852

Yang, L., L. Wang, H. Geiger, J.A. Cancelas, J. Mo, and Y. Zheng. 2007a. Rho GTPase Cdc42 coordinates hematopoietic stem cell quiescence and niche interaction in the bone marrow. *Proc. Natl. Acad. Sci. USA.* 104:5091–5096. https://doi.org/10.1073/pnas.0610819104

Yang, L., L. Wang, T.A. Kalfa, J.A. Cancelas, X. Shang, S. Pushkaran, J. Mo, D.A. Williams, and Y. Zheng. 2007b. Cdc42 critically regulates the balance between myelopoiesis and erythropoiesis. *Blood.* 110:3853–3861. https://doi.org/10.1182/blood-2007-03-079582

Zhou, Y., J.L. Johnson, R.A. Cerione, and J.W. Erickson. 2013. Prenylation and membrane localization of Cdc42 are essential for activation by DOCK7. *Biochemistry.* 52:4354–4363. https://doi.org/10.1021/bi301688g

Chapter IV

Activating Mutations of *RRAS2* Are a Rare Cause of Noonan Syndrome

Graphical abstract

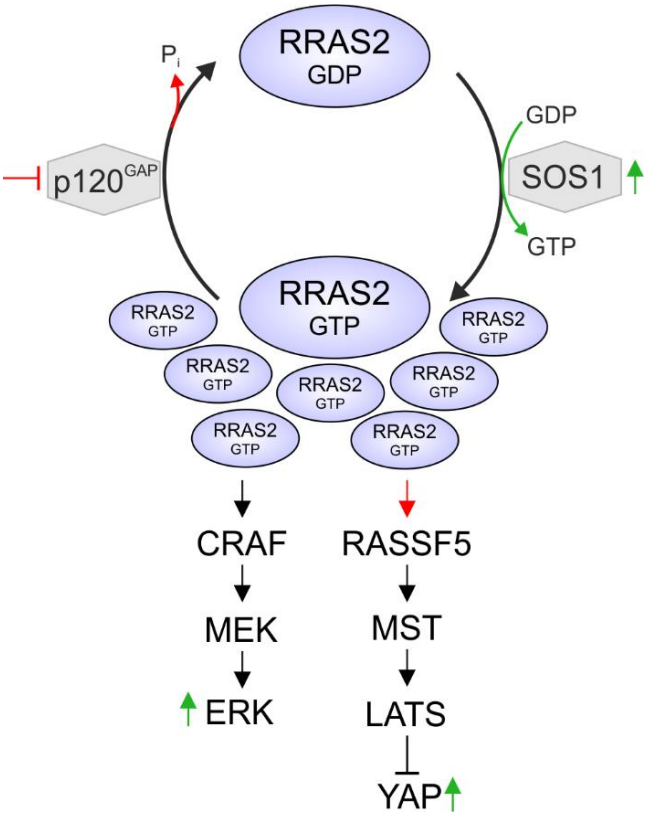

Status: Published in The American Journal of Human Genetics, June 6th, 2019

Impact factor: 9.924

Own proportion: 25 %

Expression and purification of RRAS2 variants, effectors and regulators, structural analyses, interaction studies, GTP hydrolysis assay, figure preparation, writing the manuscript, discussion.

REPORT

Activating Mutations of *RRAS2* Are a Rare Cause of Noonan Syndrome

Yline Capri,[1,20] Elisabetta Flex,[2,20] Oliver H.F. Krumbach,[3,20] Giovanna Carpentieri,[2,4] Serena Cecchetti,[5] Christina Lißewski,[6] Soheila Rezaei Adariani,[3] Denny Schanze,[6] Julia Brinkmann,[6] Juliette Piard,[7] Francesca Pantaleoni,[4] Francesca R. Lepri,[4] Elaine Suk-Ying Goh,[8] Karen Chong,[9] Elliot Stieglitz,[10] Julia Meyer,[10] Alma Kuechler,[11] Nuria C. Bramswig,[11] Stephanie Sacharow,[12] Marion Strullu,[1,13] Yoann Vial,[1,13] Cédric Vignal,[1] George Kensah,[14] Goran Cuturilo,[15,16] Neda S. Kazemein Jasemi,[3] Radovan Dvorsky,[3] Kristin G. Monaghan,[17] Lisa M. Vincent,[17,18] Hélène Cavé,[1,13] Alain Verloes,[1,19] Mohammad R. Ahmadian,[3,21] Marco Tartaglia,[4,21,*] and Martin Zenker[6,21,*]

Aberrant signaling through pathways controlling cell response to extracellular stimuli constitutes a central theme in disorders affecting development. Signaling through RAS and the MAPK cascade controls a variety of cell decisions in response to cytokines, hormones, and growth factors, and its upregulation causes Noonan syndrome (NS), a developmental disorder whose major features include a distinctive facies, a wide spectrum of cardiac defects, short stature, variable cognitive impairment, and predisposition to malignancies. NS is genetically heterogeneous, and mutations in more than ten genes have been reported to underlie this disorder. Despite the large number of genes implicated, about 10%–20% of affected individuals with a clinical diagnosis of NS do not have mutations in known RASopathy-associated genes, indicating that additional unidentified genes contribute to the disease, when mutated. By using a mixed strategy of functional candidacy and exome sequencing, we identify *RRAS2* as a gene implicated in NS in six unrelated subjects/families. We show that the NS-causing *RRAS2* variants affect highly conserved residues localized around the nucleotide binding pocket of the GTPase and are predicted to variably affect diverse aspects of RRAS2 biochemical behavior, including nucleotide binding, GTP hydrolysis, and interaction with effectors. Additionally, all pathogenic variants increase activation of the MAPK cascade and variably impact cell morphology and cytoskeletal rearrangement. Finally, we provide a characterization of the clinical phenotype associated with *RRAS2* mutations.

Noonan syndrome (NS [MIM: PS163950]) is one of the most common monogenic disorders affecting development and growth.[1] The phenotype of NS comprises a distinctive facies (e.g., hypertelorism, downslanting palpebral fissures, ptosis, and low-set/posteriorly rotated ears), cardiac abnormalities (a wide spectrum of congenital heart defects and cardiomyopathy), postnatally reduced growth, skeletal defects (chest and spine), cryptorchidism, bleeding diathesis, as well as variable neurocognitive impairment and predisposition to malignancies,[1,2] most commonly juvenile myelomonocytic leukemia (JMML [MIM: 607785]).[3] NS is generally transmitted as an autosomal-dominant trait and is genetically heterogeneous. So far, pathogenic variants in more than ten genes have been reported as causative events underlying this disorder.[4] While mutations in *PTPN11* (MIM: 176876), *SOS1* (MIM: 182530), *RAF1* (MIM: 164760), and *RIT1* (MIM: 609591) have been documented to occur most frequently,[5–11] a smaller proportion of cases has been ascribed to mutations in other functionally related genes, including *NRAS* (MIM: 164790), *KRAS* (MIM: 190070), *BRAF* (MIM: 164757), *MAP2K1* (MIM: 176872), *SOS2* (MIM: 601247), *LZTR1* (MIM: 600574), *MRAS* (MIM: 608435), and *RASA2* (MIM: 601589).[12–20] Although the causal link between mutations in a subset of these genes and the disorder still remains to be confirmed,[4] the accumulated molecular evidence strongly supports the view that NS is caused by upregulated intracellular traffic through the RAS-mitogen-activated protein kinase (MAPK) signaling pathway.[21,22] Other disorders clinically related to NS (e.g., cardio-facio-cutaneous syndrome [MIM: PS115150], Costello syndrome [MIM: 218040], neurofibromatosis type 1 [MIM: 162200], Legius syndrome [MIM: 611431], Mazzanti syndrome [MIM: 607721], and Noonan syndrome with multiple lentigines

[1]Département de Génétique, Assistance Publique des Hôpitaux de Paris (AP-HP) Hôpital Robert Debré, 75019 Paris, France; [2]Department of Oncology and Molecular Medicine, Istituto Superiore di Sanità, 00161 Rome, Italy; [3]Institute of Biochemistry and Molecular Biology II, Medical Faculty of the Heinrich Heine University, 40225 Düsseldorf, Germany; [4]Genetics and Rare Diseases Research Division, Ospedale Pediatrico Bambino Gesù, IRCCS, 00146 Rome, Italy; [5]Microscopy Area, Core Facilities, Istituto Superiore di Sanità, 00161 Rome, Italy; [6]Institute of Human Genetics, University Hospital Magdeburg, 39120 Magdeburg, Germany; [7]Human Genetic Center – CHU St Jacques, 25000 Besancon, France; [8]Laboratory Medicine and Genetics, Trillium Health Partners, Mississauga, ON L5M 2N1, Canada; [9]Department of Obstetrics and Gynecology, The Prenatal Diagnosis and Medical Genetics Program, Mount Sinai Hospital, Toronto, ON M5G 1Z5, Canada; [10]Department of Pediatrics, Benioff Children's Hospital, University of California, San Francisco, San Francisco, CA 94107, USA; [11]Institut für Humangenetik, Universitätsklinikum Essen, Universität Duisburg-Essen, 45147 Essen, Germany; [12]Boston Children's Hospital and Harvard Medical School, Boston, MA 02115, USA; [13]INSERM UMR 1131, Institut de Recherche Saint-Louis, Université de Paris, 75010 Paris, France; [14]Department of Thoracic and Cardiovascular Surgery, University Medical Center Göttingen, 37075 Göttingen, Germany; [15]Faculty of Medicine, University of Belgrade, 11000 Belgrade, Serbia; [16]University Children's Hospital, 11000 Belgrade, Serbia; [17]GeneDx, Gaithersburg, MD 20877, USA; [18]Center for Cancer of Blood Disorders, Children's National Health System, Washington, DC 20010, USA; [19]INSERM UMR 1141 - Université de Paris, 75019 Paris, France
[20]These authors contributed equally to this work
[21]These authors contributed equally to this work
*Correspondence: marco.tartaglia@opbg.net (M.T.), martin.zenker@med.ovgu.de (M.Z.)
https://doi.org/10.1016/j.ajhg.2019.04.013.

[MIM: PS151100]) are also caused by mutations in genes encoding key proteins of the RAS-MAPK signaling backbone or upstream regulators (i.e., *CBL*, *HRAS*, *KRAS*, *NF1*, *SPRED1*, *SHOC2*, *BRAF*, *MAP2K1*, and *MAP2K2*).[21,22] In all these related conditions, termed RASopathies, increased signaling through RAS and the MAPK cascade can result from upregulated activity of RAS proteins, enhanced function of upstream signal transducers (e.g., proteins positively controlling RAS function) or downstream RAS effectors, as well as from the inefficient signaling switch-off by feedback mechanisms (e.g., neurofibromin and CBL loss of function). More recently, the use of whole-exome sequencing (WES) has allowed the discovery of RASopathy-associated genes encoding signal transducers or modulators that do not belong to the canonical RAS-MAPK pathway, but when functionally perturbed, are predicted to impact RAS signaling by still poorly characterized circuits.[20,23–29]

A remarkable finding of the molecular genetics of NS and other RASopathies is the occurrence of conserved themes in the mechanism of disease. This applies in particular to mutations affecting genes encoding the various members of the RAS superfamily of GTPases that have been implicated in these disorders, including *KRAS*, *HRAS*, *NRAS*, *RRAS*, *MRAS*, and *CDC42*.[11–14,20,23–26,30] Missense mutations in these genes affect a small number of highly conserved amino acid residues that lead to overactivation of these proteins by decreasing/impairing their GTPase activity in response to GTPase-activating proteins (GAPs), increasing guanine nucleotide exchange factor (GEF)-independent GDP release, altering binding properties to effectors, or a combination of these mechanisms.[31] Notably, while these germline mutations may affect the same residues that are generally mutated in cancer, multiple lines of evidence indicate that RASopathy-causing changes are generally less activating than their respective cancer-associated somatic lesions.[21]

Despite the large number of genes implicated in NS and related phenotypes, about 10%–20% of affected individuals with a convincing clinical diagnosis of NS do not have mutations in currently known RASopathy-associated genes, indicating that other unidentified genes contribute to this disorder. Through the use of complementary approaches based on "functional candidacy" (parallel sequencing of selected gene panels containing functionally related candidate genes) or WES, we identified *RRAS2* (MIM: 600098; GenBank: NM_012250.5) as a gene implicated in NS. We provide structural, biochemical, and functional data to support the causal link between *RRAS2* mutations and NS, outline the mechanisms by which mutations perturb RRAS2 function, and characterize the clinical phenotype associated with these gene lesions.

Subjects from six unrelated families were included in the study. Clinical data and DNA samples were collected from the participating families after written informed consent was obtained. DNA samples were stored and used under research projects approved by the Review Boards of the participating institutions. Because of a suspected RASopathy, subjects 1, 2, 3-III-1, and 5 were referred for diagnostic genetic testing by sequencing of an "extended" panel of RASopathy-associated genes designed to include a set of candidate disease genes selected in the frame of the NSEuroNet Consortium, while subjects 4 and 6 were analyzed by WES (Supplemental Subjects and Methods). In five cases, the *RRAS2* variant (c.68G>T [p.Gly23Val], c.65_73dup [p.Gly22_Gly24dup], c.70_78dup [p.Gly24_Gly26dup], c.208G>A [p.Ala70Thr], c.215A>T [p.Gln72Leu]) arose *de novo* (i.e., it was not identified in parental blood DNA samples). In family 3, mutation scan in one affected family member (3-III-1) identified the heterozygous c.208G>A missense change, and subsequent co-segregation analysis confirmed the occurrence of the variant in three similarly affected relatives. All variants were validated by Sanger sequencing. In all cases, no other candidate variant was identified, further supporting the clinical relevance of this finding. In subject 4, the *RRAS2* variant was detected in both amniocyte and peripheral blood DNA, at 44% and 46% of reads, respectively, indicating the heterozygous mutation was present in the germline of the subject. The clinical data of the affected subjects from the six families are shown in Table 1, facial features of four affected individuals as well as the pedigree of family 3 are presented in Figure 1, and a detailed clinical history is provided in the Supplemental Note. Taken together, the identified *RRAS2* variants included three different nucleotide substitutions predicting missense changes of highly conserved amino acid residues (Gly23, Ala70, and Gln72) among RRAS2 orthologs and paralogs (Figure S1). Alterations to the corresponding positions in other GTPases of the RAS superfamily have already been reported to cause RASopathies or to contribute to oncogenesis (Table S1). In the remaining cases, we identified two small in-frame duplications (p.Gly22_Gly24dup, p.Gly24_Gly26dup) affecting the well-established mutational hotspot of RAS proteins (Figure 2A). Of note, p.Gly22_Gly24dup had previously been reported as somatic event in an uterine leiomyosarcoma specimen,[32] and other similar, but not identical, small in-frame duplications affecting these residues have also been reported in association with different cancers in the Catalogue of Somatic Mutations in Cancer (COSMIC database). The two small in-frame duplications and c.68G>T (p.Gly23Val) and c.215A>T (p.Gln72Leu) substitutions were absent from general population databases, while the c.208G>A (p.Ala70Thr) change had previously been reported in two subjects in gnomAD (heterozygous state, frequency < 0.00001) (Table S2). Multiple *in silico* prediction algorithms uniformly rated these changes as deleterious/pathogenic (Table S2).

RRAS2 (RAS related 2, also known as TC21, teratocarcinoma 21) is a member of the RAS superfamily of GTPases, originally described in 1990.[33] The protein shares the same four conserved functional domains with HRAS, KRAS, and NRAS, and about 55% amino acid sequence homology with HRAS (Figure 2A), which reaches 80%

Table 1. Clinical Features and Genotype of Individuals with *RRAS2* Variants

			Family 3						
	Subject 1	**Subject 2**	**3-II-1**	**3-II-2**	**3-III-1**	**3-III-2**	**Subject 4**	**Subject 5**	**Subject 6**
Origin	Algerian	Sri Lanka	German				Indian	Serbian	South American/ Ashkenazi
Gender	M	M	F	F	F	M	M	F	M
Age at last visit	7 y 11 m	12 y 2 m	32 y	40 y	7 y 1 m	1 y 7 m	2 weeks	8 y 10 m	22 m (last measurement 18 m)
RRAS2 variant	c.65_73dup (p.Gly22_Gly24dup)	c.68G>T (p.Gly23Val)	c.208G>A (p.Ala70Thr)	c.208G>A (p.Ala70Thr)	c.208G>A (p.Ala70Thr)	c.208G>A (p.Ala70Thr)	c.215A>T (p.Gln72Leu)	c.208G>A (p.Ala70Thr)	c.70_78dup (p.Gly24_ Gly26dup)
Inheritance	*de novo*	*de novo*	presumed paternal	presumed paternal	maternal	maternal	*de novo*	*de novo*	*de novo*
Prenatal features	NE, PH	PH	NA	NA	NA	N	NE, fetal ventriculo-megaly and cardiac abnormalities	NE	PH, LGA
Birth measurements: weight, length, OFC (weeks GA)	3,730 g, 50.5 cm, 37 cm (35)	3,180 g, 46.5 cm, 35 cm (35)	NA	3,740 g, 51 cm, 36 cm	3,110 g, 48 cm, 36 cm (39)	2,440 g, 48 cm, 32 cm (35)	2,400 g (33)	NA	3,600 g, 51 cm, 38 cm (35)
Feeding difficulties	PF	PF, TF	NA	NA	PF	N	NA	N	N
Height at last examination	125.5 cm (+0.3 SD)	139.5 (−1.5 SD) 85 cm (−3.3 SD)[a]	160 cm (−1.3 SD)	170 cm (+0.3 SD)	108 cm (−3.0 SD)	78 cm (−1.8 SD)	NA	122 cm (−2.1 SD)	84.5 cm (+0.5 SD)
Weight	27.5 kg (+0.5 SD)	32.5 kg (−1.4 SD)	NA	59 kg (+0.1 SD)	18.6 kg (−1.8 SD)	11 kg (−0.4 SD)	NA	22 kg (−1.9 SD)	12.5 kg (+0.7 SD)
OFC	54 cm (+1.2 SD)	57 cm (+2.5 SD)	52.5 cm (−2.2 SD)	55.5 cm (+0.2 SD)	52 cm (+0.4 SD)	49 cm (+0.2 SD)	NA	52.5 cm (+0.2 SD)	54.5 cm (+5.0 SD)
Cryptorchidism	N	N	NA	NA	NA	N	hypoplastic scrotum	NA	N
Congenital heart defect	SVAoS	VSD	VSD	N	N	N	TOF	AVSD, multiple VSDs	N
Lymphatic anomalies	N	N	N	N	N	N	N	N	N
Facial anomalies	typical NS	typical NS	suggestive NS	very mild in adulthood	typical NS	typical NS	multiple anomalies	suggestive NS	typical NS
Development	N	mild MD, mild LD	N	N	mild MD, mild LD	N	NA	N	mild global delay
Neurology	N	Chiari malformation	N	N	N	N	non-obstructive hydrocephalus	N	mild ventriculomegaly, hypotonia
Skeletal	N	N	N	N	N	N	11 rib pairs, proximally placed thumb, spinal canal stenosis	pectus excavatum	N

(*Continued on next page*)

Table 1. *Continued*

			Family 3						
	Subject 1	Subject 2	3-II-1	3-II-2	3-III-1	3-III-2	Subject 4	Subject 5	Subject 6
Hematology & oncology	N	lymphopenia	N	N	N	N	thrombocytopenia	N	N
Skin and hair	glabellar heamangioma	N	N	N	atopic dermatitis,	N	N	N	glabellar hemangioma
Ocular	N	strabismus	N	strabismus	hyperopia, bilateral ptosis	N	NA	N	strabismic amblyopia, esotropia
Other malformations/ anomalies	N	GH deficiency, GH treatment from age 4 y	unilateral duplex kidney	N	multiple allergies, bronchitis	N	labyrinth dysplasia, anteriorly placed anus	minor hippocampal malformation on brain MRI	N

Abbreviations: AVSD, atrioventricular septal defect; F, female; GA, gestational age; GD, global delay; GH, growth hormone; LD, learning difficulties; LGA, large for gestational age; M, male; m, months; MD, motor delay; N, none/normal; NA, not applicable/not available; NE, nuchal edema; OFC, occipitofrontal head circumference; PF, poor feeding reported; PH, polyhydramnios; SVAoS, supravalvular aortic stenosis; TF, tube feeding (>4 weeks); TOF, Tetralogy of Fallot; y, years.
[a]Before onset of growth hormone treatment at age 3 y 6 m.

when considering the region between residues 5 to 120 (i.e., excluding the hypervariable tail at the C terminus).[34,35] RRAS2 controls multiple cellular processes, including proliferation, survival, and migration, and its functional dysregulation has been documented to contribute to oncogenesis.[34,36,37] Indeed, a number of oncogenic RRAS2 variants have been reported, including the p.Gly23Val, p.Ala70Thr, and p.Gln72Leu changes, in a variety of solid tumors (Table S1). More recently, the p.Gln72Leu change in RRAS2 has been identified in subjects with isolated JMML,[38] which represents the archetypal somatic RASopathy. Notably, germline mutations in other *RAS* genes affecting analogous codons to those observed in the present cases have also been identified (Table S1), including the missense mutation p.Gln87Leu in RRAS (homologous to p.Gln72Leu in RRAS2), previously reported in individuals having features reminiscent of NS.[23]

In order to decipher the consequences of the observed amino acid changes and the small in-frame duplications on the molecular structure of RRAS2, we performed structural modeling. A closer view into the active site of RRAS2 structure in its active form (Figure 2B, left) revealed that the identified *RRAS2* mutations affect residues localized around the nucleotide binding pocket of the GTPase. The corresponding amino acids, including Gly22-Gly26, Ala70, and Gln72, do not only play a critical role in GDP/GTP exchange and GTP hydrolysis but also are involved in stabilization of the switch regions (Figure 2B, right), which are the binding sites for both RRAS2 regulators (GEFs and GAPs) and effectors.[39] Specifically, the amino acid stretch encompassing Gly22 to Gly26 constitutes part of the phosphate-binding loop (P loop; residues Gly21 to Ser28) that is responsible for binding to the phosphate groups of either GTP or GDP. These residues play a critical role in nucleotide binding and hydrolysis by contacting both the β-γ phosphates of GTP (shown as GppNHp, a non-hydrolyzable GTP analog in Figure 2B) and residues 67 to 69 of the switch II region (SwII; Asp68 to Arg84). Val25 stabilizes the P loop by contacting Val92, Ser94, and Ser100. The Gly22-to-Gly24 and Gly24-to-Gly26 duplications were predicted to destabilize the P loop and result in increased nucleotide exchange and decreased GTP hydrolysis reactions. Differently, Ala70 and Gln72 are located in the switch II region of the GTPase and are directly involved in Mg^{2+} coordination and GTP hydrolysis reaction. Additionally, Ala70 and Gln72 stabilize the switch I region (SwI; Phe39-Ser50) by contacting Ile47 and Glu48, respectively. Based on these considerations, the NS-associated amino acid changes were expected to affect various aspects of RRAS2 biochemical behavior, including a faster nucleotide exchange, an impaired GTP hydrolysis, and a decrease in GEF, GAP, and effector interactions. Subsequent biochemical analysis of $RRAS2^{p.Ala70Thr}$ clearly confirmed these structural predictions, as assessment of the intrinsic and stimulated nucleotide exchange demonstrated a significantly increased

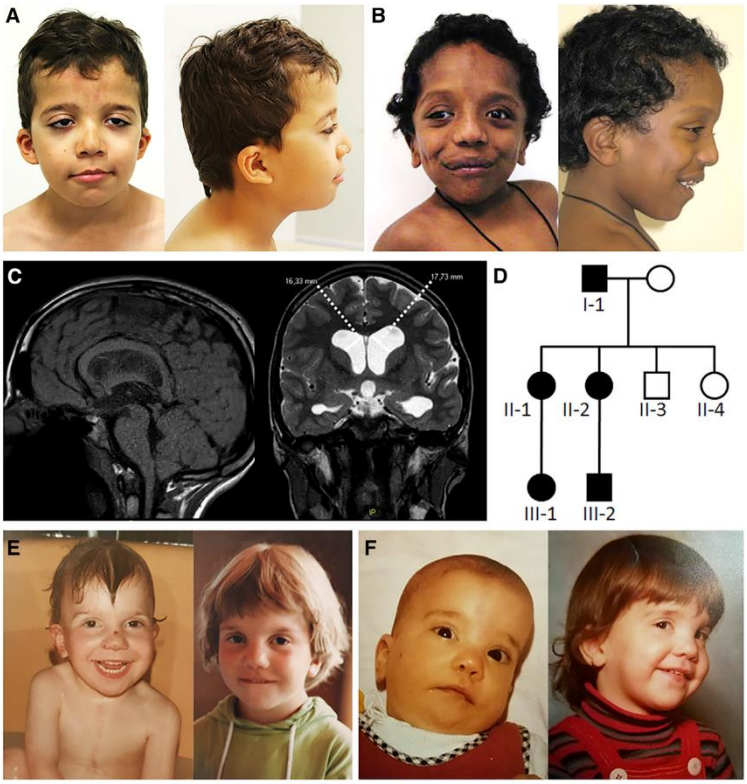

Figure 1. Clinical Features of Individuals with Heterozygous Noonan Syndrome-Causing *RRAS2* Variants
(A) Clinical appearance of subject 1 at 7 years and 11 months. Note the distinctive NS features, including bitemporal narrowing, downslanting palpebral fissures, ptosis, low-set ears, and low posterior hairline.
(B) Facial features of subject 2 at 2 years and 6 months. Facial features overlap those characterizing subject 1, even though a "coarse" face is also observed.
(C) Subject 2 brain MRI at 11 years and 9 months showing Chiari type 1 malformation and bilateral ventricular dilatation.
(D) Pedigree of family 3.
(E) Clinical appearance of subject 3-II-1 at the age of 11 months and 4.5 years.
(F) Facial features of subject 3-II-2 at 9 months and 5 years. The NS facial gestalt of subjects 3-II-1 and 3-II-2 became less obvious in adulthood.

response of the RRAS2$^{p.Ala70Thr}$ protein to GEF as compared to wild-type RRAS2 (Figure 2C). In contrast, the GTP hydrolysis reactions of the mutant were reduced compared to the wild-type protein. Particularly, the GAP-stimulated GTPase activity of RRAS2$^{p.Ala70Thr}$ was significantly decreased (9-fold) (Figure 2C). Finally, the binding properties to two RRAS2 effectors, RAF1 (CRAF) and RASSF5, were assessed. While the affinity of the interaction with CRAF was comparable to that of wild-type RRAS2, binding to RASSF5 was abolished (Figure 2C). This suggests the p.Ala70Thr change leads to a structural rearrangement of RRAS2 switch II, which is a key binding site for RASSF5 but not for CRAF. Overall, these data support that the p.Ala70Thr change leads to an accumulation of RRAS2 in its GTP-bound active state, which predicts an increase in signaling activity. The impaired binding to RASSF5, however, suggest a possible differential impact of the missense change on downstream signaling pathways.

RRAS2 shares downstream effectors with the other members of the RAS subfamily;[35] however, little information exists about the function of this protein in cellular processes and development. Similarly, scant data exist on the specific role of this protein in intracellular signaling as well as on the extent of functional overlap with the other RAS proteins implicated in RASopathies. To explore the consequences of NS-associated *RRAS2* mutations on the intracellular signaling pathways affected in NS, the signaling flows through the MAPK and phosphatidylinostiol-3 kinase (PI3K)-AKT cascades were evaluated using transient expression in HEK293T cells. Expression of all mutants resulted in variably enhanced ERK phosphorylation compared to cells overexpressing the wild-type protein (Figure 3A). Notably, RRAS2$^{p.Ala70Thr}$ and RRAS2$^{p.Gln72Leu}$ were observed to constitutively promote increased ERK phosphorylation, while only a slight increase was observed basally in cells expressing the RRAS2$^{p.Gly22_Gly24dup}$ and RRAS2$^{p.Gly23Val}$ mutants. However, this slight increase substantially strengthened after stimulation with EGF. This activating role of p.Gly22_Gly24dup is in line with previous evidence supporting the gain-of-function role of short insertional mutations in the P loop of other members of the RAS family.[40] Based on previous data indicating that upregulated RRAS2 promotes tumorigenesis in a PI3K-dependent manner,[41] the impact of NS-associated mutants on PI3K-AKT signaling was also assessed. No significant difference in the extent of AKT phosphorylation was documented, indicating a specific functional link between RRAS2 and the MAPK signaling cascade, at least in the present experimental conditions. In line with these findings, *Rras2* KO mice showed a downmodulation of Erk activation and unaltered levels of phosphorylated Akt.[42]

RAS proteins interact with multiple signaling platforms, which allow these proteins to differentially control multiple signaling pathways.[43] Such complex behavior is attained by their dynamic interaction with the plasma membrane and other intracellular membranes (i.e., endosomes, endoplasmic reticulum, and Golgi). To explore any perturbing effect of mutations on the subcellular

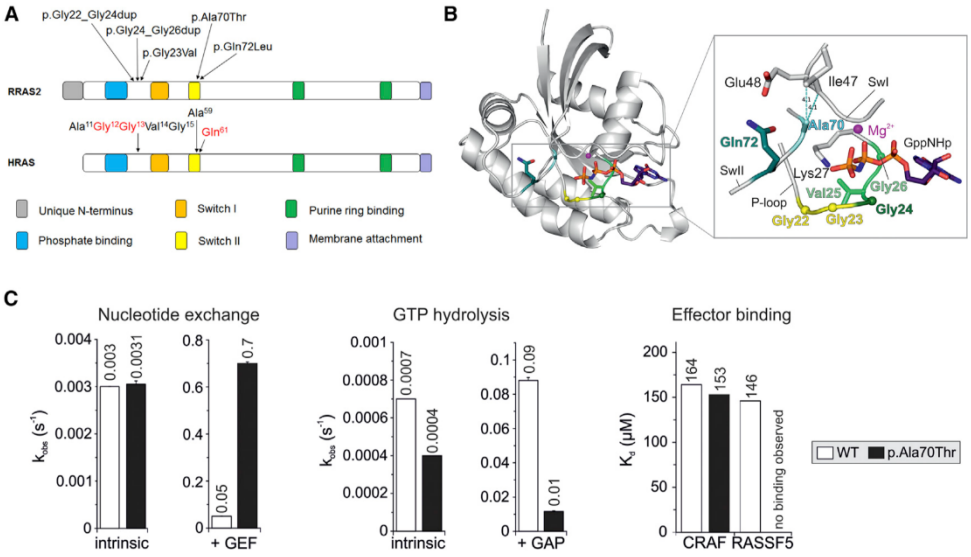

Figure 2. RRAS2 Structure and Location and Functional Impact of Noonan Syndrome-Causing Variants
(A) Schematic representation of RRAS2 and HRAS proteins. Conserved motifs critical for tight guanine nucleotide binding and hydrolysis, and position of the disease-causing RRAS2 variants are illustrated together with the homologous residues of HRAS. The three residues representing the mutational hotspots of oncogenic *HRAS* mutations are shown in red.
(B) Structural modeling of RRAS2 variants. A structural model of the active GTP-bound RRAS2 protein highlights the relative position of the disease-causing missense or insertion mutations. All *RRAS2* mutations affect residues that are located in the nucleotide binding active site region, which contains integral elements involved in GDP/GTP binding, GTP hydrolysis, and interactions with regulators (GEFs and GAPs) and effectors.
(C) Biochemical assessment of RRAS2$^{p.Ala70Thr}$. RRAS2^{WT} and RRAS2$^{p.Ala70Thr}$ proteins were biochemically characterized regarding their nucleotide exchange (left), GTP hydrolysis (middle), and effector binding (right) properties. The nucleotide exchange reaction was measured in the absence (intrinsic) and in the presence of the catalytic RASGEF domain of mouse RASGRF1, while the catalytic activity of the GTPase was assessed in the absence (intrinsic) and in the presence of the p120 RASGAP GAP domain. The RAS-binding and RAS association domains of CRAF and RASSF5 were used to evaluate the binding behavior of the RRAS2$^{p.Ala70Thr}$ mutant to RAS effectors. Overall, the data indicate that the p.Ala70Thr change leads to an accumulation of the protein in its GTP-bound active state, resulting to an increased signaling activity. The missense change, however, is predicted to differentially impact on the diverse downstream signaling pathways.

localization and distribution of RRAS2, including possible preferential targeting to specific intracellular domains, confocal laser scanning microscopy analysis was performed in HEK293T cells transiently expressing Myc-tagged RRAS2 constructs under starved condition. Similarly to the wild-type protein, a fraction of all RRAS2 mutant proteins co-localized with GM130, indicating their targeting to the Golgi apparatus, and the remainder were largely found at the plasma membrane (Figure 3B, left), indicating that mutations do not cause any overt subcellular redistribution of the GTPase. Notably, transient expression of all mutants was found to variably impact cell morphology and cytoskeletal rearrangement, with all mutant proteins promoting spreading and adhesion (Figure 3B, right). Taken together, these experimental data suggest that NS-associated *RRAS2* mutations variably upregulate MAPK signaling and are likely to affect cellular processes depending on cytoskeleton rearrangement similar to observations of RASopathy-causing KRAS mutants.[44]

Our findings establish *RRAS2* germline mutations as a cause of NS. Although previous screening of a cohort of 116 subjects with a clinical diagnosis of NS without a genetic explanation did not identify germline pathogenic *RRAS2* variants,[45] the present collaborative effort allowed to identify six unrelated affected individuals. Of the case subjects reported here, two individuals carrying *de novo* germline NS-causing *RRAS2* variants (subjects 1 and 2) were identified among 1,220 samples addressed to Robert Debré Hospital, Paris, for diagnostic testing for NS, between February 2016 and September 2018. Within the same period, 181 of these subjects were found to carry a *PTPN11* mutation. At the University Hospital of Magdeburg, screening of a multigene panel including *RRAS2* in a cohort of 280 subjects with a tentative diagnosis of NS and negative results for mutations in previously known genes yielded two *RRAS2* mutation-positive cases. Finally, no putative *RRAS2* mutation was identified among 150 case subjects with a clinical diagnosis of NS from Ospedale Pediatrico Bambino Gesù, Rome. Overall, these findings indicate that *RRAS2* mutations are rare events in NS.

The phenotypes associated with the two *RRAS2* mutation hotspots were found to fit well within the clinical spectrum of NS even though they appeared variable in terms of

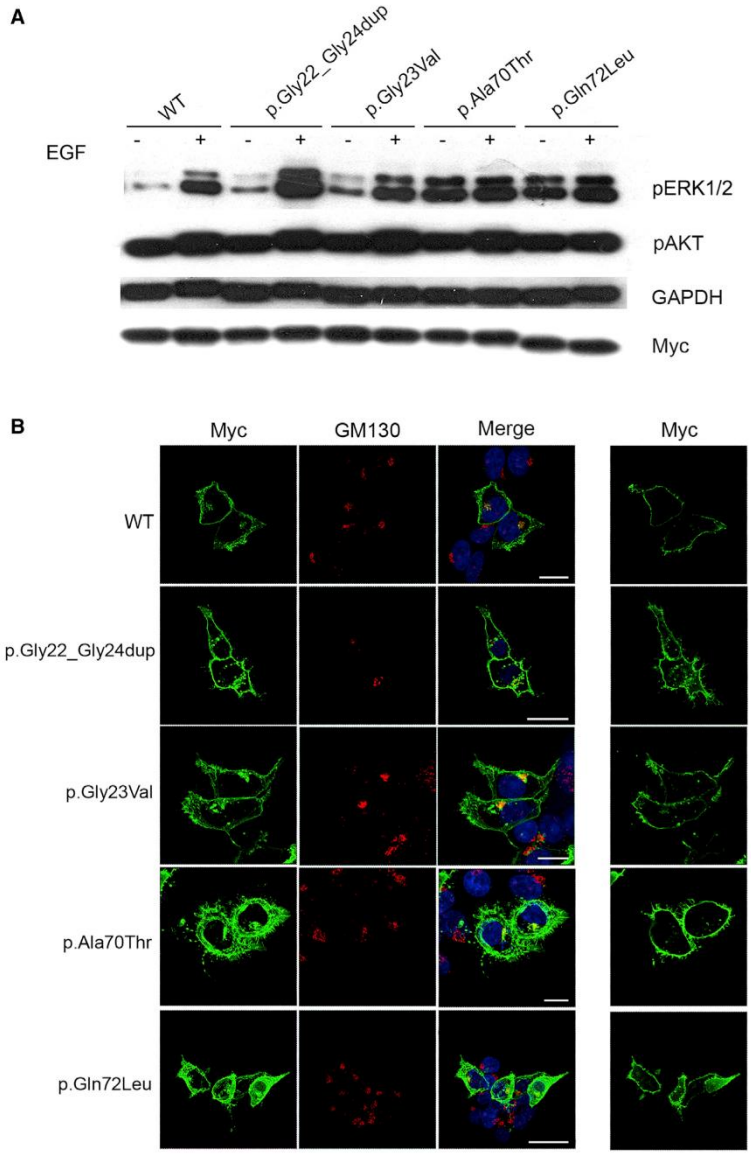

Figure 3. Biochemical and Functional Characterization of Noonan Syndrome-Causing *RRAS2* Variants

(A) ERK and AKT phosphorylation assays. HEK293T cells were transfected with the indicated Myc-tagged RRAS2 constructs. Following starvation (18 h) and EGF stimulation (30 ng/mL for 15 min), ERK and AKT phosphorylation levels were evaluated using a mouse monoclonal anti-phospho-p44/42 ERK (Thr202/Tyr204) antibody and a rabbit polyclonal anti-phospho-AKT (Ser473) antibody, respectively. To assess myc-RRAS2 protein levels, 20 μg of total lysates were immunoblotted with a mouse monoclonal anti-Myc antibody. Membranes were re-probed with mouse monoclonal anti-GAPDH antibody for protein normalization. Representative blot of three performed experiments are shown.

(B) RRAS2 subcellular localization showed by confocal laser scanning microscopy (CLSM) observations (left). Assays were performed on HEK293T cells starved overnight and stained with an anti-Myc mouse monoclonal antibody, followed by goat anti-mouse Alexa Fluor-488 (green), and an anti-GM130 (Golgi marker) rabbit polyclonal antibody, followed by goat anti-rabbit Alexa Fluor-594 (red). Nuclei are visualized by DAPI staining (blue). Co-localization areas were detected in yellow. CLSM observation were also performed at the basal level of cells to show the distinctive pattern of adhesion-like structures and cytoskeletal rearrangement in cells expressing the RRAS2 mutants (right). In all panels, bars correspond to 21 μm.

severity. While individuals 1, 2, 5, and 6 had features fitting typical NS, the phenotype in some affected members of family 3 was relatively mild. On the other hand, subject 4 showed a complex and particularly severe phenotype with multiple congenital anomalies and neonatal lethality. Of note, prenatal features (nuchal edema, polyhydramnios, and/or cardiomyopathy) were reported in five of six subjects, and none showed pulmonary valve stenosis or hypertrophic cardiomyopathy. While the small size of the studied cohort does not allow us to outline specific genotype-phenotype correlations, we hypothesize that such variable expressivity likely reflects the differential strength of individual variants to perturb RRAS2 function and intracellular signaling. Consistent with the collected functional data, p.Gln72Leu (analogous to p.Gln61Leu in HRAS, NRAS, and KRAS) is a strong activating mutation and has not been observed to occur as a germline event in *HRAS*, *KRAS*, or *NRAS*. Similar differences in the biological and phenotypic consequences have previously been reported for *HRAS*, *NRAS*, and *KRAS*,[12–14,30,31,46–53] including the positions corresponding to the presently identified *RRAS2* mutations. The genotype-phenotype correlations in *HRAS* are illustrative and correlate well with the present findings: while p.Ala59Thr has been associated with Costello syndrome and p.Gly12Val has been reported with severe expression of Costello syndrome,[46] p.Gln61Leu and other changes at this codon have only been reported as somatic events in cancer (Table S1).

A noticeable finding of this study is the observation of a diverse impact of the p.Ala70Thr on RRAS2 binding to CRAF/RAF1 and RASSF5. These data suggest the possibility that multiple signaling pathways downstream of RRAS2 may contribute to dysregulation of cellular processes

(e.g., cell proliferation). As expected, a variable hyperactivation of the MAPK pathway resulting from the hyperactive state of the GTPase and unaltered binding to CRAF was observed for the NS-causing RRAS2^{Ala70Thr} protein. Remarkably, impaired binding of this mutant to RASSF5, a known tumor suppressor protein negatively modulating YAP1 levels through activation of the Hippo pathway, was also observed. YAP1 is a transcriptional cofactor promoting cell proliferation, which undergoes RASSF5-mediated phosphorylation and degradation.[54] The impaired binding of RRAS2 to RASSF5 raises the possibility that a less effective Hippo-mediated control of YAP1 levels may contribute to disease pathogenesis in NS.

Among RAS GTPases, RRAS2 exhibits the highest amino acid identity to HRAS, KRAS, and NRAS.[35] Somatic mutations in *RRAS2* have been established to contribute to oncogenesis, even though in a substantially restricted tumor type and less frequently compared to *HRAS*, *KRAS*, and *NRAS*. Consistently, it was originally demonstrated that RRAS2 proteins containing amino acid substitutions analogous to those with oncogenic role in HRAS, KRAS, and NRAS have transforming properties comparable to the strong transforming activity of RAS oncoproteins and similarly promote constitutive activation of the MAPK cascade.[55] Our findings, which are in line with the data presented in an accompanying report by Niihori et al. published in this issue,[56] further extend these observations by demonstrating the clinical relevance of a narrow spectrum of germline pathogenic variants in *RRAS2* as the event underlying a small fraction of NS cases via upregulation of MAPK signaling. Further studies are required to more accurately define the precise mechanisms and circuits linking upregulated RRAS2 function and RAS-MAPK signaling dysregulation.

Accession Numbers

The accession numbers for the five *RRAS2* variants reported in this paper are ClinVar: SCV000902249–SCV000902253.

Supplemental Data

Supplemental Data can be found online at https://doi.org/10.1016/j.ajhg.2019.04.013.

Acknowledgments

The authors thank the subjects and their families for participating in this study. This work was supported by the ERN-ITHACA networking (A.V. and M.T.) and grants from E-Rare (NSEuroNet, ERARE15-pp-063) to H.C., M.R.A. (01GM1602B), M.T., and M.Z. (01GM1602A), AIRC (IG21614) and Ministero della Salute (Ricerca Corrente 2017, 2018) to M.T., German Federal Ministry of Education and Research - BMBF (German Network for RASopathy Research "GeNeRARe") to M.R.A. (01GM1519D and 01GM1902C) and M.Z. (01GM1519A), and the German Research Foundation through the Collaborative Research Center 974 (SFB 974) "Communication and Systems Relevance during Liver Injury and Regeneration" to M.R.A and grant number ZE 524-10/1 to M.Z.

Declaration of Interests

K.G.M. declares no additional conflicts of interest beyond her employment affiliation. L.M.V. is a former employee of GeneDx. All the other authors declare no competing interests.

Received: March 6, 2019
Accepted: April 18, 2019
Published: May 23, 2019

Web Resources

CADD, https://cadd.gs.washington.edu/
ClinVar, https://www.ncbi.nlm.nih.gov/clinvar/
COSMIC, https://cancer.sanger.ac.uk/cosmic
dbSNP, https://www.ncbi.nlm.nih.gov/snp
Exome Aggregation Consortium (ExAC) Browser, http://exac.broadinstitute.org/
GenBank, https://www.ncbi.nlm.nih.gov/genbank
GeneMatcher, https://genematcher.org
gnomAD, https://gnomad.broadinstitute.org/
Muscle, https://www.ebi.ac.uk/Tools/msa/muscle/
MutationAssessor, http://mutationassessor.org/r3/
MutationTaster, http://mutationtaster.org
MutPred2, http://mutpred.mutdb.org/
OMIM, http://www.omim.org/
PolyPhen-2, http://genetics.bwh.harvard.edu/pph2/
PROVEAN, http://provean.jcvi.org/index.php

References

1. Roberts, A.E., Allanson, J.E., Tartaglia, M., and Gelb, B.D. (2013). Noonan syndrome. Lancet *381*, 333–342.
2. Tartaglia, M., Gelb, B.D., and Zenker, M. (2011). Noonan syndrome and clinically related disorders. Best Pract. Res. Clin. Endocrinol. Metab. *25*, 161–179.
3. Strullu, M., Caye, A., Lachenaud, J., Cassinat, B., Gazal, S., Fenneteau, O., Pouvreau, N., Pereira, S., Baumann, C., Contet, A., et al. (2014). Juvenile myelomonocytic leukaemia and Noonan syndrome. J. Med. Genet. *51*, 689–697.
4. Grant, A.R., Cushman, B.J., Cavé, H., Dillon, M.W., Gelb, B.D., Gripp, K.W., Lee, J.A., Mason-Suares, H., Rauen, K.A., Tartaglia, M., et al. (2018). Assessing the gene-disease association of 19 genes with the RASopathies using the ClinGen gene curation framework. Hum. Mutat. *39*, 1485–1493.
5. Tartaglia, M., Mehler, E.L., Goldberg, R., Zampino, G., Brunner, H.G., Kremer, H., van der Burgt, I., Crosby, A.H., Ion, A., Jeffery, S., et al. (2001). Mutations in PTPN11, encoding the protein tyrosine phosphatase SHP-2, cause Noonan syndrome. Nat. Genet. *29*, 465–468.
6. Tartaglia, M., Pennacchio, L.A., Zhao, C., Yadav, K.K., Fodale, V., Sarkozy, A., Pandit, B., Oishi, K., Martinelli, S., Schackwitz, W., et al. (2007). Gain-of-function *SOS1* mutations cause a distinctive form of Noonan syndrome. Nat. Genet. *39*, 75–79.
7. Roberts, A.E., Araki, T., Swanson, K.D., Montgomery, K.T., Schiripo, T.A., Joshi, V.A., Li, L., Yassin, Y., Tamburino, A.M., Neel, B.G., and Kucherlapati, R.S. (2007). Germline gain-of-function mutations in *SOS1* cause Noonan syndrome. Nat. Genet. *39*, 70–74.
8. Zenker, M., Horn, D., Wieczorek, D., Allanson, J., Pauli, S., van der Burgt, I., Doerr, H.-G., Gaspar, H., Hofbeck, M., Gillessen-Kaesbach, G., et al. (2007). SOS1 is the second most common

Noonan gene but plays no major role in cardio-facio-cutaneous syndrome. J. Med. Genet. *44*, 651–656.

9. Pandit, B., Sarkozy, A., Pennacchio, L.A., Carta, C., Oishi, K., Martinelli, S., Pogna, E.A., Schackwitz, W., Ustaszewska, A., Landstrom, A., et al. (2007). Gain-of-function RAF1 mutations cause Noonan and LEOPARD syndromes with hypertrophic cardiomyopathy. Nat. Genet. *39*, 1007–1012.
10. Razzaque, M.A., Nishizawa, T., Komoike, Y., Yagi, H., Furutani, M., Amo, R., Kamisago, M., Momma, K., Katayama, H., Nakagawa, M., et al. (2007). Germline gain-of-function mutations in *RAF1* cause Noonan syndrome. Nat. Genet. *39*, 1013–1017.
11. Kouz, K., Lissewski, C., Spranger, S., Mitter, D., Riess, A., Lopez-Gonzalez, V., Lüttgen, S., Aydin, H., von Deimling, F., Evers, C., et al. (2016). Genotype and phenotype in patients with Noonan syndrome and a *RIT1* mutation. Genet. Med. *18*, 1226–1234.
12. Cirstea, I.C., Kutsche, K., Dvorsky, R., Gremer, L., Carta, C., Horn, D., Roberts, A.E., Lepri, F., Merbitz-Zahradnik, T., König, R., et al. (2010). A restricted spectrum of NRAS mutations causes Noonan syndrome. Nat. Genet. *42*, 27–29.
13. Schubbert, S., Zenker, M., Rowe, S.L., Böll, S., Klein, C., Bollag, G., van der Burgt, I., Musante, L., Kalscheuer, V., Wehner, L.-E., et al. (2006). Germline *KRAS* mutations cause Noonan syndrome. Nat. Genet. *38*, 331–336.
14. Zenker, M., Lehmann, K., Schulz, A.L., Barth, H., Hansmann, D., Koenig, R., Korinthenberg, R., Kreiss-Nachtsheim, M., Meinecke, P., Morlot, S., et al. (2007). Expansion of the genotypic and phenotypic spectrum in patients with KRAS germline mutations. J. Med. Genet. *44*, 131–135.
15. Sarkozy, A., Carta, C., Moretti, S., Zampino, G., Digilio, M.C., Pantaleoni, F., Scioletti, A.P., Esposito, G., Cordeddu, V., Lepri, F., et al. (2009). Germline *BRAF* mutations in Noonan, LEOPARD, and cardiofaciocutaneous syndromes: molecular diversity and associated phenotypic spectrum. Hum. Mutat. *30*, 695–702.
16. Nava, C., Hanna, N., Michot, C., Pereira, S., Pouvreau, N., Niihori, T., Aoki, Y., Matsubara, Y., Arveiler, B., Lacombe, D., et al. (2007). Cardio-facio-cutaneous and Noonan syndromes due to mutations in the RAS/MAPK signalling pathway: genotype-phenotype relationships and overlap with Costello syndrome. J. Med. Genet. *44*, 763–771.
17. Yamamoto, G.L., Aguena, M., Gos, M., Hung, C., Pilch, J., Fahiminiya, S., Abramowicz, A., Cristian, I., Buscarilli, M., Naslavsky, M.S., et al. (2015). Rare variants in *SOS2* and *LZTR1* are associated with Noonan syndrome. J. Med. Genet. *52*, 413–421.
18. Cordeddu, V., Yin, J.C., Gunnarsson, C., Virtanen, C., Drunat, S., Lepri, F., De Luca, A., Rossi, C., Ciolfi, A., Pugh, T.J., et al. (2015). Activating Mutations Affecting the Dbl Homology Domain of SOS2 Cause Noonan Syndrome. Hum. Mutat. *36*, 1080–1087.
19. Chen, P.-C., Yin, J., Yu, H.-W., Yuan, T., Fernandez, M., Yung, C.K., Trinh, Q.M., Peltekova, V.D., Reid, J.G., Tworog-Dube, E., et al. (2014). Next-generation sequencing identifies rare variants associated with Noonan syndrome. Proc. Natl. Acad. Sci. USA *111*, 11473–11478.
20. Higgins, E.M., Bos, J.M., Mason-Suares, H., Tester, D.J., Ackerman, J.P., MacRae, C.A., Sol-Church, K., Gripp, K.W., Urrutia, R., and Ackerman, M.J. (2017). Elucidation of *MRAS*-mediated Noonan syndrome with cardiac hypertrophy. JCI Insight *2*, e91225.
21. Tartaglia, M., and Gelb, B.D. (2010). Disorders of dysregulated signal traffic through the RAS-MAPK pathway: phenotypic spectrum and molecular mechanisms. Ann. N Y Acad. Sci. *1214*, 99–121.
22. Rauen, K.A. (2013). The RASopathies. Annu. Rev. Genomics Hum. Genet. *14*, 355–369.
23. Flex, E., Jaiswal, M., Pantaleoni, F., Martinelli, S., Strullu, M., Fansa, E.K., Caye, A., De Luca, A., Lepri, F., Dvorsky, R., et al. (2014). Activating mutations in RRAS underlie a phenotype within the RASopathy spectrum and contribute to leukaemogenesis. Hum. Mol. Genet. *23*, 4315–4327.
24. Gripp, K.W., Aldinger, K.A., Bennett, J.T., Baker, L., Tusi, J., Powell-Hamilton, N., Stabley, D., Sol-Church, K., Timms, A.E., and Dobyns, W.B. (2016). A novel rasopathy caused by recurrent de novo missense mutations in *PPP1CB* closely resembles Noonan syndrome with loose anagen hair. Am. J. Med. Genet. A. *170*, 2237–2247.
25. Martinelli, S., Krumbach, O.H.F., Pantaleoni, F., Coppola, S., Amin, E., Pannone, L., Nouri, K., Farina, L., Dvorsky, R., Lepri, F., et al.; University of Washington Center for Mendelian Genomics (2018). Functional Dysregulation of CDC42 Causes Diverse Developmental Phenotypes. Am. J. Hum. Genet. *102*, 309–320.
26. Young, L.C., Hartig, N., Boned Del Río, I., Sari, S., Ringham-Terry, B., Wainwright, J.R., Jones, G.G., McCormick, F., and Rodriguez-Viciana, P. (2018). SHOC2-MRAS-PP1 complex positively regulates RAF activity and contributes to Noonan syndrome pathogenesis. Proc. Natl. Acad. Sci. USA *115*, E10576–E10585.
27. Motta, M., Fidan, M., Bellacchio, E., Pantaleoni, F., Schneider-Heieck, K., Coppola, S., Borck, G., Salviati, L., Zenker, M., Cirstea, I.C., and Tartaglia, M. (2018). Dominant Noonan syndrome-causing LZTR1 mutations specifically affect the kelch domain substrate-recognition surface and enhance RAS-MAPK signaling. Hum. Mol. Genet. *28*, 1007–1022.
28. Bigenzahn, J.W., Collu, G.M., Kartnig, F., Pieraks, M., Vladimer, G.I., Heinz, L.X., Sedlyarov, V., Schischlik, F., Fauster, A., Rebsamen, M., et al. (2018). LZTR1 is a regulator of RAS ubiquitination and signaling. Science *362*, 1171–1177.
29. Steklov, M., Pandolfi, S., Baietti, M.F., Batiuk, A., Carai, P., Najm, P., Zhang, M., Jang, H., Renzi, F., Cai, Y., et al. (2018). Mutations in LZTR1 drive human disease by dysregulating RAS ubiquitination. Science *362*, 1177–1182.
30. Aoki, Y., Niihori, T., Kawame, H., Kurosawa, K., Ohashi, H., Tanaka, Y., Filocamo, M., Kato, K., Suzuki, Y., Kure, S., and Matsubara, Y. (2005). Germline mutations in *HRAS* proto-oncogene cause Costello syndrome. Nat. Genet. *37*, 1038–1040.
31. Gremer, L., Gilsbach, B., Ahmadian, M.R., and Wittinghofer, A. (2008). Fluoride complexes of oncogenic Ras mutants to study the Ras-RasGap interaction. Biol. Chem. *389*, 1163–1171.
32. Huang, Y., Saez, R., Chao, L., Santos, E., Aaronson, S.A., and Chan, A.M. (1995). A novel insertional mutation in the TC21 gene activates its transforming activity in a human leiomyosarcoma cell line. Oncogene *11*, 1255–1260.
33. Drivas, G.T., Shih, A., Coutavas, E., Rush, M.G., and D'Eustachio, P. (1990). Characterization of four novel ras-like genes expressed in a human teratocarcinoma cell line. Mol. Cell. Biol. *10*, 1793–1798.
34. Bos, J.L. (1997). Ras-like GTPases. Biochim. Biophys. Acta *1333*, M19–M31.
35. Nakhaei-Rad, S., Haghighi, F., Nouri, P., Rezaei Adariani, S., Lissy, J., Kazemein Jasemi, N.S., Dvorsky, R., and Ahmadian, M.R. (2018). Structural fingerprints, interactions, and

signaling networks of RAS family proteins beyond RAS isoforms. Crit. Rev. Biochem. Mol. Biol. *53*, 130–156.

36. Graham, S.M., Oldham, S.M., Martin, C.B., Drugan, J.K., Zohn, I.E., Campbell, S., and Der, C.J. (1999). TC21 and Ras share indistinguishable transforming and differentiating activities. Oncogene *18*, 2107–2116.
37. Erdogan, M., Pozzi, A., Bhowmick, N., Moses, H.L., and Zent, R. (2007). Signaling pathways regulating TC21-induced tumorigenesis. J. Biol. Chem. *282*, 27713–27720.
38. Stieglitz, E., Taylor-Weiner, A.N., Chang, T.Y., Gelston, L.C., Wang, Y.-D., Mazor, T., Esquivel, E., Yu, A., Seepo, S., Olsen, S., et al. (2015). The genomic landscape of juvenile myelomonocytic leukemia. Nat. Genet. *47*, 1326–1333.
39. Vetter, I.R., and Wittinghofer, A. (2001). The guanine nucleotide-binding switch in three dimensions. Science *294*, 1299–1304.
40. Klockow, B., Ahmadian, M.R., Block, C., and Wittinghofer, A. (2000). Oncogenic insertional mutations in the P-loop of Ras are overactive in MAP kinase signaling. Oncogene *19*, 5367–5376.
41. Larive, R.M., Moriggi, G., Menacho-Márquez, M., Cañamero, M., de Álava, E., Alarcón, B., Dosil, M., and Bustelo, X.R. (2014). Contribution of the R-Ras2 GTP-binding protein to primary breast tumorigenesis and late-stage metastatic disease. Nat. Commun. *5*, 3881.
42. Larive, R.M., Abad, A., Cardaba, C.M., Hernández, T., Cañamero, M., de Álava, E., Santos, E., Alarcón, B., and Bustelo, X.R. (2012). The Ras-like protein R-Ras2/TC21 is important for proper mammary gland development. Mol. Biol. Cell *23*, 2373–2387.
43. Hancock, J.F. (2003). Ras proteins: different signals from different locations. Nat. Rev. Mol. Cell Biol. *4*, 373–384.
44. Gremer, L., Merbitz-Zahradnik, T., Dvorsky, R., Cirstea, I.C., Kratz, C.P., Zenker, M., Wittinghofer, A., and Ahmadian, M.R. (2011). Germline KRAS mutations cause aberrant biochemical and physical properties leading to developmental disorders. Hum. Mutat. *32*, 33–43.
45. Ceremsak, J.J., Yu, A., Esquivel, E., Lissewski, C., Zenker, M., Loh, M.L., and Stieglitz, E. (2016). Germline *RRAS2* mutations are not associated with Noonan syndrome. J. Med. Genet. *53*, 728.
46. Quélin, C., Loget, P., Rozel, C., D'Hervé, D., Fradin, M., Demurger, F., Odent, S., Pasquier, L., Cavé, H., and Marcorelles, P. (2017). Fetal costello syndrome with neuromuscular spindles excess and p.Gly12Val HRAS mutation. Eur. J. Med. Genet. *60*, 395–398.
47. Carta, C., Pantaleoni, F., Bocchinfuso, G., Stella, L., Vasta, I., Sarkozy, A., Digilio, C., Palleschi, A., Pizzuti, A., Grammatico, P., et al. (2006). Germline missense mutations affecting KRAS Isoform B are associated with a severe Noonan syndrome phenotype. Am. J. Hum. Genet. *79*, 129–135.
48. Gripp, K.W., Hopkins, E., Sol-Church, K., Stabley, D.L., Axelrad, M.E., Doyle, D., Dobyns, W.B., Hudson, C., Johnson, J., Tenconi, R., et al. (2011). Phenotypic analysis of individuals with Costello syndrome due to HRAS p.G13C. Am. J. Med. Genet. A. *155A*, 706–716.
49. Gripp, K.W., Sol-Church, K., Smpokou, P., Graham, G.E., Stevenson, D.A., Hanson, H., Viskochil, D.H., Baker, L.C., Russo, B., Gardner, N., et al. (2015). An attenuated phenotype of Costello syndrome in three unrelated individuals with a *HRAS* c.179G>A (p.Gly60Asp) mutation correlates with uncommon functional consequences. Am. J. Med. Genet. A. *167A*, 2085–2097.
50. Bertola, D., Buscarilli, M., Stabley, D.L., Baker, L., Doyle, D., Bartholomew, D.W., Sol-Church, K., and Gripp, K.W. (2017). Phenotypic spectrum of Costello syndrome individuals harboring the rare *HRAS* mutation p.Gly13Asp. Am. J. Med. Genet. A. *173*, 1309–1318.
51. Pantaleoni, F., Lev, D., Cirstea, I.C., Motta, M., Lepri, F.R., Bottero, L., Cecchetti, S., Linger, I., Paolacci, S., Flex, E., et al. (2017). Aberrant HRAS transcript processing underlies a distinctive phenotype within the RASopathy clinical spectrum. Hum. Mutat. *38*, 798–804.
52. Altmüller, F., Lissewski, C., Bertola, D., Flex, E., Stark, Z., Spranger, S., Baynam, G., Buscarilli, M., Dyack, S., Gillis, J., et al. (2017). Genotype and phenotype spectrum of NRAS germline variants. Eur. J. Hum. Genet. *25*, 823–831.
53. Stark, Z., Gillessen-Kaesbach, G., Ryan, M.M., Cirstea, I.C., Gremer, L., Ahmadian, M.R., Savarirayan, R., and Zenker, M. (2012). Two novel germline KRAS mutations: expanding the molecular and clinical phenotype. Clin. Genet. *81*, 590–594.
54. Nussinov, R., Zhang, M., Tsai, C.J., Liao, T.J., Fushman, D., and Jang, H. (2018). Autoinhibition in Ras effectors Raf, PI3Kα, and RASSF5: a comprehensive review underscoring the challenges in pharmacological intervention. Biophys. Rev. *10*, 1263–1282.
55. Graham, S.M., Cox, A.D., Drivas, G., Rush, M.G., D'Eustachio, P., and Der, C.J. (1994). Aberrant function of the Ras-related protein TC21/R-Ras2 triggers malignant transformation. Mol. Cell. Biol. *14*, 4108–4115.
56. Niihori, T., Nagai, K., Fujita, A., Ohashi, H., Okamoto, N., Okada, S., Harada, A., Kihara, H., Arbogast, T., Funayama, R., et al. (2019). Germline activating *RRAS2* mutations cause Noonan syndrome. Am. J. Hum. Genet. *104*, this issue, 1233–1240.

Chapter V

Activating *MRAS* Mutations Cause Noonan Syndrome Associated With Hypertrophic Cardiomyopathy

Graphical abstract

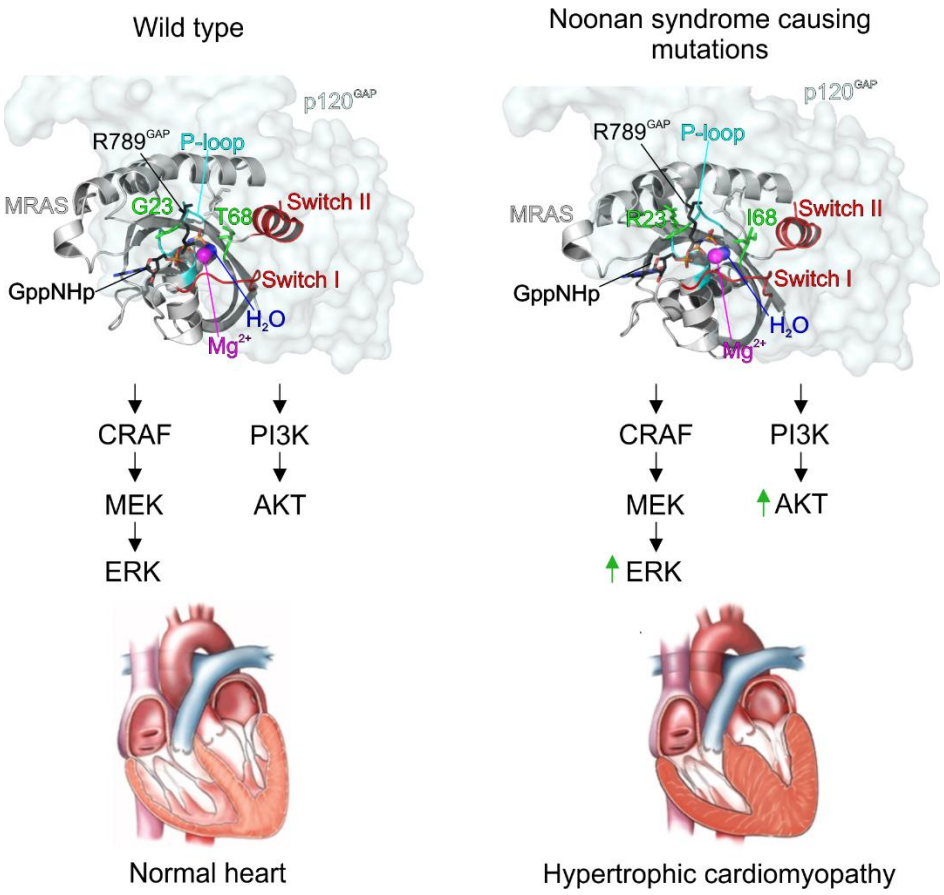

Status: Published in Human Molecular Genetics, May 21th 2019

Impact factor: 4.544

Own proportion: 15 %

Structural modeling, figure preparation, writing the manuscript, discussion.

ACTIVATING *MRAS* MUTATIONS CAUSE NOONAN SYNDROME ASSOCIATED WITH HYPERTROPHIC CARDIOMYOPATHY

Marialetizia Motta[1,#], Lena Sagi-Dain[2,#], Oliver H.F. Krumbach[3], Andreas Hahn[4], Amir Peleg[2], Alina German[5], Christina Lissewski[6], Simona Coppola[7], Francesca Pantaleoni[1], Luisa Kocherscheid[6], Franziska Altmüller[6], Denny Schanze[6], Thushiha Logeswaran[8], Soheyla Chahrokh-Zadeh[9], Anna Munzig[9], Saeideh Nakhaei-Rad[3,§], Hélène Cavé[10,11], Mohammad R. Ahmadian[3], Marco Tartaglia[1,^,*], Martin Zenker[6,^]

[1]Genetics and Rare Diseases Research Division, Ospedale Pediatrico Bambino Gesù, IRCCS, Rome, Italy

[2]The Human Genetic institute, Carmel Medical Center, Ruth and Bruce Rappaport Faculty of Medicine, Israel Institute of Technology, Haifa, Israel

[3]Institute of Biochemistry and Molecular Biology II, Medical Faculty of the Heinrich Heine University, Düsseldorf, Germany.

[4]Department of Child Neurology, University Hospital, Gießen, Germany

[5]Pediatric Department, Bnai-Zion Medical Center and Clalit Health Maintenance Organization, Haifa, Israel

[6]Institute of Human Genetics, University Hospital, Magdeburg, Germany

[7]National Centre for Rare Diseases, Istituto Superiore di Sanità, Rome, Italy

[8]Pediatric Heart Center, University Hospital, Gießen, Germany

[9]Center of Human Genetics and Laboratory Diagnostics, Martinsried, Germany

[10]Assistance Publique des Hôpitaux de Paris (AP-HP), Hôpital Robert Debré, Département de Génétique, 75019 Paris, France

[11]INSERM UMR 1131, Institut de Recherche Saint-Louis, Université de Paris, 75010 Paris, France

[#]These authors contributed equally to this work.

[§]Current address: Stem Cell Biology and Regenerative Medicine, Institute of Biotechnology, Ferdowsi University of Mashhad, Mashhad, Iran.

[^]These authors jointly coordinated this work.

*Corresponding author.

Correspondence:

Marco Tartaglia, PhD

Genetics and Rare Diseases Research Division

Ospedale Pediatrico Bambino Gesù

Viale di San Paolo 15

00146 Rome, Italy

Phone: +39 06 68593742

Fax: +39 06 68594584

Email: marco.tartaglia@opbg.net

ABSTRACT

The RASopathies are a group of genetic syndromes caused by upregulated RAS signaling. Noonan syndrome (NS), the most common entity among the RASopathies, is characterized mainly by short stature, cardiac anomalies and distinctive facial features. Mutations in multiple RAS-MAPK pathway-related genes have been associated with NS and related phenotypes.

We describe two unrelated patients presenting with hypertrophic cardiomyopathy (HCM) and dysmorphic features suggestive of NS. One of them died in the neonatal period because of cardiac failure. Targeted sequencing revealed *de novo MRAS* variants, c.203C>T (p.Thr68Ile) and c.67G>C (p.Gly23Arg) as causative events. *MRAS* has only recently been related to NS based on the observation of two unrelated affected individuals with *de novo* variants involving the same codons here found mutated. Gly23 and Thr68 are highly conserved residues, and the corresponding codons are known hotspots for RASopathy-associated mutations in other RAS proteins. Functional analyses documented high level of activation of MRAS mutants due to impaired GTPase activity, which was associated with constitutive plasma membrane targeting, prolonged localization in non-raft microdomains, enhanced binding to PPP1CB and SHOC2 protein, and variably increased MAPK and PI3K-AKT activation.

This report provides additional evidence that a narrow spectrum of activating mutations in *MRAS* represents another rare cause of NS, and that *MRAS* has to be counted among the RASopathy genes predisposing to HCM. Moreover, our findings further emphasize the relevance of the MRAS-SHOC2-PPP1CB axis in the control of MAPK signaling, and the contribution of both MAPK and PI3K-AKT pathways in MRAS functional upregulation.

INTRODUCTION

The RASopathies are a group of genetic disorders caused by germline mutations in genes that encode components and regulators of the RAS/mitogen activated protein kinase (MAPK) pathway, an intracellular signaling cascade that is involved in many cellular, developmental and physiological processes (1-3). Taken together, the RASopathies represent the most common non-chromosomal diseases affecting development, with an estimated prevalence of 1 in 2000 individuals. This clinically variable group of disorders includes Noonan syndrome (NS, OMIM PS163950), Costello syndrome (OMIM 218040), cardiofaciocutaneous syndrome (OMIM PS115150), NS with multiple lentigines (LEOPARD syndrome; OMIM PS151100), Mazzanti syndrome (NS-like disorder with loose anagen hair; OMIM PS607721), neurofibromatosis type 1 (OMIM 162200), Legius syndrome (OMIM 611431), and an increasing number of related conditions. These disorders share some major clinical features, such as a distinctive pattern of facial dysmorphisms, post-natal growth failure, cutaneous, cardiac and skeletal defects, cognitive deficits, behavioral abnormalities, and a variable increased risk for cancer (1-3).

NS, the most common entity among the RASopathies, is characterized mainly by short stature, a wide spectrum of congenital cardiac anomalies and hypertrophic cardiomyopathy (HCM) (50%-80% of the affected subjects), and a recognizable facies, which includes hypertelorism with down-slanting palpebral fissures and low-set, posteriorly rotated ears as major features (4, 5). In addition, patients with NS show an increased risk for bleeding disorders and certain malignancies, and may have variable developmental delay and cognitive deficits. The syndrome has been associated with mutations in more than 10 genes (6), and it is mainly transmitted as an autosomal dominant trait with a high proportion of *de novo* mutations, although a recessive form of NS related to biallelic inactivating/hypomorphic mutations in *LZTR1* gene (OMIM #600574) has recently been recognized and characterized (7-9). Mutations affect genes encoding signal transducers participating in the RAS-MAPK backbone as well as proteins functioning in signaling circuits with positive or negative modulatory role on this signaling cascade. While this evidence strongly points

to the upregulation of MAPK signaling as a major event implicated in disease pathogenesis, the contribution of other signaling pathways to disease pathogenesis has recently been suggested and documented (10-14). Notably, several clinically relevant genotype-phenotype correlations have been recognized. Among these, an increased prevalence of HCM among affected subjects heterozygous for a specific class of missense mutations in *RAF1*, and mutations affecting the *RIT1* and *LZTR1* genes has been described (15-20).

One of the genes recently reported to be implicated in NS is *MRAS* (MIM #608435), encoding a small monomeric GTPase belonging to the RAS family controlling multiple signaling pathways, including the MAPK and PI3K-AKT cascades (20, 21). One subject with clinical diagnosis of NS showing HCM as associated feature was reported to carry a *de novo* missense mutation (p.Gly23Val) that was documented to stabilize MRAS in its active conformation, and to slightly enhance signaling through the MAPK cascade (22). The same team identified a second subject carrying a different *de novo MRAS* variant (p.Thr68Ile) among a relatively large cohort of mutation-negative patients with clinical diagnosis of NS associated with HCM (22), pointing to *MRAS* as a novel disease gene implicated in NS and predisposing to HCM, when mutated.

In this work, we report on two patients with clinical features of NS caused by a *de novo* activating mutation of *MRAS*, representing the third and fourth individual with this particular genetic etiology reported to date. We characterize the biochemical consequences of the three NS-causing mutations reported thus far on MRAS protein behavior and demonstrate their activating effect in modulating the MAPK and PI3K-AKT cascades, with the former found to be upregulated in a cell-specific manner. We also provide evidence that the upregulation of MAPK signaling is associated with enhanced binding of the three NS-causing MRAS mutants to PPP1CB and SHOC2 proteins, confirming further the relevance of the MRAS-SHOC2-PPP1CB complex in positively modulating MAPK signaling. The presence of cardiac hypertrophy in all reported individuals with *MRAS* mutations suggests that *MRAS* has to be counted among the RASopathy genes predisposing

to HCM, further emphasizing the importance of a comprehensive mutation screening approach for a more effective patient management.

RESULTS

Clinical description

Patient 1, first child of healthy non-consanguineous, North African Jewish parents, was born after 38 weeks of an uneventful pregnancy and was delivered without complications. His birth weight, head circumference and body length were 2,945 g (-1.1 SD), 33.5 cm (-1.1 SD) and 47 cm (-1.6 SD), respectively. Apgar score was 9/10, and initial physical examination noted only mild pectus excavatum. Three days after the delivery, the patient was admitted to neonatal intensive care unit due to dyspnea and treated by intravenous antibiotics due to suspected pneumonia. Echocardiography at the age of four days demonstrated a patent foramen ovale and an atrial septal defect. After recovery from his infection the patient was discharged at age 10 days. Repeated echocardiography at age 10 months revealed dilatation of coronary sinus, with normal ventricular function. However, at age 14 months mild left ventricular hypertrophy was first noted, together with a small septal defect causing left-to-right shunting. At the age of 15 months, growth delay with appropriate weight was noted (height and weight at -2.0 SD), along with obstructive sleep apnea. Ophthalmological examination demonstrated intermittent exotropia, mainly on the right. The patient was hospitalized few times due to infectious diseases (RSV bronchiolitis at age four months, and recurrent otitis media and infectious mononucleosis at age 15 months). Sweat test and nasal nitric oxide were normal. Audiological examination showed moderate hearing loss due to middle ear effusions. At age 20 months, adenoidectomy and myringotomy with hollow tube insertion were performed. Independent walking was achieved at the age of 17 months. At age two years, the child had no active speech and was diagnosed with mild global developmental delay. Endocrinological evaluation at that age showed normal levels of prolactin, IGF1, IGFBP3, and thyroid function tests. However, glucagon stimulation test was suggestive of growth hormone (GH) deficiency (GH values ranging from 1.1 to 4.2 µg/L, lower than the accepted cutoff of 7.5 µg/L). The patient was referred for genetic evaluation at age two years and three months. His height and weight were both slightly below normal values (82 cm and 10.7 kg, respectively; both -2.0 SD), head circumference was 47.5

cm (+1.0 SD). Facial features were suggestive of NS, with hypertelorism, downslanting palpebral fissures, palpebral ptosis, a short bulbous nose with low nasal bridge and upturned nostrils, long and smooth philtrum, full drooping cheeks with prominent nasolabial folds, small mouth, and mild retrognathia. Parents declined the publication of photos, but the evaluation of the craniofacial phenotype by a RASopathy expert (M.Z.) confirmed it to be typical of NS. In addition, evaluation of the facial photograph using face2gene (https://www.face2gene.com/) yielded NS and cardiofaciocutaneous syndrome as the best hits. One café-au-lait spot sized 10x3 mm was noted on his right lower abdomen, as well as mild pectus excavatum and relatively thin scalp hair. Following the genetic diagnosis, treatment with GH was started. Follow-up neurodevelopmental evaluation showed significant global developmental delay in all fields (Developmental Quotient score of 56). Echocardiography at the age of 3 years documented concentric hypertrophy of cardiac ventricles.

Patient 2, a first child of healthy, non-consanguineous German parents, was born spontaneously without complications at 37 gestational weeks after uneventful pregnancy. Apgar scores were 6/8/10 and umbilical cord pH was 7.34. Her birth weight was 3,440 g (+0.5 SD), length was 49 cm (-0.7 SD), and head circumference was 34 cm (-0.5 SD). Respiratory distress was noticed immediately after birth and required CPAP support. Clinical examination showed a short neck with excess skin folds, low set ears, a broad forehead, mild ptosis, hypertelorism, and a systolic heart murmur. X-ray examination of the chest and echocardiography were performed because of persistent tachydyspnea without laboratory signs of a neonatal infection. These tests disclosed significant cardiomegaly (Fig. 1A) with marked biventricular hypertrophic cardiomyopathy (HCM). The patient was treated with propranolol. Although respiratory support could be discontinued after two weeks, cardiac hypertrophy worsened, obstruction of the left-ventricular outflow tract occurred, and cardiac function declined. At age four weeks, echocardiography revealed HCM with severe diastolic dysfunction and mitral valve insufficiency grade 3. Interventricular septal (IVS) thickness was 12 mm (z-score +5.6) during diastole and 15 mm (z-score +6) during systole. Left-ventricular posterior wall thickness was 10 mm (z-score + 5.4)

during diastole and 12 mm (z-score +5.6) during systole. The left ventricular outflow gradient was increased to 70 mmHg reflecting marked obstruction (Fig. 1B, C). In addition, an increasing obstruction of the right ventricular outflow tract with a moderate stenosis of 35 mmHg was observed. A RASopathy was suspected because of the facial gestalt in conjunction with the severe biventricular obstructive HCM. After discussing the limited therapeutic options with the parents, they voted for palliative care. The girl was discharged home and deceased at age two months due to cardiac failure. Facial photos are not available.

Mutation analyses

In patient 1, multi-gene panel sequencing identified a heterozygous missense variant c.203C>T in exon 3 of *MRAS*, predicting the substitution of a threonine residue by isoleucine (p.Thr68Ile) (Supplementary Fig. 1). No other variants in NS-related genes were qualified as clinically relevant. Molecular genetic testing of both parents excluded the *MRAS* variant in leukocyte DNA, indicating a *de novo* origin of the missense substitution. The identical sequence change in this gene had recently been reported as a *de novo* event in a patient affected by NS with cardiac hypertrophy (22). Patient 1 belonged to a cohort of 288 individuals with a clinical diagnosis of a RASopathy who had previously been tested negative for all known RASopathy-associated genes. The absence of a specific bias in enrollment of these subjects suggest that *MRAS* mutations account for a very small proportion of NS cases. In patient 2, multi-gene panel sequencing revealed the heterozygous *MRAS* missense variant, c.67G>C (p.Gly23Arg), which was again confirmed to be *de novo* (not present in parental leukocyte DNA samples) (Supplementary Fig. 1). A different amino acid substitution at the same codon, p.Gly23Val, had been reported as NS-causing mutation previously (22). Both variants were not reported in major databases (ExAC, gnomAD, 1000G) (Supplementary Table 1). The amino acid residues corresponding to Gly^{23} and Thr^{68} in MRAS are highly conserved in all RAS paralogs and orthologs, from bacteria to mammals (Supplementary Fig. 2). According to various prediction programs, the variants were consistently predicted as pathogenic (Supplementary Table

1). Finally, *MRAS* mutation scan was also performed on a cohort of 1,840 consecutive patients with clinical diagnosis of RASopathy or having a phenotype suggestive of these disorders. No putative pathogenic *MRAS* change was identified, while a large proportion of subjects was found positive for disease-causing mutations in other genes (*e.g.*, *PTPN11*, n=213; *SOS1*, n=56; *BRAF*, n=49, *RAF1*, n=23). Overall, these findings indicate that *MRAS* mutations represent a rare event in NS.

Structural and biochemical characterization of the NS-causing *MRAS* mutations

Similar to the other members of the RAS superfamily of GTPases, MRAS cycles between a GTP-bound (active) and a GDP-bound (inactive) form. The transition between the two states is tightly regulated by proteins promoting GDP release (guanine nucleotide exchange factors, GEFs) and those stimulating the basally low GTPase activity (GTPase-activating proteins, GAPs). In their GTP-bound, active state, MRAS interacts with effector proteins *via* its effector binding regions (switch I and switch II). Of note, MRAS possesses a different structure of the switch I region (residues 33 to 49) as compared to other human paralogs, which has been proposed to be based on an impaired intramolecular interaction of Thr^{45} and the γ-phosphate of GTP (23, 24). Though this uniqueness, the functions of Gly^{23} and Thr^{68} in MRAS are comparable to those of the corresponding residues of other RAS paralogs, as they are part of the highly conserved guanine nucleotide binding motifs 1 and 3, which are also known as the phosphate-binding loop (Gly^{20} to Ser^{27}) and the switch II region (Asp^{67} to Arg^{83}), respectively (Fig. 2A). These amino acid residues stabilize the nucleotide bound state by contacting Asp^{67} with Ser^{27} and a water molecule coordinating the magnesium ion in the MRAS active site (Fig. 2B) (22, 25). Notably, the P-loop region is critical for the GTP binding and hydrolysis and thus for the function of GAPs, which stimulate GTP hydrolysis by stabilizing the transition state of this reaction. Substitution of the glycine residue by arginine or valine causes a steric clash, resulting in an impaired or defective response of the GTPase to GAPs (26). A similar consideration applies for Thr^{68}, which is adjacent to the catalytic Gln^{71}, and is located in the interswitch region of MRAS stabilizing the active site. Based on these considerations, the

p.Gly23Val/Arg and p.Thr68Ile changes are predicted to affect proper GDP/GTP exchange and GTP hydrolysis, and thus cause a gain of function effect. Based on the tight interaction of Thr^{68} with the switch II, however, a perturbation of proper binding with effector proteins as the result of the substitution of this residue by isoleucine cannot be ruled out.

To evaluate the impact of the mutations on MRAS functional behavior, HEK 293T cells were transiently transfected to express wild-type MRAS or each of three generated mutants ($MRAS^{G23R}$, $MRAS^{G23V}$ and $MRAS^{T68I}$) and the active state and subcellular localization of the GTPases were assessed. Pull-down assays directed to measure the GTP-bound levels of the four Myc-tagged proteins revealed a higher level of GTP-bound $MRAS^{G23R}$, $MRAS^{G23V}$ and $MRAS^{T68I}$ compared to the wild-type protein in both serum-free condition and following EGF stimulation (Fig. 3A). This finding indicates hyperactivation of the three mutants, which is likely to be the result of defective nucleotide binding and/or impaired GTPase activity, as predicted by the structural analysis.

Localization of RAS proteins is finely modulated, and controls the specific activation of different signaling platforms, which mediate both the extent and dynamics of signal flow and the differential activation of effectors. Based on these considerations, we assessed the subcellular localization of wild-type and mutant MRAS proteins. To this goal, immunofluorescence microscopy analysis was performed in COS-1 cells transiently expressing the Myc-tagged MRAS constructs. The wild-type MRAS protein was widely distributed in endomembranes in cells under serum-starved condition, but massively translocated to the plasma membrane following stimulation, as shown by the extensive colocalization with cortical actin (Fig. 3B). In contrast, $MRAS^{G23R}$, $MRAS^{G23V}$ and $MRAS^{T68I}$ appeared to be specifically targeted to the cell membrane both in serum-starved and EGF-stimulated cells. Of note, it has been shown that the dynamic redistribution in intracellular membranes of the RAS proteins includes their reallocation in structurally distinct microdomains of the plasma membrane. Among these, lipid rafts are cholesterol/sphingolipid-rich domains documented to serve as reservoirs for inactive signal transducers or sorting platforms for signal transduction mediating both compartmentalization and fine tuning of signaling events (27-

29). By using cell fractionation experiments, localization of MRAS in lipid rafts was found to be dynamic since it was distributed in insoluble fractions containing lipid rafts (fractions 4-6) as well as in soluble fractions (fractions 7-10), the latter including proteins located in other membrane domains or in the cytosol, under serum starved condition (Fig. 3C). The GTPase translocated to non-raft domains of the plasma membrane following 1 minute of EGF stimulation, but redistributed from non-raft to raft domains after 10 minutes of stimulation, strongly suggesting that MRAS exerts its function in non-raft plasma membrane subdomains, similarly to what documented for HRAS (30, 31). We assessed the dynamic distribution of the $MRAS^{G23V}$ and $MRAS^{T68I}$ mutants in different plasma membrane domains. As we previously documented for other RAS mutants (32), differently from the wild-type protein, a prolonged localization of both $MRAS^{G23V}$ and $MRAS^{T68I}$ in non-rafts fractions was appreciated (Fig. 3C). This finding and the prevalent GTP-bound state of both $MRAS^{G23V}$ and $MRAS^{T68I}$ proteins supports the idea that, similarly to what has been reported for HRAS, hyperactive MRAS mutants are preferentially associated with non-raft domains of the plasma membrane.

NS-causing *MRAS* mutations promote enhanced MAPK and PI3K-AKT signaling and increased binding to SHOC2 and PPP1CB

To evaluate the consequences of constitutive activation of the mutants on intracellular signaling, the extent of ERK and AKT phosphorylation was assessed. Transient overexpression of the $MRAS^{G23V}$ and $MRAS^{T68I}$ mutants in HEK 293T cells was found to promote only a slightly increased, transient EGF-dependent ERK phosphorylation after 5 minutes of stimulation. By contrast, a more evident increased level of AKT phosphorylation was observed basally in cells expressing each of the two mutants (Fig. 4A). Increased levels of phosphorylated AKT were further boosted by EGF stimulation. Remarkably, the same assays performed in transiently transfected Neuro2A cells provided evidence for a significantly enhanced stimulus-dependent ERK phosphorylation promoted by the three MRAS mutants and confirmed the constitutive increased level of AKT phosphorylation

even though to a lesser extent (Fig. 4B). These data document that the three MRAS mutants behave as hypermorph proteins promoting the activation of the RAF-MEK-ERK and PI3K-AKT pathways, with a modulatory effect depending on the cellular context in both cascades, at least in our experimental conditions.

MRAS positively modulates MAPK signaling by promoting SHOC2-mediated translocation of the catalytic protein phosphatase 1 (PP1C) subunit to the plasma membrane, which is a required step for a stable interaction of RAF1 with RAS proteins and subsequent activation of the kinase (33). Based on these considerations, we evaluated the binding properties of the three MRAS mutants to both SHOC2 and PPP1CB, the latter being one of the three catalytic PP1 subunits. Co-immunoprecipitation assays were performed using cell lysates collected from Neuro2A cells transiently co-expressing each of the four Myc-tagged MRAS proteins with V5-tagged SHOC2 (Fig. 4C, left panel). As shown, the three mutants showed an increased binding to SHOC2 when compared to the wild-type protein. Similarly, co-immunoprecipitation analyses using lysates collected from cells transfected to co-express the Myc-tagged MRAS proteins with V5-tagged PPP1CB documented an augmented binding of the three mutants to the catalytic subunit of PP1 compared to wild-type MRAS (Fig. 4C, right panel). These data indicate that the three NS-causing *MRAS* mutations are activating and enhance signaling through the MAPK cascade by promoting an increased and/or more stable binding of MRAS to both SHOC2 and PP1C, which is in line with recently published data (34).

DISCUSSION

Here, we report on two patients in whom the clinical diagnosis of NS was found to be causally associated with *de novo* activating mutations of *MRAS*, and provide biochemical and functional data documenting the activating effect of these mutations on MAPK and PI3K-AKT signaling. Our findings strengthen a recent report proposing the involvement of upregulated MRAS function in NS, emphasize the association between *MRAS* mutations and HCM, and support the view that multiple signaling pathways triggered by MRAS functional upregulation are likely implicated in disease pathogenesis.

MRAS mutations had previously been reported to underlie NS in two unrelated subjects (22). One patient was a 15-year-old girl with clinical features fitting NS and having cardiac hypertrophy. Trio-based whole exome sequencing revealed a *de novo* missense mutation (c.68G>T, p.Gly23Val). The second subject was heterozygous for a different *de novo MRAS* variant (c.203C>T, p.Thr68Ile), identified by the same team through targeted mutational analysis in 109 unrelated patients with a suspected RASopathy and concomitant cardiac hypertrophy, who had previously been tested negative for mutations in previously identified genes implicated in NS. Notably, the latter variant is identical to the one identified as a *de novo* event in patient 1 of the present report, while the other missense change reported by Higgins et al. (22) affects the same codon as in our patient 2. These findings indicate that a narrow spectrum of missense mutations of *MRAS* cause NS. In the present study, patient 1 was the only case identified with a *MRAS* mutation among 288 individuals with a clinical diagnosis of a RASopathy who had previously been tested negative for all known RASopathy-associated genes, and no *MRAS* mutation was identified in an unselected cohort of 1,840 subjects with a clinical diagnosis of RASopathy or with features suggestive of these disorders. We therefore assume that the frequency of *MRAS*-related NS is relatively rare.

The RAS superfamily of GTP/GDP-binding proteins includes a number of membrane-associated GTPases that control several cellular processes in response to a variety of extracellular stimuli, by cycling between an active, GTP-bound state and an inactive, GDP-bound state (20, 21,

35). Within this large group, a relatively small subfamily of structurally and functionally related proteins (*i.e.*, HRAS, NRAS, and two KRAS isoforms) play a major role in controlling key cellular processes (*e.g.*, proliferation, differentiation, survival and metabolism) as well as early and late developmental programs. Their importance in these processes is exemplified by the role of somatic mutations in these genes as driver events in oncogenesis, and the involvement of these genes in RASopathies when their mutations have germline origin (1-3, 36; COSMIC database, https://cancer.sanger.ac.uk/cosmic). Germline mutations in *NRAS* account for a small proportion of NS, while those affecting *HRAS* and *KRAS* underlie CS and a fraction of CFCS and NS, respectively (37-41). A closely related subfamily of GTPases includes RRAS, RRAS2 and MRAS. Similarly to the classical p21 RAS proteins, these GTPases control multiple cellular and developmental processes, and contribute to cancer when mutated (COSMIC database). Remarkably, recent studies have also established that activating mutations in these proteins underlie a small fraction of NS or related phenotypes when inherited from the germline (22, 42-44). Likewise the other RAS members, MRAS is a membrane-associated protein. It shares about 50% sequence identity with the four classical p21 RAS proteins, and a higher level of conservation within the regions that mediate GTP/GDP binding and interactions with positive and negative regulators, and several effector proteins (20, 21, 35, 45). MRAS is expressed in multiple tissues and cell types (Human Protein Atlas, https://www.proteinatlas.org/), and participates in a wide variety of signaling pathways with functions in various biological processes including bone and neural tissue formation (45-49). While MRAS has been shown to be a relatively weak activator of the RAF-MEK-ERK cascade when compared to HRAS, it has been reported to more efficiently enhance PI3K-AKT signaling (50). Higgins and colleagues were able to show that p.Gly23Val results in a protein that is more abundant in its active GTP-bound form and that weakly enhances MAPK signaling in response to growth factors (22). Biochemical/functional validation assays were not performed for the p.Thr68Ile variant. In a more recent study, the two MRAS mutants, p.Gly23Val and p.Thr68Ile, have been shown to confer MAPK pathway upregulation (34). Those observations are consistent

with our findings indicating an activating role of all the three NS-causing *MRAS* mutations in promoting a GTP-bound, active state of the GTPase, its steady targeting to the plasma membrane, and a variable upregulation of the MAPK cascade, which however appears to be dependent on the cellular context. Of note, we observed that all mutants are also able to substantially upregulate the PI3K-AKT cascade, at both the basal level and upon EGF stimulation, which is in line with the known modulatory role of MRAS on this signal cascade (50).

In the context of the RAF-MEK-ERK signaling cascade, MRAS has specific functions that appear to be unique among the RAS family: active GTP-bound MRAS together with SHOC2 form a ternary complex with PP1C that has a key role in promoting SHOC2-mediated PP1C translocation to the plasma membrane, which is required for dephosphorylating a regulatory serine residue of RAF1 inhibiting stable interaction of the kinase with RAS proteins (33, 34). Remarkably, missense mutations in *SHOC2* and *PPP1CB* cause Mazzanti syndrome (51, 52), a RASopathy clinically related to NS, by promoting a more stable and/or prolonged formation of the complex, which in turn promotes an enhanced and sustained activation of the MAPK cascade (34, 51; our present and unpublished observations). We originally reported that the recurrent missense change in SHOC2 (p.Ser2Gly) underlying Mazzanti syndrome promotes *N*-myristoylation and constitutive plasma membrane targeting of the mutant protein, and enhanced ERK activation in a cell type-specific fashion (51). Recent studies have shown that myristylated SHOC2 has enhanced/stable binding to both MRAS and PPP1CB (34), suggesting a more efficient plasma membrane targeting of the ternary complex. Young and colleagues also demonstrated a similar behavior for disease-causing MRAS and PPP1CB mutants, which were further confirmed by the present observations, supporting a model in which the perturbing role of *SHOC2*, *PPP1CB* and *MRAS* mutations on MAPK signaling is exerted by enhancing the MRAS-SHOC2-PPP1CB complex formation at the plasma membrane, with consequent more efficient/prolonged RAF1 dephosphorylation at Ser^{259} (34). Notably, the constitutive targeting of all MRAS mutants and their abnormal cycling between lipid rafts and non-raft membrane microdomains here documented reinforce the concept of the required targeting of

this protein to the plasma membrane for the specific function of the MRAS-SHOC2-PPP1CB complex, and that formation and function of this ternary complex is attained in non-raft microdomains of the plasma membrane.

Missense changes p.Gly13Arg and p.Thr58Ile in KRAS, NRAS, and HRAS, which are corresponding to p.Gly23Arg and p.Thr68Ile in MRAS, have been reported in tumors, mosaic RASopathies and RASopathies (*i.e.*, NS and Costello syndrome) (Supplementary Table 1), respectively, and have activating effects (39, 53-55). HRAS substitutions at codon 13 (*e.g.*, p.Gly13Cys, p.Gly13Ser, and Gly13Val) have been shown to confer impaired GAP-stimulated GTPase acivity (56). Similarly, mutant RAS proteins with the p.Thr58Ile substitution have been shown to upregulate the function of the protein, even though with a milder extent compared with the Gly^{12} and Gly^{13} changes (25, 39, 54). As in the case of $KRAS^{T58I}$ (25), substitution at Thr^{68} to Ile in MRAS most likely leads to increased GDP/GTP exchange and thus to its accumulation in the active state of the GTPase. Being integral parts of the nucleotide binding motifs of MRAS, Gly^{23} is responsible for binding to the phosphate groups of GTP/GDP, while Thr^{68} contacts Ser^{27} and Asp^{67} from the P-loop and switch II region of MRAS and is involved in magnesium ion coordination. Substitution of Gly^{23} and Thr^{68} thus is predicted to impair GTP hydrolysis and GTP/GDP binding, respectively, thereby promoting an overall stabilized GTP-bound state of the protein and enhanced downstream signaling, which was confirmed experimentally.

Analysis of clinical characteristics of the two previously published cases with *MRAS* mutations and the ones reported here (Table 1) shows that generally the individuals affected by these mutations appear to have all the characteristic signs and symptoms of NS, making it impossible at the current stage to distinguish *MRAS* mutation-related NS from NS of other genetic etiologies. Of note, the presence of cardiac hypertrophy in all four patients reported to date suggests that *MRAS* belongs to the NS genes with particular association to HCM (similar to *RAF1* and *RIT1*). This was already suggested by Higgins et al. (22) and it is further corroborated by the two additional observations we present here. The course of HCM was variable in the four patients with

MRAS mutation-related NS known so far. One patient reported in the original paper required myectomy for biventricular outflow tract obstruction at age 8 years, while little information is available from the second case. The present patient 2 displayed progressive HCM leading to early lethality. This patient had the most severe outcome, which may be related to more severe activating effects of this particular mutation.

Based on the specific association between heterozygous mutations in genes encoding other partners of the complex, SHOC2 and PPP1CB, and Mazzanti syndrome, activating mutations in *MRAS* gene might also be anticipated to lead to phenotypic features characteristic of this RASopathy (*e.g.*, loose anagen hair, characteristic facies, high frequency of growth hormone deficiency). However, typical phenotypic features of Mazzanti syndrome have not been documented in the previously reported cases and were not obvious in the present patients either. While the number of reported individuals with *MRAS* mutations are insufficient to make a final conclusion about a possible relation of *MRAS* mutations with Mazzanti syndrome, the available clinical data support the idea that *MRAS* mutations are specifically linked to NS, which is likely to be associated with the more articulated impact of dysregulated *MRAS* function on intracellular signaling (e.g., enhanced PI3K-AKT signaling).

We documented that depending upon the cellular context, NS-causing MRAS mutants differentially impact MAPK and PI3K-AKT signaling cascades. This finding has relevant clinical implications, which are linked to the current effort to generate pharmacological targeted therapeutic approaches to treat the evolutive complications of RASopathies, including HCM. Indeed, accumulated evidence indicates that both the MAPK and PI3K-AKT-mTOR pathways contribute to HCM in RASopathies. Enhanced MAPK signaling has been demonstrated to contribute to HCM in the case of activating NS-causing mutations affecting *PTPN11*, *SOS1* and *RAF1* in multiple experimental models (57-59). These findings suggest that blockade of MAPK signaling by inhibitors targeting signal transducers participating in this cassette (*e.g.*, the MEK inhibitor, PD0325901) could be efficacious in post-natal treatments directed to block the

emergence of HCM or disease progression, depending upon when therapy is initiated. On the other hand, a specific class of mutations of *PTPN11* affecting the catalytic activity of the phosphatase and causing LEOPARD syndrome has been demonstrated to promote enhanced signaling through the PI3K-AKT-mTOR cascade (60). In this case, treatment with rapamycin, a drug specifically targeting MTOR, was found to prevent the emergence of HCM or reverse it depending on the age at which the drug was started in a mouse model of disease (61-63). These observations indicate that multiple pathways underlie HCM in RASopathies, and that distinct therapeutic approaches tailored for the specific molecular perturbation are required. For these reasons, understanding of the mechanism of disease is a required step for the identification of appropriate small molecules directed to treat HCM in RASopathies, including the form of NS caused by *MRAS* mutations.

In conclusion, the demonstration of *de novo* activating *MRAS* mutations in two patients with NS reinforces the evidence causally linking variants in *MRAS* to NS and confirms codons 23 and 68 as hot spots for NS-associated mutations in this gene. Importantly, our findings further strengthen the specific association of *MRAS* mutations with HCM and point to both the MAPK and PI3K-AKT-mTOR pathways as contributing to disease pathogenesis. Further studies are required to dissect the specific contribution of individual signaling cascades in HCM, a major evolutive complication of *MRAS*-associated NS, to the design of targeted therapeutic approaches.

MATERIALS AND METHODS

Mutation screening

Diagnostic genetic analysis was performed after obtaining parental consent according to national regulations. Genomic DNA derived from venous blood samples was analyzed by sequencing of a custom multi-gene panel covering the previously published RASopathy genes (*PTPN11*, *SOS1*, *SOS2*, *RAF1*, *RIT1*, *KRAS*, *NRAS*, *RRAS*, *HRAS*, *MRAS*, *SHOC2*, *LZTR1*, *CBL*, *CDC42*, *A2ML1*, *BRAF*, *MAP2K1*, *MAP2K2*, *NF1*, *SPRED1*, *PPP1CB*, and *RASA2*). Coverage was >50x for the entire coding region of the aforementioned genes. Enrichment of exonic and flanking intronic regions of these genes was achieved using a Nextera Rapid Capture Custom Enrichment Kit (Illumina, San Diego, CA) (patient 1) and a custom SureSelect XT Target Enrichment kit (Agilent Technologies Inc., Santa Clara, CA) (patient 2). Libraries were analyzed by parallel sequencing on a MiSeq (patient 1)/NextSeq 500 (patient 2) Sequencing System (Illumina). Obtained reads were aligned and compared to the reference sequences (hg37) using the CLC Genomics Workbench (Quiagen, Venlo, The Netherlands). Filtering of variants was based on occurrence in public databases (MAF<0.5% in ExAC and gnomAD) and predicted functional impact (PolyPhen-2, SIFT, MutationTaster, PROVEAN, and CADD). Identified variants of presumed pathogenic relevance were validated on the original DNA sample as well as parental DNA samples using conventional Sanger sequencing on an automated capillary sequencer (3500xL Genetic Analyzer, Applied Biosystems, Foster City, CA).

Structural analysis

The crystal structure of active, GppNHp-bound MRAS (PDB: 1X1S) was used to assess the impact of the identified substitutions affecting residues Gly^{23} and Thr^{68} (Gly^{13} and Thr^{58} in HRAS). To elucidate the consequence of the NS-causing mutations on GTP hydrolysis function, the structure of HRAS in complex with the catalytic domain of p120 RASGAP (PDB: 1WQ1) was analyzed, using Pymol molecular viewer (64).

Antibodies

The following antibodies were used: mouse monoclonal anti-Myc, rabbit polyclonal anti-p44/42 MAPK, mouse monoclonal anti-phospho-p44/42 MAPK (Thr^{202}/Tyr^{204}), rabbit monoclonal anti-AKT, rabbit monoclonal anti-phospho-AKT (Ser473) (Cell Signaling Technology, Danvers, MA); mouse monoclonal anti-Flotillin (BD Transduction Laboratories, Franklin Lakes, NJ); mouse monoclonal anti-V5 (Invitrogen, Carlsbad, CA); mouse monoclonal anti-GAPDH (Santa Cruz, Dallas, CA); mouse monoclonal anti-β-actin, horseradish peroxidase-conjugated anti-rabbit or anti-mouse (Sigma-Aldrich); anti-mouse conjugated to Alexa Fluor 594 (Molecular Probes, Eugene, OR).

Constructs

The entire coding sequence of wild-type (WT) *MRAS* was cloned into the pcDNA3.1/Myc A eukaryotic expression vector (Addgene, Cambridge, MA). Mutant MRAS constructs carrying the p.Gly23Val, p.Gly23Arg and p.Thr68Ile amino acid substitutions were generated by PCR-based site-directed mutagenesis using the QuikChange II Site-Directed Mutagenesis Kit (Stratagene, La Jolla, CA). The identity of each construct was verified by bidirectional Sanger sequencing.

Cell culture, transfection, and EGF stimulation

COS-1, Neuro2A and HEK 293T cells (American Type Culture Collection, Manassas, VA) were cultured in DMEM supplemented with 10% heat-inactivated FBS, 2 mM glutamine, 100 units/ml of penicillin and 100 μg/ml of streptomycin (Euroclone, Wetherby, UK), and maintained at 37 °C in a humidified atmosphere containing 5% CO2. Subconfluent cells were transfected using the Fugene6 transfection reagent (Roche Diagnostics, Mannheim, Germany), according to the manufacturer's instructions. Serum-free DMEM and EGF (30 ng/ml) (Invitrogen, Carlsbad, CA) were utilized to starve and stimulate cells, respectively.

Immunoblotting

Assays were preformed as previously reported (8, 65). Briefly, cells were lysed in radio-immunoprecipitation assay (RIPA) buffer, pH 8.0, containing 20 mM NaF, 1mM Na_3VO_4 and protease inhibitors. Lysates were kept on ice for 30 min and then centrifuged at 16,000*g* for 20 min at 4 °C. Supernatants were collected and their protein concentration was determined by bicinchoninic acid (BCA) assay (66), using bovine serum albumin (BSA) as a standard. Load samples containing equal amount of total proteins were resolved by 10% sodium dodecyl sulphate (SDS)-polyacrylamide gel. After electrophoresis, proteins were transferred to nitrocellulose membrane using the Trans-Blot Turbo transfer system (Bio-Rad Laboratories, Hercules, CA). Blots were blocked with 5% non-fat milk powder in PBS containing 0.1% Tween-20 for 1 h and incubated with specific antibodies for 1 h. Primary and secondary antibodies were diluted in blocking solution. Immunoreactive proteins were detected by an enhanced chemiluminescence (ECL) detection kit (Pierce Biotechnology, Rockford, IL). Densitometric analysis of protein bands was performed using Alpha View SA image software (Protein Simple, Santa Clara, CA).

Confocal laser scanning microscopy

COS-1 cells (3×10^4) were seeded on glass coverslips, transfected with the various Myc-tagged constructs for 24 h, serum starved for 16 h and stimulated with EGF for 5 or 15 min. Cells were fixed with 4% paraformaldehyde for 30 min at 4 °C and permeabilized with 0.5% Triton X-100 for 10 min at room temperature. Cells were then incubated with mouse anti-Myc antibody for 1 h at room temperature, rinsed twice with PBS, and incubated with a secondary goat anti-mouse antibody conjugated with Alexa Fluor 594 for 1 h at room temperature. After washing with PBS, cells were stained with Alexa Fluor 488 phalloidin dye to stain the filamentous actin (F-actin). Finally, glass coverslips were mounted on microscope slides using the Vectashield antifade medium containing DAPI (Vector Laboratories, Burlingame, CA) and analyzed by an Olympus FluoView FV1000

apparatus, using excitation spectral laser lines at 405, 488 and 568 nm. Signals from different fluorescent probes were taken in sequential scanning mode. Image processing used Adobe Photoshop 7.0 (Adobe Systems Incorporated, San Jose, CA).

RAS activation assay

RAS activation assays were carried out using a RAS activation assay kit (Millipore, Temecula, CA), according to the manufacturer's instructions. In brief, HEK 293T cells were transfected with the various constructs for 24 h, serum starved for 16 h, stimulated with EGF for 5 min or left untreated, washed in ice-cold PBS and collected in Magnesium-containing Lysis Buffer (MLB). Cell lysates were further subjected to pull-down, using glutathione S-transferase fused to the RAS binding domain of the RAF1 kinase (GST-RAF1-RBD). Pulled down samples and whole cell lysates for immunoblotting analyses were mixed with sample buffer and denatured at 95 °C for 5 min.

Isolation of lipid raft-enriched membrane fractions

Lipid raft-enriched membrane fractions were isolated as previously described (32, 65, 67). Briefly, HEK 293T cells were transfected with different constructs for 24 h, starved 4 h, stimulated with EGF at the specified time or left untreated, rinsed twice with cold PBS, and harvested in MES-buffered saline [(MBS) 25 mM 2-(N-morpholino) ethanesulfonic acid, pH 6.5, 150 mM NaCl] containing 1% Triton X-100, 1mM Na_3VO_4 and protease inhibitors. Each cell lysate was Dounce homogenized, adjusted to 40% sucrose and placed at the bottom of an ultracentrifuge tube. A 5-30% linear sucrose gradient was then placed above the homogenate and the mixture was centrifuged at 45,000 rpm for 18 h at 4 °C in a SW60Ti rotor (Beckman Instruments, Palo Alto, CA). Twelve fractions were harvested from top of gradient and stored at - 20 °C until analysis.

Co-immunoprecipitation assays

For co-immunoprecipitation (co-IP) analyses, Neuro2A cells were co-transfected with wild-type *SHOC2* (pcDNA6-V5-SHOC2) or *PPP1CB* (pcDNA6-V5-PPP1CB), and each of the various *MRAS* constructs for 24 h, serum starved for 16 h, stimulated with EGF for 5 min, and then lysed in IP buffer containing 25 mM Tris-HCl, pH 7.4, 1% Triton X-100, 2 mM EDTA, pH 8.0, 150 mM NaCl and protease inhibitors. Samples were centrifuged at 10,000*g* for 20 min at 4 °C, supernatants were collected, and equal amounts of total proteins were immunoprecipitated with 2 µg of anti-Myc antibody for 2 h at 4 °C, followed by a 2 h incubation with 20 µl protein G-sepharose beads (GE Healthcare, Freiburg, Germany) at 4 °C. The beads were recovered by centrifugation and washed six times with IP buffer. Finally, the immunoprecipitated proteins were eluted with sample buffer by incubating for 5 min at 95 °C and stored at -20 °C for western blot analyses.

ACKNOWLEDGEMENTS

We thank the families for participation. This work was supported by grants from the German Federal Ministry of Education and Research (GeNeRARe, to M.R.A. [01GM1519D and 01GM1902C] and M.Z. [01GM1519A]), E-Rare (NSEuroNet, to H.C., M.R.A. [01GM1602B], M.T., and M.Z. [01GM1602A]), German Research Foundation (to M.Z. [ZE 524/10-1]), AIRC (to M.T. [IG 21614]), and Italian Ministry of Health (Ricerca Corrente 2018 and 2019, to M.T.).

CONFLICT OF INTEREST STATEMENT

The authors do not have any conflict of interest.

REFERENCES

1. Tartaglia, M. and Gelb, B.D. (2010) Disorders of dysregulated signal traffic through the RAS-MAPK pathway: phenotypic spectrum and molecular mechanisms. *Ann. N. Y. Acad. Sci*., **1214**, 99-121.
2. Rauen, K.A. (2013) The RASopathies. *Annu. Rev. Genomics Hum. Genet*., **14**, 355-369.
3. Tajan, M., Paccoud, R., Branka, S., Edouard, T. and Yart, A. (2018) The RASopathy Family: Consequences of Germline Activation of the RAS/MAPK Pathway. *Endocr. Rev*., **39**, 676-700.
4. Roberts, A.E., Allanson, J.E., Tartaglia, M. and Gelb, B.D. (2013) Noonan syndrome. *Lancet*, **381**, 333-342.
5. Tartaglia, M., Gelb, B.D. and Zenker, M. (2011) Noonan syndrome and clinically related disorders. *Best Pract. Res. Clin. Endocrinol. Metab*., **25**, 161-179.
6. Grant, A.R., Cushman, B.J., Cave, H., Dillon, M.W., Gelb, B.D., Gripp, K.W., Lee, J.A., Mason-Suares, H., Rauen, K.A., Tartaglia, M. et al. (2018) Assessing the gene-disease association of 19 genes with the RASopathies using the ClinGen gene curation framework. *Hum. Mutat*., **39**, 1485-1493.
7. Johnston, J.J., van der Smagt, J.J., Rosenfeld, J.A., Pagnamenta, A.T., Alswaid, A., Baker, E.H., Blair, E., Borck, G., Brinkmann, J., Craigen, W. et al. (2018) Autosomal recessive Noonan syndrome associated with biallelic LZTR1 variants. *Genet. Med*., **20**, 1175-1185.
8. Motta, M., Fidan, M., Bellacchio, E., Pantaleoni, F., Schneider-Heieck, K., Coppola, S., Borck, G., Salviati, L., Zenker, M., Cirstea I.C. et al. (2018) Dominant Noonan syndrome-causing LZTR1 mutations specifically affect the kelch domain substrate-recognition surface and enhance RAS-MAPK signaling. *Hum. Mol. Genet*., doi: 10.1093/hmg/ddy412.
9. Pagnamenta, A.T., Kaisaki, P.J., Bennett, F., Burkitt-Wright, E., Martin, H.C., Ferla, M.P., Taylor, J.M., Gompertz, L., Lahiri, N., Tatton-Brown, K. et al. (2019) Delineation of dominant

and recessive forms of LZTR1-associated Noonan syndrome. *Clin. Genet.*, doi: 10.1111/cge.13533.

10 Sini, P., Cannas, A., Koleske, A.J., Di Fiore, P.P., and Scita, G. (2004) Abl-dependent tyrosine phosphorylation of Sos-1 mediates growth-factor-induced Rac activation. *Nat. Cell Biol.*, **6**, 268-274.

11 Holly, S.P., Larson, M.K., and Parise, L. (2005) The unique N-terminus of R-ras is required for Rac activation and precise regulation of cell migration. *Mol. Biol. Cell*, **16**, 2458-2469.

12 Kaduwal, S., Jeong, W.J., Park, J.C., Lee, K.H., Lee, Y.M., Jeon, S.H., Lim, Y.B., Min do, S., and Choi, K.Y. (2015) Sur8/Shoc2 promotes cell motility and metastasis through activation of Ras-PI3K signaling. *Oncotarget*, **6**, 33091-33105.

13 Martinelli, S., Krumbach, O.H.F., Pantaleoni, F., Coppola, S., Amin, E., Pannone, L., Nouri, K., Farina, L., Dvorsky, R., Lepri, F. et al. (2018) Functional Dysregulation of CDC42 Causes Diverse Developmental Phenotypes. *Am. J. Hum. Genet.*, **102**, 309-320.

14 Meyer Zum Buschenfelde, U., Brandenstein, L.I., von Elsner, L., Flato, K., Holling, T., Zenker, M., Rosenberger, G. and Kutsche, K. (2018) RIT1 controls actin dynamics via complex formation with RAC1/CDC42 and PAK1. *PLoS Genet.*, **14**, e1007370.

15 Pandit, B., Sarkozy, A., Pennacchio, L.A., Carta, C. Oishi, K., Martinelli, S., Pogna, E.A., Schackwitz, W., Ustaszewska, A., Landstrom, A. et al. (2007) Gain-of-function RAF1 mutations cause Noonan and LEOPARD syndromes with hypertrophic cardiomyopathy. *Nat. Genet.*, **39**, 1007-1012.

16 Razzaque, M.A., Nishizawa, T., Komoike, Y., Yagi, H., Furutani, M., Amo, R., Kamisago, M., Momma, K., Katayama, H., Nakagawa, M. et al. (2007) Germline gain-of-function mutations in RAF1 cause Noonan syndrome. *Nat Genet.*, **39**, 1013-1017.

17 Yaoita, M., Niihori, T., Mizuno, S., Okamoto, N., Hayashi, S., Watanabe, A., Yokozawa, M., Suzumura, H., Nakahara, A., Nakano, Y. et al. (2016) Spectrum of mutations and

genotype-phenotype analysis in Noonan syndrome patients with RIT1 mutations. *Hum. Genet.*, **135**, 209-222.

18 Kouz, K., Lissewski, C., Spranger, S., Mitter, D., Riess, A., Lopez-Gonzalez, V., Lüttgen, S., Aydin, H., von Deimling, F., Evers, C. et al. (2016) Genotype and phenotype in patients with Noonan syndrome and a RIT1 mutation. *Genet. Med.*, **18**, 1226-1234.

19 Calcagni, G., Baban, A., Lepri, F.R., Marino, B., Tartaglia, M. and Digilio, M.C. (2016) Congenital heart defects in Noonan syndrome and RIT1 mutation. *Genet. Med.*, **18**, 1320.

20 Wennerberg, K., Rossman, K.L. and Der, C.J. (2005) The Ras superfamily at a glance. *J. Cell Sci.*, **118**, 843-846.

21 Nakhaei-Rad, S., Haghighi, F., Nouri, P., Rezaei Adariani, S., Lissy, J., Kazemein Jasemi, N.S., Dvorsky, R. and Ahmadian, R. (2018) Structural fingerprints, interactions, and signaling networks of RAS family proteins beyond RAS isoforms. *Crit. Rev. Biochem. Mol. Biol.*, **53**, 130-156.

22 Higgins, E.M., Bos, J.M., Mason-Suares, H., Tester, D.J., Ackerman, J.P., MacRae, C.A., Sol-Church, K., Gripp, K.W., Urrutia, R. and Ackerman, M.J. (2017) Elucidation of MRAS-mediated Noonan syndrome with cardiac hypertrophy. *JCI Insight*, **2**, e91225.

23 Ye, M., Shima, F., Muraoka, S., Liao, J., Okamoto, H., Yamamoto, M., Tamura, A., Yagi, N., Ueki, T. and Kataoka, T. (2005) Crystal structure of M-Ras reveals a GTP-bound "off" state conformation of Ras family small GTPases. *J. Biol. Chem.*, **280**, 31267-31275.

24 Matsumoto, K., Shima, F., Muraoka, S., Araki, M., Hu, L., Ijiri, Y., Hirai, R., Liao, J., Yoshioka, T., Kumasaka, T. et al. (2011) Critical roles of interactions among switch I-preceding residues and between switch II and its neighboring alpha-helix in conformational dynamics of the GTP-bound Ras family small GTPases. *J. Biol. Chem.*, **286**, 15403-15412.

25 Gremer, L., Merbitz-Zahradnik, T., Dvorsky, R., Cirstea, I.C., Kratz, C.P., Zenker, M., Wittinghofer, A. and Ahmadian, M.R. (2011) Germline KRAS mutations cause aberrant

biochemical and physical properties leading to developmental disorders. *Hum. Mutat*., **32**, 33-43.

26 Scheffzek, K., Ahmadian, M.R., Kabsch, W., Wiesmüller, L., Lautwein, A., Schmitz, F., Wittinghofer, A. (1997) The Ras-RasGAP complex: structural basis for GTPase activation and its loss in oncogenic Ras mutants. *Science*, **277**, 333-338.

27 Niv, H., Gutman, O., Kloog, Y. and Henis, Y.I. (2002) Activated K-Ras and H-Ras display different interactions with saturable nonraft sites at the surface of live cells. *J. Cell Biol*., **157**, 865-872.

28 Plowman, S.J., Muncke, C., Parton, R.G. and Hancock, J.F. (2005) H-ras, K-ras, and inner plasma membrane raft proteins operate in nanoclusters with differential dependence on the actin cytoskeleton. *Proc. Natl. Acad. Sci. U. S. A*., **102**, 15500-15505.

29 Nicolau, D.V., Jr. Burrage, K., Parton, R.G. and Hancock, J.F. (2006) Identifying optimal lipid raft characteristics required to promote nanoscale protein-protein interactions on the plasma membrane. *Mol. Cell. Biol*., **26**, 313-323.

30 Prior, I.A., Harding, A., Yan, J., Sluimer, J., Parton, R.G. and Hancock, J.F. (2001) GTP-dependent segregation of H-ras from lipid rafts is required for biological activity. *Nat. Cell Biol.*, **3**, 368-375.

31 Prior, I.A., Muncke, C., Parton, R.G. and Hancock, J.F. (2003) Direct visualization of Ras proteins in spatially distinct cell surface microdomains. *J. Cell Biol.*, **160**, 165-170.

32 Pantaleoni, F., Lev, D., Cirstea, I.C., Motta, M., Lepri, F.R., Bottero, L., Cecchetti, S., Linger, I., Paolacci, S., Flex, E. et al. (2017) Aberrant HRAS transcript processing underlies a distinctive phenotype within the RASopathy clinical spectrum. *Hum. Mutat*., **38**, 798-804.

33 Rodriguez-Viciana, P., Oses-Prieto, J., Burlingame, A., Fried, M. and McCormick, F. (2006) A phosphatase holoenzyme comprised of Shoc2/Sur8 and the catalytic subunit of PP1 functions as an M-Ras effector to modulate Raf activity. *Mol. Cell*, **22**, 217-230.

34 Young, L.C., Hartig, N., Boned Del Rio, I., Sari, S., Ringham-Terry, B., Wainwright, J.R., Jones, G.G., McCormick, F. and Rodriguez-Viciana, P. (2018) SHOC2-MRAS-PP1 complex positively regulates RAF activity and contributes to Noonan syndrome pathogenesis. *Proc. Natl. Acad. Sci. U.S.A.*, **115**, E10576-E10585.

35 Bourne, H.R., Sanders, D.A. and McCormick, F.T. (1991) The GTPase superfamily: conserved structure and molecular mechanism. *Nature*, **349**, 117-127.

36 Bos, J.L. (1989) ras oncogenes in human cancer: a review. *Cancer Res.*, **49**, 4682-4689.

37 Cirstea, I.C., Kutsche, K., Dvorsky, R., Gremer, L., Carta, C., Horn, D., Roberts, A.E., Lepri ,F., Merbitz-Zahradnik, T., König, R. et al. (2010) A restricted spectrum of NRAS mutations causes Noonan syndrome. *Nat. Genet.*, **42**, 27-29.

38 Aoki, Y., Niihori, T., Kawame, H., Kurosawa, K., Ohashi, H., Tanaka, Y., Filocamo, M., Kato, K., Suzuki, Y., Kure, S. et al. (2005) Germline mutations in HRAS proto-oncogene cause Costello syndrome. *Nat. Genet.*, **37**, 1038-1040.

39 Schubbert, S., Zenker, M., Rowe, S.L., Boll, S., Klein, C., Bollag, G., van der Burgt, I., Musante, L., Kalscheuer, V., Whenner, L.E. et al. (2006) Germline KRAS mutations cause Noonan syndrome. *Nat. Genet.*, **38**, 331-336.

40 Carta, C., Pantaleoni, F., Bocchinfuso, G., Stella, L., Vasta, I., Sarkozy, A., Digilio, C., Palleschi, A., Pizzuti, A., Grammatico, P. et al. (2006) Germline missense mutations affecting KRAS Isoform B are associated with a severe Noonan syndrome phenotype. *Am. J. Hum. Genet.*, **79**, 129-135.

41 Niihori, T., Aoki, Y., Narumi, Y., Neri, G., Cavé, H., Verloes, A., Okamoto, N., Hennekam, R.C., Gillessen-Kaesbach, G., Wieczorek, D. et al. (2006) Germline KRAS and BRAF mutations in cardio-facio-cutaneous syndrome. *Nat. Genet.*, **38**, 294-296.

42 Flex, E., Jaiswal, M., Pantaleoni, F., Martinelli, S., Strullu, M., Fansa, E.K., Caye, A., De Luca, A., Lepri, F., Dvorsky, R. et al. (2014) Activating mutations in RRAS underlie a phenotype

within the RASopathy spectrum and contribute to leukaemogenesis. *Hum. Mol. Genet.*, **23**, 4315-4327.

43 Capri, Y., Flex, E., Krumbach, O.H.F., Carpentieri, G., Cecchetti, S., Lißewski, C., Rezaei Adariani, S., Schanze, D., Brinkmann, J., Piard, J. et al. (2019) Activating mutations of RRAS2 are a rare cause of Noonan syndrome. *Am. J. Hum. Genet.*, in press.

44 Niihori, T., Nagai, K., Fujita, A., Ohashi, H., Okamoto, N., Okada, S., Harada, A., Kihara, H., Arbogast, T., Funayama, R. et al. (2019) Germline activating RRAS2 mutations cause Noonan syndrome. *Am. J. Hum. Genet.*, in press.

45 Kimmelman, A., Tolkacheva, T., Lorenzi, M.V., Osada, M. and Chan, A.M. (1997). Identification and characterization of R-ras3: a novel member of the RAS gene family with a non-ubiquitous pattern of tissue distribution. *Oncogene*, **15**, 2675-2685.

46 Ehrhardt, G.R., Leslie, K.B., Lee, F., Wieler, J.S. and Schrader, J.W. (1999) M-Ras, a widely expressed 29-kD homologue of p21 Ras: expression of a constitutively active mutant results in factor-independent growth of an interleukin-3-dependent cell line. *Blood*, **94**, 2433-2444.

47 Young, L.C., Hartig, N., Munoz-Alegre, M., Oses-Prieto, J.A., Durdu, S., Bender, S., Vijayakumar, V., Vietri Rudan, M., Gewinner, C. et al. (2013) An MRAS, SHOC2, and SCRIB complex coordinates ERK pathway activation with polarity and tumorigenic growth. *Mol. Cell*, **52**, 679-692.

48 Watanabe-Takano, H., Takano, K., Keduka, E. and Endo, T. (2010) M-Ras is activated by bone morphogenetic protein-2 and participates in osteoblastic determination, differentiation, and transdifferentiation. *Exp. Cell Res.*, **316**, 477-490.

49 Mathieu, M.E., Faucheux, C., Saucourt, C., Soulet, F., Gauthereau, X., Fedou, S., Trouillas, M., Thézé, N., Thiébaud, P. and Boeuf, H. (2013) MRAS GTPase is a novel stemness marker that impacts mouse embryonic stem cell plasticity and Xenopus embryonic cell fate. *Development*, **140**, 3311-3322.

50 Kimmelman, A.C., Osada, M. and Chan, A.M. (2000) R-Ras3, a brain-specific Ras-related protein, activates Akt and promotes cell survival in PC12 cells. *Oncogene*, **19**, 2014-2022.

51 Cordeddu, V., Di Schiavi, E., Pennacchio, L.A., Ma'ayan, A., Sarkozy, A., Fodale, V., Cecchetti, S., Cardinale, A., Martin, J., Schackwitz, W. et al. (2009) Mutation of SHOC2 promotes aberrant protein N-myristoylation and causes Noonan-like syndrome with loose anagen hair. *Nat. Genet.*, **41**, 1022-1026.

52 Gripp, K.W., Aldinger, K.A., Bennett, J.T., Baker, L., Tusi, J., Powell-Hamilton, N., Stabley, D., Sol-Church, K., Timms, A.E., Dobyns, W.B. (2016) A novel rasopathy caused by recurrent de novo missense mutations in PPP1CB closely resembles Noonan syndrome with loose anagen hair. *Am. J. Med. Genet. A*, **170**, 2237-2247.

53 Gripp, K.W., Innes, A.M., Axelrad, M.E., Gillan, T.L., Parboosingh, J.S., Davies, C., Leonard, N.J., Lapointe, M., Doyle, D., Catalano, S. et al. (2008) Costello syndrome associated with novel germline HRAS mutations: an attenuated phenotype? *Am. J. Med. Genet. A*, **146A**, 683-690.

54 Altmuller, F., Lissewski, C., Bertola, D., Flex, E., Stark, Z., Spranger, S., Baynam, G., Buscarilli, M., Dyack, S., Gillis, J. et al. (2017) Genotype and phenotype spectrum of NRAS germline variants. *Eur. J. Hum. Genet.*, **25**, 823-831.

55 Groesser, L., Herschberger, E., Ruetten, A., Ruivenkamp, C., Lopriore, E., Zutt, M., Langmann, T., Singer, S., Klingseisen, L., Schneider-Brachert, W. et al. (2012) Postzygotic HRAS and KRAS mutations cause nevus sebaceous and Schimmelpenning syndrome. *Nat. Genet.*, **44**, 783-787.

56 Wey, M., Lee, J., Jeong, S.S., Kim, J. and Heo, J. (2013) Kinetic mechanisms of mutation-dependent Harvey Ras activation and their relevance for the development of Costello syndrome. *Biochemistry*, **52**, 8465-8479.

57 Chen, P.C., Wakimoto, H., Conner, D., Araki, T., Yuan, T., Roberts, A., Seidman, C., Bronson, R., Neel, B., Seidman, J.G. et al. (2010) Activation of multiple signaling pathways

causes developmental defects in mice with a Noonan syndrome–associated Sos1 mutation. *J. Clin. Invest*., **120**, 4353-4365.

58 Wu, X., Simpson, J., Hong, J.H., Kim, K.H., Thavarajah, N.K., Backx, P.H., Neel, B.G. and Araki, T. (2011) MEK-ERK pathway modulation ameliorates disease phenotypes in a mouse model of Noonan syndrome associated with the Raf1(L613V) mutation. *J. Clin. Invest.*, **121**, 1009-1025.

59 Nakamura, T., Colbert, M., Krenz, M., Molkentin, J.D., Hahn, H.S., Dorn, G.W. 2nd, and Robbins, J. (2007) Mediating ERK 1/2 signaling rescues congenital heart defects in a mouse model of Noonan syndrome. *J. Clin. Invest.,* **117**, 2123-2132.

60 Edouard, T., Combier, J.P., Nédélec, A., Bel-Vialar, S., Métrich, M., Conte-Auriol, F., Lyonnet, S., Parfait, B., Tauber, M., Salles, J.P. et al. (2010) Functional effects of PTPN11 (SHP2) mutations causing LEOPARD syndrome on epidermal growth factor-induced phosphoinositide 3-kinase/AKT/glycogen synthase kinase 3beta signaling. *Mol. Cell Biol*., **30**, 2498-2507.

61 Marin, T.M., Keith, K., Davies, B., Conner, D.A., Guha, P., Kalaitzidis, D., Wu, X., Lauriol, J., Wang, B., Bauer, M. et al. (2011) Rapamycin reverses hypertrophic cardiomyopathy in a mouse model of LEOPARD syndrome-associated PTPN11 mutation. *J. Clin. Invest*., **121**, 1026-1043.

62 Hahn, A., Lauriol, J., Thul, J., Behnke-Hall, K., Logeswaran, T., Schänzer, A., Böğürcü, N., Garvalov, B.K., Zenker, M., Gelb, B.D. et al. (2015) Rapidly progressive hypertrophic cardiomyopathy in an infant with Noonan syndrome with multiple lentigines: palliative treatment with a rapamycin analog. *Am. J. Med. Genet. A*, **167A**, 744-751.

63 Wang, J., Chandrasekhar, V., Abbadessa, G., Yu, Y., Schwartz, B. and Kontaridis, M.I. (2017) In vivo efficacy of the AKT inhibitor ARQ 092 in Noonan Syndrome with multiple lentigines-associated hypertrophic cardiomyopathy. *PLoS One*, **12**, e0178905.

64 DeLano W. The PyMOL Molecular Graphics System, Version 1.8.2.3. DeLano Scientific LLC, San Carlos, CA. 2002.

65 Motta, M., Chillemi, G., Fodale, V., Cecchetti, S., Coppola, S., Stipo, S., Cordeddu, V., Macioce, P., Gelb, B.D. and Tartaglia, M. (2016) SHOC2 subcellular shuttling requires the KEKE motif-rich region and N-terminal leucine-rich repeat domain and impacts on ERK signalling. *Hum. Mol. Genet.*, **25**, 3824-3835.

66 Smith, P.K., Krohn, R.I., Hermanson, G.T., Mallia, A.K., Gartner, F.H., Provenzano, M.D., Fujimoto, E.K., Goeke, N.M., Olson, B.J. and Klenk, D.C. (1987) Measurement of protein using bicinchoninic acid. *Anal. Biochem.*, **150**, 76-85.

67 Sargiacomo, M., Sudol, M., Tang,. Z and Lisanti, M.P. (1993) Signal transducing molecules and glycosyl-phosphatidylinositol-linked proteins form a caveolin-rich insoluble complex in MDCK cells. *J. Cell Biol.*, **122**, 789-807.

LEGENDS TO FIGURES

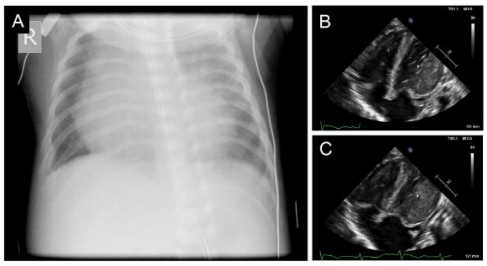

Figure 1. X-ray and echocardiographic findings in patient 2. A, Chest x-ray of the patient at birth revealing marked cardiomegaly. **B**-**C**, Echocardiography during diastole (**B**) and systole (**C**) of the patient at age 4 weeks demonstrating biventricular hypertrophy, increased echogenicity, "kissing" phenomenon of the left ventricular walls during systole, and substantially reduced left ventricular lumen during systole.

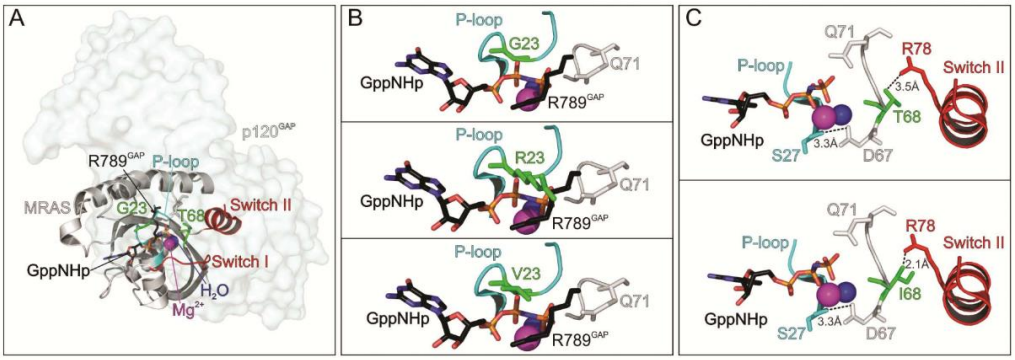

Figure 2. Location of disease-causing *MRAS* mutations and their structural impact. A, Structural modeling of MRAS in complex with p120 RASGAP showing conserved regions and the positions of affected residues. Gly^{23} and Thr^{68}, which are affected in Noonan syndrome, are shown (green), together with the catalytic Arg^{789} of p120 RASGAP. **B**, Gly^{23} (upper panel) is located in the P-loop of MRAS, which is involved in GDP/GTP binding. Arg^{789} of p120 RASGAP interacts with the P-loop and the catalytic Gln^{71}, and stimulates GTP hydrolysis by stabilizing the transition state of this reaction. Substitution of the glycine residue by arginine (middle panel) or valine (lower panel) lead

to steric clashes of this interaction, and consequently in an impaired RASGAP function to stimulate the GTPase reaction; as a consequence, MRAS accumulates in its active form. **C**, Thr^{68} is located in the interswitch region of MRAS stabilizing the active site. Asp^{67} of MRAS interacts with Ser^{27} and a water molecule, leading to an indirect interaction with the Mg^{2+} ion and stabilizing the conformation of the switch regions (upper panel). Substitution by isoleucine (lower panel) is predicted to lead to a stronger interaction with Arg^{78} of the switch II region, and potentiate the interaction with effector proteins.

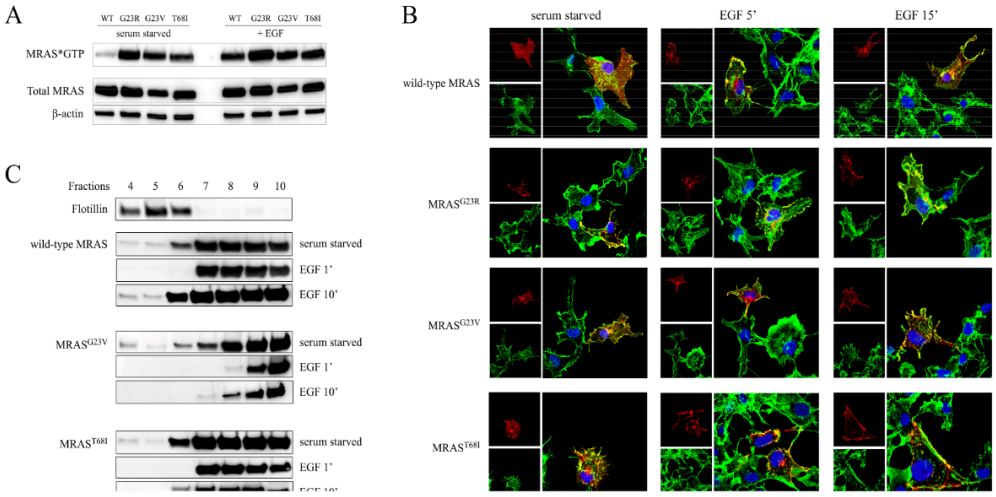

Figure 3. Biochemical and functional characterization of the MRAS mutants. A, Determination of active GTP-bound MRAS levels in HEK 293T cells transiently expressing wild-type or mutant Myc-tagged MRAS proteins. Pull-down assays were performed using glutathione S-transferase fused to the RAS binding domain of the RAF1 kinase (GST-RAF1-RBD) in serum starved condition or after EGF (30 ng/ml) stimulation for 5 min. An anti-Myc antibody was used for MRAS detection and the β-actin was utilized as loading control. **B**, Subcellular localization of transiently expressed Myc-tagged wild-type or mutated MRAS proteins in COS-1 cells during starvation or following EGF stimulation revealed by confocal microscopy analysis. Cells were stained with anti-Myc antibody and

Alexa Fluor 594 goat anti-mouse secondary antibody (red). The F-actin dye Alexa Fluor 488 phalloidin was used to stain the cortical actin associated with the plasma membrane (green). Merged images with nuclei (blue) are displayed on the right panels. Colocalization of MRAS with F-actin is shown in yellow. Note the extensive colocalization of the MRAS mutants with cortical actin even in the absence of EGF stimulation. Scale bar, 10 µm. **C**, Membrane microdomain partitioning of Myc-tagged wild-type and mutant MRAS proteins transiently expressed in HEK 293T cells, serum starved and then stimulated with EGF (30 ng/ml) or left untreated. Wild-type and mutant MRAS proteins localize in both insoluble fractions (fractions 4 to 6, containing lipid rafts) and soluble fractions (fractions 7 to 10, including other membrane domains and cytosol) basally. Note that the relocalization of MRAS mutants in the lipid rafts after 10 min of stimulation with EGF is retarded compared to that of wild-type protein. The detergent-insoluble lipid rafts were separated by sucrose gradient ultracentrifugation, and fractions were analyzed by western blotting using flotillin as lipid raft marker.

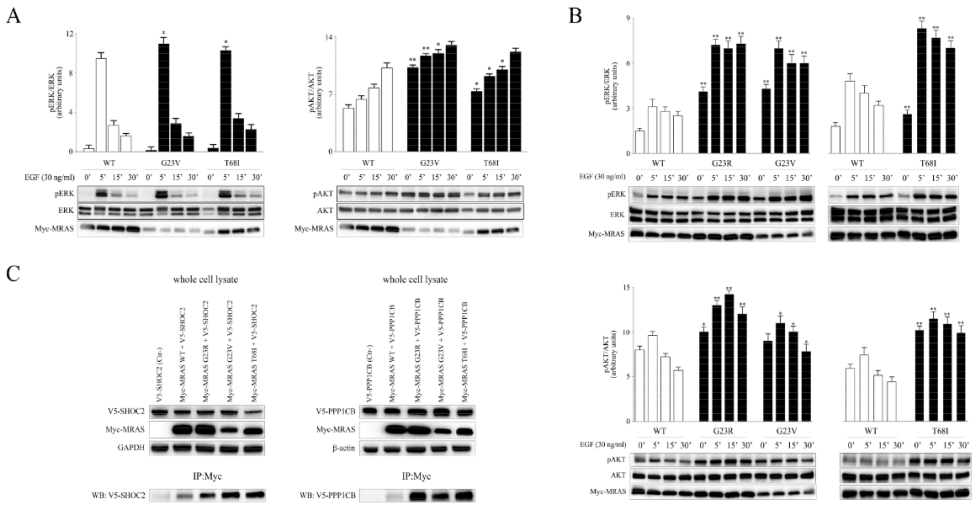

Figure 4. Disease-causing *MRAS* mutations promote enhanced activation of the MAPK and PI3K-AKT pathways. A, Transient overexpression of MRAS mutants in HEK 293T cells promotes

enhanced AKT phosphorylation basally and after EGF stimulation, and a weak increased stimulus-dependent phosphorylation of ERK, as assessed by time-course experiments. Representative blots (below) and mean ± SD densitometry values (above) of three independent experiments are shown. HEK 293T cells were transiently transfected with the Myc-tagged MRAS constructs, serum starved and treated with 30 ng/ml EGF for 5, 15 or 30 min or left unstimulated. Equal amounts of cell lysates were resolved on 10% polyacrylamide gel. Asterisks indicate significant differences compared with wild-type MRAS at the corresponding time upon EGF stimulation (*P < 0.05, **P < 0.01; Student's t-test). **B**, Transient overexpression of MRAS mutants in Neuro2A cells promotes enhanced stimulus-dependent ERK phosphorylation (above) and increases the level of AKT phosphorylation (below) basally and after growth factor stimulation, as assessed by time-course experiments. Experiments were performed as reported above. **C**, NS-causing MRAS mutants show enhanced/more stable binding to SHOC2 and PPP1CB. Co-immunoprecipitation assays were performed using cell lysates collected from Neuro2A cells transiently co-expressing each of the four Myc-tagged MRAS proteins with V5-tagged SHOC2 (left panel) or V5-tagged PPP1CB (right panel).

Chapter VI

Selectivity determinants of RHO GTPase binding to the IQ motif containing GTPase activating proteins

Graphical abstract

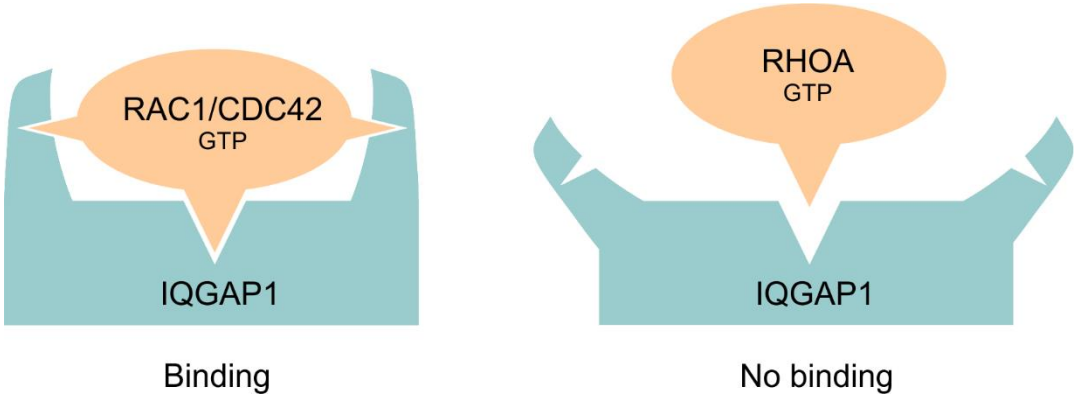

Status: In preparation

Impact factor: None

Own proportion: 40 %

Cloning, expression and purification of RHO GTPases, and IQGAPs, interaction studies, *in silico* analyses, structural modeling, experiment design, figure preparation, writing the manuscript, discussion.

Selectivity determinants of RHO GTPase binding to the IQ motif containing GTPase activating proteins

Oliver H.F. Krumbach*, Kazem Nouri*§, Radovan Dvorsky, Ehsan Amin§, Mohammad R. Ahmadian

Institute of Biochemistry and Molecular Biology II, Medical faculty of the Heinrich-Heine University, 40225 Düsseldorf, Germany

Running title: Selectivity determinants of IQGAP-RHO GTPase binding

§Current Addresses: Kazem Nouri (PhD), Department of Pathology & Molecular Medicine, Richardson Laboratory, Queen's University, Kingston, Ontario, K7L 3N6, Canada; Ehsan Amin (PhD) Institute of Neural and Sensory Physiology, Medical Faculty, Heinrich Heine University Düsseldorf, 40225, Düsseldorf, Germany

*These authors equally contributed to this study

Corresponding author: Reza Ahmadian, Institut für Biochemie und Molekularbiologie II, Medizinische Fakultät der Heinrich-Heine-Universität, Universitätsstr. 1, Gebäude 22.03, 40255 Düsseldorf, Germany, Tel.: +49-211-811 2384, Fax: +49-211-811 2726, e-mail: reza.ahmadian@hhu.de

Key words: RHO GTPases, IQGAP1, IQGAP2, IQGAP3, binding determinants, RAC1, CDC42, RHOA

SUMMARY

The IQ motif-containing GTPase-activating proteins (IQGAPs) modulate a wide range of cellular processes, including adhesion, polarity, and migration by scaffolding and pooling protein components into distinct signaling networks. Their functional states have been proposed to be controlled, among other regulators, by the members of the RHO family GTPases. In this study, we show that IQGAP1 and IQGAP2 are able to associate with CDC42-/RAC1-like proteins but not RIF, RHOD, and RHO-like proteins. As the switch regions of RHO GTPases apparently allocate the first binding site for effector proteins additional contacts outside these regions are required to achieve effector activation. Sequence alignment, structural, mutational, and competitive biochemical analyses revealed that RHO GTPases possess paralog-specific residues apart from the two highly conserved switch regions that essentially determine the selectivity of IQGAP-RHO GTPase binding. Amino acid substitution of these specific residues in RHOA to corresponding residues in RAC1 resulted in association with IQGAP1. Electrostatic potentials turned out to play crucial roles for this bimolecular interaction.

INTRODUCTION

The IQ motif-containing GTPase-activating proteins (IQGAPs) belong to the class of multidomain scaffold proteins, which play a central role in the assembly of protein complexes and signaling networks (1-7). Three IQGAPs are described in humans. Ubiquitously expressed IQGAP1 is the best-characterized paralog. IQGAP2 is mostly expressed in the liver, prostate, kidney, thyroid, stomach, testis, platelets and salivary glands, while IQGAP3 is found in the brain, lung, testis, and intestine (8). Multiple domains enable IQGAPs to interact with a large number of proteins and to modulate

spatiotemporal distributions of distinct signal transducing protein complexes, including B/CRAF-MEK1/2-ERK1/2 (9-11), FGFR1-CDC42-NWASP-Arp2/3-actin (12-14), Tiam1-RAC1-PAK6 (15,16), and CDC42/RAC1/CLIP170 (17,18). The IQGAP paralogs share a similar domain organization and high sequence homology. The N-terminal calponin homology domain (CHD) binds F-actin (19). The polyproline-binding region (WW) binds ERK1/2 (9). The IQ motif (IQ) binds to HER1/2, KRAS, B/CRAF, MEK1/2, and Calmodulin (4,20-24). The RASGAP-related domain (GRD) and the RASGAP C-terminal domain (RGCT) bind to CDC42 and RAC1. The very C-terminal domain (CT) binds E-cadherin, β-catenin, APC, and CLIP170 (3).

CDC42 and RAC1 belong to the RHO GTPase family consisting of 20 classical paralogs and isoforms (25), which control diverse cellular functions (26,27). They are molecular switches that cycle between an inactive (GDP-bound) and an active (GTP-bound) form (28). In the active state, they interact with a multitude of target (effector) proteins, such as IQGAPs, to induce cellular responses (29-31). Interaction with CDC42 or RAC1 and/or phosphorylation of Ser-1441 and Ser-1443 may release IQGAPs from an autoinhibited state to an activated signaling competent state (20,22,23,32). The interaction of the C-terminal part of IQGAP1, encompassing the GRD, RGCT and CT domains (here called GRD-CT), with RAC1 and CDC42 has been intensively studied by several groups (21,23,32-38). In spite of common binding properties of CDC42 and RAC1 for IQGAPs there are significant differences which may be attributed to diverging IQGAP-RHO GTPase complexes that control distinct cellular processes (23,24,35,39,40). As the switch I and II regions (encompassing amino acids 29–42 and 62–68, respectively) (30) are almost identical between CDC42 and RAC1, the selectivity-determining residues have to be located outside these two regions.

However, the binding selectivity of this and the other two IQGAP paralogs for a larger number of RHO family GTPases has not been analyzed to date. In this study, we investigate the IQGAP-RHO GTPase interactions using the GRD-CTs of IQGAP1 and IQGAP2 towards 14 RHO GTPases. This analysis revealed that IQGAPs bind RAC-/CDC42-like proteins but not RHO-like proteins. Additional competition experiments with other binding proteins of CDC42 and RAC1 along with mutational and structural analysis uncovered three distinct regions outside but in the vicinity of the switch regions which are differently involved in selective IQGAP binding.

RESULTS

IQGAP1/2 selectively bind RAC-like and CDC42-like members of RHO family—The C-terminal part of IQGAP1 and IQGAP2, encompassing the GRD, RGCT and CT domains, were successfully purified to measure their binding properties over a broader range of RHO GTPases. We excluded IQGAP3, RHOH, RHOU (WRCH1), RHOV (WRCH2) and TCL from this study due to their physical instability. Interaction studies were performed using time-resolved stopped-flow fluorescence spectrometry under the same conditions described previously (23). Accordingly, both IQGAPs similarly associated with RAC1, RAC2, RAC3, RHOG, CDC42 and TC10, but not with RHOA, RHOB, RHOC, RIF, and RHOD proteins (supplemental Fig. S1). Since a GTP exchange of RND proteins (RND1, RND2 and RND3) for mantGppNHp was not possible, we measured their interactions with IQGAPs in an indirect competitive assay. We measured IQGAP association with RAC1 in the presence and the absence of excess amount of GTP-bound RND proteins. As a positive control, we used GppNHp-bound CDC42. In contrast to CDC42, which competitively blocked IQGAP-RAC1 interaction, there was no effects of RND proteins observed (Supplemental Fig. S1), suggesting that IQGAP1 and IQGAP2 do not interact with these unconventional members of the RHO family (28).

RAC2 exhibited highest affinity for IQGAP1—To examine binding properties, the respective association rate constants (k_{on}) and the dissociation rate constants (k_{off}) were determined for the interaction of IQGAP1 with individual RAC/CDC42-like proteins under conditions described previously (Supplemental Fig. S2) (23). All kinetic parameters along with calculated dissociation constants (K_d) are summarized in Table 1. The data are very similar for RAC1, RAC3, RHOG and CDC42 except for RAC2, which strikingly showed with a K_d value of 27 nM, the highest affinity for IQGAP1 (Figure 2A). Most remarkable are thereby very fast association and slow dissociation rates, which proposes RAC2-IQGAP1 interaction as an event with long residence time.

Potential hotspots for IQGAP binding appear outside the switch regions—The switch regions, which are generally known as the effector binding site, are required but obviously not sufficient for binding (23,30,35,39). These two regions are, with some exceptions, almost identical, if we especially compare IQGAP1 binders, *e.g.*, RAC subfamily, with non-binders, e.g., RHO subfamily (Figure 2A). In this context, it is interesting to note that the CDC42 subfamily includes IQGAP binders and non-binders. Thus, a set of specificity determining residues in IQGAP-RHO GTPase interactions must reside outside of the switch regions. Accordingly, we found four different sites, including 24/25, 45/52, 74, and 85/88 (CDC42/RAC numbering), which are highly conserved in IQGAP binders and clearly deviating from non-binders (Figure 2A). Moreover, an inspection of the crystal structures of RHO GTPases from five different subfamilies showed that the four sites do not significantly contribute local structural differences (Figure 2C, upper panel). These residues rather surround the switch regions and most interestingly are all located on the surface of the respective proteins and available for intermolecular interactions (Figure 2C, middle panel). A striking insight was provided from electrostatic surface potential, which is conserved across RAC1 and CDC42 proteins and strongly negative in the case of RHOA and RND1, in particular in the region of the identified hotspots that may interfere with the IQGAP-binding (Figure 2C, lower panel). The overall electrostatic potential of RHOD considerably differs as compared to the other RHO GTPases.

PAK1 and p50GAP compete with IQGAP1 for binding to RAC1—To further map the IQGAP binding sites on RAC1 we performed competitive binding experiments by measuring IQGAP1 association with mantGppNHp-bound RAC1 in the absence and in the presence of excess amounts of several other purified RAC1 interacting proteins. RAC1-IQGAP1 interaction was not affected by RHOGDI1, TIAM1, TRIO, Plexin B1, and $p67^{phox}$, while significantly reduced in the presence of p50GAP and completely abolished in the presence of PAK1 (Supplemental Fig. S3A and Fig. 3B). Similar result was observed when $RAC1^{\Delta C}$ was used instead of $RAC1^{FL}$ (Supplemental Fig. S3B) suggesting that the hypervariable region (HVR; Fig. 2A) of RAC1 does not play a critical role in this interaction. Moreover, the same experiments were performed for CDC42 and comparable results to RAC1 were observed (data not shown) suggesting the RHO GTPase binding similarity of IQGAP. In addition, we measured the impact of IQGAP1 binding to RAC1 on GEF and GAP activities of TIAM1 and p50GAP, respectively. Notably, RHO GEFs do not largely discriminate between GDP- and GTP- (or GppNHp-) bound RHO GTPases (41). However, no change was observed for the mantGppNHp exchange reaction catalyzed by TIAM1, whereas p50GAP-stimulated GTP hydrolysis activity showed a drastic reduction of 25-fold in the presence of IQGAP1 (Fig. 3C and 3D). This was consistent with the data obtained from the competition experiments.
To correlate functional data to binding sites of the respective RAC1 binding proteins, we first overlaid the structures of investigated binding proteins (Fig. 3E, left panel) and extracted assigned interacting interfaces on a single, GppNHp-bound RAC1 molecule (Fig. 3E, right panel). The interfaces are accordingly shown in dark grey for non-interfering proteins, yellow for p50GAP and green for PAK1, which do interfere with IQGAP1 binding to RAC1. In the next step, we analyzed the crystal structure of RAC3 in complex with PAK1 GBD, which fully interfere with IQGAP1 binding to RAC1, and may thus share overlapping binding regions. Remarkably, potential residues identified by sequence structural analysis of the RHO GTPases, such as Thr-25, Asn-26, Met-45, Asn-52, and Gln-74 of RAC3, are located in close vicinity of RAC1 binding region of PAK1 GBD (Figure 3F). Visualizing the electrostatic potential of this complex structure showed that PAK1 GBD generates on overall negative electrostatic potential on the surface of RAC3 (Figure 3F right panel).

Hotspot mutations differently diminish IQGAP1 binding properties for RAC1 versus CDC42, and generate RHOA binding—To determine whether predicted hotspots determine IQGAP-RHO protein interactions we performed mutational analysis where these residues were replaced by the corresponding amino acids in RHOA (Fig. 2A). Interestingly, we observed a different binding properties of the RAC1 and CDC42 variants when we measured their interaction with IQGAP1 und the same condition as described above. On the one hand, $RAC1^{M45E\_N52E}$ exhibited in a 19-fold reduced binding affinity for IQGAP1 compared to $RAC1^{WT}$, whereas $CDC42^{M45E\_T52E}$ did not show any significant difference to

$CDC42^{WT}$. On the other hand, $CDC42^{Q74D}$ revealed in a 26-fold decrease in binding affinity for IQGAP1, while no significant change was observed for $RAC1^{Q74D}$. Both $RAC1^{T25K\_N26D}$ and $CDC42^{T25K\_N26D}$ showed a reduction of around 4-fold compared to the wild type proteins. Mutation of residues 85 and 88 of RAC1 and CDC42 to RHOA did not affect the binding with IQGAP1 significantly (Figure 4A and B). Moreover, we generated a RHOA variant containing five mutations, such as K27T, D28N, E47M, E54N, and D76Q to mimic RAC1. Interestingly, this variant was capable of associating with IQGAP1, while RHOA WT did not show any association.

DISCUSSION

A large number of studies have examined the protein- protein interaction between IQGAPs and the RHO family of small GTPases. Among the 20 classical RHO proteins, RAC1 and CDC42 have been extensively investigated regarding their binding behavior towards IQGAPs (21,23,32,35,38,42). Accordingly, the C- terminal half of IQGAP (863-1657 in IQGAP1) is able to interact with RHO GTPases. To understand how IQGAPs are able to orchestrate many signaling events by acting as a scaffold protein it is of major interest to know how small GTPases interact with IQGAPs in detail. In this study, we measured the direct protein-protein interaction of 14 RHO GTPases with IQGAP1 and 2 to identify selectivity determinants of IQGAP-RHO GTPase interactions. Time- resolved stopped- flow fluorescence spectrometry was used to monitor the kinetics of IQGAP1/2 C-terminal association with RHO GTPases. The results clearly show that the two IQGAP paralogs bind to RAC- and CDC42- like proteins.

The RAC-related proteins have been shown to be involved in the formation of lamellipodia and membrane ruffles, while CDC42 stimulates the formation of membrane protrusions, called filopodia, at the leading edge of a migrating cell (43-45). Considering that IQGAP1 is able to form complexes with small GTPases, as well as with their regulators and effectors, IQGAP1 possibly integrates several signaling pathways and thus regulates different cellular activities at the same time (15,16). Both Casteel *et al.* and Bhattacharya *et al.* have shown the complex formation of IQGAP1 with RHOA and RHOC, but not RHOB, while our results clearly did not show any direct binding of RHOA and RHOC towards IQGAP1/2 (46,47). In our opinion, the observed interactions of IQGAP1 and RHOA or RHOC are either indirect, since these proteins were co-immunoprecipitated from cells overexpressing tagged RHO proteins or this interaction is mediated *via* a different IQGAP domain than that one used for the interaction with RAC- and CDC42- like proteins. Moreover, we show in this study that RHOA mutations to RAC1 at position xxx and xxx are able to bind IQGAP1 but not RHOA WT.

The interaction between TC10 and IQGAP1 has been previously shown (48). However, Bridges *et al.* showed that TC10 does not undergo the same structural conformational changes upon exchanging GDP to GTP. Most of the RHO GTPases result in a so called “closed” conformation after binding to GTP, while the switch I region of TC10 has been shown to stay in the GDP-like conformation even when GTP is bound (49) (50). This conformational differences may explain why we did not observed the kinetic of interaction between TC10 with IQGAP1/2. Therefore, to confirm our data we investigated this interaction using fluorescence polarization, a different method to determine the binding affinity of two proteins at equilibrium. Interestingly, we were able to see an interaction between TC10 and IQGAP1/2 by fluorescence polarization indicating that TC10 is using a different binding mechanism for IQGAPs compared to RAC1 or CDC42. Owen *et al.* analyzed a multitude of CDC42 and RAC1 variants to study the interaction with IQGAP1 by mutational analysis of the switch I, switch II and insert helix. This study suggest that CDC42 and RAC1 associate with IQGAP1 in a significantly different manner (35,39). Studies by LeCour *et al.* and Ozdemir *et al.* showed that the insert helix of CDC42, especially residue Asn-132, might be important for an additional binding site of CDC42 towards the GRD of IQGAP2 leading to an IQGAP dimerization, which does not take place in case of RAC1 and IQGAP binding

(24,40). However, these studies did not explain why RAC- and CDC42-related proteins are able to interact with IQGAP, while for example the RHO-related proteins do not associate directly with IQGAP1/2.

In silico analyses, including sequence alignment, comparison of different crystal structures and the electrostatic potential, along with competition assays in this study revealed four different sites in RHO GTPases that might define a selective binding mechanism towards IQGAPs. Accordingly, we were able to show that three different hotspots indeed dictate the interaction of RAC1 and CDC42 with IQGAPs. Furthermore, these data support the hypothesis that CDC42 and RAC1 use different mechanisms for IQGAP-binding, since mutations at different sites of RAC1 and CDC42 interfered with the protein-protein interaction. Considering the high sequence identity between the RHO GTPases within the switch regions and that they are generally known as the main binding sites for three classes of regulators and of downstream effectors (30) we assumed that further contact sites apart the switch regions are required to define the selectivity of the respective interactions. Recently, nine different missense mutations in *CDC42* were identified causing a phenotype resembling Noonan syndrome. Among these, $CDC42^{R66G}$ and $CDC42^{R68Q}$ showed defective interaction with IQGAP1 (42). However, these residues are part of the switch II region and do not differ significantly within the RHO GTPases. Another recently described disease, called NOCARH syndrome, caused by a specific missense mutation in *CDC42* (R186C) was identified by Lam and colleagues. Biochemical analysis has shown a dramatically reduced interaction with IQGAP1 (38). It has been thus proposed that this mutant localizes to Golgi apparatus, since IQGAP1 has been shown to promote CDC42 translocation from the Golgi apparatus to the plasma membrane (51).

Conclusions:
However, the molecular mechanism of RHO GTPase-mediated IQGAP integration in signal processes is still unclear.

EXPERIMENTAL PROCEDURES
Constructs—Different variants of pGEX vectors (pGEX2T, pGEX4T-1) encoding an N-terminal glutathione S-transferase (GST) fusion protein were used for the overexpression of human IQGAP1 (Acc. no. P46940; aa 863-1657), human Plexin B1 (Acc. no. O43157; aa 1724-1903), human $p67^{phox}$ (Acc. no. P19878; aa 1-203), human PAK1 (Acc. No. Q13153; aa 57-141), murine TIAM1 DH-PH (Acc. no. Q60610; aa 1033–1404), human TrioN DH-PH (Acc. no. O75962; aa 1226–1535), and human RHOGDIα (Acc. no. P52565) as well as human RHO-related genes, i.e. RAC1 (Acc. no. P63000; aa 1-179), RAC2 (Acc. no. P15153; aa 1-192), RAC3 (Acc. no. P60763; aa 1-192), RHOG (Acc. no. P84095; aa 1-178), RHOA (Acc. no. P61586; aa 1-181), RHOB (Acc. no. P62745; aa 1-181), RHOC (Acc. no. P08134; aa 1-181), CDC42 (Acc. no. P60953; aa 1-178), TC10 (Acc. no. P17081; aa 2-193), RND1 (Acc. no. Q92730; aa 1-232), RND2 (Acc. no. P52198; aa 26-184), RND3 (Acc. no. P61587; aa, 1-244), RIF (Acc. no. Q9HBH0; aa 1-195), and mouse RHOD (Acc. no. P97348; aa 2-193). pET23b was used for the expression of IQGAP2 (Acc. No. Q13576); aa 780-1575).

Proteins—All proteins were purified according to the protocols describe (23). All proteins, except IQGAP2, were isolated in a first step as glutathione S-transferase (GST) fusion proteins by affinity chromatography on a glutathione sepharose column and purified in a second step by size exclusion chromatography after proteolytic cleavage of GST (23,69). IQGAP2 was purified as his-tagged protein. This protein was isolated from the supernatant via Ni-NTA affinity purification. Nucleotide-free RHO proteins were prepared using alkaline phosphatase (Roche) and phosphodiesterase (Sigma Aldrich) at 4 ° C as described (70). Fuorescent methylanthraniloyl (mant) was used to generate mantGppNHp bound RHO proteins, where GppNHp is non hydrolysable analog of GTP, quality and concentrations of labeled proteins were determined as described (70). RND proteins were isolated in the GTP-bound form (71).

Fluorescence stopped-flow spectrometry—Kinetic measurements of the direct association of an effector to a mantGppNHp bound RHO proteins, the GEF-catalyzed nucleotide exchange, and the GAP-stimulated GTP hydrolysis were monitored by stopped-flow apparatus (Applied Photophysics, SX18MV, Surrey, UK), and performed as described (69,72,73) using an excitation wavelength of 362 nm. The emission was detected with a cut-off filter above 408 nm. All measurements were performed in 30 mM Tris-HCl (pH 7.5), 10 mM K_2HPO_4 /KH_2PO_4 (pH 7.4) 2 mM MgCl2 and 3 mM DTT at 25°C. Obtained data are averages of at least four independent measurements. Dissociation experiments were performed by displacing the bound effector from the complex with the mantGppNHp bound RHO protein by an excess amount of unlabeled GppNHp bound GTPase. Competition experiments were carried out by mixing the mantGppNHp bound RHO protein with excess amount of competitor. The observed rate constants were fitted single exponentially using the GraFit program (Erithacus software).

Fluorescence polarization—Experiments were performed in a Fluoromax 4 fluorimeter in polarization mode as described (72,74). Briefly, increasing amounts of IQGAP1 and IQGAP2 were titrated to mGppNHp- TC10 (1 μM) in a buffer containing 30 mM Tris/HCl (pH 7.5), 150 mM NaCl, 5 mM MgCl2, 3 mM DTT and a total volume of 200 μl at 25°C. For excitation, wavelength of 360 nm (slit width: 8 micron) was used, and 450 nm was used for emission (slit width: 10 micron). The dissociation constant (K_d) were calculated by fitting the concentration dependent binding curve using a quadratic ligand binding equation.

Structural analysis—Structural analysis and the electrostatic potential maps were obtained using PyMol molecular viewer, version 1.5.0.4 Schrödinger, LLC and APBS (75), respectively. To be able to compare the electrostatic potentials of proteins with different total charges, positive and negative charges of the proteins were separately scaled so that their overall sum was +1 and -1, respectively.

REFERENCES

1. Abel, A. M., Schuldt, K. M., Rajasekaran, K., Hwang, D., Riese, M. J., Rao, S., Thakar, M. S., and Malarkannan, S. (2015) IQGAP1: insights into the function of a molecular puppeteer. *Mol Immunol* **65**, 336-349
2. Choi, S., and Anderson, R. A. (2016) IQGAP1 is a phosphoinositide effector and kinase scaffold. *Adv Biol Regul* **60**, 29-35
3. Hedman, A. C., Smith, J. M., and Sacks, D. B. (2015) The biology of IQGAP proteins: beyond the cytoskeleton. *EMBO Rep* **16**, 427-446
4. Smith, J. M., Hedman, A. C., and Sacks, D. B. (2015) IQGAPs choreograph cellular signaling from the membrane to the nucleus. *Trends Cell Biol* **25**, 171-184
5. Watanabe, T., Wang, S., and Kaibuchi, K. (2015) IQGAPs as Key Regulators of Actin-cytoskeleton Dynamics. *Cell Struct Funct* **40**, 69-77
6. Tanos, B. E., Yeaman, C., and Rodriguez-Boulan, E. (2018) An emerging role for IQGAP1 in tight junction control. *Small GTPases* **9**, 375-383
7. Nussinov, R., Zhang, M., Tsai, C. J., and Jang, H. (2018) Calmodulin and IQGAP1 activation of PI3Kalpha and Akt in KRAS, HRAS and NRAS-driven cancers. *Biochim Biophys Acta Mol Basis Dis* **1864**, 2304-2314
8. White, C. D., Brown, M. D., and Sacks, D. B. (2009) IQGAPs in cancer: a family of scaffold proteins underlying tumorigenesis. *FEBS Lett* **583**, 1817-1824
9. Roy, M., Li, Z., and Sacks, D. B. (2004) IQGAP1 binds ERK2 and modulates its activity. *J Biol Chem* **279**, 17329-17337
10. Roy, M., Li, Z., and Sacks, D. B. (2005) IQGAP1 is a scaffold for mitogen-activated protein kinase signaling. *Mol Cell Biol* **25**, 7940-7952
11. Ren, J. G., Li, Z., and Sacks, D. B. (2007) IQGAP1 modulates activation of B-Raf. *Proc Natl Acad Sci U S A* **104**, 10465-10469
12. Bensenor, L. B., Kan, H. M., Wang, N., Wallrabe, H., Davidson, L. A., Cai, Y., Schafer, D. A., and Bloom, G. S. (2007) IQGAP1 regulates cell motility by linking growth factor signaling to actin assembly. *J Cell Sci* **120**, 658-669
13. Le Clainche, C., Schlaepfer, D., Ferrari, A., Klingauf, M., Grohmanova, K., Veligodskiy, A., Didry, D., Le, D., Egile, C., Carlier, M. F., and Kroschewski, R. (2007) IQGAP1 stimulates actin assembly through the N-WASP-Arp2/3 pathway. *J Biol Chem* **282**, 426-435
14. Pelikan-Conchaudron, A., Le Clainche, C., Didry, D., and Carlier, M. F. (2011) The IQGAP1 protein is a calmodulin-regulated barbed end capper of actin filaments: possible implications in its function in cell migration. *J Biol Chem* **286**, 35119-35128
15. Usatyuk, P. V., Gorshkova, I. A., He, D., Zhao, Y., Kalari, S. K., Garcia, J. G., and Natarajan, V. (2009) Phospholipase D-mediated activation of IQGAP1 through Rac1 regulates hyperoxia-induced p47phox translocation and reactive oxygen species generation in lung endothelial cells. *J Biol Chem* **284**, 15339-15352
16. Kaur, R., Yuan, X., Lu, M. L., and Balk, S. P. (2008) Increased PAK6 expression in prostate cancer and identification of PAK6 associated proteins. *Prostate* **68**, 1510-1516
17. Fukata, M., Watanabe, T., Noritake, J., Nakagawa, M., Yamaga, M., Kuroda, S., Matsuura, Y., Iwamatsu, A., Perez, F., and Kaibuchi, K. (2002) Rac1 and Cdc42 capture microtubules through IQGAP1 and CLIP-170. *Cell* **109**, 873-885
18. Watanabe, T., Wang, S., Noritake, J., Sato, K., Fukata, M., Takefuji, M., Nakagawa, M., Izumi, N., Akiyama, T., and Kaibuchi, K. (2004) Interaction with IQGAP1 links APC to Rac1, Cdc42, and actin filaments during cell polarization and migration. *Dev Cell* **7**, 871-883
19. Mateer, S. C., Morris, L. E., Cromer, D. A., Bensenor, L. B., and Bloom, G. S. (2004) Actin filament binding by a monomeric IQGAP1 fragment with a single calponin homology domain. *Cell Motil Cytoskeleton* **58**, 231-241

20. Grohmanova, K., Schlaepfer, D., Hess, D., Gutierrez, P., Beck, M., and Kroschewski, R. (2004) Phosphorylation of IQGAP1 modulates its binding to Cdc42, revealing a new type of rho-GTPase regulator. *J Biol Chem* **279**, 48495-48504
21. Kurella, V. B., Richard, J. M., Parke, C. L., Lecour, L. F., Jr., Bellamy, H. D., and Worthylake, D. K. (2009) Crystal structure of the GTPase-activating protein-related domain from IQGAP1. *J Biol Chem* **284**, 14857-14865
22. Li, Z., McNulty, D. E., Marler, K. J., Lim, L., Hall, C., Annan, R. S., and Sacks, D. B. (2005) IQGAP1 promotes neurite outgrowth in a phosphorylation-dependent manner. *J Biol Chem* **280**, 13871-13878
23. Nouri, K., Fansa, E. K., Amin, E., Dvorsky, R., Gremer, L., Willbold, D., Schmitt, L., Timson, D. J., and Ahmadian, M. R. (2016) IQGAP1 Interaction with RHO Family Proteins Revisited: KINETIC AND EQUILIBRIUM EVIDENCE FOR MULTIPLE DISTINCT BINDING SITES. *J Biol Chem* **291**, 26364-26376
24. Ozdemir, E. S., Jang, H., Gursoy, A., Keskin, O., Li, Z., Sacks, D. B., and Nussinov, R. (2018) Unraveling the molecular mechanism of interactions of the Rho GTPases Cdc42 and Rac1 with the scaffolding protein IQGAP2. *J Biol Chem* **293**, 3685-3699
25. Wennerberg, K., and Der, C. J. (2004) Rho-family GTPases: it's not only Rac and Rho (and I like it). *J Cell Sci* **117**, 1301-1312
26. Jaffe, A. B., and Hall, A. (2005) Rho GTPases: biochemistry and biology. *Annu Rev Cell Dev Biol* **21**, 247-269
27. Haga, R. B., and Ridley, A. J. (2016) Rho GTPases: Regulation and roles in cancer cell biology. *Small GTPases* **7**, 207-221
28. Jaiswal, M., Fansa, E. K., Dvorsky, R., and Ahmadian, M. R. (2013) New insight into the molecular switch mechanism of human Rho family proteins: shifting a paradigm. *Biol Chem* **394**, 89-95
29. Bishop, A. L., and Hall, A. (2000) Rho GTPases and their effector proteins. *Biochem J* **348 Pt 2**, 241-255
30. Dvorsky, R., and Ahmadian, M. R. (2004) Always look on the bright site of Rho: structural implications for a conserved intermolecular interface. *EMBO Rep* **5**, 1130-1136
31. Hall, A. (2012) Rho family GTPases. *Biochem Soc Trans* **40**, 1378-1382
32. Elliott, S. F., Allen, G., and Timson, D. J. (2012) Biochemical analysis of the interactions of IQGAP1 C-terminal domain with CDC42. *World J Biol Chem* **3**, 53-60
33. Zhang, B., Wang, Z. X., and Zheng, Y. (1997) Characterization of the interactions between the small GTPase Cdc42 and its GTPase-activating proteins and putative effectors. Comparison of kinetic properties of Cdc42 binding to the Cdc42-interactive domains. *J Biol Chem* **272**, 21999-22007
34. Zhang, B., Chernoff, J., and Zheng, Y. (1998) Interaction of Rac1 with GTPase-activating proteins and putative effectors. A comparison with Cdc42 and RhoA. *J Biol Chem* **273**, 8776-8782
35. Owen, D., Campbell, L. J., Littlefield, K., Evetts, K. A., Li, Z., Sacks, D. B., Lowe, P. N., and Mott, H. R. (2008) The IQGAP1-Rac1 and IQGAP1-Cdc42 interactions: interfaces differ between the complexes. *J Biol Chem* **283**, 1692-1704
36. Mataraza, J. M., Briggs, M. W., Li, Z., Frank, R., and Sacks, D. B. (2003) Identification and characterization of the Cdc42-binding site of IQGAP1. *Biochem Biophys Res Commun* **305**, 315-321
37. Li, R., Debreceni, B., Jia, B., Gao, Y., Tigyi, G., and Zheng, Y. (1999) Localization of the PAK1-, WASP-, and IQGAP1-specifying regions of Cdc42. *J Biol Chem* **274**, 29648-29654
38. Lam, M. T., Coppola, S., Krumbach, O. H. F., Prencipe, G., Insalaco, A., Cifaldi, C., Brigida, I., Zara, E., Scala, S., Di Cesare, S., Martinelli, S., Di Rocco, M., Pascarella, A., Niceta, M., Pantaleoni, F., Ciolfi, A., Netter, P., Carisey, A. F., Diehl, M., Akbarzadeh, M., Conti, F., Merli, P., Pastore, A., Levi Mortera, S., Camerini, S., Farina, L., Buchholzer, M., Pannone, L., Cao, T. N.,

Coban-Akdemir, Z. H., Jhangiani, S. N., Muzny, D. M., Gibbs, R. A., Basso-Ricci, L., Chiriaco, M., Dvorsky, R., Putignani, L., Carsetti, R., Janning, P., Stray-Pedersen, A., Erichsen, H. C., Horne, A., Bryceson, Y. T., Torralba-Raga, L., Ramme, K., Rosti, V., Bracaglia, C., Messia, V., Palma, P., Finocchi, A., Locatelli, F., Chinn, I. K., Lupski, J. R., Mace, E. M., Cancrini, C., Aiuti, A., Ahmadian, M. R., Orange, J. S., De Benedetti, F., and Tartaglia, M. (2019) A novel disorder involving dyshematopoiesis, inflammation, and HLH due to aberrant CDC42 function. *J Exp Med*

39. Nouri, K., Timson, D. J., and Ahmadian, M. R. (2017) New model for the interaction of IQGAP1 with CDC42 and RAC1. *Small GTPases*, 1-7
40. LeCour, L., Jr., Boyapati, V. K., Liu, J., Li, Z., Sacks, D. B., and Worthylake, D. K. (2016) The Structural Basis for Cdc42-Induced Dimerization of IQGAPs. *Structure* **24**, 1499-1508
41. Jaiswal, M., Gremer, L., Dvorsky, R., Haeusler, L. C., Cirstea, I. C., Uhlenbrock, K., and Ahmadian, M. R. (2011) Mechanistic insights into specificity, activity, and regulatory elements of the regulator of G-protein signaling (RGS)-containing Rho-specific guanine nucleotide exchange factors (GEFs) p115, PDZ-RhoGEF (PRG), and leukemia-associated RhoGEF (LARG). *J Biol Chem* **286**, 18202-18212
42. Martinelli, S., Krumbach, O. H. F., Pantaleoni, F., Coppola, S., Amin, E., Pannone, L., Nouri, K., Farina, L., Dvorsky, R., Lepri, F., Buchholzer, M., Konopatzki, R., Walsh, L., Payne, K., Pierpont, M. E., Vergano, S. S., Langley, K. G., Larsen, D., Farwell, K. D., Tang, S., Mroske, C., Gallotta, I., Di Schiavi, E., Della Monica, M., Lugli, L., Rossi, C., Seri, M., Cocchi, G., Henderson, L., Baskin, B., Alders, M., Mendoza-Londono, R., Dupuis, L., Nickerson, D. A., Chong, J. X., University of Washington Center for Mendelian, G., Meeks, N., Brown, K., Causey, T., Cho, M. T., Demuth, S., Digilio, M. C., Gelb, B. D., Bamshad, M. J., Zenker, M., Ahmadian, M. R., Hennekam, R. C., Tartaglia, M., and Mirzaa, G. M. (2018) Functional Dysregulation of CDC42 Causes Diverse Developmental Phenotypes. *Am J Hum Genet*
43. Eden, S., Rohatgi, R., Podtelejnikov, A. V., Mann, M., and Kirschner, M. W. (2002) Mechanism of regulation of WAVE1-induced actin nucleation by Rac1 and Nck. *Nature* **418**, 790-793
44. Etienne-Manneville, S. (2004) Cdc42--the centre of polarity. *J Cell Sci* **117**, 1291-1300
45. Heasman, S. J., and Ridley, A. J. (2008) Mammalian Rho GTPases: new insights into their functions from in vivo studies. *Nat Rev Mol Cell Biol* **9**, 690-701
46. Bhattacharya, M., Sundaram, A., Kudo, M., Farmer, J., Ganesan, P., Khalifeh-Soltani, A., Arjomandi, M., Atabai, K., Huang, X., and Sheppard, D. (2014) IQGAP1-dependent scaffold suppresses RhoA and inhibits airway smooth muscle contraction. *J Clin Invest* **124**, 4895-4898
47. Casteel, D. E., Turner, S., Schwappacher, R., Rangaswami, H., Su-Yuo, J., Zhuang, S., Boss, G. R., and Pilz, R. B. (2012) Rho isoform-specific interaction with IQGAP1 promotes breast cancer cell proliferation and migration. *J Biol Chem* **287**, 38367-38378
48. Neudauer, C. L., Joberty, G., Tatsis, N., and Macara, I. G. (1998) Distinct cellular effects and interactions of the Rho-family GTPase TC10. *Curr Biol* **8**, 1151-1160
49. Bridges, D., Chang, L., Lodhi, I. J., Clark, N. A., and Saltiel, A. R. (2012) TC10 is regulated by caveolin in 3T3-L1 adipocytes. *PLoS One* **7**, e42451
50. Hemsath, L., Dvorsky, R., Fiegen, D., Carlier, M. F., and Ahmadian, M. R. (2005) An electrostatic steering mechanism of Cdc42 recognition by Wiskott-Aldrich syndrome proteins. *Mol Cell* **20**, 313-324
51. Swart-Mataraza, J. M., Li, Z., and Sacks, D. B. (2002) IQGAP1 is a component of Cdc42 signaling to the cytoskeleton. *J Biol Chem* **277**, 24753-24763
52. Casteel, D. E., Turner, S., Schwappacher, R., Rangaswami, H., Su-Yuo, J., Zhuang, S., Boss, G. R., and Pilz, R. B. (2012) Rho isoform-specific interaction with IQGAP1 promotes breast cancer cell proliferation and migration. *J Biol Chem* **287**, 38367-38378
53. Wennerberg, K., Ellerbroek, S. M., Liu, R. Y., Karnoub, A. E., Burridge, K., and Der, C. J. (2002) RhoG signals in parallel with Rac1 and Cdc42. *J Biol Chem* **277**, 47810-47817

54. McCallum, S. J., Wu, W. J., and Cerione, R. A. (1996) Identification of a putative effector for Cdc42Hs with high sequence similarity to the RasGAP-related protein IQGAP1 and a Cdc42Hs binding partner with similarity to IQGAP2. *J Biol Chem* **271**, 21732-21737
55. Hedman, A. C., Smith, J. M., and Sacks, D. B. (2015) The biology of IQGAP proteins: beyond the cytoskeleton. *EMBO reports* **16**, 427-446
56. Etienne-Manneville, S., and Hall, A. (2002) Rho GTPases in cell biology. *Nature* **420**, 629-635
57. Wu, Y., Tao, Y., Chen, Y., and Xu, W. (2012) RhoC regulates the proliferation of gastric cancer cells through interaction with IQGAP1. *PLoS ONE* **7**, 7
58. Clark, E. A., Golub, T. R., Lander, E. S., and Hynes, R. O. (2000) Genomic analysis of metastasis reveals an essential role for RhoC. *Nature* **406**, 532-535
59. Prieto-Sanchez, R. M., and Bustelo, X. R. (2003) Structural basis for the signaling specificity of RhoG and Rac1 GTPases. *J Biol Chem* **278**, 37916-37925
60. Inoue, M., Chang, L., Hwang, J., Chiang, S. H., and Saltiel, A. R. (2003) The exocyst complex is required for targeting of Glut4 to the plasma membrane by insulin. *Nature* **422**, 629-633
61. Inoue, M., Chiang, S. H., Chang, L., Chen, X. W., and Saltiel, A. R. (2006) Compartmentalization of the exocyst complex in lipid rafts controls Glut4 vesicle tethering. *Mol Biol Cell* **17**, 2303-2311
62. Chiang, S. H., Chang, L., and Saltiel, A. R. (2006) TC10 and insulin-stimulated glucose transport. *Methods Enzymol* **406**, 701-714
63. Pommereit, D., and Wouters, F. S. (2007) An NGF-induced Exo70-TC10 complex locally antagonises Cdc42-mediated activation of N-WASP to modulate neurite outgrowth. *J Cell Sci* **120**, 2694-2705
64. Dupraz, S., Grassi, D., Bernis, M. E., Sosa, L., Bisbal, M., Gastaldi, L., Jausoro, I., Caceres, A., Pfenninger, K. H., and Quiroga, S. (2009) The TC10-Exo70 complex is essential for membrane expansion and axonal specification in developing neurons. *J Neurosci* **29**, 13292-13301
65. Fujita, A., Koinuma, S., Yasuda, S., Nagai, H., Kamiguchi, H., Wada, N., and Nakamura, T. (2013) GTP hydrolysis of TC10 promotes neurite outgrowth through exocytic fusion of Rab11- and L1-containing vesicles by releasing exocyst component Exo70. *PLoS ONE* **8**
66. Ory, S., and Gasman, S. (2011) Rho GTPases and exocytosis: what are the molecular links? *Semin Cell Dev Biol* **22**, 27-32
67. Wang, S., Watanabe, T., Noritake, J., Fukata, M., Yoshimura, T., Itoh, N., Harada, T., Nakagawa, M., Matsuura, Y., Arimura, N., and Kaibuchi, K. (2007) IQGAP3, a novel effector of Rac1 and Cdc42, regulates neurite outgrowth. *J Cell Sci* **120**, 567-577
68. Haeusler, L. C., Blumenstein, L., Stege, P., Dvorsky, R., and Ahmadian, M. R. (2003) Comparative functional analysis of the Rac GTPases. *FEBS Lett* **555**, 556-560
69. Hemsath, L., and Ahmadian, M. R. (2005) Fluorescence approaches for monitoring interactions of Rho GTPases with nucleotides, regulators, and effectors. *Methods* **37**, 173-182
70. Jaiswal, M., Dubey, B. N., Koessmeier, K. T., Gremer, L., and Ahmadian, M. R. (2012) Biochemical assays to characterize Rho GTPases. *Methods Mol Biol* **827**, 37-58
71. Fiegen, D., Blumenstein, L., Stege, P., Vetter, I. R., and Ahmadian, M. R. (2002) Crystal structure of Rnd3/RhoE: functional implications. *FEBS Lett* **525**, 100-104
72. Nouri, K., Fansa, E. K., Amin, E., Dvorsky, R., Gremer, L., Willbold, D., Schmitt, L., Timson, D. J., and Ahmadian, M. R. (2016) IQGAP1 interaction with RHO family proteins revisited: Kinetic and equilibrium evidence for multiple distinct binding sites. *J Biol Chem*
73. Jaiswal, M., Dvorsky, R., and Ahmadian, M. R. (2013) Deciphering the molecular and functional basis of Dbl family proteins: a novel systematic approach toward classification of selective activation of the Rho family proteins. *J Biol Chem* **288**, 4486-4500
74. Nouri, K., J., M. M., Milroy LG, Hain, A., Dvorsky, R., Amin, E., Lenders, M., Nagel-Steger, L., Howe, S., Smits, S. H. J., Hengel, H., Schmitt, L., Münk, C., Brunsveld, L., and Ahmadian, M. R.

(2015) Biophysical Characterization of Nucleophosmin Interactions with Human Immunodeficiency Virus Rev and Herpes Simplex Virus US11. *PLoS ONE*

75. Baker, N. A., Sept, D., Joseph, S., Holst, M. J., and McCammon, J. A. (2001) Electrostatics of nanosystems: application to microtubules and the ribosome. *Proc Natl Acad Sci U S A* **98**, 10037-10041

FIGURE LEGENDS

Figure 1. IQGAP1 and IQGAP2 selectively associate with various RAC- and CDC42- like proteins. (A) Association of 2 µM GRD-CT of IQGAP1 and IQGAP2 with various mantGppNHp-bound RHO GTPases (0.2µM) was investigated (Figure S1). The k_{obs} values for the interaction of IQGAP1 and IQGAP2 with several RHO GTPases, shown as bars, illustrate that both IQGAPs associate with RAC- and CDC42-like proteins. RHO-like proteins, RND1, RND2, RND3, TC10, RIF, and RHOD did not show any association for the IQGAPs under these conditions. Data are expressed as the ± S.D. All measurements were accomplished in triplicates. **(B)** The association rates (k_{on}) were measured using 0.2µM mantGppNHp-bound RHO GTPases with increasing concentrations (2-8µM) of $IQGAP1^{GRD-CT}$. Dissociation rates (k_{off}) were measured using 2µM $IQGAP1^{GRD-CT}$ with (0.2µM) mantGppNHp-bound RHO GTPases in the presence of unlabeled RAC1-GppNHp (10µM). Calculated individual rate constants for the interaction of the $IQGAP1^{GRD-CT}$ with RAC- and CDC42- like proteins, plotted as bar charts. Association rates (k_{on}), dissociation rates (k_{off}), and dissociation constants (K_d) for the $IQGAP1^{GRD-CT}$-RHO protein binding are shown. RAC2 showed the highest binding affinity for $IQGAP1^{GRD-CT}$, followed by CDC42, RAC3, RHOG, and RAC1. Data are expressed as the ± S.D. All measurements were accomplished in duplicates.

Figure 2. Difference in the overall electrostatic potential of RHO GTPases. (A) Sequence alignment of RHO GTPases revealed several residues outside the switch regions that may play a role in IQGAP binding. RHO GTPases that associate and do not associate with IQGAPs are colored in green or red, respectively. **(B)** Family tree of the RHO-family shows that GTPases of the RAC subfamily and CDC42 are able to bind IQGAPs. **(C)** Electrostatic potential maps of one representative of each RHO subfamily, such as RAC1 (PDB code: 1MH1), CDC42 (PDB code: 2QRZ), RHOA (PDB code: 1A2B), RND1 (PDB code: 2CLS), and RHOD (PDB code: 2J1L). T25, N26, M45, N52, Q74, V85, and A88 of RAC1 are located on the surface and generate neutral potentials, while corresponding residues in for example RHOA cause significant negative electrostatic potentials. Analysis and illustrations were made using PyMOL molecular viewer.

Figure 3. IQGAP1 structurally compete with PAK1 (GBD) and p50GAP (A) Association competition of mantGppNHp-RAC1 (0,2µM) with IQGAP1 (GRD-CT) (2µM) in the presence of excess amount of competitive interacting partners (100µM). **(B)** Evaluated observed rate constants (k_{obs}), shown as bars, demonstrate that IQGAP1 (GRD-CT) associates with RAC1 regardless of the presence of RHOGDI, Tiam1, Plexin-B1, p67phox, and TRIO while the association was blocked in the presence of PAK1 and p50GAP. **(C)** GAP stimulated GTP hydrolysis. The catalytic domain of p50GAP was used to measure the GAP-stimulated GTP hydrolysis of RAC1 using a stopped flow instrument and a fluorescently labelled GTP (tamraGTP). GAP stimulated GTPase activity was drastically reduced (25fold) in the presence of IQGAP1 (GRD-CT). **(D)** The release of a fluorescently labelled GDP (mantGDP) from RAC1 catalyzed by the catalytic domain of Tiam1 was measured in a fluorimeter and single exponentially fitted to obtain the observed rate constants (k_{obs} values) for the reactions in the presence and absence of IQGAP1 (GRD-CT). The nucleotide exchange reaction was not affected by IQGAP1 (GRD-CT). **(E)** Left panel shows the structure of RAC1 (grey) in complex with different RAC and CDC42 interacting partners, including plexin-B1 (PDB code: 3SU8), TRIO (PDB code: 2NZ8), RHOGDI (PDB code: 1HH4), Tiam1 (PDB code: 1FOE), p67phox (PDB code: 1E96), PAK1 (PDB code: 1E0A), and p50GAP (PDB code: 1AM4). In the right panel interfaces of RAC and CDC42 binding proteins are colored in black (Tiam1, TRIO, RHOGDI, Plexin-B1, and p67phox). Interface of PAK1 and p50GAP which are not covered by other proteins are colored in green and orange, respectively. **(F)** Complex structure of RAC3 and the CRIB-motif of PAK1 (PDB code: 2QME) shows that T25, N26, M45, N52, and Q74 of RAC3 are in close vicinity of the CRIB-motif binding region. Electrostatic potentials (right panel) show that PAK1 (CRIB-motif) generates an overall negative electrostatic potential. Analysis and illustrations were made using PyMOL molecular viewer.

Figure 4. Kinetic measurements of RAC1 and CDC42 mutants with IQGAP1. (A) Calculated individual rate constants for the interaction of the $IQGAP1^{GRD-CT}$ with RAC1 WT and mutants, plotted

as bar charts. Association rates (k_{on}), dissociation rates (k_{off}), and dissociation constants (K_d) for the IQGAP1^{GRD-CT} –RAC1 protein binding are shown. RAC1 double mutant (Met45Glu_Asn52Glu) resulted in a 19-fold decreased binding affinity for IQGAP1 compared to wild type RAC1. **(B)** Calculated individual rate constants for the interaction of the IQGAP1^{GRD-CT} with CDC42 WT and mutants, plotted as bar charts. Association rates (k_{on}), dissociation rates (k_{off}), and dissociation constants (K_d) for the IQGAP1^{GRD-CT} –CDC42 protein binding are shown. CDC42^{Gln74Asp} resulted in a 26-fold decreased binding affinity for IQGAP1 compared to wild type CDC42. The association rates (k_{on}) were measured using 0.2μM mantGppNHp-bound RHO GTPases with increasing concentrations (2-8μM) of IQGAP1^{GRD-CT}. Dissociation rates (k_{off}) were measured using 2μM IQGAP1^{GRD-CT} with (0.2μM) mantGppNHp-bound RHO GTPases in the presence of unlabeled RAC1-GppNHp (10μM). Data were obtained from >4 independent experiments.

Table 1. Data summary for the interaction of RHO proteins with IQGAP (GRD-CT)

Proteins	K_{on} ($\mu M^{-1}s^{-1}$)	K_{off} (s^{-1})	K_d (μM)	Method
RAC1	0.7	0.65	0.93	SFF
RAC2	2.88	0.08	0.027	SFF
RAC3	1.53	0.69	0.45	SFF
RHOG	1.14	0.56	0.49	SFF
CDC42	1.32	0.39	0.29	SFF
TC10	n. i.	n. i.	38.5	FP
TCL	n. i.	n. i.	n. i.	n. i.
WRCH1	n. i.	n. i.	n. i.	n. i.
WRCH2	n. i.	n. i.	n. i.	n. i.
RHOA	n. s. o.	n. s. o.	n. s. o.	n. s. o.
RHOB	n. s. o.	n. s. o.	n. s. o.	n. s. o.
RHOC	n. s. o.	n. s. o.	n. s. o.	n. s. o.
RND1	n. s. o.	n. s. o.	n. s. o.	n. s. o.
RND2	n. s. o.	n. s. o.	n. s. o.	n. s. o.
RND3	n. s. o.	n. s. o.	n. s. o.	n. s. o.
RHOD	n. s. o.	n. s. o.	n. s. o.	n. s. o.
RIF	n. s. o.	n. s. o.	n. s. o.	n. s. o.
RHOH	n. i.	n. i.	n. i.	n. i.
$RAC1^{T25K\_N26D}$	0.11	0.45	4.09	SFF
$RAC1^{M45E\_N52E}$	0.14	2.44	17.46	SFF
$RAC1^{Q74D}$	0.18	0.51	2.8	SFF
$RAC1^{V85D\_A88D}$	0.44	0.75	1.64	SFF
$CDC42^{T25K\_N26D}$	0.9	1.13	1.25	SFF
$CDC42^{M45E\_T52E}$	1.19	0.15	0.13	SFF
$CDC42^{Q74D}$	0.15	1.11	7.4	SFF
$CDC42^{V85D\_S88D}$	0.6	0.25	0.41	SFF
$RHOA^{K27T\_D28N\_E47M\_E54N\_D76Q}$	0.28	3.6	12.5	SFF

n.i. = not investigated

n.s.o.= no signal observed

SFF= stopped-flow fluorimetry

FP= fluorescence polarization

Figure 1

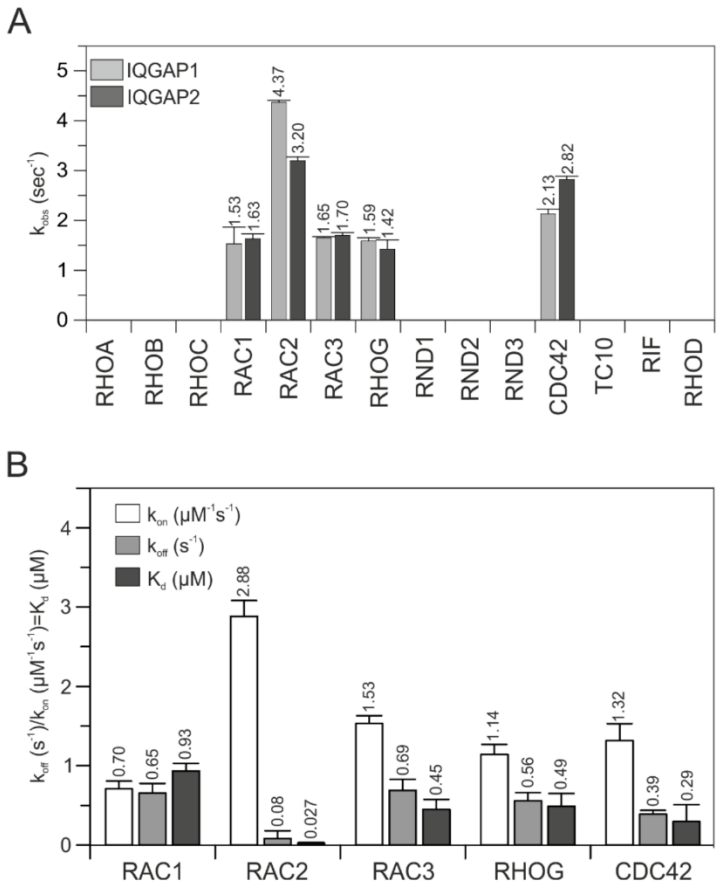
A
IQGAP1
IQGAP2
k_{obs} (sec^{-1})
1.53
1.63
4.37
3.20
1.65
1.70
1.59
1.42
2.13
2.82
RHOA
RHOB
RHOC
RAC1
RAC2
RAC3
RHOG
RND1
RND2
RND3
CDC42
TC10
RIF
RHOD
B
k_{on} ($\mu M^{-1}s^{-1}$)
k_{off} (s^{-1})
K_d (μM)
k_{off} (s^{-1})/k_{on} ($\mu M^{-1}s^{-1}$)=K_d (μM)
0.70
0.65
0.93
2.88
0.08
0.027
1.53
0.69
0.45
1.14
0.56
0.49
1.32
0.39
0.29
RAC1
RAC2
RAC3
RHOG
CDC42

Figure 2

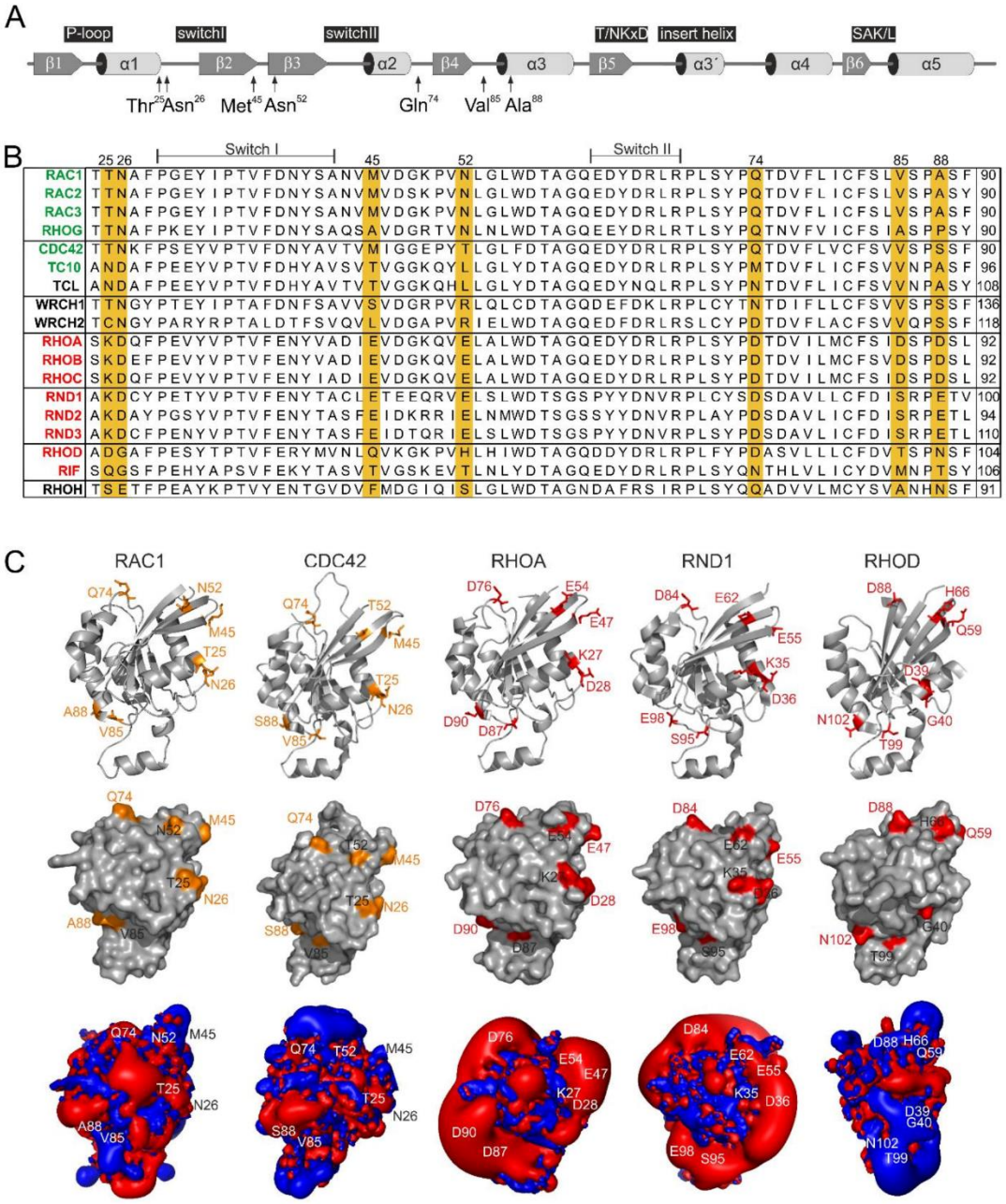
A
P-loop
switchI
switchII
T/NKxD
insert helix
SAK/L
β1 α1 β2 β3 α2 β4 α3 β5 α3' α4 β6 α5
Thr25Asn26 Met45Asn52 Gln74 Val85 Ala88
B
Switch I
Switch II
25 26 45 52 74 85 88
RAC1 TTNAFPGEYIPTVFDNYSANVMVDGKPVNLGLWDTAGQEDYDRLRPLSYPQTDVFLICFSLVSPASF 90
RAC2 TTNAFPGEYIPTVFDNYSANVMVDSKPVNLGLWDTAGQEDYDRLRPLSYPQTDVFLICFSLVSPASY 90
RAC3 TTNAFPGEYIPTVFDNYSANVMVDGKPVNLGLWDTAGQEDYDRLRPLSYPQTDVFLICFSLVSPASF 90
RHOG TTNAFPKEYIPTVFDNYSAQSAVDGRTVNLNLWDTAGQEEYDRLRTLSYPQTNVFVICFSIASPPSY 90
CDC42 TTNKFPSEYVPTVFDNYAVTVMIGGEPYTLGLFDTAGQEDYDRLRPLSYPQTDVFLVCFSVVSPSSF 90
TC10 ANDAFPEEYVPTVFDHYAVSVTVGGKQYLLGLYDTAGQEDYDRLRPLSYPMTDVFLICFSVVNPASF 96
TCL ANDAFPEEYVPTVFDHYAVTVTVGGKQHLLGLYDTAGQEDYNQLRPLSYPNTDVFLICFSVVNPASY 108
WRCH1 TTNGYPTEYIPTAFDNFSAVVSVDGRPVRLQLCDTAGQDEFDKLRPLCYTNTDIFLLCFSVVSPSSF 136
WRCH2 TCNGYPARYRPTALDTFSVQVLVDGAPVRIELWDTAGQEDFDRLRSLCYPDTDVFLACFSVVQPSSF 118
RHOA SKDQFPEVYVPTVFENYVADIEVDGKQVELALWDTAGQEDYDRLRPLSYPDTDVILMCFSIDSPDSL 92
RHOB SKDEFPEVYVPTVFENYVADIEVDGKQVELALWDTAGQEDYDRLRPLSYPDTDVILMCFSVDSPDSL 92
RHOC SKDQFPEVYVPTVFENYIADIEVDGKQVELALWDTAGQEDYDRLRPLSYPDTDVILMCFSIDSPDSL 92
RND1 AKDCYPETYVPTVFENYTACLETEEQRVELSLWDTSGSPYYDNVRPLCYSDSDAVLLCFDISRPETV 100
RND2 AKDAYPGSYVPTVFENYTASFEIDKRRIELNMWDTSGSSYYDNVRPLAYPDSDAVLICFDISRPETL 94
RND3 AKDCFPENYVPTVFENYTASFEIDTQRIELSLWDTSGSPYYDNVRPLSYPDSDAVLICFDISRPETL 110
RHOD ADGAFPESYTPTVFERYMVNLQVKGKPVHLHIWDTAGQDDYDRLRPLFYPDASVLLLCFDVTSPNSF 104
RIF SQGSFPEHYAPSVFEKYTASVTVGSKEVTLNLYDTAGQEDYDRLRPLSYQNTHLVLICYDVMNPTSY 106
RHOH TSETFPEAYKPTVYENTGVDVFMDGIQISLGLWDTAGNDAFRSIRPLSYQQADVVLMCYSVANHNSF 91
C
RAC1
CDC42
RHOA
RND1
RHOD

Figure 3

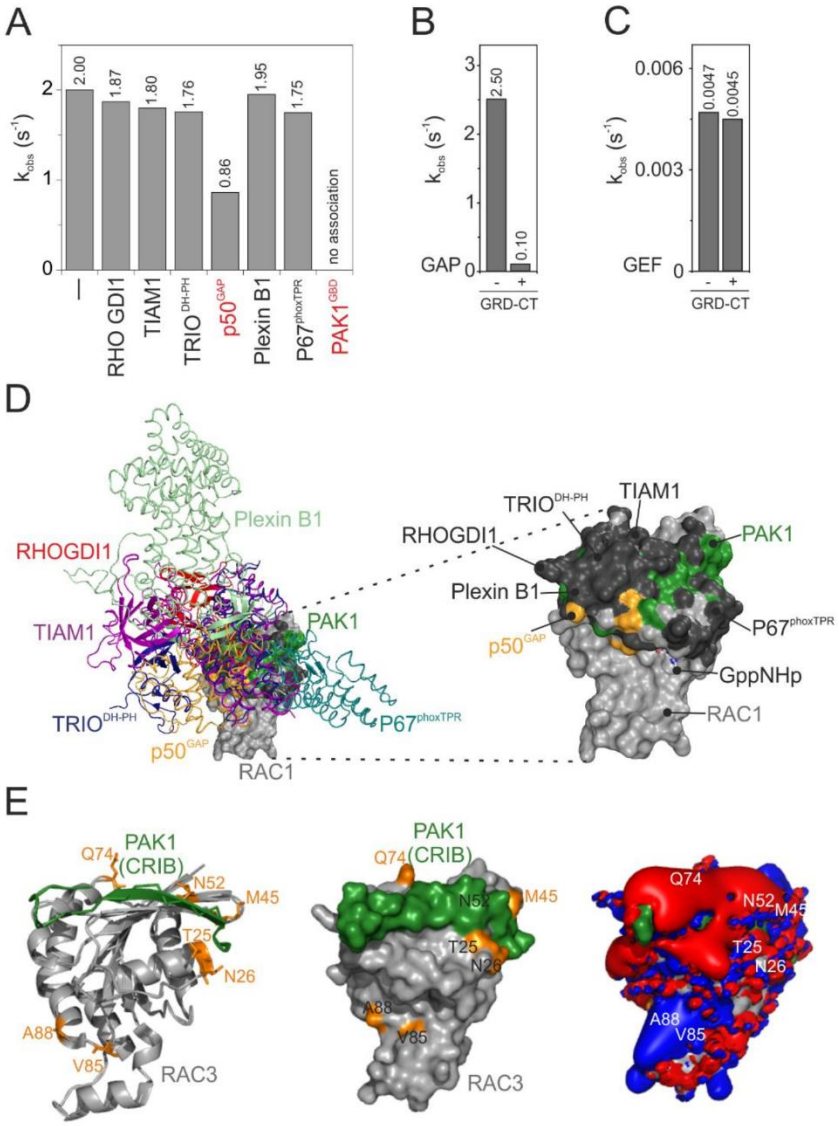
A
B
C
D
E
k_{obs} (s^{-1})
2.00
1.87
1.80
1.76
0.86
1.95
1.75
no association
—
RHO GDI1
TIAM1
TRIO DH-PH
p50 GAP
Plexin B1
P67 phoxTPR
PAK1 GBD
2.50
0.10
GAP
GRD-CT
0.0047
0.0045
GEF
Plexin B1
RHOGDI1
TIAM1
TRIO DH-PH
p50 GAP
PAK1
P67 phoxTPR
RAC1
GppNHp
PAK1 (CRIB)
Q74
N52
M45
T25
N26
A88
V85
RAC3

Figure 4

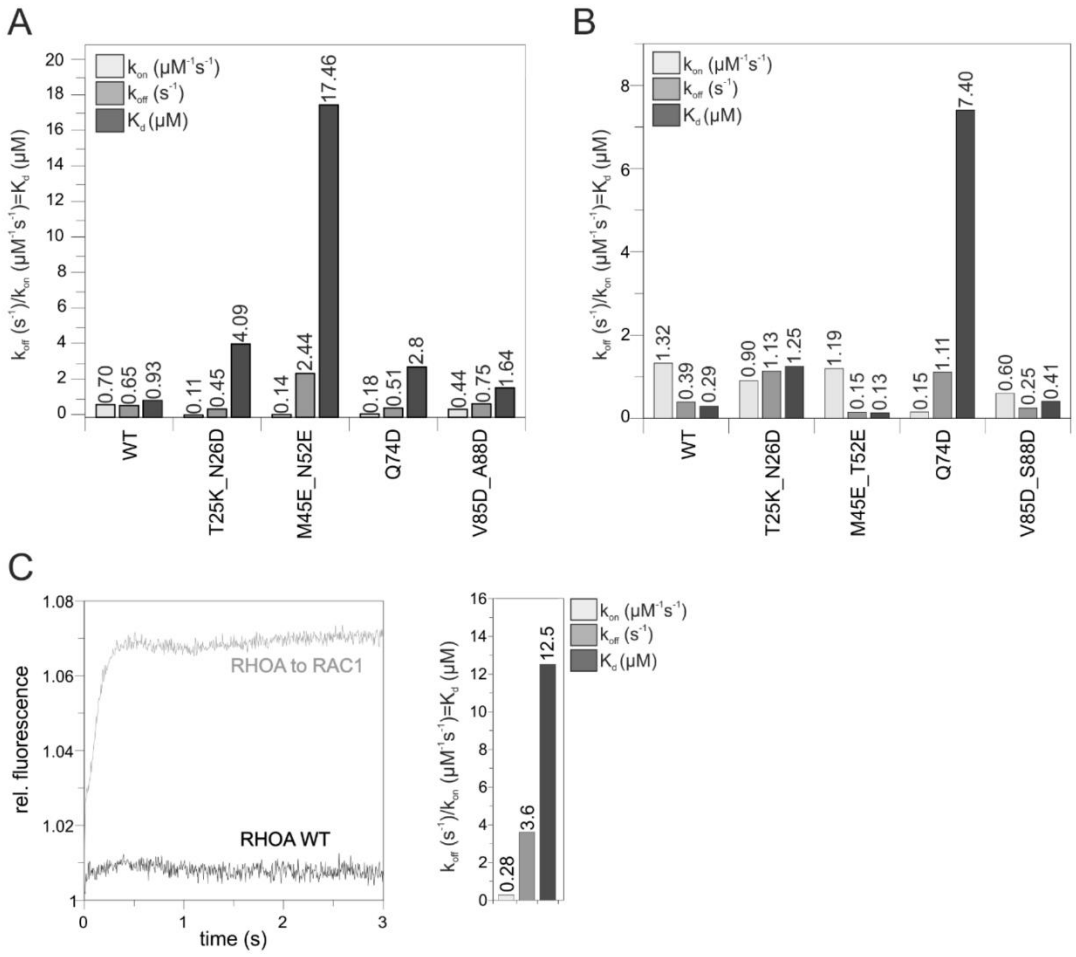
A
B
C
k_{on} ($\mu M^{-1}s^{-1}$)
k_{off} (s^{-1})
K_d (μM)
k_{off} (s^{-1})/k_{on} ($\mu M^{-1}s^{-1}$)=K_d (μM)
0.70
0.65
0.93
0.11
0.45
4.09
0.14
2.44
17.46
0.18
0.51
2.8
0.44
0.75
1.64
WT
T25K_N26D
M45E_N52E
Q74D
V85D_A88D
1.32
0.39
0.29
0.90
1.13
1.25
1.19
0.15
0.13
0.15
1.11
7.40
0.60
0.25
0.41
M45E_T52E
V85D_S88D
rel. fluorescence
time (s)
RHOA to RAC1
RHOA WT
0.28
3.6
12.5

SUP Figure 1

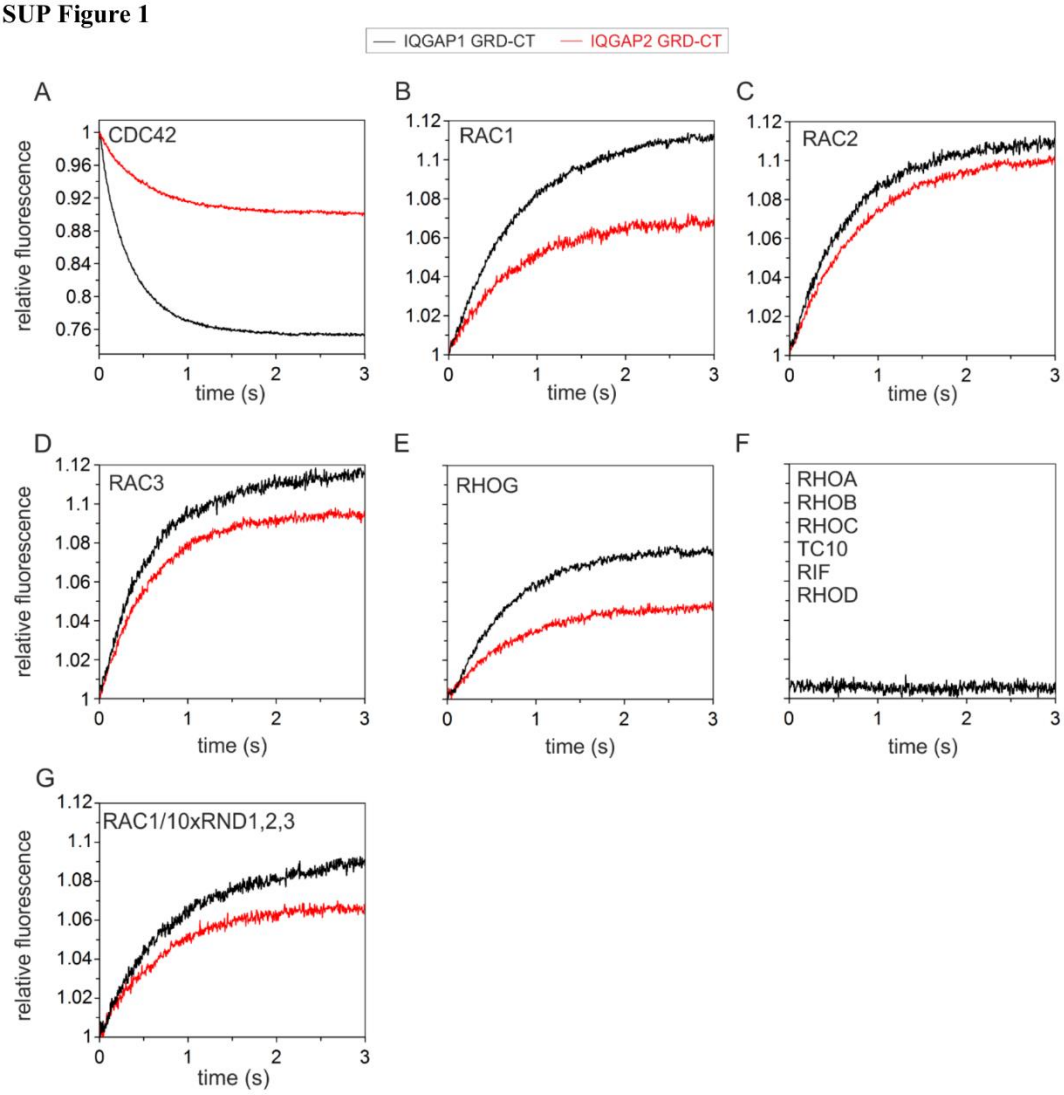

SUP Figure 2

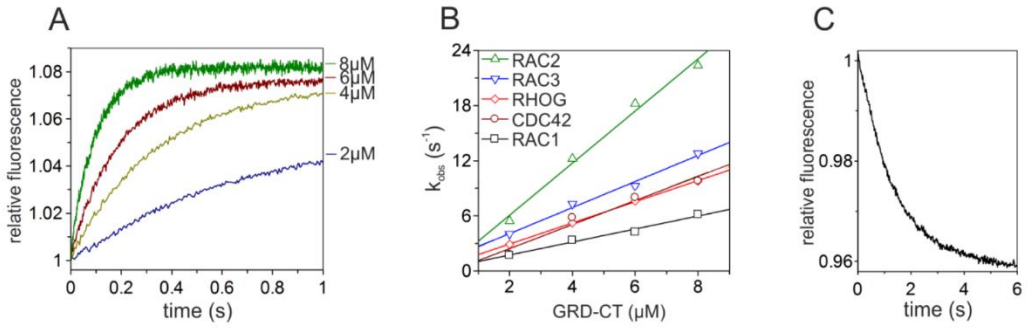

SUP Figure 3

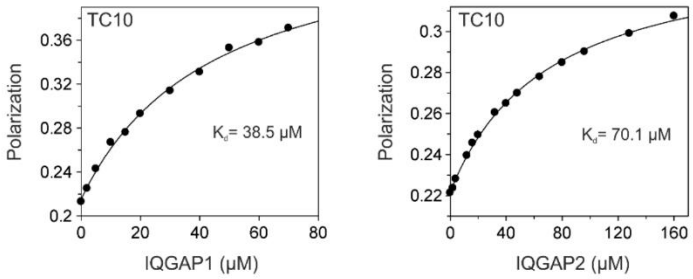

SUP Figure 4

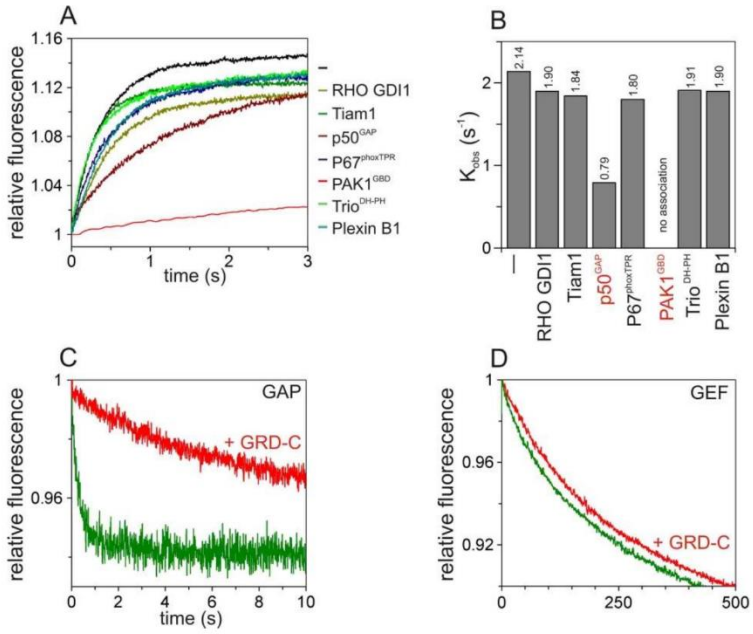

Chapter VII

Inhibition of the DBL-Family Member VAV3 by the Small Molecule IODVA1 Impedes RAC Signaling and Overcomes Resistance to Tyrosine Kinase Inhibition in Lymphoblastic Leukemia

Graphical abstract

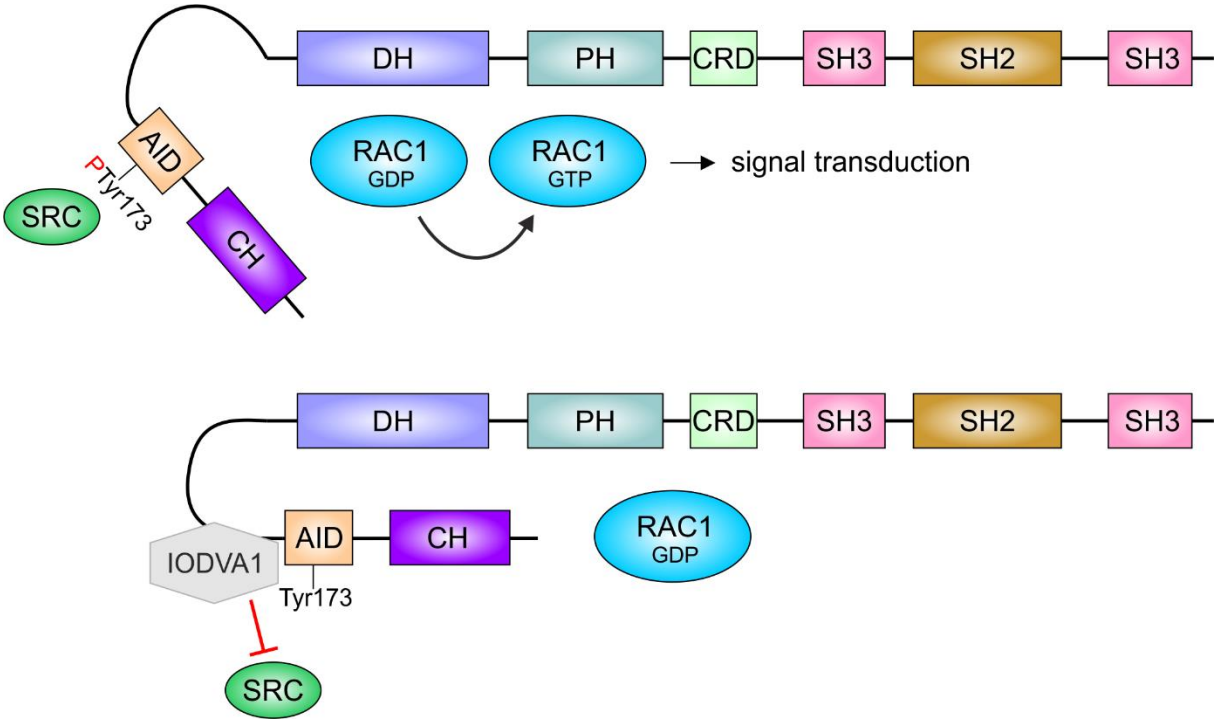

Status: In preparation

Impact factor: None

Own proportion: 10 %

Expression and purification of RAC1, IQGAP1, and p50RHOGAP. Interaction studies and GTP hydrolysis assay.

Running title:

Inhibition of the Dbl-Family Member Vav3 by the Small Molecule IODVA1 Impedes Rac Signaling and Overcomes Resistance to Tyrosine Kinase Inhibition in Lymphoblastic Leukemia

Shailaja Hegde [1,2], Anjelika Gasilina [1], Mark Wunderlich [1], Yuan Lin [1], Gurdat Premnauth [3], Edward J. Merino [3], Marcel Buchholzer [4], Oliver H.F. Krumbach [4], Mohammad Akbarzadeh [4], Mohammad Reza Ahmadian [4], William Seibel [5], Yi Zheng [1,6], Benjamin Mizukawa [1], Lisa Privette Vinnedge [5,6], José A. Cancelas [1,2,6], and Nicolas N. Nassar [1,6*]

[1]: Division of Experimental Hematology and Cancer Biology, Children's Hospital Research foundation, 3333 Burnet Ave, Cincinnati, OH 45229

[2]: Hoxworth Blood Center, University of Cincinnati Academic Health Center, OH, USA

[3]: Department of Chemistry, University of Cincinnati, 404 Crosley Tower, Cincinnati, Ohio 45221

[4]: Institute of Biochemistry and Molecular Biology II, Medical Faculty, Heinrich-Heine-University, Düsseldorf 40225, Germany

[5]: Division of Oncology, Cincinnati Children's Hospital Medical Center, Cancer and Blood Diseases Institute, 3333 Burnet Ave, Cincinnati, OH 45229

[6]: Department of Pediatrics, University of Cincinnati College of Medicine, 3230 Eden Ave, Cincinnati, OH 45267

*: To whom correspondence should be addressed at nicolas.nassar@cchmc.org

1- Summary

Aberrant activation of Rho guanine nucleotide exchange factors (RhoGEFs) is a chief mechanism driving abnormal activation of their RhoGTPase targets in transformation and tumorigenesis. Consequently, a small molecule inhibitor of RhoGEF activities can be used as an anti-cancer drug. Here, we used cellular, mouse, and humanized models of Rac-dependent BCR-ABL1-driven leukemia to identify Vav3, a tyrosine phosphorylation–dependent RacGEF, as the target of the small molecule IODVA1. We show that IODVA1 binds tightly to Vav3, inhibits Rac activation and signaling, and increases pro-apoptotic activity in BCR-ABL expressing cells only. Consistent with this mechanism of action, both Vav3-deficient leukemic cells and mouse models of BCR-ABL leukemia do not respond to IODVA1. Importantly, IODVA1 eradicates leukemic propagating activity of TKI-resistant BCR-ABL1(T315I) B-ALL cells after treatment withdrawal by decreasing Rac signaling *in vivo*. Cells representing pediatric ALL patients are highly sensitive to IODVA1 *ex vivo*. IODVA1 thus spearheads a novel class of drugs that inhibits a RacGEF and holds promise as an anti-tumor therapeutic agent.

Keywords: Rac, RacGEF, Vav3, Philadelphia chromosome positive (Ph^+), Ph-like, MLL-rearrangement, TKI-resistance, drug discovery, small molecule inhibitor, Ras-driven cancer, leukemia, BCR-ABL, pediatric ALL.

2- Introduction

Rac GTPases (Rac1, Rac2, Rac3, and RhoG) are tightly regulated signaling switches that mediate inputs from various receptors and oncogenes to regulate growth, apoptosis, cell-cell and cell-matrix interactions in response to growth factors such as EGF, PDGF, and HGF. Regulation of the actin cytoskeleton, which plays a key role in cell shape, polarity, division, migration and metastasis, is a major function of Rac, as it promotes membrane ruffling and formation of lamellipodia and circular dorsal ruffles [1-6]. Rac also controls cell cycle progression and cell survival, integrin-mediated adhesion, and is required for Ras transformation [7-11]. Furthermore, Rac is pivotal in most aggressive types of leukemias [12-19]. Thus, Rac has been associated with pro-tumorigenic functions and linked to the development of cancer. Moreover, Rac is characteristic of resistance to chemo-, radio-, and targeted-therapies and associated with persistence of leukemic stem cell [2,20-27].

Reducing Rac activity, specifically in cancer cells, is desirable and is an active area of research. However, no small molecule inhibitor of Rac signaling is in clinical use despite the many efforts. Rac activity is regulated by an intricate and well-orchestrated set of proteins comprised of guanine nucleotide exchange factors (GEFs), GTPase-activating proteins (GAPs), and guanine dissociation inhibitors (GDIs). RacGEFs activate Rac by exchanging the bound GDP to GTP to initiate signaling while GAPs deactivate Rac by increasing the rate of GTP hydrolysis to arrest signaling. GDIs extract Rac from membranes, thereby preventing it from signaling. When activated, Rac binds to and activates downstream effectors such as the p21-activated kinases (PAKs), which in turn activate pro-survival pathways and actin-regulating proteins. Rac regulators and effectors

are themselves subject to tight regulation. For example, Vav proteins (Vav1, Vav2, and Vav3) are multi-domain tyrosine phosphorylation–dependent RacGEFs. Phosphorylation of specific tyrosine residues releases an N-and C-terminal autoinhibition mechanism allowing Rac to access the Dbl-homology (DH) domain necessary for the GTP-exchange reaction. Therefore, finding a small molecule inhibitor of Rac itself or its activator, such as the Vav proteins, will provide an effective strategy for treatment of malignancies with aberrant Rac signaling.

In this study, we reveal the mechanism of action (MoA) of IODVA1, a 2-guanidinobenzimidazole derivative we identified as the active ingredient in NSC124205. Initial characterization of IODVA1 showed that it is not a kinase inhibitor but that it prevents lamellipodia and circular dorsal ruffle formation at low concentrations and within minutes of cell exposure. It also decreases cell-cell and cell-extra cellular matrix interactions and reduces growth of Ras-driven tumors (Gasilina *et al.*, 2019). These properties and the specificity of IODVA1 to oncogene expressing cells hinted that it targets Rac activation. We used *in vitro* and *in vivo* leukemic models of the chimeric BCR-ABL1 oncoprotein B-cell acute lymphoblastic leukemia (Ph^+ B-ALL) to study the MoA of IODVA1. BCR-ABL1 B-ALL models are well-suited for our endeavor for several reasons. First, BCR-ABL B-ALL is a single-driver genetic model. Expression of BCR-ABL, which has constitutive kinase activity is sufficient to promote the growth advantage of leukemic cells. When expressed, BCR-ABL1 activates a variety of pathways including the Ras-mitogen-activated protein kinase (MAPK) leading to abnormal cell proliferation, the Janus-activated kinase (JAK)-STAT pathway leading to impaired transcriptional activity, and the phosphoinositide 3-kinase (PI-3K)/AKT

pathway resulting in prolonged survival [28]. In addition, expression of p190- or p210-BCR-ABL activates Rac signaling pathways to regulate leukemogenesis [16,29-31] and deleting Rac2 or the combination of Rac1 and Rac2, impairs myeloid leukemogenesis induced by p210-BCR-ABL expression in the hematopoietic stem and progenitor cell compartment [12,15]. Second, seemingly complex pathways activated by BCR-ABL all depend on the deregulated kinase activity of BCR-ABL [32] and ABL1-tyrosine kinase inhibitors (ABL1-TKIs), *e.g.* imatinib, are used as first-line therapy. Thus, imatinib can be used as positive control to assess the efficacy of IODVA1. Third, despite their tremendous success in treating B-ALL in the clinic, appearance of mechanisms of TKI-dependent and -independent resistance limited their efficacy [33,34]. Thus, there is an unmet need for novel treatments of patients with TKI-resistant leukemia and treatments that prevent leukemic-cell persistence.

Here, we show that IODVA1 binds tightly and inhibits Vav3, consequently leading to the deactivation of Rac and of its downstream signaling and to the induction of apoptosis specifically in BCR-ABL expressing cells *in vivo* and *in vitro*. Further, we show that IODVA1 prolongates the survival of a mouse model of TKI-resistance and reduces its leukemic burden long after treatment was withdrawn. We also show that IODVA1 is effective in decreasing proliferation and survival of relapsed and *de novo* primary patient-derived cells. To the best of our knowledge, IODVA1 is the first inhibitor of a RhoGEF with *in vivo* activity against xenograft mouse models of cancer. Our findings have direct implications for overcoming TKI-resistance in the clinic and for treating cancers where Vav3 is a target, including Ras-driven cancers.

Results

IODVA1 specifically targets BCR-ABL B-ALL cells in vitro. To confirm that IODVA1 is specific for oncogene-expressing cells, we tested its efficacy on the proliferation and survival of $CD34^+$ human peripheral blood mononuclear cells transduced with retroviral bicistronic p190-BCR-ABL or Mieg3 empty vector [35]. As expected, expression of BCR-ABL increased cell proliferation (**Fig. 1a**). Treatment with IODVA1 (IO1, 1 μM) decreased proliferation of BCR-ABL-transformed cells, while proliferation of Mieg3 transduced cells was not affected. We then assessed survival of p190-BCR-ABL-transformed $CD34^+$ cells in the presence of IODVA1 by trypan blue exclusion. The survival of p190-BCR-ABL expressing cells decreased in a dose-dependent manner to 60 ± 16% (SD, N = 3) at 1 μM on day 5 and to 1 ± 0.2% (SD, N = 3) at 3 μM on day 3 (**Fig. 1b**). Survival of Mieg3 expressing cells was not affected by IODVA1. IODVA1 irreversibly inhibits survival of p190- and p210-BCR-ABL but not Mieg3 expressing Ba/F3 cells with a half maximal effective concentration (EC50) of 0.8 μM and inhibits the clonogenic ability of BCR-ABL expressing Ba/F3 cells in methylcellulose (**Supplemental data, Fig. S1a-S1c**). Together, these results indicate that IODVA1 specifically targets proliferation and survival of BCR-ABL-transformed cells and are consistent with our previous report that IODVA1 is more specific to oncogene expressing cells (Gasilina *et al.*, 2019).

IODVA1 prevents leukemia-related death and significantly decreases the leukemia burden in a BCR-ABL-induced leukemic murine model. To test if IODVA1's potency on cells can be recapitulated *in vivo*, we probed its efficacy on a murine model of p190-

BCR-ABL induced B-ALL and compared it to imatinib, an ABL1-TKI with well-characterized MoA in mouse models of Ph^+ B-ALL used as first-line therapy in Ph^+-induced malignancies in the clinic. C57Bl/6 mice were used as donors and/or recipients of transduction/transplantation model. Mouse low-density bone marrow (LDBM) cells were transduced with a MSCV-driven bicistronic retroviral vector (MSCV-IRES-EGFP) encoding p190-BCR-ABL. Transduced LDBM cells (1×10^6) were intravenously transplanted into lethally irradiated C57Bl/6 mice. Mice were bled post 23 days and GFP^+ cells were analyzed by flow cytometry. All mice had developed leukemia by day 28. Leukemic mice were stratified into 5 groups (7 mice per group) and administered either PBS control vehicle, 0.25 or 0.5 mM IODVA1, 0.5 mM imatinib, or the combination 0.25 mM IODVA1 + 0.5 mM imatinib. Vehicle control group had the same DMSO amount (0.1%) as the other groups. Drugs were administered subcutaneously in osmotic pumps for continuous slow release for 4 weeks. Mice survival plot shows that while the control group had died within 7 to 10 days post administration of the PBS vehicle, the low IODVA1 dose (0.25 mM) increased survival by an average of 10 days. Mice treated with imatinib or 0.5 mM IODVA1 or the combination were alive for the 4-week duration of the therapy (**Fig. 1c)**. Significantly, IODVA1 decreased the residual p190-BCR-ABL expressing leukemic progenitor B-cells ($EGFP^+/B220^+$) from peripheral blood (PB) of treated mice (**Supplementary data, Fig. S1d**).

IODVA1 eradicates leukemic propagating activity assessed by serial transplantation. Despite its significant clinical success, imatinib and, more generally, TKIs do not eliminate leukemic stem/progenitor cells in the bone marrow (BM), which can lead to

residual disease, appearance of mechanisms of resistance, and ultimately relapse [36,37]. To determine if IODVA1 eradicates progenitor B-cells with ability to propagate tumors as a functional surrogate of minimal residual disease capable of leukemia relapse, BM cells from vehicle-control and treated mice from **Fig. 1c** (without the 0.25 mM IODVA1-treated mice) were transplanted into lethally irradiated secondary C57BL/6 mice in a limiting dilution series of 1 x 10^6, 0.3 x 10^6, and 0.1 x 10^6 cell doses and analyzed for leukemia development and survival in the absence of any additional therapy. Kaplan-Meier survival plots for the 10^6-cell dilution transplant indicate that administration of IODVA1 alone or in combination with imatinib resulted in survival of p190-BCR-ABL chimeric mice beyond the 70-day endpoint analysis (**Fig. 1d**). Mice transplanted with BM cells from primary recipient mice treated with imatinib alone died by day 40 post-transplantation. Analysis at week 5 post transplantation of the leukemic progenitor cells ($EGFP^+/B220^+$) from the peripheral blood of secondary transplanted mice (**Supplemental data, Fig. S1e**) indicate that IODVA1 is superior than imatinib at eradicating leukemic cell burden. Poisson's distribution analysis of the lower cell dose transplantations (**Supplemental Fig. S1f-S1i**) indicates >10-fold depletion of tumor propagating activity in grafts from IODVA1- or IODVA1+imatinib-treated leukemic mice compared with leukemic mice treated with imatinib alone.

IODVA1 eradicates TKI-resistant BCR-ABL B-ALL. We have previously reported that IODVA1 has no inhibitory activity against major wild-type kinases including ABL1 and SRC-like kinases. Thus, the anti-proliferative activity of IODVA1 towards *in vitro* and *in vivo* BCR-ABL B-ALL models and its ability to eradicate residual disease cannot be

explained by ABL1 inhibition. To further test this idea, we evaluated the ability of IODVA1 to increase the survival of mice harboring p210-BCR-ABL(T315I). We chose this ABL1 mutant because it is one of the most frequent mutations arising in chronic myelogenous leukemia (CML) patients on imatinib therapy [38-42]. Mice were treated for 4 weeks with two rounds of pumps containing vehicle control, imatinib, or IODVA1. At the end of the 4-week treatment, surviving mice were kept in their cages without any additional treatment. As expected, p210(T315I) mice did not respond to the TKI as all imatinib-treated mice died by day 22, before the end of the treatment (**Fig. 2a**). 80% of IODVA1-treated mice survived until day 65, 37 days post last treatment. 60% of IODVA1-treated mice survived till day 80, 52 days post last treatment (**Fig. 2a**). Counts of $EGFP^+/B220^+$ leukemic progenitor cells from the T315I-leukemic mice peripheral blood indicated that IODVA1 significantly decreased leukemic progenitor levels by 24% by week two, by 84% by week 5, and by 91% by week 10 (**Fig. 2b**).

To assess signaling pathways affected by IODVA1, $EGFP^+/B220^+$ LDBM cells were isolated from two-week treated p210(T315I) mice, stained with phospho-antibodies against the pro-proliferative Rac-dependent effectors JNK, PAK, 4EBP, and S6 and the Rac-independent effectors ERK1/2, STAT3, STAT5, p38, and AKT, and analyzed by flow cytometry. IODVA1 resulted in significant decreases in pJNK by 55% ($p = 0.0029$), pPAK by 56% ($p = 0.0016$), p4EBP by 20.3% ($p = 0.037$), and pS6 by 17.8% ($p = 0.0012$), respectively (**Fig. 2c)**. Phosphorylation levels of p38, ERK, STAT3, STAT5, and AKT were not affected by IODVA1. Interestingly, imatinib had the opposite effect, it decreased the levels of pERK, pSTAT3, and pAKT but did not affect the phosphorylation levels of the Rac-dependent effectors. Taken together, IODVA1 not only overcomes

TKI-resistance but also eliminates TKI-resistant leukemic stem/progenitor cells likely by acting on imatinib-independent growth signaling pathways that involve Rac effectors.

IODVA1 decreases Rac activity and downstream signaling. We have previously shown that IODVA1 prevents formation of F-actin suprastructures, such as lamellipodia and circular dorsal ruffles, within minutes of cell incubation (Gasilina *et al.*, 2019). Rac is a major regulator of lamellipodia formation and of JNK and TORC1 activities [43,44] and is required for circular dorsal ruffles formation and is also activated downstream of BCR-ABL. We thus tested if IODVA1 inhibits Rac activation and measured levels of Rac-GTP during treatment using PAK-GBD (GTPase-binding domain). A 70% decrease in the levels of active Rac occurs 10-15 minutes post incubation of p190-BCR-ABL transformed Ba/F3 cells with IODVA1 (3 μM, **Fig. 3a**). Interestingly, this 10-minute time point is consistent with the IODVA1-driven decrease in lamellipodia formation in MDA-MB-231 breast cancer cells (Gasilina *et al.*, 2019). IODVA1 is specific to Rac (IC50 = 1 μM) and is less effective on Cdc42 and not on RhoA (**Supplemental data, Fig. S2a & S2c**).

To test if the decrease in Rac activation is translated into a decrease in its downstream signaling *in vitro* as was observed with xenograft-derived TKI-resistant cells (**Fig. 2c**), we analyzed vehicle- and IODVA1-treated p190-BCR-ABL- or Mieg3-expressing Ba/F3 cells by phosphor-flow. **Fig. 3b** shows that the phosphorylation levels of JNK, S6, 4EBP, PAK, and AKT were increased by more than 2.5 times in the BCR-ABL- than in the Mieg3-expressing cells. IODVA1 decreases the phosphorylation levels of JNK by 1.8 ($p = 0.015$), S6 by 1.5 ($p = 0.05$), 4EBP by 3.0 ($p = 0.009$), and PAK by 6.1 ($p = 0.004$)

fold, respectively. Importantly, the decrease in effectors phosphorylation levels induced by IODVA1 treatment is specific to BCR-ABL- but not Mieg3-expressing cells. IODVA1 did not affect the phosphorylation levels of AKT regardless of the oncogene BCR-ABL status (**Fig. 3b**). The decrease in JNK, S6, and 4EBP activity in IODVA1-treated Ba/F3 cells mirrors the decrease observed in LDBM cells from IODVA1-treated p210-T315I mice in pharmacodynamics studies (**Fig. 2c**). Together, our *in vitro* and *in vivo* data are consistent with IODVA1 targeting activation of Rac and its downstream signaling.

Significantly, IODVA1 decreases Rac downstream pro-survival PAK and decreases inhibitory phosphorylation of pro-apoptotic BAD Ser136 activities within minutes of cell exposure (**Supplemental data, Fig. S2b**). The decrease in PAK and BAD phosphorylation suggests that IODVA1 promotes reduction in survival and induction of apoptosis. To further test this hypothesis, we analyzed the cell cycle of murine p190-BCR-ABL leukemic progenitor cells ($EGFP^{+}/B220^{dim}$) incubated with vehicle control or IODVA1 (1-10 μM) for 20 h, followed by *in vitro* BrdU incorporation and flow cytometry analysis (**Fig. 3c**). IODVA1 did not affect the G0+G1 phase, it significantly affected the distribution of the G2+M, S, and apoptotic phases. It increased the percentage of cells in the G2+M phases from $7 \pm 1\%$ (SD, N = 3) in the presence of vehicle control to 22 ± 6.6, 32 ± 3, and $36 \pm 7\%$ (SD, N = 3) at 1, 3, and 10 μM, respectively. At 1 μM, it reduced the S-phase 8-fold ($p = 0.0002$) and increased apoptosis by at least 5.3-times ($p = 0.007$). Therefore, IODVA1 induces a G2/M arrest.

Rac-deficient cells do not respond to IODVA1. To confirm that IODVA1 targets Rac-dependent pathways, we assessed its effects in a Rac2-null background. $Rac1^{\Delta/\Delta}$+$Rac2^{-/-}$

murine leukemic cells show severe reduction in Rac1 expression and are deficient in Rac2 (**Fig. S2d**). $Rac1^{\Delta/\Delta}$+$Rac2^{-/-}$ or wild-type murine leukemic cells expressing p190-BCR-ABL [29] were tested for clonogenic ability in the presence of IODVA1 (**Fig. 3d**). $Rac1^{\Delta/\Delta}$+$Rac2^{-/-}$ leukemic cells formed 3.8-times less colonies than wild-type leukemic cells ($p = 0.0003$). IODVA1 did not alter the number of colonies formed by $Rac1^{\Delta/\Delta}$+$Rac2^{-/-}$ cells, suggesting these they are insensitive to IODVA1. Interestingly, $Rac1^{\Delta/\Delta}$+$Rac2^{-/-}$ leukemic cells treated with vehicle or IODVA1 formed 2.4-times more colonies than wild-type cells treated with IODVA1 ($p = 0.0091$). Combined with the biochemical data, these data support the idea that IODVA1 targets Rac activity and thus, inhibits its downstream pro-survival signals, and induces a G2/M arrest that correlates with apoptosis.

IODVA1 is an inhibitor of the RacGEF Vav3. Rac activity and signaling is regulated by GAPs, GDIs, and RacGEFs. We argued that the decrease in Rac activity might be caused by IODVA1 targeting one Rac regulator. Using biochemical assays, we show that IODVA1 does not stimulate the activity of the Rac negative regulators p50GAP and RhoGDI1 (**Supplemental data, Fig. S2e-S2g**). We next turned to GEFs and posited that IODVA1 inhibits one Rac-specific GEF leading to its inactivation. While several RacGEFs have been associated with leukemogenesis [45-51], Vav3 was shown to play an important role in leukemogenesis [52]. We thus focused on Vav3 and tested if IODVA1 inhibits Vav3 binding to Rac. Ba/F3 cells expressing either p190-BCR-ABL or Mieg3 empty vector were incubated with IODVA1 (3 μM) or vehicle control for 30 min and subjected to GST-Rac pull-down. The pull-down protein complex was separated on SDS-

PAGE and immunoblotted for pVav3 and Vav3 and quantified (**Fig. 4a & S3a**). There was no significant change in Vav3 or pVav3 bound to Rac in empty vector expressing Ba/F3 cells treated with IODVA1 or vehicle control (**Fig. 4a**, lanes 1 & 2) suggesting that IODVA1 did not affect Vav3 binding to Rac in cells expressing the empty vector. Strong pVav3 and Vav3 bands appeared in cells expressing the p190-BCR-ABL oncogene and treated with vehicle (**Fig. 4a**, lane 3) implying strong binding between active Vav3 and Rac. Specifically, the 5-fold increase in the pVav3 intensity in Ba/F3 leukemic cells is consistent with similar observation that BCR-ABL increases Vav3 activation [52]. The intensity of this band is decreased 8-times in cells treated with IODVA1 (**Fig. 4a**, lane 4) suggesting that IODVA1 inhibited Vav3 binding to Rac in BCR-ABL expressing cells. This inhibition is likely due to the overall decrease in pVav3 levels in IODVA1 treated cells (**Fig. 4a**, input pVav3 band, lanes 3 & 4). Taken together, our data suggest that IODVA1 interferes with Vav3 activation and binding to Rac thus preventing the activation of the latter.

The previous observation suggests that IODVA1 binds to Vav3. To test this hypothesis, we measured its binding affinity (K_d) to recombinant Vav3 and Rac1 using microscale thermophoresis (MST); the catalytic domain (DH/PH) of the RhoGEF LARG served as negative control. We used LARG for two reasons. First, we reasoned that if Rho-activation is not affected by IODVA1 (**Fig. S2c**), we should not detect any binding between LARG and IODVA1. Second, like Vav3, LARG contains a DH/PH domain responsible for the exchange activity such that any non-specific binding to this domain should be detected. The MST signal for Vav3 reaches saturation at 10 µM IODVA1 and beyond (**Fig. 4b**). The MST signal for Rac1 and LARG showed no saturation at the

highest IODVA1 concentration tested. Fitting of the MST titration data shows that one molecule of IODVA1 binds to Vav3 with a K_d of 0.4 μM. The best estimate for the K_d for Rac and LARG is 35.5 and 7.7 μM, respectively. Thus, IODVA1 binds tightly and specifically to Vav3.

Vav3-deficient leukemic cells do not respond to IODVA1 in vitro and in vivo. To further validate Vav3 as IODVA1's target, we studied the effects of IODVA1 on leukemic cells from the Vav3-KO ($Vav3^{-/-}$) mice we published previously [12,29,52]. We argued that if IODVA1 targets Vav3, then $Vav3^{-/-}$ cells should be insensitive to its action. Wild-type or $Vav3^{-/-}$ murine BM leukemic cells expressing p190-BCR-ABL ($EGFP^{+}/B220^{+}$) were tested in colony formation assay in the presence of IODVA1 (**Fig. 4c**). The number of colonies formed by leukemic cells expressing Vav3 decreased on average by 3- and 7-folds in the presence of 1 and 3 μM IODVA1, respectively. $Vav3^{-/-}$ cells on the other hand formed similar number of colonies when grown in the presence of vehicle control or IODVA1 suggesting they lost sensitivity to our drug. Interestingly, the difference in the number of colonies formed by $Vav3^{-/-}$ leukemic cells and by IODVA1-treated wild-type leukemic cells is not statistically significant ($p = 0.13$). Similarly, cell cycle analysis shows that $Vav3^{-/-}$ cells expressing p190-BCR-ABL were not affected by IODVA1 (**Supplementary data & Fig. S3d**). Taken together, our data suggest that while wild-type leukemic cells respond to IODVA1, $Vav3^{-/-}$ leukemic cells are irresponsive and mimic IODVA1-treated wild-type leukemic cells.

Next, we tested if the lack of response to IODVA1 by $Vav3^{-/-}$ cells holds *in vivo*. We transplanted wild-type or $Vav3^{-/-}$ LDBM cells transduced with p190-BCR-ABL retrovirus

into lethally irradiated C57BL/6 mice, waited for the leukemia to develop, and treated the mice with either vehicle control or IODVA1 administered through osmotic pumps as before. $Vav3^{-/-}$ leukemic mice did not respond to IODVA1 supporting the hypothesis that Vav3 is IODVA1's target *in vivo* (**Supplemental Data, Fig. S3b).** Taken together, our data show that Vav3-deficient leukemia progenitor cells do not respond to IODVA1 in cellular and *in vivo* assays consistent with the idea that Vav3 is IODVA1's target *in vivo* and *in vitro*. The persistency of leukemia *in vivo* in $Vav3^{-/-}$ mice suggests that $Vav3^{-/-}$ BCR-ABL leukemia has evolved mechanisms of escape relying on Rac-independent pathways such as AKT and STAT3 signaling pathways (**Fig. S3c & S3d**).

IODVA1 targets Vav3 in MDA-MB-231 cells and xenograft tumors. Next, we tested if IODVA1 is effective in another model of Vav3-dependent cancer. We chose MDA-MB-231 triple negative breast cancer cells because these cells express high endogenous levels of Vav3 [53] and because Vav3 is an acknowledged target in breast cancer [53-57]. In addition, we have previously shown that these cells are sensitive to IODVA1 and that IODVA1 halts tumor growth and induces apoptosis in MDA-MB-231 xenograft mice (Gasilina *et al.*, 2019). First, we showed that reduction in Vav3 expression levels by targeting shRNA severely reduces proliferation of MDA-MB-231 cells. IODVA1 (0.1 – 1 μM) reduces, in a dose-dependent manner, the viability and proliferation of scrambled MDA-MB-231, it has no effect on the shVav3 expressing cells (**Fig. 5a**). Second, we incubated MDA-MB-231 cells with IODVA1 (3 μM) for 15 min and analyzed the levels of phosphorylated Vav3 (pY173) by immunoblotting. **Fig. 5b** shows that IODVA1 treatment results in a significant decrease in pY173 signal. Since phosphorylation of this Tyr173 is indicative

of Vav3 activation, we conclude that IODVA1 inhibits Vav3 activity shortly after exposure.

To test if IODVA1 inhibits Vav3 *in vivo*, we took advantage of the MDA-MB-231 xenograft tumors we generated (Gasilina *et al*., 2019) and stained them by immunohistochemistry for pVav3. Comparison of pVav3 stained tumor sections treated with vehicle control and with IODVA1 shows significant decrease in pVav3 staining for tumors treated with IODVA1 than with vehicle control (**Fig. 5c**). Thus, IODVA1 also inhibits Vav3 *in vitro* and *in vivo* in solid tumor models and in a cell-independent manner.

IODVA1 decreases survival of patient-derived leukemia cells. Consistent with our findings with peripheral $CD34^+$ BCR-ABL cells (**Fig. 1a-1b**), cells from PDX models representing pediatric Ph^+ B-ALL patients (**Table 1)** were found to be highly sensitive to IODVA1 *ex vivo* (**Fig. 6)**.

Cells from relapsed patient #2018-136 with Ph^+ (BCR-ABL1) were treated with ABL-TKI dasatinib, JAK-inhibitor ruxolitinib, dasatinib and ruxolitinib combination (das + rux), CDK-inhibitor abemaciclib, and IODVA1. Dasatinib (20 nM) reduced the proliferation of #2018-136 cells by 56%; ruxolitinib or abemaciclib (1 μM) had no effect. The das+rux combination resulted in 63% decrease in proliferation, which is likely due to dasatinib's inhibitory action. IODVA1 (0.5 μM) reduced the proliferation of these cells by 78%. When tested in the colony formation assay, IODVA1 (1 μM) reduced the number of colonies by 60% ($p = 0.001$) (**Fig. 6a)**.

Cells from patient #2017-58 with a dual Ph^+ (BCR-ABL1) and Ph-like (P2RY8-CRLF2) rearrangement were similarly treated. These cells clearly responded to dasatinib, ruxolitinib, and the combination. IODVA1 was not as potent as it decreased their proliferation by only 40% at 1 μM and had no effect at 0.2 μM (**Fig. 6b**). Original $CD19^+$ cells from patient #2017-129 with Ph^+ B-ALL (BCR-ABL1; T315I) who relapsed after initial treatment were treated with vehicle control, dasatinib, ruxolitinib, (das + rux), and IODVA1. As expected dasatinib, ruxolitinib, or the combination had no effect on proliferation of the $CD19^+$ cells (**Fig. 6c,** left panel). In contrast, IODVA1 at 1 μM but not at 0.2 μM reduced the $CD19^+$ B-ALL cell counts by 80%. Additionally, we confirmed that IODVA1 does not exert toxic effects to cells of normal stroma (**Fig. 6c**, right panel arrows). Thus, IODVA1 decreases the proliferation of Ph^+ B-ALL (BCR-ABL1) primary cells including cells expressing the TKI-resistant T315I mutant consistent with our findings that Ph^+ B-ALL (BCR-ABL1) model cells express high-levels of Vav3. The fact that #2017-58 cells did not respond to IODVA1 as well as the other two patient samples is probably due to the existence of other genetic mutations (*e.g.* P2RY8-CRLF2) that promote cell growth independently of Vav3.

Our cohort of samples also contained numerous cases of Ph-like disease with a diverse series of genetic aberrations and a few cases of MLL-rearranged B-ALL. These patient cells generally responded positively to IODVA1 (**Supplementary data, Fig. S4a-S4h**).

DISCUSSION

Vav3 is a multi-domain tyrosine phosphorylation–dependent RacGEF that functions downstream of several different signaling molecules including immune response receptors, G-protein-coupled receptors (GPCRs), protein tyrosine kinases and integrins [58-64] and is a critical component of BCR-ABL induced Rac activation [52]. Thus far, no small molecule inhibitor of a Vav family-member has been reported. Small molecule inhibitors of the RhoGEFs LARG, AKAP13, DOCK2, and DOCK5 [65-69] have been identified in *in vitro* and cellular assays however, these molecules work at high concentrations and both their mechanism of action and their potential drug-likeness is questionable [70].

This study in cellular and murine models of the chimeric BCR-ABL1 oncoprotein demonstrates that inhibitor of oncogene-driven Vav3 activation, IODVA1, binds tightly to Vav3 (K_d = 400 nM, **Fig. 4b**), prevents its activation, and the activation of Rac *in vitro* and *in vivo*. In accordance with this MoA, IODVA1 also significantly decreased the levels of active Vav3 in xenograft tumors of triple negative breast cancer mouse model (**Fig. 5c**) suggesting that IODVA1 inhibition of Vav3 is not specific to leukemia models. One can argue that IODVA1 inhibits the transmembrane or cytosolic protein tyrosine kinases such as Syk, Janus, Tec, Abl, and Src family kinases responsible for Vav3 phosphorylation [61,71] however, this is unlikely since IODVA1 is not a kinase inhibitor (Gasilina *et al.*, 2019). IODVA1 binding to Vav3 seems specific as it does not bind Rac or LARG and does not interfere with the actions of p50GAP or RhoGDI1. The possibility that IODVA1 binds to the homologous Vav1/2 exists but based on the loss of IODVA1's efficacy in $Vav3^{-/-}$ models (**Fig. 4c & 4d**), this binding is unlikely. Significantly, IODVA1 has no effect on $Vav3^{-/-}$ murine bone marrow leukemic cells and does not affect

the survival of a mouse model of $Vav3^{-/-}$ p190-BCR-ABL-induced leukemia. In addition, IODVA1 has no effect on $Rac1^{\Delta/\Delta}$+$Rac2^{-/-}$ leukemic cells (**Fig. 3d**). These *in vivo* and *in vitro* results are relevant because if IODVA1 had off-targets with a contribution to BCR-ABL-driven leukemia, an increase in mouse survival and in cell proliferation would have been detected, which is not the case.

Our *in vitro* cell cycle and colony formation data indicate that IODVA1's pharmacological action on leukemic cells mimics the genetic deletion of Vav3 (**Fig. 4c & 4d**). The IODVA1-triggered increase in apoptosis (**Fig. 3c**) is also in line with the increase in apoptosis observed in $Vav3^{-/-}$ leukemic cells [52]. Results from the colony formation assays with the $Rac1^{\Delta/\Delta}$+$Rac2^{-/-}$ leukemic cells (**Fig. 3d**) and from viability of shVav3 MDA-MB-231 cells (**Fig. 5a**) are also consistent with this idea. We noticed however, that the $Rac1^{\Delta/\Delta}$+$Rac2^{-/-}$ leukemic cells resulted in higher number of colonies than cells treated with IODVA1. This can be explained by residual Rac1 (**Fig. S2d**), which is pro cell-proliferation or by the Rac-independent pathways regulated by Vav3 that are not inhibited by IODVA1. Likewise, there is a noticeable difference between IODVA1's pharmacological action, which increases survival of leukemic mice and Vav3 genetic deletion, which results in premature leukemic mice death (**Fig. S3b**). Our phosphor-flow data show however, that in the background of $Vav3^{-/-}$, BCR-ABL leukemic cells increase signaling through the pro-survival and Vav3/Rac-independent effectors AKT and STAT3. This mechanism of adaptation is likely responsible for the proliferation of LSCs and the death of $Vav3^{-/-}$ leukemic mice (see also [52]).

IODVA1 decreases Rac activation and the activity of several of its downstream effectors such as PAK, JNK, S6, and 4EBP *in vitro* and *in vivo*. The decrease in PAK

activity leads to dephosphorylation and therefore activation of BAD [72]. BAD activation prevents its association with Bcl2/Bcl-xL and promotes cell apoptosis. IODVA1's induction of apoptosis of BCR-ABL expressing cells is supported by our cell cycle analysis *in vitro* and *in vivo* (**Fig. 3c & 4d**). Most relevant to this MoA is the decrease in levels of pJNK, pPAK, pS6, and p4EBP following IODVA1 administration to TKI-resistant BCR-ABL(T315I) leukemia model and the associated decrease in leukemic burden (**Fig. 2c**).

The expression of BCR-ABL in B-ALL confers a much poorer prognosis compared to other cytogenetic or molecular abnormalities [73]. Treatment with the imatinib and second-generation ABL-TKI inhibitors (*e.g.* dasatinib/ponatinib) has proven to be only partly effective in Ph^+ B-ALL patients. The relative failure of TKI therapy in these types of ALL is due to, among others, the development of resistance-inducing mutations such as ABL1-T315I [38,74] and primary resistance of leukemic stem cells to TKI therapy [75]. In studies of patients with high-risk B-cell ALL that were resistant to conventional treatment, a high frequency of recurrent somatic alterations was found in key signaling pathways such as the Ras/ERK, PI3K/AKT, B-cell development and differentiation, Rac/PAK, and Janus kinases [76-78]. An emerging concept to overcome TKI-shortcomings is to target leukemic stem cells (LSCs), which are responsible for disease initiation and propagation. Whereas imatinib alone does not eradicate LSCs *in vivo*, deletion of Rac2 in p210-BCR-ABL–transduced hematopoietic cells prolonged the survival of leukemic mice [12,15,16,29]. Similarly, genetic deficiency of Vav3 but not of Vav1/Vav2 delays leukemogenesis by p190-BCR-ABL and phenocopies the effect of Rac2 deficiency [52] suggesting that Vav3 and Rac GTPases are targets in BCR-ABL LSCs. IODVA1

eliminates residual leukemic stem/progenitor cells responsible for BCR-ABL B-ALL disease relapse in secondary transplant mice better than imatinib (**Fig. 1d**) and overcomes resistance to ABL1-TKI (**Fig. 2**). It reduces the viability of primary cells from pediatric patients with Ph^+ B-ALL including TKI-resistant BCR-ABL1(T315I), Ph-like, and MLL-rearrangements with superior potency than currently administered therapies. This is interesting because Ph-like lymphoblastic leukemias are known to depend largely directly or indirectly on JAK-STAT tyrosine kinase signaling activation [79]. Our data using pre-clinical models of CLRF2 mutant B-ALL (**Fig. S4**), the most frequent mutation in Ph-like B-ALL which induces activation downstream of IL7R through the JAK/STAT signaling pathway illustrates the effect of IODVA1 in an alternative tyrosine kinase receptor signaling pathway. On the other hand, MLL-rearranged lymphoblastic leukemias have been shown to have high expression of and exquisite dependence on Flt3, a tyrosine kinase receptor signaling in many [80], but not all [81] cases, which probably illustrates the heterogeneity of results observed in the responses to IODVA1 in primary human ALL specimens. The specificity of IODVA1 to the oncoprotein expressing cells (**Fig. 1a**) explains its low toxicity *in vivo*. IODVA1 is thus well-suited to treat Ph^+ leukemias with a superior outcome.

Although our data are consistent with IODVA1 binding to Vav3, they do not reveal where it binds. Vav3 is a multidomain signaling protein that can be roughly divided into two halves: (1) a catalytic N-terminal half responsible for Rac binding and activation and (2) an adaptor C-terminal half involved in protein-protein interactions. The nucleotide exchange activity of Vav3 is subject to tight regulation. It is accepted that upon cell stimulation, phosphorylation of conserved Tyr-residues (*e.g.* Tyr173) releases an

autoinhibitory mechanism by the N-terminus calponin-homology CH-domain and acidic stretch (Ac) and the C-terminal SH3 domain, thus allowing GTPase access to the DH domain [82-86]. Based on our biochemical data (**Fig. 4a & 5b**), we argue that IODVA1 inhibits Vav3 phosphorylation by preventing the access of tyrosine residues in the Ac-stretch to Src kinases. We postulate that IODVA1 likely locks Vav3 into the autoinhibitory state, thus preventing Rac from accessing the DH domain for activation. Dissection of the exact binding site is currently underway.

In conclusion, we have shown that pharmacological inhibition of Vav3 by IODVA1 is an attractive therapeutic strategy to treat TKI-resistant BCR-ABL B-ALL. This strategy should benefit other malignancies where Vav3 is a target [52-56,87-100]. We thus expect IODVA1 to have a broader therapeutic application. In addition, IODVA1 constitutes an exceptional tool to dissect the Vav3/Rac signaling axis. Broadly, RhoGEFs are multi-domain proteins that are regulated by an autoinhibition mechanism [101-104]. Consequently, small molecules that stabilize the autoinhibited conformation of RhoGEFs and inhibit their activity could be developed into drugs to treat human cancers.

ACKNOWLEDGMENTS. We thank Drs. Marie-Dominique Filippi, Daniel Starczynowski, Damien Reynaud, and their lab members for valuable advice, Yuting Tang for help with figure preparation, and Ashley Wellendorf for retrovirus preparation and mouse colony maintenance. This project was funded by NIH grant (R01CA115611 to N.N.N.), a Translational Research Program from the Leukemia Lymphoma Society (6076-14; to N.N.N. and J.A.C.), an Affinity Group Award from the Cincinnati Cancer Center (N.N.N, J.A.C, and E.J.M.), a FY19 Cincinnati Children's Innovation Fund award (N.N.N and J.A.C.), the German Research Foundation (Deutsche Forschungsgemeinschaft; AH 92/8-1 to M.A. and M.R.A.), the European Network on Noonan Syndrome and Related Disorders (NSEuroNet, 01GM1602B to O.H.F.K. and M.R.A.), the German Federal Ministry of Education and Research (BMBF) – German Network of RASopathy Research (GeNeRARe, 01GM1519D and 01GM1902C to M.R.A.), and the International Research Training Group 1902 Intra- and Interorgan Communication of the Cardiovascular System (IRTG 1902-P6 to M.B. and M.R.A.).

Experimental Methods

Plasmids, Cell Lines, and Reagents: Plasmid set for purification of fixed-arm carrier fusions pMalX (A-E) was a kind gift from Dr. Lars C. Pedersen (NIEHS), pET28b-N_9-MBP-mOrange plasmid was from Addgene (#29748), chaperone co-expression plasmid set was from TaKaRa (cat #3340). Primers were from Integrated DNA Technologies (IDT, Inc.). Primer and construct design was performed with NEBuilder Tool. Restriction enzymes, polymerases, cloning assembly kits and competent cells were from New England Biolabs and Invitrogen.

MDA-MB-231 cells were maintained in IMEM (Invitrogen) supplemented with 10% FBS, 1% penicillin/streptomycin, and 1% amphotericin B. Ba/F3 cells were cultured in RPMI (GIBCO) supplemented with 10% FBS and IL-3 (10 ng/ml). HEK293T cells were maintained with DMEM supplemented with 10% FBS and 1% penicillin/streptomycin. All cell lines were cultured at 37°C in a 5% CO_2 humidified incubator. Cell viability was assessed by trypan blue exclusion assay as previously described (Gasilina *et al*., 2019). Cytokines were from Peprotech.

The following antibodies were used: GAPDH (#627408, GeneTex), pERK1/2 (#4370), pAKT (#9271 and #9018), Cdc42 (#2462), RhoA (#2117), pPAK1 (#9018S), pS6 (#48515), PAK1/3 (#2602S), pBAD (#4366), and BAD (#9292), anti-mouse HRP (#7076), anti-rabbit HRP (#7074) were from Cell Signaling Technologies, pVav3(Y173) (#ab109544) and total Vav3 (#ab203315) were from Abcam, pJNK (Alexa Fluor 647 conjugated, #562481), p-p38 (PE-conjugated, #612565), Rac2 (#610850), pStat3 (#55385), and pStat5 (Alexa Fluor 647 conjugated, #612599), and B220 APC-Cy7

antibody (#552094) were from BD Bioscience, p4EBP1 (PE-conjugated, #12-9107-42) was form Thermofisher Scientific.

Lipids (Phosphatidylserine (PS), Phosphatidylcholine (PC), phosphatidylethanolamine (PE) and sphingomyelin (SM), and phosphatidylinositol 4,5-bisphosphate (PIP_2) for membrane displacement assays were from Avanti.

IODVA1 was synthesized from 2-guanidinobenzimidazole and purified as described (Gasilina *et al*., 2019). Imatinib (#SML1027) was from SIGMA-Aldrich, dasatinib (#S1021), and ruxolitinib (#S1378) from Selleck.

Retroviral and Lentiviral Particle Production, Transduction and Transplantation of Transduced Leukemic cells: Production of lentivirus and retrovirus for stable transduction of murine and human cells were done as described previously [105]. Scrambled and Vav3-specific shRNAs (Sigma-Aldrich MISSION shRNA) were obtained from Cincinnati Children's Lenti-shRNA Library Core. Retroviral and lentiviral vectors, viral transduction of cell lines and mouse LDBM, and transplantation of transduced leukemic cells were previously described [52].

SDS-PAGE, Pull-down Assays and Immunoblotting: Exponentially growing (6×10^6) p190-BCR-ABL Ba/F3 cells were treated with either vehicle or IODVA1 at indicated concentrations and time points. Active GTPase pulldown was done according to the manufacturer's instructions using GST-PAK1-GBD or GST-Rhotekin (Thermofisher, #16118 and #16116). Protein complexes was separated on SDS-PAGE and immunoblotted with anti-Rac1, anti-Cdc42 and anti-RhoA antibodies.

For analysis of expression, cells were lysed in RIPA buffer, supplemented with phosphatase and protease inhibitors, separated on SDS-PAGE, transferred on PVDF or nitrocellulose membrane and blotted with appropriate primary and secondary antibodies, as described previously [52,105]. Relative signals were normalized to the unstimulated conditions after normalization to the total protein amount. Quantification was performed using Licor Image Studio.

Cloning: Human *Rac1* (GenBank accession n° NM_006908.4) was subcloned into pFastBacHTB vector (Invitrogen) and fused with an N-terminal His_6-tag.

For pMalX(E)-based expression, full-length Vav3 was amplified with primers overlapping NotI restriction site of pMalX(E) vector with N-terminal linkers AAAA, AAAASEF or AAAASEFGS linkers. The finalized construct encoded MBPX(E)-linker-Vav3. For His_6-MBP-N_9-TEV-Vav3 construct, full-length Vav3 cDNA with a stop codon at the end of the coding sequence was amplified by PCR with primers overlapping pET28a-MBP-N_9TEV-mOrange vector at the *Ssp*I site. The resulting construct encoded MBP-N_9-Vav3-His_6. All constructs were verified using Sanger sequencing using CCHCM DNA Core. To minimize aggregation and improve on quality of purified protein, the expression clones were tested with chaperone plasmids according to the manufacturer's protocol.

Protein Expression and Purification: For membrane displacement assays, full-length human Rac1 was purified from baculovirus. pFastBacHTB-Rac1 was transformed into

DH10 cells and the resulting bacmid was used to generate baculovirus in Sf9 cells. Rac1 was produced in TNAO38 insect cells and purified using Ni-IMAC chromatography [106].

For production of recombinant Vav3, plasmids were co-transformed with chaperone plasmid Gro7 groEL-groES in BL21 (DE3) or T7 Express. Cultures were grown in LB, supplemented with metal mix [107]. Protein was purified using Ni-IMAC chromatography, dialyzed and further purified using size-exclusion gel filtration (HiLoad Superdex 200 16/60). Fractions were analyzed by SDS-PAGE and protein fractions containing Vav3 were pooled, concentrated to ~10 mg/mL and flash frozen in liquid nitrogen. Final yields for MBP-N9-Vav3 and MBPXE-Vav3 were 5 mg and 20 mg per 6 L of culture, respectively.

Recombinant LARG (DH/PH) was purified as a MBP-fusion protein as described previously (Kristelly R. et al., 2003).

RhoGDI extracting prenylated Rac1 from liposomes: Displacement of prenylated-Rac1-GDP from synthetic liposomes by GST RhoGDI1 in the presence and absence of IODVA1 was studied using liposome sedimentation assay as in [106]. Briefly, liposomes were generated by using a defined composition of lipids (194 μg) containing 39% w/w phosphatidylethanolamine, 16% w/w phosphatidylcholine, 36% w/w phosphatidylserine, 4% sphingomyelin, and 5 % w/w phosphatidylinositol 4,5-bisphosphate. Prenylated Rac1-GDP (1 μM) was added to liposomes suspended in protein buffer (20 mM Hepes, pH 7.4, 150 mM NaCl, 5 mM $MgCl_2$, 3 mM DTT) and incubated for 20 min on ice. GST RHOGDI1 (2 μM) in the absence or presence of IODVA1 was added to the liposome/prenylated Rac1 and further incubated on ice for 30 min. The samples were

then centrifuged at 20,000 x g for 20 min at 4 °C. Pellet and supernatant fractions were collected, separated on SDS-PAGE and immunoblotted for Rac1.

Microscale Thermophoresis (MST): Purified Vav3, LARG or Rac (1 µM) were incubated with the indicated concentrations of IODVA1 at room temperature for 30 min. Samples were loaded into Zero Background MST Premium Coated capillaries and binding events were measured on Monolith NT.LabelFree (NanoTemper Technologies). Binding data were analyzed using Thermophoresis or Thermophoresis with Temperature Jump analysis as described previously [108]. Data were normalized using fraction-bound binding. The 95% confidence interval for K_d values was 0.27 to 0.98 µM for Vav3, 5.9 to 10.37 µM for LARG, and 19.6 to 105.8 µM for Rac.

Stopped-flow spectrometry. GTPase assay and nucleotide exchange reaction were performed with a Hi- Tech Scientific (SF-61) stopped-flow instrument as described [109] The excitation wavelengths were 543 nm and 362 nm for tamraGTP and mantGppNHp, respectively. For GTPase assay, equal volumes (600 µl) of 0.2 µM RAC1- tamraGTP and 10 µM of p50GAP were used. GTPase assay as well the protein-protein interaction were performed in presence of 5% DMSO.

Animals and *in vivo* Drug Administration: Vav3-deficient mice [110] and $Rac1^{\Delta/\Delta}$+Rac2-deficient [12] mice have been described previously. C57Bl/6 mice were commercially obtained (The Jackson Laboratory and Harlan Laboratories) and used as donors and/or recipients of transduction/transplantation models under a protocol approved by The

Cincinnati Children's Hospital Medical Center Institutional Animal Care and Use Committee. For *in vivo* drug administration, Alzet implantable osmotic pumps (Model 2002, Durect) were used according to the manufacturer's protocol and implantation was done as described previously [12].

Histology: Embedded tissues were cut into 4 μm sections then immunohistochemically stained using the Mouse on Mouse kit (MoM kit, Vector Laboratories). Tissue sections were subjected to sodium citrate antigen retrieval, pretreated with 0.3% hydrogen peroxide, blocked according to kit directions, and incubated with an antibody to phosphorylated Vav3 (1:200 dilution, Abcam) and HRP-conjugated anti-rabbit secondary (Vector Laboratories). Staining was completed with the DAB Peroxidase kit (Vector Laboraties) and counterstained with hematoxylin. Tissue sections were coverslipped with Cytoseal 60 and images acquired with a Nikon Eclipse Ci microscope.

CFU-proB assay: B-cell lineage colony-forming units (CFU-proB) were quantified post 9-day culture of leukemic BM cells or sorted for p190-BCR-ABL–expressing B-cell progenitors in M3134 methylcellulose (StemCell Technologies) supplemented with 30% FBS (for mouse B lymphoid colony forming cells; StemCell Technologies), 2 mM L-glutamine (Invitrogen), 1% penicillin-streptomycin (Invitrogen), 100 μM β-mercaptoethanol (Fisher-Scientific), 1% BSA (Sigma-Aldrich), 20 ng/mL of recombinant mouse IL-7 (PeproTech), and 100 ng/mL of recombinant mouse SCF (PeproTech).

Cell cycle analysis: Cell cycle was analyzed by using *in vitro* incorporation of 5-Bromo-2-deoxyuridine using Brdu Flow kit (BD Pharmingen, Cat# 552598). Briefly, mice leukemic progenitors were incubated with 1 mM BrdU solution for 45 minutes, cells were further fixed and permeabilized. DNAse treatment was done according to the instructions and stained with anti BrdU and apoptosis was analyzed by 7-AAD staining through flow cytometry analysis.

Flow cytometry analysis: Peripheral blood flow cytometry analysis was done by lysing the RBCs using BD pharma lyse (BD bioscience, Cat# 555899). Cells were washed once with PBS then stained with anti-B220 APC-Cy7 antibody. Stained cells were washed once and analyzed by flow cytometry.

Primary PDX ex vivo drug treatments: Primary patient specimens were obtained from patients at CCHMC according to Institutional Review Board Approved protocols (#2008-0021 and #2008-0658). Samples were subjected to RBC lysis and the isolated WBCs were mixed with OKT3 anti-CD3 antibody to eliminate the potential for xenogenic Graft Versus Host Disease before injection into busulfan conditioned NSG or NRG mice [111]. Spleen preparations from mice successfully engrafted with B-ALL were co-cultured with MS-5 or OP9 stroma in MEMα media supplemented with 20% FBS and 10 ng/mL recombinant human SCF (Kit-L), Flt3L, and IL-7 (KF7). IODVA1 was added 24 h after initial seeding. Co-cultures were collected by trypsinization after 7 days and cell counts were performed with trypan blue. Flow cytometry was performed with mCD45-APC-Cy7 (BD), hCD45-FITC (BD), hCD19-VioBlue (Miltenyi Biotech), and 7-AAd (for viability)

to determine percentage of human ALL in the cultures. Total absolute ALL cell numbers were determined by multiplying cell counts by percentage human ALL cells.

Figure Legends

Fig. 1: **IODVA1 inhibits the proliferation and survival of BCR-ABL expressing cells *in vitro* and *in vivo* and eradicates leukemia propagating cells in secondary transplants.** (**A**) Human peripheral $CD34^+$ blood cells transduced with p190-BCR-ABL (grey line, squares, and black line, inverted triangles) or Mieg3 vector control (lilac lines, circles and triangles) virus were co-cultured on OP-9 stromal cells and incubated with either vehicle or IODVA1 (IO1, 1 μM). Cell proliferation was assessed by flow cytometry. (**B**) Cells were transduced and cultured as in (**A**) but incubated with either vehicle or IODVA1 (IO1, 1 or 3 μM) and survival (%) was determined by trypan blue exclusion. (**C**) Kaplan-Meier plot showing survival of p190-BCR-ABL leukemic mice post treatment with vehicle control, IODVA1 (IO1), imatinib (IM), or the combination at the indicated concentrations in the pump. LDBM cells were transduced with bicistronic p190-BCR-ABL/EGFP retrovirus and transplanted into recipient mice. After initial assessment of leukemic burden, drugs were delivered in subcutaneously implanted osmotic pumps, each lasting two weeks. (**D**) Kaplan-Meier survival plot of secondary mice transplants. Bone marrow cells from mice treated with vehicle, imatinib (IM), IODVA1 (IO1) or the combination at the indicated concentrations were transplanted into secondary recipients. Results for the 10^6 cell-dilution are shown.

Fig. 2: IODVA1 but not imatinib increases the survival of a mouse model of TKI-resistant B-ALL. LDBM cells were transduced with TKI-resistant (gate-keeper) p210-BCR-ABL(T315I) and transplanted into recipient mice as in **Fig. 1**. Pumps were

surgically introduced into mice (N = 5 per treatment group) and treatment lasted 28 days or two rounds of pumps. After 28 days, mice were monitored without any additional treatment. (**A**) Kaplan-Meier survival plot of imatinib-resistant mice. Pumps either carried vehicle control (black line), 0.5 mM imatinib (IM, grey line), or 0.5 mM IODVA1 (IO1, lilac line). (**B**) Flow cytometric analysis of leukemic progenitor ($EGFP^{+}$) B-cells in peripheral blood (PB) at the indicated week. Only IODVA1-treated mice remained alive for analysis at weeks 5, 7, and 10. (**C**) Pharmacodynamic assessment of leukemic progenitor cells (%) from the 2-week treated mice with vehicle control (black), imatinib (grey), or IODVA1 (lilac) using phospho-flow analysis of the indicated Rac-dependent and -independent effectors (* $p \leq 0.05$; ** $p \leq 0.01$).

Fig. 3: **IODVA1 decreases Rac activation and signaling.** (**A**) Ba/F3 cells expressing p190-BCR-ABL were treated with IODVA1 (3 μM) as indicated and levels of active Rac (Rac-GTP) were assessed by pull-down using GST-PAK-GBD, followed by immunoblotting (upper panel) and densitometric quantification (lower panel). (**B**) Flow-cytometry analysis of pJNK, pS6, p4EBP, pPAK, and pAKT of Ba/F3 cells expressing Mieg3 empty vector (light and dark blue) or p190-BCR-ABL (light and dark salmon) and treated with vehicle control or IODVA1 (3 μM) for 30 min. (**C**) Representative histogram data of the cell cycle analysis of Ba/F3 cells expressing p190-BCR-ABL and treated with vehicle control or IODVA1 (1, 3, and 10 μM) for 20 h. (**D**) Quantification of the average number of colonies of bone marrow wild-type (black) and $Rac1^{\Delta/\Delta}$+$Rac2^{-/-}$ (red) p190-BCR-ABL leukemic cells treated with vehicle control or IODVA1 (IO1, 1 μM) (** $p \leq 0.01$; *** $p \leq 0.001$).

Fig. 4: IODVA1 targets Vav3 *in vitro* and *in vivo*. (**A**) Ba/F3 cells expressing Mieg3 or p190-BCR-ABL were treated with vehicle control or IODVA1 (IO1, 3 μM) for 30 min and incubated with GST-Rac and glutathione beads. Beads were washed and the protein complex separated on SDS-PAGE and immunoblotted for pVav3. Input Vav3 was used as control. (**B**) Binding affinity (K_d) between IODVA1 and Vav3 (green), LARG (brown), and RacGDP (blue). The miscroscale thermophoresis signal expressed as fractional occupancy was plotted against IODVA1 (0.1 nM – 20 μM) and fitted to yield K_d. Error bars = s.d.; n = 3. (**C**) Quantification of the average number of colonies made by bone marrow wild-type (black) and $Vav3^{-/-}$ (lilac) p190-BCR-ABL leukemic cells treated with vehicle control or IODVA1 (IO1, 1 and 3 μM) (* $p \leq 0.05$; ** $p \leq 0.01$; *** $p \leq 0.001$; ns non-significant). (**D**) Representative histogram data of the cell cycle analysis of wild-type (black and grey bars) and $Vav3^{-/-}$ (dark and light lilac) bone marrow cells expressing p190-BCR-ABL and treated with vehicle control or IODVA1 (IO1, 3 μM) for 20 h.

Figure 5: IODVA1 decreases levels of pVav3 in *in vitro* and *in vivo* models of triple negative breast cancer. (**A**) Immunoblot and quantification of Vav3 protein in lysates of MDA-MB-231 triple negative breast cancer cells stably expressing scrambled or Vav3-targeting shRNAs. Viability of the MDA-MB-231 cells stably expressing shVav3 in the presence of IODVA1 (0 - 1 μM). Cells were grown in the presence of IODVA1 and counted by trypan blue exclusion at the indicated time points. (**B**) MDA-MB-231 cells were incubated with IODVA1 (3 μM) for 15 min and the levels of phosphorylated Vav3

(pY173) were assessed by immunoblotting. (**C**) Immunohistochemical staining of phosphorylated Vav3 in tissue derived from MDA-MB-231 xenografts treated with vehicle control or IODVA1.

Figure 6: IODVA1 reduces survival of relapsed and *de novo* pediatric patient derived Ph^+ leukemia cells. Patient derived xenograft (PDX) cells were co-cultured *ex vivo* on MS-5 or OP-9 stromal cells and treated with dasatinib (Das, ABL1-inhibitor), ruxolitinib (Rux, JAK-inhibitor), combination of dasarinib and ruxolitinib (Das + Rux), abemaciclib (CDK inhibitor), or IODVA1 and assessed for survival. (**A**) Representative survival of patient #2018-136 treated cells and of colony number in the presence of IODVA1 (IO1). Representative survival of patient #2017-58 (**B**) and BCR-ABL1(T315I) patient #2017-129 (**C**) treated cells. Note lack of toxicity of IODVA1 to normal stromal cells (black arrows) in the accompanying image.

References

1. Etienne-Manneville, S. & Hall, A. Rho GTPases in cell biology. *Nature* **420**, 629-35 (2002).
2. Jaffe, A.B. & Hall, A. Rho GTPases: biochemistry and biology. *Annu Rev Cell Dev Biol* **21**, 247-69 (2005).
3. Bustelo, X.R. RHO GTPases in cancer: known facts, open questions, and therapeutic challenges. *Biochem Soc Trans* **46**, 741-760 (2018).
4. Ridley, A.J. Rho GTPase signalling in cell migration. *Curr Opin Cell Biol* **36**, 103-12 (2015).
5. Ridley, A.J., Paterson, H.F., Johnston, C.L., Diekmann, D. & Hall, A. The small GTP-binding protein rac regulates growth factor-induced membrane ruffling. *Cell* **70**, 401-10 (1992).
6. Steffen, A. et al. Rac function is crucial for cell migration but is not required for spreading and focal adhesion formation. *J Cell Sci* **126**, 4572-88 (2013).
7. Coleman, M.L., Marshall, C.J. & Olson, M.F. RAS and RHO GTPases in G1-phase cell-cycle regulation. *Nat Rev Mol Cell Biol* **5**, 355-66 (2004).
8. Kiosses, W.B., Shattil, S.J., Pampori, N. & Schwartz, M.A. Rac recruits high-affinity integrin alphavbeta3 to lamellipodia in endothelial cell migration. *Nat Cell Biol* **3**, 316-20 (2001).
9. Sundaresan, M. et al. Regulation of reactive-oxygen-species generation in fibroblasts by Rac1. *Biochem J* **318 (Pt 2)**, 379-82 (1996).
10. Mack, N.A., Whalley, H.J., Castillo-Lluva, S. & Malliri, A. The diverse roles of Rac signaling in tumorigenesis. *Cell Cycle* **10**, 1571-81 (2011).
11. Qiu, R.G., Chen, J., Kirn, D., McCormick, F. & Symons, M. An essential role for Rac in Ras transformation. *Nature* **374**, 457-9 (1995).
12. Thomas, E.K. et al. Rac guanosine triphosphatases represent integrating molecular therapeutic targets for BCR-ABL-induced myeloproliferative disease. *Cancer Cell* **12**, 467-78 (2007).
13. Somervaille, T.C. & Cleary, M.L. Identification and characterization of leukemia stem cells in murine MLL-AF9 acute myeloid leukemia. *Cancer Cell* **10**, 257-68 (2006).
14. Wei, J. et al. Microenvironment determines lineage fate in a human model of MLL-AF9 leukemia. *Cancer Cell* **13**, 483-95 (2008).
15. Sengupta, A., Arnett, J., Dunn, S., Williams, D.A. & Cancelas, J.A. Rac2 GTPase deficiency depletes BCR-ABL+ leukemic stem cells and progenitors in vivo. *Blood* **116**, 81-4 (2010).

16. Skorski, T. et al. BCR/ABL-mediated leukemogenesis requires the activity of the small GTP-binding protein Rac. *Proc Natl Acad Sci U S A* **95**, 11858-62 (1998).

17. Mizukawa, B. et al. Inhibition of Rac GTPase signaling and downstream prosurvival Bcl-2 proteins as combination targeted therapy in MLL-AF9 leukemia. *Blood* **118**, 5235-45 (2011).

18. Bassermann, F. et al. Association of Bcr-Abl with the proto-oncogene Vav is implicated in activation of the Rac-1 pathway. *J Biol Chem* **277**, 12437-45 (2002).

19. Nieborowska-Skorska, M. et al. Rac2-MRC-cIII-generated ROS cause genomic instability in chronic myeloid leukemia stem cells and primitive progenitors. *Blood* **119**, 4253-63 (2012).

20. Loirand, G. & Pacaud, P. The role of Rho protein signaling in hypertension. *Nat Rev Cardiol* **7**, 637-47 (2010).

21. Mulloy, J.C. et al. Rho GTPases in hematopoiesis and hemopathies. *Blood* **115**, 936-47 (2010).

22. Newey, S.E., Velamoor, V., Govek, E.E. & Van Aelst, L. Rho GTPases, dendritic structure, and mental retardation. *J Neurobiol* **64**, 58-74 (2005).

23. Sahai, E. & Marshall, C.J. RHO-GTPases and cancer. *Nat Rev Cancer* **2**, 133-42 (2002).

24. Vigil, D., Cherfils, J., Rossman, K.L. & Der, C.J. Ras superfamily GEFs and GAPs: validated and tractable targets for cancer therapy? *Nat Rev Cancer* **10**, 842-57 (2010).

25. Porter, A.P., Papaioannou, A. & Malliri, A. Deregulation of Rho GTPases in cancer. *Small GTPases* **7**, 123-38 (2016).

26. Zandvakili, I., Lin, Y., Morris, J.C. & Zheng, Y. Rho GTPases: Anti- or pro-neoplastic targets? *Oncogene* **36**, 3213-3222 (2017).

27. Cardama, G.A. et al. Relevance of small GTPase Rac1 pathway in drug and radio-resistance mechanisms: Opportunities in cancer therapeutics. *Crit Rev Oncol Hematol* **124**, 29-36 (2018).

28. Cilloni, D. & Saglio, G. Molecular pathways: BCR-ABL. *Clinical cancer research : an official journal of the American Association for Cancer Research* **18**, 930-7 (2012).

29. Thomas, E.K., Cancelas, J.A., Zheng, Y. & Williams, D.A. Rac GTPases as key regulators of p210-BCR-ABL-dependent leukemogenesis. *Leukemia* **22**, 898-904 (2008).

30. Harnois, T. et al. Differential interaction and activation of Rho family GTPases by p210bcr-abl and p190bcr-abl. *Oncogene* **22**, 6445-54 (2003).

31. Sahay, S. et al. The RhoGEF domain of p210 Bcr-Abl activates RhoA and is required for transformation. *Oncogene* **27**, 2064-71 (2008).

32. Lugo, T.G., Pendergast, A.M., Muller, A.J. & Witte, O.N. Tyrosine kinase activity and transformation potency of bcr-abl oncogene products. *Science* **247**, 1079-82 (1990).

33. Arrigoni, E. et al. Concise Review: Chronic Myeloid Leukemia: Stem Cell Niche and Response to Pharmacologic Treatment. *Stem Cells Transl Med* **7**, 305-314 (2018).

34. Hamilton, A. et al. Chronic myeloid leukemia stem cells are not dependent on Bcr-Abl kinase activity for their survival. *Blood* **119**, 1501-10 (2012).

35. Williams, D.A. et al. Dominant negative mutation of the hematopoietic-specific Rho GTPase, Rac2, is associated with a human phagocyte immunodeficiency. *Blood* **96**, 1646-54 (2000).

36. Milojkovic, D. & Apperley, J. Mechanisms of Resistance to Imatinib and Second-Generation Tyrosine Inhibitors in Chronic Myeloid Leukemia. *Clin Cancer Res* **15**, 7519-7527 (2009).

37. Bixby, D. & Talpaz, M. Mechanisms of resistance to tyrosine kinase inhibitors in chronic myeloid leukemia and recent therapeutic strategies to overcome resistance. *Hematology Am Soc Hematol Educ Program*, 461-76 (2009).

38. Gorre, M.E. et al. Clinical resistance to STI-571 cancer therapy caused by BCR-ABL gene mutation or amplification. *Science* **293**, 876-80 (2001).

39. Azam, M., Latek, R.R. & Daley, G.Q. Mechanisms of autoinhibition and STI-571/imatinib resistance revealed by mutagenesis of BCR-ABL. *Cell* **112**, 831-43 (2003).

40. Jabbour, E. et al. Frequency and clinical significance of BCR-ABL mutations in patients with chronic myeloid leukemia treated with imatinib mesylate. *Leukemia* **20**, 1767-73 (2006).

41. Nicolini, F.E. et al. Mutation status and clinical outcome of 89 imatinib mesylate-resistant chronic myelogenous leukemia patients: a retrospective analysis from the French intergroup of CML (Fi(phi)-LMC GROUP). *Leukemia* **20**, 1061-6 (2006).

42. Jabbour, E. et al. Characteristics and outcomes of patients with chronic myeloid leukemia and T315I mutation following failure of imatinib mesylate therapy. *Blood* **112**, 53-5 (2008).

43. Minden, A., Lin, A., Claret, F.X., Abo, A. & Karin, M. Selective activation of the JNK signaling cascade and c-Jun transcriptional activity by the small GTPases Rac and Cdc42Hs. *Cell* **81**, 1147-57 (1995).

44. Saci, A., Cantley, L.C. & Carpenter, C.L. Rac1 regulates the activity of mTORC1 and mTORC2 and controls cellular size. *Mol Cell* **42**, 50-61 (2011).

45. Biswas, M. et al. MBD3/NuRD loss participates with KDM6A program to promote DOCK5/8 expression and Rac GTPase activation in human acute myeloid leukemia. *FASEB J* **33**, 5268-5286 (2019).

46. Chatterjee, S.S., Biswas, M., Boila, L.D., Banerjee, D. & Sengupta, A. SMARCB1 Deficiency Integrates Epigenetic Signals to Oncogenic Gene Expression Program Maintenance in Human Acute Myeloid Leukemia. *Mol Cancer Res* **16**, 791-804 (2018).

47. Martin, H. et al. Pak and Rac GTPases promote oncogenic KIT-induced neoplasms. *J Clin Invest* **123**, 4449-63 (2013).

48. Lyons, R. et al. The RAC specific guanine nucleotide exchange factor Asef functions downstream from TEL-AML1 to promote leukaemic transformation. *Leuk Res* **34**, 109-15 (2010).

49. Reuther, G.W. et al. Leukemia-associated Rho guanine nucleotide exchange factor, a Dbl family protein found mutated in leukemia, causes transformation by activation of RhoA. *J Biol Chem* **276**, 27145-51 (2001).

50. Rouard, H., Tamasdan, S., Fridman, W.H. & Teillaud, J.L. Vav and SLP-76 recruitment by cross-linking of FcgammaRIIa1 in promyelocytic HL-60 cells. *Immunol Lett* **68**, 347-53 (1999).

51. Bourgoin, S., Harbour, D., Desmarais, Y., Takai, Y. & Beaulieu, A. Low molecular weight GTP-binding proteins in HL-60 granulocytes. Assessment of the role of ARF and of a 50-kDa cytosolic protein in phospholipase D activation. *J Biol Chem* **270**, 3172-8 (1995).

52. Chang, K.H. et al. Vav3 collaborates with p190-BCR-ABL in lymphoid progenitor leukemogenesis, proliferation, and survival. *Blood* **120**, 800-11 (2012).

53. Chen, X. et al. Vav3 oncogene is upregulated and a poor prognostic factor in breast cancer patients. *Oncol Lett* **9**, 2143-2148 (2015).

54. Lee, K. et al. Vav3 oncogene activates estrogen receptor and its overexpression may be involved in human breast cancer. *BMC Cancer* **8**, 158 (2008).

55. Aguilar, H. et al. VAV3 mediates resistance to breast cancer endocrine therapy. *Breast Cancer Res* **16**, R53 (2014).

56. Citterio, C. et al. The rho exchange factors vav2 and vav3 control a lung metastasis-specific transcriptional program in breast cancer cells. *Sci Signal* **5**, ra71 (2012).

57. Lorenzo-Martin, L.F. et al. Vav proteins maintain epithelial traits in breast cancer cells using miR-200c-dependent and independent mechanisms. *Oncogene* **38**, 209-227 (2019).

58. Bustelo, X.R. & Barbacid, M. Tyrosine phosphorylation of the vav proto-oncogene product in activated B cells. *Science* **256**, 1196-9 (1992).

59. Bustelo, X.R., Ledbetter, J.A. & Barbacid, M. Product of vav proto-oncogene defines a new class of tyrosine protein kinase substrates. *Nature* **356**, 68-71 (1992).

60. Turner, M. & Billadeau, D.D. VAV proteins as signal integrators for multi-subunit immune-recognition receptors. *Nat Rev Immunol* **2**, 476-86 (2002).

61. Bustelo, X.R. Regulatory and signaling properties of the Vav family. *Mol Cell Biol* **20**, 1461-77 (2000).

62. Schuebel, K.E., Movilla, N., Rosa, J.L. & Bustelo, X.R. Phosphorylation-dependent and constitutive activation of Rho proteins by wild-type and oncogenic Vav-2. *EMBO J* **17**, 6608-21 (1998).

63. Movilla, N. & Bustelo, X.R. Biological and regulatory properties of Vav-3, a new member of the Vav family of oncoproteins. *Mol Cell Biol* **19**, 7870-85 (1999).

64. Crespo, P., Schuebel, K.E., Ostrom, A.A., Gutkind, J.S. & Bustelo, X.R. Phosphotyrosine-dependent activation of Rac-1 GDP/GTP exchange by the vav proto-oncogene product. *Nature* **385**, 169-72 (1997).

65. Shang, X. et al. Small-molecule inhibitors targeting G-protein-coupled Rho guanine nucleotide exchange factors. *Proc Natl Acad Sci U S A* **110**, 3155-60 (2013).

66. Diviani, D. et al. Small-Molecule Protein-Protein Interaction Inhibitor of Oncogenic Rho Signaling. *Cell Chem Biol* **23**, 1135-1146 (2016).

67. Nishikimi, A. et al. Blockade of inflammatory responses by a small-molecule inhibitor of the Rac activator DOCK2. *Chem Biol* **19**, 488-97 (2012).

68. Vives, V. et al. The Rac1 exchange factor Dock5 is essential for bone resorption by osteoclasts. *J Bone Miner Res* **26**, 1099-110 (2011).

69. Bouquier, N. et al. A cell active chemical GEF inhibitor selectively targets the Trio/RhoG/Rac1 signaling pathway. *Chem Biol* **16**, 657-66 (2009).

70. Gray, J.L., von Delft, F. & Brennan, P. Targeting the Small GTPase Superfamily through their Regulatory Proteins. *Angew Chem Int Ed Engl* (2019).

71. Bustelo, X.R. Vav family exchange factors: an integrated regulatory and functional view. *Small GTPases* **5**, 9 (2014).

72. Schurmann, A. et al. p21-activated kinase 1 phosphorylates the death agonist bad and protects cells from apoptosis. *Mol Cell Biol* **20**, 453-61 (2000).

73. Arico, M. et al. Outcome of treatment in children with Philadelphia chromosome-positive acute lymphoblastic leukemia. *The New England journal of medicine* **342**, 998-1006 (2000).

74. Azam, M., Seeliger, M.A., Gray, N.S., Kuriyan, J. & Daley, G.Q. Activation of tyrosine kinases by mutation of the gatekeeper threonine. *Nat Struct Mol Biol* **15**, 1109-18 (2008).

75. Corbin, A.S. et al. Human chronic myeloid leukemia stem cells are insensitive to imatinib despite inhibition of BCR-ABL activity. *The Journal of clinical investigation* **121**, 396-409 (2011).

76. Hunger, S.P. & Mullighan, C.G. Redefining ALL classification: toward detecting high-risk ALL and implementing precision medicine. *Blood* **125**, 3977-87 (2015).

77. Roberts, K.G. et al. Targetable kinase-activating lesions in Ph-like acute lymphoblastic leukemia. *N Engl J Med* **371**, 1005-15 (2014).

78. Zhang, J. et al. Key pathways are frequently mutated in high-risk childhood acute lymphoblastic leukemia: a report from the Children's Oncology Group. *Blood* **118**, 3080-7 (2011).

79. Tran, T.H. & Loh, M.L. Ph-like acute lymphoblastic leukemia. *Hematology Am Soc Hematol Educ Program* **2016**, 561-566 (2016).

80. Furuichi, Y. et al. Fms-like tyrosine kinase 3 ligand stimulation induces MLL-rearranged leukemia cells into quiescence resistant to antileukemic agents. *Cancer Res* **67**, 9852-61 (2007).

81. Stam, R.W. et al. Targeting FLT3 in primary MLL-gene-rearranged infant acute lymphoblastic leukemia. *Blood* **106**, 2484-90 (2005).

82. Llorca, O., Arias-Palomo, E., Zugaza, J.L. & Bustelo, X.R. Global conformational rearrangements during the activation of the GDP/GTP exchange factor Vav3. *EMBO J* **24**, 1330-40 (2005).

83. Yu, B. et al. Structural and energetic mechanisms of cooperative autoinhibition and activation of Vav1. *Cell* **140**, 246-56 (2010).

84. Aghazadeh, B., Lowry, W.E., Huang, X.Y. & Rosen, M.K. Structural basis for relief of autoinhibition of the Dbl homology domain of proto-oncogene Vav by tyrosine phosphorylation. *Cell* **102**, 625-33 (2000).

85. Rapley, J., Tybulewicz, V.L. & Rittinger, K. Crucial structural role for the PH and C1 domains of the Vav1 exchange factor. *EMBO Rep* **9**, 655-61 (2008).

86. Chrencik, J.E. et al. Structural basis of guanine nucleotide exchange mediated by the T-cell essential Vav1. *J Mol Biol* **380**, 828-43 (2008).

87. Katzav, S., Martin-Zanca, D. & Barbacid, M. vav, a novel human oncogene derived from a locus ubiquitously expressed in hematopoietic cells. *EMBO J* **8**, 2283-90 (1989).

88. Fernandez-Zapico, M.E. et al. Ectopic expression of VAV1 reveals an unexpected role in pancreatic cancer tumorigenesis. *Cancer Cell* **7**, 39-49 (2005).

89. Menacho-Marquez, M. et al. The Rho exchange factors Vav2 and Vav3 favor skin tumor initiation and promotion by engaging extracellular signaling loops. *PLoS Biol* **11**, e1001615 (2013).

90. Liu, Y., Wu, X., Dong, Z. & Lu, S. The molecular mechanism of Vav3 oncogene on upregulation of androgen receptor activity in prostate cancer cells. *Int J Oncol* **36**, 623-33 (2010).

91. Dong, Z. et al. Vav3 oncogene is involved in regulation of secretory phospholipase A2-IIa expression in prostate cancer. *Oncol Rep* **25**, 1511-6 (2011).

92. Liu, Y. et al. Targeted overexpression of vav3 oncogene in prostatic epithelium induces nonbacterial prostatitis and prostate cancer. *Cancer Res* **68**, 6396-406 (2008).

93. Dong, Z. et al. Vav3 oncogene is overexpressed and regulates cell growth and androgen receptor activity in human prostate cancer. *Mol Endocrinol* **20**, 2315-25 (2006).

94. Lyons, L.S. & Burnstein, K.L. Vav3, a Rho GTPase guanine nucleotide exchange factor, increases during progression to androgen independence in prostate cancer cells and potentiates androgen receptor transcriptional activity. *Mol Endocrinol* **20**, 1061-72 (2006).

95. Lin, K.T. et al. Vav3-rac1 signaling regulates prostate cancer metastasis with elevated Vav3 expression correlating with prostate cancer progression and posttreatment recurrence. *Cancer Res* **72**, 3000-9 (2012).

96. Lin, K.Y. et al. Clinical significance of increased guanine nucleotide exchange factor Vav3 expression in human gastric cancer. *Mol Cancer Res* **10**, 750-9 (2012).

97. Tan, B.B. et al. Inhibition of Vav3 gene can promote apoptosis of human gastric cancer cell line MGC803 by regulating ERK pathway. *Tumour Biol* **37**, 7823-33 (2016).

98. Tan, B. et al. The clinical value of Vav3 in peripheral blood for predicting lymphatic metastasis of gastric cancer. *Br J Biomed Sci* **74**, 133-137 (2017).

99. Salhia, B. et al. The guanine nucleotide exchange factors trio, Ect2, and Vav3 mediate the invasive behavior of glioblastoma. *Am J Pathol* **173**, 1828-38 (2008).

100. Liu, J.K. et al. Phage display discovery of novel molecular targets in glioblastoma-initiating cells. *Cell Death Differ* **21**, 1325-39 (2014).

101. Zheng, Y. Dbl family guanine nucleotide exchange factors. *Trends Biochem Sci* **26**, 724-32 (2001).

102. Rossman, K.L., Der, C.J. & Sondek, J. GEF means go: turning on RHO GTPases with guanine nucleotide-exchange factors. *Nat Rev Mol Cell Biol* **6**, 167-80 (2005).

103. Hoffman, G.R. & Cerione, R.A. Signaling to the Rho GTPases: networking with the DH domain. *FEBS Lett* **513**, 85-91 (2002).

104. Schmidt, A. & Hall, A. Guanine nucleotide exchange factors for Rho GTPases: turning on the switch. *Genes Dev* **16**, 1587-609 (2002).

105. Lee, L.H. et al. Real-time genomic profiling of histiocytoses identifies early-kinase domain BRAF alterations while improving treatment outcomes. *JCI Insight* **2**, e89473 (2017).

106. Zhang, S.C. et al. Liposome reconstitution and modulation of recombinant prenylated human Rac1 by GEFs, GDI1 and Pak1. *PLoS One* **9**, e102425 (2014).

107. Studier, F.W. Protein production by auto-induction in high density shaking cultures. *Protein Expr Purif* **41**, 207-34 (2005).

108. Jerabek-Willemsen, M., Wienken, C.J., Braun, D., Baaske, P. & Duhr, S. Molecular interaction studies using microscale thermophoresis. *Assay Drug Dev Technol* **9**, 342-53 (2011).

109. Nouri, K. et al. IQGAP1 Interaction with RHO Family Proteins Revisited: KINETIC AND EQUILIBRIUM EVIDENCE FOR MULTIPLE DISTINCT BINDING SITES. *J Biol Chem* **291**, 26364-26376 (2016).

110. Fujikawa, K. et al. Vav1/2/3-null mice define an essential role for Vav family proteins in lymphocyte development and activation but a differential requirement in MAPK signaling in T and B cells. *J Exp Med* **198**, 1595-608 (2003).

111. Wunderlich, M. et al. OKT3 prevents xenogeneic GVHD and allows reliable xenograft initiation from unfractionated human hematopoietic tissues. *Blood* **123**, e134-44 (2014).

Figure 1

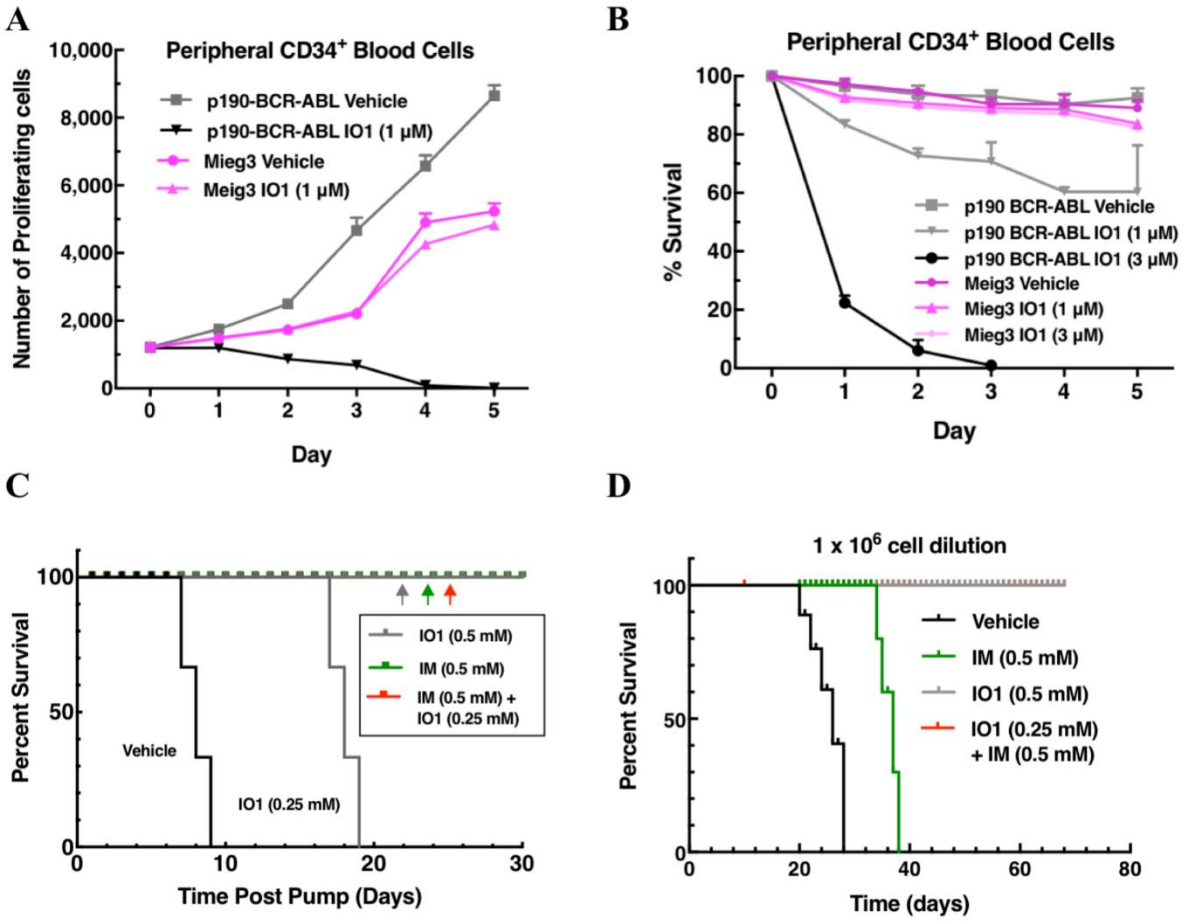
A
Peripheral CD34+ Blood Cells
Number of Proliferating cells
10,000
8,000
6,000
4,000
2,000
0
0
1
2
3
4
5
Day
p190-BCR-ABL Vehicle
p190-BCR-ABL IO1 (1 μM)
Mieg3 Vehicle
Meig3 IO1 (1 μM)
B
Peripheral CD34+ Blood Cells
% Survival
100
80
60
40
20
0
0
1
2
3
4
5
Day
p190 BCR-ABL Vehicle
p190 BCR-ABL IO1 (1 μM)
p190 BCR-ABL IO1 (3 μM)
Meig3 Vehicle
Mieg3 IO1 (1 μM)
Mieg3 IO1 (3 μM)
C
Percent Survival
100
50
0
0
10
20
30
Time Post Pump (Days)
Vehicle
IO1 (0.25 mM)
IO1 (0.5 mM)
IM (0.5 mM)
IM (0.5 mM) +
IO1 (0.25 mM)
D
1 x 10^6 cell dilution
Percent Survival
100
50
0
0
20
40
60
80
Time (days)
Vehicle
IM (0.5 mM)
IO1 (0.5 mM)
IO1 (0.25 mM)
+ IM (0.5 mM)

Figure 2

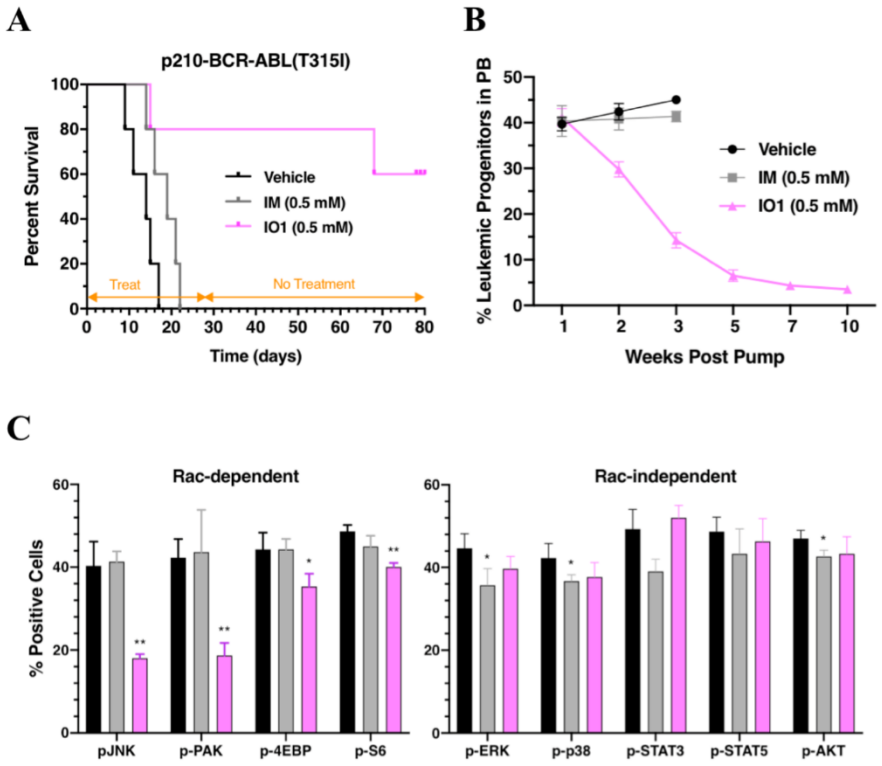
A
p210-BCR-ABL(T315I)
Percent Survival
Time (days)
Vehicle
IM (0.5 mM)
IO1 (0.5 mM)
Treat
No Treatment
B
% Leukemic Progenitors in PB
Weeks Post Pump
Vehicle
IM (0.5 mM)
IO1 (0.5 mM)
C
Rac-dependent
Rac-independent
% Positive Cells
pJNK
p-PAK
p-4EBP
p-S6
p-ERK
p-p38
p-STAT3
p-STAT5
p-AKT

Figure 3

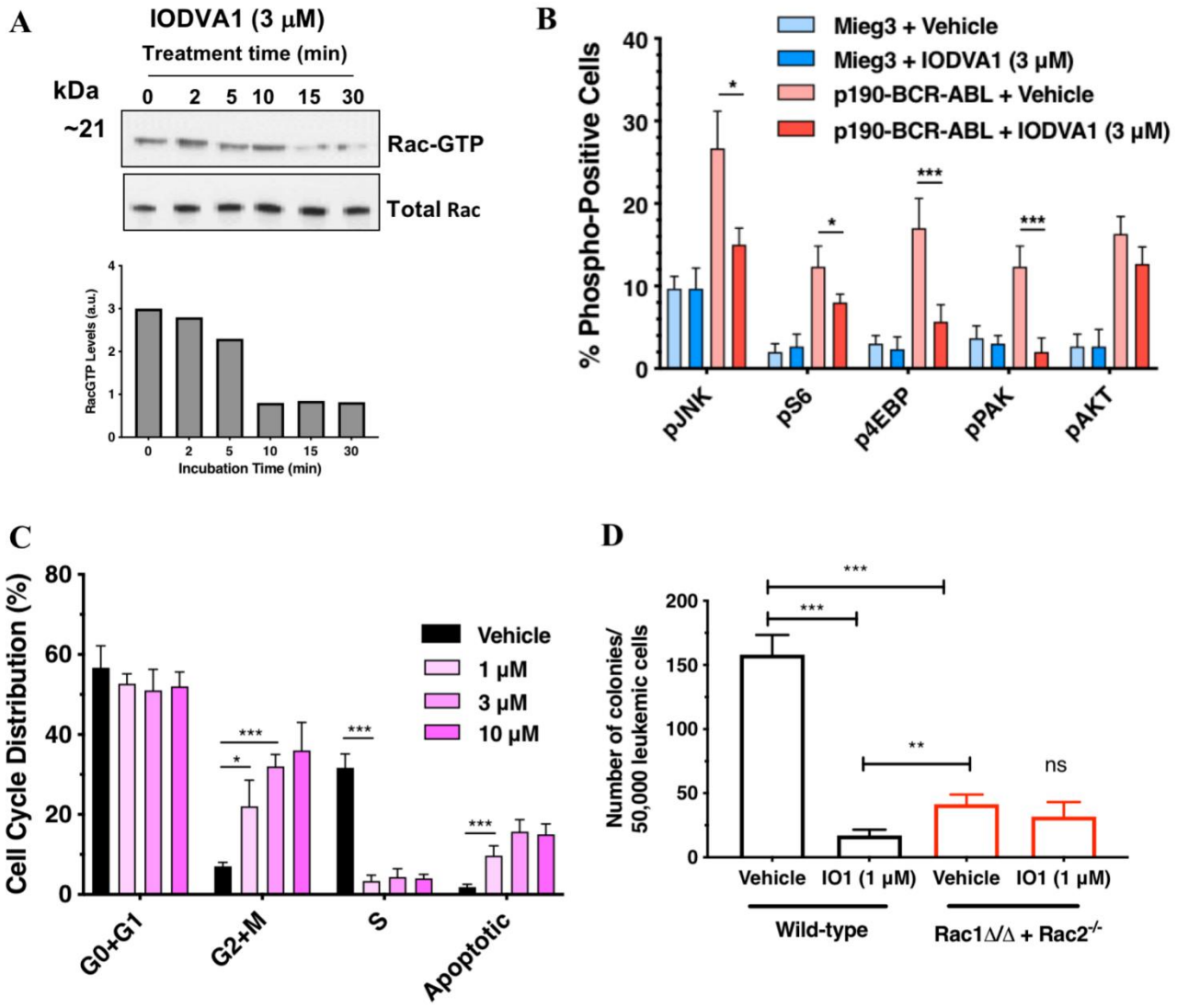
A
IODVA1 (3 µM)
Treatment time (min)
kDa
0 2 5 10 15 30
~21
Rac-GTP
Total Rac
RacGTP Levels (a.u.)
Incubation Time (min)
B
Mieg3 + Vehicle
Mieg3 + IODVA1 (3 µM)
p190-BCR-ABL + Vehicle
p190-BCR-ABL + IODVA1 (3 µM)
% Phospho-Positive Cells
pJNK
pS6
p4EBP
pPAK
pAKT
C
Cell Cycle Distribution (%)
Vehicle
1 µM
3 µM
10 µM
G0+G1
G2+M
S
Apoptotic
D
Number of colonies/ 50,000 leukemic cells
Vehicle
IO1 (1 µM)
Vehicle
IO1 (1 µM)
Wild-type
Rac1Δ/Δ + Rac2-/-
ns

Figure 4

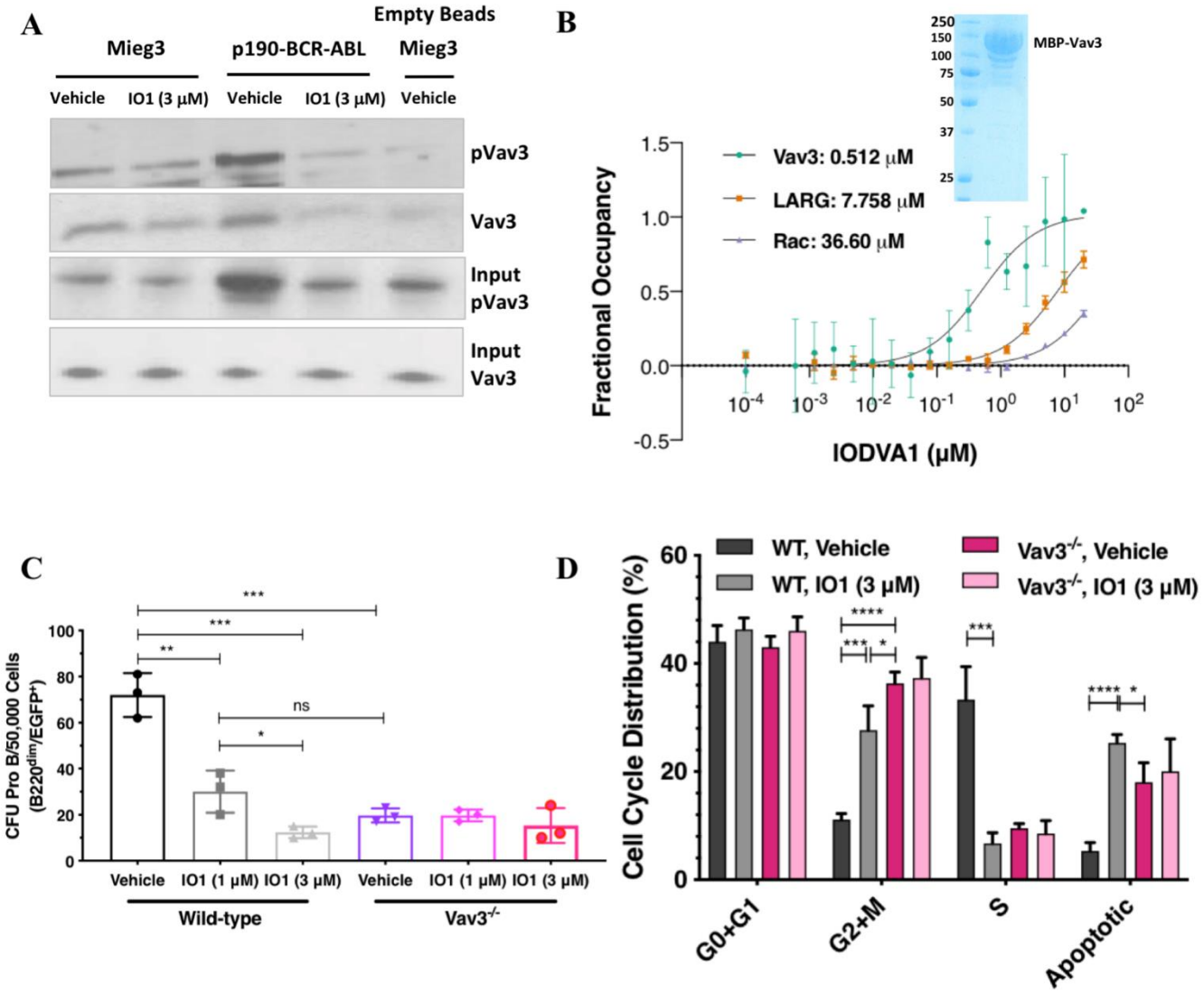
A
Empty Beads
Mieg3
p190-BCR-ABL
Mieg3
Vehicle
IO1 (3 μM)
Vehicle
IO1 (3 μM)
Vehicle
pVav3
Vav3
Input pVav3
Input Vav3
B
MBP-Vav3
250
150
100
75
50
37
25
Vav3: 0.512 μM
LARG: 7.758 μM
Rac: 36.60 μM
Fractional Occupancy
IODVA1 (μM)
C
CFU Pro B/50,000 Cells (B220dim/EGFP+)
Vehicle
IO1 (1 μM)
IO1 (3 μM)
Vehicle
IO1 (1 μM)
IO1 (3 μM)
Wild-type
Vav3-/-
ns
D
WT, Vehicle
WT, IO1 (3 μM)
Vav3-/-, Vehicle
Vav3-/-, IO1 (3 μM)
Cell Cycle Distribution (%)
G0+G1
G2+M
S
Apoptotic

Figure 5

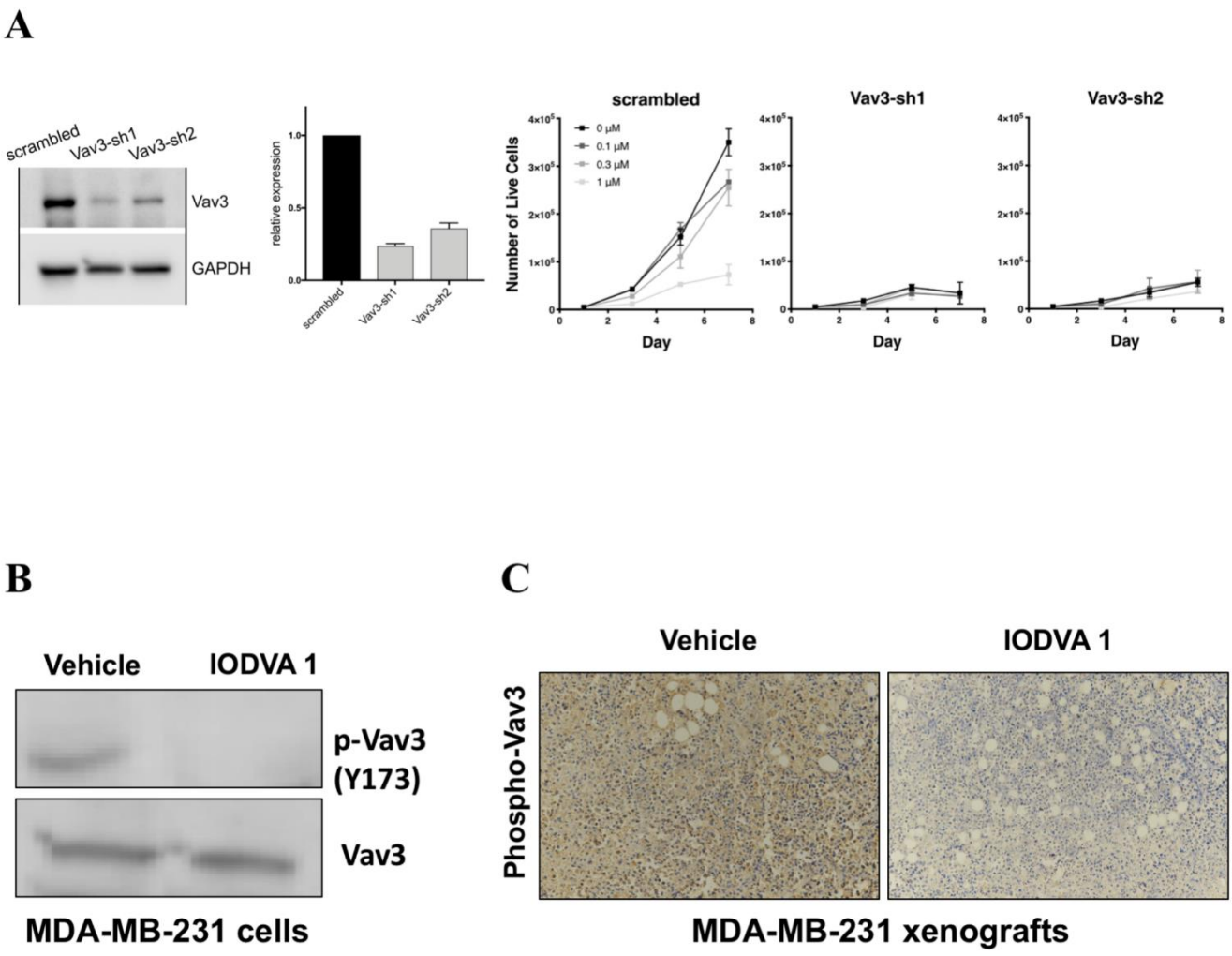
A
scrambled
Vav3-sh1
Vav3-sh2
Vav3
GAPDH
relative expression
scrambled
Vav3-sh1
Vav3-sh2
Number of Live Cells
0 µM
0.1 µM
0.3 µM
1 µM
Day
B
Vehicle
IODVA 1
p-Vav3 (Y173)
Vav3
MDA-MB-231 cells
C
Vehicle
IODVA 1
Phospho-Vav3
MDA-MB-231 xenografts

Figure 6

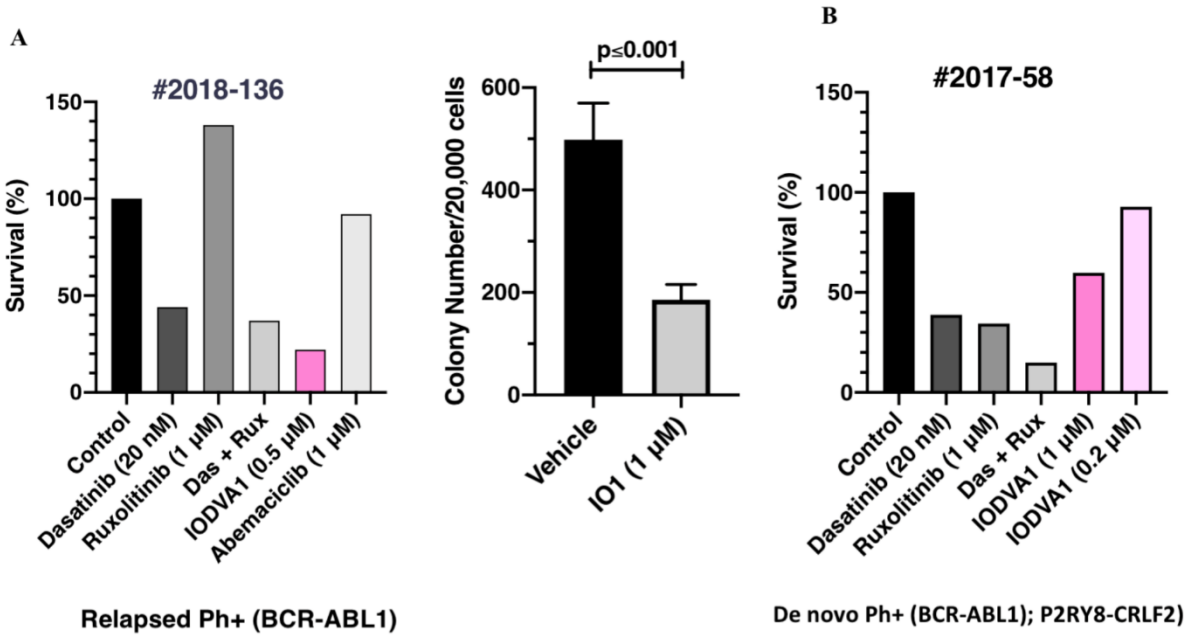

Relapsed Ph+ (BCR-ABL1)

De novo Ph+ (BCR-ABL1); P2RY8-CRLF2)

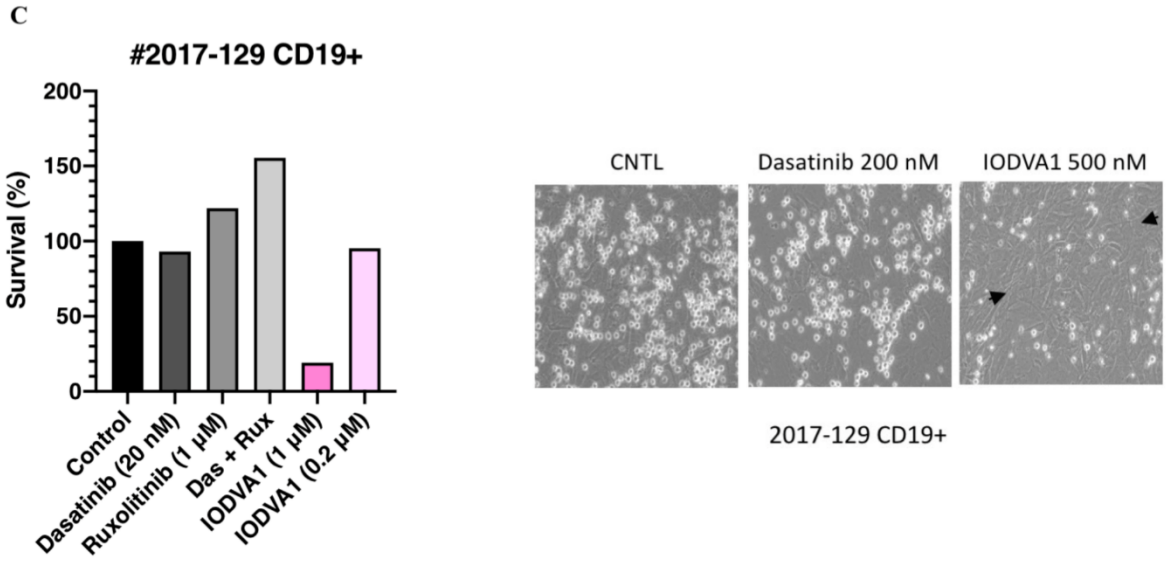

Relapsed Ph⁺ (BCR-ABL1, T315I).
Original TKI-resistant patient cells.

Table 1

PDX ALL models				
Patient #	Sample ID	Disease Stage	Mutations/Group	TKI History
ALL-009	2016-116 *	R/R	t(1;11), t(6;6)	
ALL-011	2016-79	De Novo	Ph-like (IGH-CRLF2; JAK2)	Ruxolitinib
ALL-012	2016-88	De Novo	Ph-like (CNTRL-FGFR1)	
ALL-014	2017-49	De Novo	Ph-like (P2RY8-CLRF2; ETV6-NTRK3)	Larotrectinib
ALL-015	2017-58 *	De Novo	Ph+ (BCR-ABL1); Ph-like (P2RY8-CRLF2)	Dasatinib
ALL-017	2017-129 *	R/R	Ph+ (BCR-ABL1, T315I)	Ponatinib
ALL-019	2018-132	De Novo	Ph-like (IGH-CRLF2; JAK2)	
ALL-004	2018-136	R/R	Ph+ (BCR-ABL1)	
ALL-032	2018-190	De novo	B-ALL (MLL/AF9)	
ALL-011	2016-70	De novo	Ph-like (NUP214/ABL1, IKZF-1, P2RY8/CD99, SETD2, VHL)	

List of ALL patients with samples available through the Pediatric Leukemia Avatar Program at CCHMC, including those with cytokine receptor, tyrosine kinase (TKI), or RAS pathway mutations. Clinical history of TKI treatment is indicated with the TKI received. All samples have confirmed patient-derived xenografts (PDXs) with disease latency as noted. Highlighted samples indicate those selected for Ph+/Ph-like cohort. Patient samples that have established in vitro culture are marked (*). Next-Gen Sequencing (NGS) was performed using the FoundationOne Heme panel (Cambridge, MA). Other abbreviations: relapsed or refractory (R/R), busulfan (BU), Philadelphia chromosome (Ph+), Philadelphia-like (Ph-like), minimal residual disease (MRD), bone marrow transplant (BMT).

Chapter VIII

General discussion

5 Discussion

The RAS superfamily of GTP/GDP-binding proteins comprises a large number of membrane-localized proteins controlling a multitude of cellular functions in response to several extracellular stimuli [33]. Most of the small GTPases cycle between an active, GTP-bound state and an inactive, GDP-bound state. This cycle is tightly regulated by GEFs and GAPs which accelerate the intrinsic nucleotide exchange reaction and stimulate the slow intrinsic GTP hydrolysis, respectively [219]. RHO GTPases are also controlled by a third class of regulators, called RHOGDIs. RHOGDIs play a key role in cytoplasm-membrane shuttling of RHO proteins thereby preventing proteasomal degradation [109]. In their active, GTP-bound conformation GTPases are capable of physically interacting with effector proteins and transduce extracellular stimuli through the cell. Several mutations in genes encoding members of the RAS superfamily have been described to be implicated in human diseases, such as RASopathies and cancer. RASopathies are a group of genetic syndromes caused by germline mutations in genes encoding key components of the RAS/MAPK pathway or upstream regulators. However, about 10-20% of individuals with RASopathies do not show mutations in known RASopathy-associated genes, indicating still unidentified genetic alterations [2, 17]. Exome sequencing has enhanced the discovery of genes implicated in genetic disorders and helped to identify novel mutations as the cause for human diseases, especially the Noonan syndrome. We were able to structurally, biochemically, and functionally characterize these mutations for a better understanding of the molecular mechanisms underlying these syndromes.

5.1 Missense mutations variably perturb CDC42 function

In Chapter II, we observed for the first time that missense mutations in *CDC42*, a gene encoding a small GTPase of the RHO subfamily, underlie a clinically heterogeneous group of developmental phenotypes which are characterized by short stature, facial dysmorphism, brain malformations, and thrombocytopenia. Nine different missense mutations were identified and divided into three groups based on their localization. Group I mutations affected the switch II region of CDC42 (p.Tyr64Cys, p.Arg66Gly, and p.Arg68Gln). Tyr64 and Arg66 are located on the protein surface and were proposed to directly affect the interaction with effectors and regulatory proteins like GEFs and GAPs, while Arg68 is embedded in the protein interior and stabilizes the switch II region due to intramolecular interactions with

several residues, such as Ala59, Gln61, and Glu100. Group II mutations showed substitutions in residues located within or in close vicinity to the nucleotide-binding pocket (p.Cys81Phe, p.Ser83Pro, p. Ala159Val) which were predicted to perturb the nucleotide binding properties of CDC42. The group III mutations (p.Ile21Thr, p.Tyr23Cys, p.Glu171Lys) or also called CRIB mutations are located on the protein surface and were predicted to affect the interaction with proteins containing a CRIB motif. Interaction studies with several direct interaction partners of CDC42, including WASP, PAK1, IQGAP1, and FMNL2 were performed to elucidate the impact of these mutations on protein-protein interaction. The interaction with WASP was completely abolished for the Glu171Lys variant and resulted in a 21-fold decreased binding affinity for $CDC42^{Tyr23Cys}$ supporting our notion that these mutations affect binding towards CRIB motif containing proteins. The complex structure of CDC42 and WASP (GBD) solved in 1999 by Abdul-Manan *et al.* illustrates that Glu171 plays a major role in the electrostatic steering mechanism by binding Lys235 of WASP [220, 221]. Substitution of lysine for glutamic acid at residue 171 results in repulsion and consequently in loss of WASP-binding. The interaction studies with PAK1 showed an impaired binding for $CDC42^{Tyr23Cys}$ and $CDC42^{Tyr64Cys}$ and a reduced binding affinity for $CDC42^{Arg68Gln}$ and $CDC42^{Glu171Lys}$ supporting our prediction that group I and group III mutations affect effector binding and interactions with CRIB motif containing proteins, respectively. Obtained data for the interaction between the different CDC42 variants and FMNL2 showed loss of binding for the group I mutations. Structural analysis revealed that residues of CDC42 switch II region are involved in hydrophobic and polar interactions with FMNL2. Tyr64 forms a hydrophobic contact with Leu44 of FMNL2, whereas Arg66 forms a hydrophobic interaction with Met42, as well as polar interactions with Leu114, Asn117, and Asn233 [222]. The interaction to the scaffold protein IQGAP1 showed a decreased binding affinity for $CDC42^{Arg66Gly}$ and $CDC42^{Arg68Glu}$. Previous studies have shown that interaction between CDC42 and IQGAP1 regulates the cadherin-mediated cell adhesion, indicating that dysregulation of protein-protein interaction negatively affects this cellular function [223, 224]. RASopathy-associated missense mutations in small GTPases have been shown to result in overactivation of these proteins due to impaired intrinsic GTPase activity, GAP insensitivity, increased nucleotide exchange rates, or a combination of these mechanisms [225]. To further reveal the underlying mechanism, the CDC42 variants have been investigated regarding their regulatory function. The GTP hydrolysis assay stimulated by p50RHOGAP, a

specific GAP for CDC42, exhibited a robust GAP insensitivity for the CDC42 variants Tyr64Cys, Arg68Gln, and Ala159Val resulting in an increased amount of active, GTP-bound CDC42 and enhanced signal flow. Furthermore, the GEF-catalyzed nucleotide exchange reaction showed a 5-fold increase for $CDC42^{Ala159Val}$. Obtained data clearly indicate an intracellular accumulation of $CDC42^{Ala159Val}$ in its active conformation due to a fast cycling effect induced by increased nucleotide exchange and decreased GTP hydrolysis. Overall, we were able to show in this study that different groups of *CDC42* mutations variably perturb CDC42 function and consequently result in a phenotype resembling the Noonan syndrome. Generally, RASopathies are mediated by mutations affecting genes of the RAS/MAPK backbone. However, recent studies showed other affected genes, such as *RIT1*, *RRAS*, and *LZTR1* which had not been shown to directly have an impact on the RAS/MAPK cascade yet [30, 226, 227]. Further studies are needed to understand whether *CDC42* mutations affect the RAS/MAPK signaling directly, or if other signaling pathways may contribute to disease progression.

5.2 Identification of a novel disorder caused by altered CDC42 function

Chapter III deals with the identification of a novel disease in four unrelated individuals due to the same de novo missense mutation of *CDC42* (p.Arg186Cys), characterized by neonatal onset of pancytopenia, autoinflammation, rash, and episodes of HLH (NOCARH). Our *in silico*, *in vitro*, and *in vivo* studies elucidated a unique impact of the p.Arg186Cys mutation on CDC42 function. Arg186 is located on the surface of CDC42 in the hypervariable region which has been shown to be one of two major binding sites for RHOGDI1 [178]. Structural analysis showed that Arg186 is in contact with several residues of RHOGDI1, such as Asp140, Thr142, Tyr144, and Glu163. The *in silico* prediction of the CDC42 mutation revealed a disruption of this contacts resulting in a destabilized RHOGDI1 interaction. To further confirm this hypothesis, pull-down assays, as well as SPR analysis were performed. Obtained data clearly demonstrated a loss of binding to geranylgeranylated CDC42 with RHOGDI1. This interaction has been shown to play a key role in the control of CDC42 function. Therefore, perturbation in subcellular localization and trafficking may contribute to pathogenesis. The previously reported CDC42 mutations which were described in chapter II have been analyzed regarding their regulatory function and their capability to transduce signals *via* effector proteins. The regulatory function of $CDC42^{Arg186Cys}$ was not affected, whereas the interaction with IQGAP1 was dramatically reduced. IQGAP1 has been shown to promote the translocation of CDC42

from the Golgi apparatus to the plasma membrane [117]. For this reason, we analyzed the subcellular localization of CDC42^{Arg186Cys} by confocal microscopy and observed a Golgi-restricted localization. It was also recently shown by another group that the Arg186Cys variant is posttranslationally modified by an additional palmitate on this new cysteine resulting in enhanced interaction with the Golgi apparatus, as well as inhibition of extraction by RHOGDI and as a consequence in impaired cytoplasm-membrane shuttling [228]. Furthermore, we were able to show functional changes, including actin cytoskeleton rearrangements, reduced migration, and impaired proliferation. Various mutations in genes involved in remodeling of the actin cytoskeleton, such as *CFL1*, *WAS*, *DOCK8*, and *RAC2* have been shown to cause hematological and autoinflammatory phenotypes due to changed migration and/or impaired proliferation [229-233]. Moreover, *Fukata et al.* showed that IQGAP1 mutants incapable of binding CDC42 displayed aberrant multipolar morphology supporting our findings of the cytoskeletal rearrangements with multiple leading edges [210]. In conclusion, NOCARH syndrome caused by a *de novo* missense mutation in *CDC42* results in an autoinflammatory disease due to small GTPase mislocalization to the Golgi apparatus. Markedly elevated IL-18 levels may serve as a potential biomarker for diagnosing NOCARH. However, early recognition and bone marrow transplantation have turned out to be crucial in preventing multiorgan failure and thus, survival of the patient.

5.3 Identification of *RRAS2* as a gene implicated in Noonan syndrome

Noonan syndrome is the most prevalent disorder among the RASopathies and is characterized by several pathogenic features, including facial dysmorphism, cardiac abnormalities, reduced growth, and neurocognitive impairment. In chapter IV we, identified *RRAS2* mutations underlying Noonan syndrome variably affecting the biochemical properties of the protein. Six unrelated individuals showed *de novo* germline mutations in *RRAS2*, such as p.Gly23Val, p.Gly22_Gly24dup, p.Gly24_Gly26dup, p.Ala70Thr, and p.Glu72Leu. RRAS2, a member of the RAS superfamily of GTPases, shares high amino acid sequence homology with the most prominent RAS-members HRAS, KRAS, and NRAS [46, 47]. Several somatic cancer mutations in *RRAS2* have been reported, including our identified missense germline mutations p.Gly23Val, p.Ala70Thr, and p.Glu72Leu. Corresponding residues in other RAS genes have been already reported as a cause for Noonan syndrome [12]. Structural modeling revealed that all mutations are located in the nucleotide binding region, suggesting aberrant nucleotide

binding properties, dysregulation of the GTPase cycle, as well as impaired effector binding. P-loop residues (Gly21-Ser28) are responsible for phosphate binding of either GTP or GDP. These residues contact the nucleotide β-and γ-phosphates and residues 67-69 of switch II to control GTP hydrolysis. Therefore, the two genetic duplications p.Gly22_Gly24 and p.Gly24_Gly26 were predicted to decrease the GTP hydrolysis. Ala70 and Gln72 are located in the switch II region of RRAS2 and have been shown to be involved in Mg^{2+} coordination and GTP hydrolysis. Furthermore, they stabilize the switch I region *via* intramolecular interactions with residues Ile47 and Glu48. Biochemical analyses with $RRAS2^{Ala70Thr}$ resulted in a reduced GTP hydrolysis stimulated by p120RASGAP and in an increased nucleotide exchange reaction accelerated by SOS1, suggesting an accumulation of the GTPase in its active, GTP-bound form. Interaction studies with two common RAS effectors revealed an unaffected CRAF binding, whereas binding to RASSF5 was abolished. These data suggest that signaling pathways, beside RAF-MEK-ERK, may also contribute to the pathogenesis of Noonan syndrome. However, since the obtained binding affinities for RRAS2 with their effectors are comparatively low, other unknown effector proteins might be considered as downstream targets of RRAS2. Further studies are needed to precisely uncover the molecular mechanism underlying Noonan syndrome mediated by germline pathogenic variants in *RRAS2*.

5.4 *De novo* MRAS variants as another rare cause of Noonan syndrome

Upregulation of the canonical RAS-MAPK cascade has been suggested as major event for pathogenesis of RASopathies. However, other signaling pathways have been reported to be involved in developmental disorders like Noonan syndrome, as well [234-236]. MRAS or RRAS3 belongs to the RAS family of GTPases and has been shown to control the MAPK and PI3K-AKT cascades [36, 41]. In chapter V, we reported two MRAS variants, p.Gly23Arg and p.Thr68Ile as a rare cause of Noonan syndrome associated with hypertrophic cardiomyopathy (HCM). Corresponding residues in other RAS genes are known hotspots for mutations related to disease progression. As already described in chapter IV, the same glycine residue was identified in RRAS2 to be involved in the development of Noonan syndrome [237]. Interestingly, MRAS shows a different switch I structure compared to other members of the RAS superfamily. Due to an impaired intramolecular interaction between Thr45 and the γ-phosphate of GTP, MRAS exists in an open conformation independent of its activation state [50, 51]. Structural analyses were performed to illustrate the location of the disease-causing

MRAS variants and to elucidate their structural impact. Gly23 is located in the P-loop, while Thr68 is part of the interswitch region which are involved in nucleotide binding and stabilization of the active state, respectively. Many studies have been performed regarding substitution of glycine 13 (Gly23 in MRAS) by various amino acids which resulted in hyperactive variants in several RAS paralogs [27, 238]. The crystal structure of HRAS in complex with the GAP domain of p120 revealed that Arg789 of p120 is in contact with the P-loop residues and Gln61 (Gln71 in MRAS) stimulating the GTP hydrolysis *via* stabilization of the transition state [239]. Substitution of glycine to any other residue, such as valine or arginine lead to steric clashes of this interaction and as a consequence in GAP insensitivity. The p.Thr68Ile variant is predicted to result in a stronger intramolecular association with Arg78 resulting in a more stabilized active conformation and consequently in increased interaction with effectors. Biochemical analyses of the MRAS variants resulted in increased levels of GTP-bound MRAS, as well as elevated ERK and AKT phosphorylation levels, thereby confirming the structural predictions. It has been shown that a ternary complex of MRAS with SHOC2 and PP1C is required for membrane localization of PP1C which is needed for dephosphorylation of the inhibitory Ser259 in RAF1. This dephosphorylation was shown to be crucial for a conformational change of RAF1, thereby encouraging RAS-RAF interaction [240, 241]. Moreover, obtained data showed an increased binding towards SHOC2 and PP1C, supporting the increased ERK phosphorylation levels. Overall, we were able to structurally and biochemically reveal the molecular mechanism underlying Noonan syndrome due to germline mutations in *MRAS*. Both, the MAPK cascade and the PI3K-AKT axis are affected by the pathogenic variants. However, MRAS has been reported to have a significantly higher impact on signaling through PI3K. Recently, elevated activation of MAPK signaling has been shown to contribute to HCM mediated by mutations in genes, including *PTPN11*, *SOS1*, and *RAF1* [242-244]. Further studies are needed to explain in detail why mutations in *MRAS* cause Noonan syndrome associated with HCM.

5.5 Selectivity determinants of IQGAP-RHO GTPase binding

Scaffold proteins are multidomain proteins that modulate many cellular processes in the cell by supporting protein complex formation of two or more signaling molecules. IQGAPs, especially IQGAP1, have been shown to be part of the canonical MAPK cascade binding the key components, such as RAS, RAF, MEK, and also ERK [213, 245-247]. Overactivation of RAS

proteins or downstream molecules have been reported in many studies as a cause for disease progression. Targeting RAS has turned out to be extremely challenging [248, 249]. Therefore, many drugs were designed to inhibit different kinases of the MAPK cascade. Scaffold proteins have been proposed as potential drug targets. Since RHO protein binding has been accepted as one of the activation mechanisms of IQGAPs chapter VI investigates the interaction of IQGAP1 and 2 towards RHO GTPases [214, 216, 217]. Although, RAC1 and CDC42 have been extensively investigated in terms of IQGAP binding, the selectivity of IQGAPs for other members of the RHO family has not been analyzed so far. To understand the exact mechanism how IQGAPs achieve their scaffolding function and orchestrate many signaling events it is necessary to elucidate how RHO GTPases interact with IQGAPs in detail. Protein-protein interaction studies revealed that IQGAP1 and 2 selectively bind RAC-like and CDC42-like members, but not RHO-like proteins. The switch regions have been proposed as the main binding sites for IQGAPs. However, additional contacts outside the switch regions seem to be required for IQGAP binding since the switch regions are highly conserved within the RHO family proteins. Various other studies have been performed regarding direct protein-protein interaction of RAC1 and CDC42 with IQGAP1, where it has been proposed that they associate with IQGAP1 in a significantly different manner after analyzing a multitude of RAC1 and CDC42 mutations in the switch regions and the insert helix [218]. Moreover, different groups were able to uncover a CDC42-induced dimerization mechanism of IQGAP due to a direct contact of the insert helix with the GRD of IQGAP2 [250, 251]. However, these studies did not explain the inability of binding other RHO GTPases, such as RHOA, RHOB, or RHOC. Several works showed a complex formation of IQGAP1 with RHOA and RHOC using co-immunoprecipitation [252, 253]. Based on the performed experiment, these interactions might be indirect or are mediated *via* another IQGAP domain. Sequence alignment, structural, mutational, and competitive biochemical analyses uncovered three regions outside the switch regions modulating this bimolecular interaction. Overall, we were able to show that residues Thr25, Asn26, Met45, Asn52, and Gln74 (RAC1 numbering) serve as selectivity determinants for the interaction between IQGAP1 and RHO GTPases. Obtained data support the idea proposed by *Nouri et al.* and *Owen et al.* that RAC1 and CDC42 use a different binding mechanism, since different regions, when mutated, interfered with the interaction. Met45 and Asn52 of RAC1 are key residues for IQGAP1 association, while Gln74 of CDC42 seems to play a major role for

this interaction. RHOA wild type did not show any association towards IQGAP1/2, whereas a RHOA variant containing five mutations to mimic RAC1 in these selective residues was able to interact with IQGAP1, indicating that these regions are crucial for IQGAP-RHO GTPase interaction. However, the molecular mechanism of RHO GTPase-mediated IQGAP integration in signal processes still remains unclear.

5.6 Inhibition of RAC signaling by targeting VAV3

Chapter VII deals with the discovery and characterization of a small molecule inhibitor against the RACGEF VAV3. VAV3 is a multidomain tyrosine phosphorylation-dependent GEF which has been shown to function downstream of different membrane receptors, such as GPCRs, RTKs, and integrins [254-257]. Furthermore, VAV3 is a key component of BCR-ABL induced activation of RAC [258]. The BCR-ABL1 oncoprotein activates many signaling pathways, including the canonical MAPK cascade, JAK-STAT signaling, and the PI3K-AKT pathway which have been shown to result in abnormal cell proliferation, impaired transcriptional activity and prolonged survival [259]. Moreover, RAC signaling pathways are activated due to expression of p190-or p210-BCR-ABL to regulate leukemogenesis [260]. Here, we describe an inhibitor, termed inhibitor of oncogene driven VAV3 activation (IODVA1) that tightly binds VAV3 *in vitro* and *in vivo* resulting in decreased RAC activation, reduced activation of its downstream signaling molecules including PAK, JNK, S6, and 4EBP, as well as in the induction of apoptosis in BCR-ABL expressing cells. Decreased PAK activation results in activating dephosphorylation of BAD, preventing its association with Bcl2/Bcl-xL, consequently promoting apoptosis [261]. Most of the RHOGEFs are regulated by an autoinhibitory mechanism. Phosphorylation of Tyr173 in VAV3 releases the N-terminal CH-domain and the C-terminal SH3-domain. Consequently, GTPases are capable of associating with the DH-domain leading to their activation [262]. Based on our biochemical data, we propose a mechanism, in which IODVA1 prevents tyrosine phosphorylation resulting in VAV3 accumulation in its autoinhibited state. Overall, we were able to show that inhibition of VAV3 by the small inhibitor molecule IODVA1 is a potential therapeutic strategy to treat TKI-resistant BCR-ABL leukemia, as well as any other malignancy with aberrant RAC signaling.

6 References

1. Zhang, W. and H.T. Liu, *MAPK signal pathways in the regulation of cell proliferation in mammalian cells.* Cell Res, 2002. **12**(1): p. 9-18.
2. Rauen, K.A., *The RASopathies.* Annu Rev Genomics Hum Genet, 2013. **14**: p. 355-69.
3. Dailey, L., et al., *Mechanisms underlying differential responses to FGF signaling.* Cytokine Growth Factor Rev, 2005. **16**(2): p. 233-47.
4. Schlessinger, J., *Cell signaling by receptor tyrosine kinases.* Cell, 2000. **103**(2): p. 211-25.
5. Pawson, T., *Protein modules and signalling networks.* Nature, 1995. **373**(6515): p. 573-80.
6. Schlessinger, J., *SH2/SH3 signaling proteins.* Curr Opin Genet Dev, 1994. **4**(1): p. 25-30.
7. Desideri, E., A.L. Cavallo, and M. Baccarini, *Alike but Different: RAF Paralogs and Their Signaling Outputs.* Cell, 2015. **161**(5): p. 967-970.
8. Unal, E.B., F. Uhlitz, and N. Bluthgen, *A compendium of ERK targets.* FEBS Lett, 2017. **591**(17): p. 2607-2615.
9. Roberts, A.E., et al., *Noonan syndrome.* Lancet, 2013. **381**(9863): p. 333-42.
10. Wood, K.W., et al., *ras mediates nerve growth factor receptor modulation of three signal-transducing protein kinases: MAP kinase, Raf-1, and RSK.* Cell, 1992. **68**(6): p. 1041-50.
11. Rattanasinchai, C. and K.A. Gallo, *MLK3 Signaling in Cancer Invasion.* Cancers (Basel), 2016. **8**(5).
12. Tartaglia, M. and B.D. Gelb, *Disorders of dysregulated signal traffic through the RAS-MAPK pathway: phenotypic spectrum and molecular mechanisms.* Ann N Y Acad Sci, 2010. **1214**: p. 99-121.
13. Tajan, M., et al., *The RASopathy Family: Consequences of Germline Activation of the RAS/MAPK Pathway.* Endocr Rev, 2018. **39**(5): p. 676-700.
14. Tartaglia, M., B.D. Gelb, and M. Zenker, *Noonan syndrome and clinically related disorders.* Best Pract Res Clin Endocrinol Metab, 2011. **25**(1): p. 161-79.
15. Jorge, A.A., et al., *Noonan syndrome and related disorders: a review of clinical features and mutations in genes of the RAS/MAPK pathway.* Horm Res, 2009. **71**(4): p. 185-93.
16. Hasle, H., *Malignant diseases in Noonan syndrome and related disorders.* Horm Res, 2009. **72 Suppl 2**: p. 8-14.
17. Tidyman, W.E. and K.A. Rauen, *Pathogenetics of the RASopathies.* Hum Mol Genet, 2016. **25**(R2): p. R123-R132.
18. Chen, P.C., et al., *Next-generation sequencing identifies rare variants associated with Noonan syndrome.* Proc Natl Acad Sci U S A, 2014. **111**(31): p. 11473-8.
19. Cirstea, I.C., et al., *A restricted spectrum of NRAS mutations causes Noonan syndrome.* Nat Genet, 2010. **42**(1): p. 27-9.
20. Cordeddu, V., et al., *Activating Mutations Affecting the Dbl Homology Domain of SOS2 Cause Noonan Syndrome.* Hum Mutat, 2015. **36**(11): p. 1080-7.
21. Higgins, E.M., et al., *Elucidation of MRAS-mediated Noonan syndrome with cardiac hypertrophy.* JCI Insight, 2017. **2**(5): p. e91225.

22. Kouz, K., et al., *Genotype and phenotype in patients with Noonan syndrome and a RIT1 mutation.* Genet Med, 2016. **18**(12): p. 1226-1234.

23. Nava, C., et al., *Cardio-facio-cutaneous and Noonan syndromes due to mutations in the RAS/MAPK signalling pathway: genotype-phenotype relationships and overlap with Costello syndrome.* J Med Genet, 2007. **44**(12): p. 763-71.

24. Razzaque, M.A., et al., *Germline gain-of-function mutations in RAF1 cause Noonan syndrome.* Nat Genet, 2007. **39**(8): p. 1013-7.

25. Roberts, A.E., et al., *Germline gain-of-function mutations in SOS1 cause Noonan syndrome.* Nat Genet, 2007. **39**(1): p. 70-4.

26. Sarkozy, A., et al., *Germline BRAF mutations in Noonan, LEOPARD, and cardiofaciocutaneous syndromes: molecular diversity and associated phenotypic spectrum.* Hum Mutat, 2009. **30**(4): p. 695-702.

27. Schubbert, S., et al., *Germline KRAS mutations cause Noonan syndrome.* Nat Genet, 2006. **38**(3): p. 331-6.

28. Tartaglia, M., et al., *Mutations in PTPN11, encoding the protein tyrosine phosphatase SHP-2, cause Noonan syndrome.* Nat Genet, 2001. **29**(4): p. 465-8.

29. Tartaglia, M., et al., *Gain-of-function SOS1 mutations cause a distinctive form of Noonan syndrome.* Nat Genet, 2007. **39**(1): p. 75-9.

30. Yamamoto, G.L., et al., *Rare variants in SOS2 and LZTR1 are associated with Noonan syndrome.* J Med Genet, 2015. **52**(6): p. 413-21.

31. Zenker, M., et al., *SOS1 is the second most common Noonan gene but plays no major role in cardio-facio-cutaneous syndrome.* J Med Genet, 2007. **44**(10): p. 651-6.

32. Bourne, H.R., D.A. Sanders, and F. McCormick, *The GTPase superfamily: conserved structure and molecular mechanism.* Nature, 1991. **349**(6305): p. 117-27.

33. Colicelli, J., *Human RAS superfamily proteins and related GTPases.* Sci STKE, 2004. **2004**(250): p. RE13.

34. Rojas, A.M., et al., *The Ras protein superfamily: evolutionary tree and role of conserved amino acids.* J Cell Biol, 2012. **196**(2): p. 189-201.

35. Vetter, I.R. and A. Wittinghofer, *The guanine nucleotide-binding switch in three dimensions.* Science, 2001. **294**(5545): p. 1299-304.

36. Wennerberg, K., K.L. Rossman, and C.J. Der, *The Ras superfamily at a glance.* J Cell Sci, 2005. **118**(Pt 5): p. 843-6.

37. Bernards, A. and J. Settleman, *GAP control: regulating the regulators of small GTPases.* Trends Cell Biol, 2004. **14**(7): p. 377-85.

38. Schmidt, A. and A. Hall, *Guanine nucleotide exchange factors for Rho GTPases: turning on the switch.* Genes Dev, 2002. **16**(13): p. 1587-609.

39. Bishop, A.L. and A. Hall, *Rho GTPases and their effector proteins.* Biochem J, 2000. **348 Pt 2**: p. 241-55.

40. Repasky, G.A., E.J. Chenette, and C.J. Der, *Renewing the conspiracy theory debate: does Raf function alone to mediate Ras oncogenesis?* Trends Cell Biol, 2004. **14**(11): p. 639-47.

41. Nakhaei-Rad, S., et al., *Structural fingerprints, interactions, and signaling networks of RAS family proteins beyond RAS isoforms.* Crit Rev Biochem Mol Biol, 2018. **53**(2): p. 130-156.

42. Harvey, J.J., *An Unidentified Virus Which Causes the Rapid Production of Tumours in Mice.* Nature, 1964. **204**: p. 1104-5.

43. Kirsten, W.H. and L.A. Mayer, *Morphologic responses to a murine erythroblastosis virus.* J Natl Cancer Inst, 1967. **39**(2): p. 311-35.

44. Willumsen, B.M., et al., *The p21 ras C-terminus is required for transformation and membrane association.* Nature, 1984. **310**(5978): p. 583-6.

45. Willumsen, B.M., et al., *Harvey murine sarcoma virus p21 ras protein: biological and biochemical significance of the cysteine nearest the carboxy terminus.* EMBO J, 1984. **3**(11): p. 2581-5.

46. Drivas, G.T., et al., *Characterization of four novel ras-like genes expressed in a human teratocarcinoma cell line.* Mol Cell Biol, 1990. **10**(4): p. 1793-8.

47. Bos, J.L., *Ras-like GTPases.* Biochim Biophys Acta, 1997. **1333**(2): p. M19-31.

48. Erdogan, M., et al., *Signaling pathways regulating TC21-induced tumorigenesis.* J Biol Chem, 2007. **282**(38): p. 27713-20.

49. Graham, S.M., et al., *TC21 and Ras share indistinguishable transforming and differentiating activities.* Oncogene, 1999. **18**(12): p. 2107-16.

50. Matsumoto, K., et al., *Critical roles of interactions among switch I-preceding residues and between switch II and its neighboring alpha-helix in conformational dynamics of the GTP-bound Ras family small GTPases.* J Biol Chem, 2011. **286**(17): p. 15403-12.

51. Ye, M., et al., *Crystal structure of M-Ras reveals a GTP-bound "off" state conformation of Ras family small GTPases.* J Biol Chem, 2005. **280**(35): p. 31267-75.

52. Shima, F., et al., *Structural basis for conformational dynamics of GTP-bound Ras protein.* J Biol Chem, 2010. **285**(29): p. 22696-705.

53. Bourne, H.R., D.A. Sanders, and F. McCormick, *The GTPase superfamily: a conserved switch for diverse cell functions.* Nature, 1990. **348**(6297): p. 125-32.

54. Bos, J.L., *ras oncogenes in human cancer: a review.* Cancer Res, 1989. **49**(17): p. 4682-9.

55. Barbacid, M., *ras genes.* Annu Rev Biochem, 1987. **56**: p. 779-827.

56. Malumbres, M. and M. Barbacid, *RAS oncogenes: the first 30 years.* Nat Rev Cancer, 2003. **3**(6): p. 459-65.

57. Kontani, K., et al., *Di-Ras, a distinct subgroup of ras family GTPases with unique biochemical properties.* J Biol Chem, 2002. **277**(43): p. 41070-8.

58. Nakhaei-Rad, S., et al., *The Function of Embryonic Stem Cell-expressed RAS (E-RAS), a Unique RAS Family Member, Correlates with Its Additional Motifs and Its Structural Properties.* J Biol Chem, 2015. **290**(25): p. 15892-903.

59. Shao, H., et al., *Biochemical characterization of the Ras-related GTPases Rit and Rin.* Arch Biochem Biophys, 1999. **371**(2): p. 207-19.

60. Spoerner, M., et al., *Dynamic properties of the Ras switch I region and its importance for binding to effectors.* Proc Natl Acad Sci U S A, 2001. **98**(9): p. 4944-9.

61. Wittinghofer, A., et al., *Three-dimensional structure and properties of wild-type and mutant H-ras-encoded p21.* Ciba Found Symp, 1993. **176**: p. 6-21; discussion 21-7.

62. Cox, A.D. and C.J. Der, *Ras history: The saga continues.* Small GTPases, 2010. **1**(1): p. 2-27.

63. Casey, P.J., et al., *p21ras is modified by a farnesyl isoprenoid.* Proc Natl Acad Sci U S A, 1989. **86**(21): p. 8323-7.

64. Tamanoi, F., et al., *Posttranslational modification of ras proteins: detection of a modification prior to fatty acid acylation and cloning of a gene responsible for the modification.* J Cell Biochem, 1988. **36**(3): p. 261-73.

65. Cox, A.D., C.J. Der, and M.R. Philips, *Targeting RAS Membrane Association: Back to the Future for Anti-RAS Drug Discovery?* Clin Cancer Res, 2015. **21**(8): p. 1819-27.

66. Cox, A.D. and C.J. Der, *The dark side of Ras: regulation of apoptosis.* Oncogene, 2003. **22**(56): p. 8999-9006.

67. Bos, J.L., *Linking Rap to cell adhesion.* Curr Opin Cell Biol, 2005. **17**(2): p. 123-8.

68. Karnoub, A.E. and R.A. Weinberg, *Ras oncogenes: split personalities.* Nat Rev Mol Cell Biol, 2008. **9**(7): p. 517-31.

69. Nakhaeizadeh, H., et al., *The RAS-Effector Interface: Isoform-Specific Differences in the Effector Binding Regions.* PLoS One, 2016. **11**(12): p. e0167145.

70. Wohlgemuth, S., et al., *Recognizing and defining true Ras binding domains I: biochemical analysis.* J Mol Biol, 2005. **348**(3): p. 741-58.

71. Morrison, D.K., *The Raf-1 kinase as a transducer of mitogenic signals.* Cancer Cells, 1990. **2**(12): p. 377-82.

72. Avruch, J., et al., *Ras activation of the Raf kinase: tyrosine kinase recruitment of the MAP kinase cascade.* Recent Prog Horm Res, 2001. **56**: p. 127-55.

73. Wellbrock, C., M. Karasarides, and R. Marais, *The RAF proteins take centre stage.* Nat Rev Mol Cell Biol, 2004. **5**(11): p. 875-85.

74. Leicht, D.T., et al., *Raf kinases: function, regulation and role in human cancer.* Biochim Biophys Acta, 2007. **1773**(8): p. 1196-212.

75. Zhang, X.F., et al., *Normal and oncogenic p21ras proteins bind to the amino-terminal regulatory domain of c-Raf-1.* Nature, 1993. **364**(6435): p. 308-13.

76. Vojtek, A.B., S.M. Hollenberg, and J.A. Cooper, *Mammalian Ras interacts directly with the serine/threonine kinase Raf.* Cell, 1993. **74**(1): p. 205-14.

77. Van Aelst, L., et al., *Complex formation between RAS and RAF and other protein kinases.* Proc Natl Acad Sci U S A, 1993. **90**(13): p. 6213-7.

78. Baljuls, A., B.N. Kholodenko, and W. Kolch, *It takes two to tango--signalling by dimeric Raf kinases.* Mol Biosyst, 2013. **9**(4): p. 551-8.

79. Kyriakis, J.M., et al., *Raf-1 activates MAP kinase-kinase.* Nature, 1992. **358**(6385): p. 417-21.

80. Matallanas, D., et al., *Raf family kinases: old dogs have learned new tricks.* Genes Cancer, 2011. **2**(3): p. 232-60.

81. Engelman, J.A., J. Luo, and L.C. Cantley, *The evolution of phosphatidylinositol 3-kinases as regulators of growth and metabolism.* Nat Rev Genet, 2006. **7**(8): p. 606-19.

82. Hawkins, P.T., et al., *Signalling through Class I PI3Ks in mammalian cells.* Biochem Soc Trans, 2006. **34**(Pt 5): p. 647-62.

83. Vanhaesebroeck, B., et al., *The emerging mechanisms of isoform-specific PI3K signalling.* Nat Rev Mol Cell Biol, 2010. **11**(5): p. 329-41.

84. Rodriguez-Viciana, P., et al., *Phosphatidylinositol-3-OH kinase as a direct target of Ras.* Nature, 1994. **370**(6490): p. 527-32.

85. Rodriguez-Viciana, P. and J. Downward, *Ras activation of phosphatidylinositol 3-kinase and Akt.* Methods Enzymol, 2001. **333**: p. 37-44.

86. Rodriguez-Viciana, P., et al., *Activation of phosphoinositide 3-kinase by interaction with Ras and by point mutation.* EMBO J, 1996. **15**(10): p. 2442-51.

87. Fritsch, R., et al., *RAS and RHO families of GTPases directly regulate distinct phosphoinositide 3-kinase isoforms.* Cell, 2013. **153**(5): p. 1050-63.

88. Vanhaesebroeck, B., et al., *Synthesis and function of 3-phosphorylated inositol lipids.* Annu Rev Biochem, 2001. **70**: p. 535-602.

89. Gordon, M. and S. Baksh, *RASSF1A: Not a prototypical Ras effector.* Small GTPases, 2011. **2**(3): p. 148-157.

90. Richter, A.M., G.P. Pfeifer, and R.H. Dammann, *The RASSF proteins in cancer; from epigenetic silencing to functional characterization.* Biochim Biophys Acta, 2009. **1796**(2): p. 114-28.

91. Sherwood, V., et al., *The N-terminal RASSF family: a new group of Ras-association-domain-containing proteins, with emerging links to cancer formation.* Biochem J, 2009. **425**(2): p. 303-11.

92. Lock, F.E., et al., *The RASSF8 candidate tumor suppressor inhibits cell growth and regulates the Wnt and NF-kappaB signaling pathways.* Oncogene, 2010. **29**(30): p. 4307-16.

93. Estrabaud, E., et al., *RASSF1C, an isoform of the tumor suppressor RASSF1A, promotes the accumulation of beta-catenin by interacting with betaTrCP.* Cancer Res, 2007. **67**(3): p. 1054-61.

94. Vos, M.D., et al., *The pro-apoptotic Ras effector Nore1 may serve as a Ras-regulated tumor suppressor in the lung.* J Biol Chem, 2003. **278**(24): p. 21938-43.

95. Eckfeld, K., et al., *RASSF4/AD037 is a potential ras effector/tumor suppressor of the RASSF family.* Cancer Res, 2004. **64**(23): p. 8688-93.

96. Pfeifer, G.P., R. Dammann, and S. Tommasi, *RASSF proteins.* Curr Biol, 2010. **20**(8): p. R344-5.

97. Praskova, M., et al., *Regulation of the MST1 kinase by autophosphorylation, by the growth inhibitory proteins, RASSF1 and NORE1, and by Ras.* Biochem J, 2004. **381**(Pt 2): p. 453-62.

98. Oh, H.J., et al., *Role of the tumor suppressor RASSF1A in Mst1-mediated apoptosis.* Cancer Res, 2006. **66**(5): p. 2562-9.

99. Ghazaleh, H.A., et al., *14-3-3 mediated regulation of the tumor suppressor protein, RASSF1A.* Apoptosis, 2010. **15**(2): p. 117-27.

100. Bee, C., et al., *Growth and tumor suppressor NORE1A is a regulatory node between Ras signaling and microtubule nucleation.* J Biol Chem, 2010. **285**(21): p. 16258-66.

101. Calvisi, D.F., et al., *Ubiquitous activation of Ras and Jak/Stat pathways in human HCC.* Gastroenterology, 2006. **130**(4): p. 1117-28.

102. Vos, M.D., et al., *RASSF2 is a novel K-Ras-specific effector and potential tumor suppressor.* J Biol Chem, 2003. **278**(30): p. 28045-51.

103. Wennerberg, K. and C.J. Der, *Rho-family GTPases: it's not only Rac and Rho (and I like it).* J Cell Sci, 2004. **117**(Pt 8): p. 1301-12.

104. Boureux, A., et al., *Evolution of the Rho family of ras-like GTPases in eukaryotes.* Mol Biol Evol, 2007. **24**(1): p. 203-16.

105. Heasman, S.J. and A.J. Ridley, *Mammalian Rho GTPases: new insights into their functions from in vivo studies.* Nat Rev Mol Cell Biol, 2008. **9**(9): p. 690-701.

106. Hall, A., *Rho family GTPases.* Biochem Soc Trans, 2012. **40**(6): p. 1378-82.

107. Jaiswal, M., R. Dvorsky, and M.R. Ahmadian, *Deciphering the molecular and functional basis of Dbl family proteins: a novel systematic approach toward classification of selective activation of the Rho family proteins.* J Biol Chem, 2013. **288**(6): p. 4486-500.

108. Goffinet, M., et al., *Identification of a GTP-bound Rho specific scFv molecular sensor by phage display selection.* BMC Biotechnol, 2008. **8**: p. 34.

109. Garcia-Mata, R., E. Boulter, and K. Burridge, *The 'invisible hand': regulation of RHO GTPases by RHOGDIs.* Nat Rev Mol Cell Biol, 2011. **12**(8): p. 493-504.

110. Etienne-Manneville, S., *Cdc42--the centre of polarity.* J Cell Sci, 2004. **117**(Pt 8): p. 1291-300.

111. Marks, P.W. and D.J. Kwiatkowski, *Genomic organization and chromosomal location of murine Cdc42.* Genomics, 1996. **38**(1): p. 13-8.

112. Nicole, S., et al., *The human CDC42 gene: genomic organization, evidence for the existence of a putative pseudogene and exclusion as a SJS1 candidate gene.* Hum Genet, 1999. **105**(1-2): p. 98-103.

113. Hunter, M.P., A. Russo, and J.P. O'Bryan, *Emerging roles for intersectin (ITSN) in regulating signaling and disease pathways.* Int J Mol Sci, 2013. **14**(4): p. 7829-52.

114. Neudauer, C.L., et al., *Distinct cellular effects and interactions of the Rho-family GTPase TC10.* Curr Biol, 1998. **8**(21): p. 1151-60.

115. Gibson, R.M., et al., *An activating mutant of Cdc42 that fails to interact with Rho GDP-dissociation inhibitor localizes to the plasma membrane and mediates actin reorganization.* Exp Cell Res, 2004. **301**(2): p. 211-22.

116. Gibson, R.M. and A.L. Wilson-Delfosse, *RhoGDI-binding-defective mutant of Cdc42Hs targets to membranes and activates filopodia formation but does not cycle with the cytosol of mammalian cells.* Biochem J, 2001. **359**(Pt 2): p. 285-94.

117. Swart-Mataraza, J.M., Z. Li, and D.B. Sacks, *IQGAP1 is a component of Cdc42 signaling to the cytoskeleton.* J Biol Chem, 2002. **277**(27): p. 24753-63.

118. Aicart-Ramos, C., R.A. Valero, and I. Rodriguez-Crespo, *Protein palmitoylation and subcellular trafficking.* Biochim Biophys Acta, 2011. **1808**(12): p. 2981-94.

119. Phillips, M.J., et al., *Effector proteins exert an important influence on the signaling-active state of the small GTPase Cdc42.* J Biol Chem, 2008. **283**(20): p. 14153-64.

120. Murphy, G.A., et al., *Cellular functions of TC10, a Rho family GTPase: regulation of morphology, signal transduction and cell growth.* Oncogene, 1999. **18**(26): p. 3831-45.

121. Michaelson, D., et al., *Differential localization of Rho GTPases in live cells: regulation by hypervariable regions and RhoGDI binding.* J Cell Biol, 2001. **152**(1): p. 111-26.

122. Eden, S., et al., *Mechanism of regulation of WAVE1-induced actin nucleation by Rac1 and Nck.* Nature, 2002. **418**(6899): p. 790-3.

123. Jordan, P., et al., *Cloning of a novel human Rac1b splice variant with increased expression in colorectal tumors.* Oncogene, 1999. **18**(48): p. 6835-9.

124. Schnelzer, A., et al., *Rac1 in human breast cancer: overexpression, mutation analysis, and characterization of a new isoform, Rac1b.* Oncogene, 2000. **19**(26): p. 3013-20.

125. Matos, P., J.G. Collard, and P. Jordan, *Tumor-related alternatively spliced Rac1b is not regulated by Rho-GDP dissociation inhibitors and exhibits selective downstream signaling.* J Biol Chem, 2003. **278**(50): p. 50442-8.

126. Didsbury, J., et al., *rac, a novel ras-related family of proteins that are botulinum toxin substrates.* J Biol Chem, 1989. **264**(28): p. 16378-82.

127. Haataja, L., J. Groffen, and N. Heisterkamp, *Characterization of RAC3, a novel member of the Rho family.* J Biol Chem, 1997. **272**(33): p. 20384-8.

128. Vincent, S., P. Jeanteur, and P. Fort, *Growth-regulated expression of rhoG, a new member of the ras homolog gene family.* Mol Cell Biol, 1992. **12**(7): p. 3138-48.

129. Adamson, P., H.F. Paterson, and A. Hall, *Intracellular localization of the P21rho proteins.* J Cell Biol, 1992. **119**(3): p. 617-27.

130. Wang, L., et al., *A novel strategy for specifically down-regulating individual Rho GTPase activity in tumor cells.* J Biol Chem, 2003. **278**(45): p. 44617-25.

131. Dvorsky, R. and M.R. Ahmadian, *Always look on the bright site of Rho: structural implications for a conserved intermolecular interface.* EMBO Rep, 2004. **5**(12): p. 1130-6.

132. ten Klooster, J.P. and P.L. Hordijk, *Targeting and localized signalling by small GTPases.* Biol Cell, 2007. **99**(1): p. 1-12.

133. Roberts, P.J., et al., *Rho Family GTPase modification and dependence on CAAX motif-signaled posttranslational modification.* J Biol Chem, 2008. **283**(37): p. 25150-63.

134. Freeman, J.L., A. Abo, and J.D. Lambeth, *Rac "insert region" is a novel effector region that is implicated in the activation of NADPH oxidase, but not PAK65.* J Biol Chem, 1996. **271**(33): p. 19794-801.

135. Nisimoto, Y., et al., *Rac binding to p67(phox). Structural basis for interactions of the Rac1 effector region and insert region with components of the respiratory burst oxidase.* J Biol Chem, 1997. **272**(30): p. 18834-41.

136. McCallum, S.J., W.J. Wu, and R.A. Cerione, *Identification of a putative effector for Cdc42Hs with high sequence similarity to the RasGAP-related protein IQGAP1 and a Cdc42Hs binding partner with similarity to IQGAP2.* J Biol Chem, 1996. **271**(36): p. 21732-7.

137. Zong, H., K. Kaibuchi, and L.A. Quilliam, *The insert region of RhoA is essential for Rho kinase activation and cellular transformation.* Mol Cell Biol, 2001. **21**(16): p. 5287-98.

138. Lammers, M., et al., *Specificity of interactions between mDia isoforms and Rho proteins.* J Biol Chem, 2008. **283**(50): p. 35236-46.

139. Rivers, E. and A.J. Thrasher, *Wiskott-Aldrich syndrome protein: Emerging mechanisms in immunity.* Eur J Immunol, 2017. **47**(11): p. 1857-1866.

140. Derry, J.M., H.D. Ochs, and U. Francke, *Isolation of a novel gene mutated in Wiskott-Aldrich syndrome.* Cell, 1994. **79**(5): p. following 922.

141. Worth, A.J. and A.J. Thrasher, *Current and emerging treatment options for Wiskott-Aldrich syndrome.* Expert Rev Clin Immunol, 2015. **11**(9): p. 1015-32.

142. Kim, A.S., et al., *Autoinhibition and activation mechanisms of the Wiskott-Aldrich syndrome protein.* Nature, 2000. **404**(6774): p. 151-8.

143. Cory, G.O., et al., *Phosphorylation of tyrosine 291 enhances the ability of WASp to stimulate actin polymerization and filopodium formation. Wiskott-Aldrich Syndrome protein.* J Biol Chem, 2002. **277**(47): p. 45115-21.

144. Tomasevic, N., et al., *Differential regulation of WASP and N-WASP by Cdc42, Rac1, Nck, and PI(4,5)P2.* Biochemistry, 2007. **46**(11): p. 3494-502.

145. Blanchoin, L., et al., *Direct observation of dendritic actin filament networks nucleated by Arp2/3 complex and WASP/Scar proteins.* Nature, 2000. **404**(6781): p. 1007-11.

146. Cory, G.O., et al., *Phosphorylation of the WASP-VCA domain increases its affinity for the Arp2/3 complex and enhances actin polymerization by WASP.* Mol Cell, 2003. **11**(5): p. 1229-39.

147. Chou, H.C., et al., *WIP regulates the stability and localization of WASP to podosomes in migrating dendritic cells.* Curr Biol, 2006. **16**(23): p. 2337-44.

148. Ramesh, N., et al., *WIP, a protein associated with wiskott-aldrich syndrome protein, induces actin polymerization and redistribution in lymphoid cells.* Proc Natl Acad Sci U S A, 1997. **94**(26): p. 14671-6.

149. Manser, E., et al., *A brain serine/threonine protein kinase activated by Cdc42 and Rac1.* Nature, 1994. **367**(6458): p. 40-6.

150. Zhao, Z.S. and E. Manser, *PAK family kinases: Physiological roles and regulation.* Cell Logist, 2012. **2**(2): p. 59-68.

151. Manser, E., et al., *PAK kinases are directly coupled to the PIX family of nucleotide exchange factors.* Mol Cell, 1998. **1**(2): p. 183-92.

152. Kiosses, W.B., et al., *A dominant-negative p65 PAK peptide inhibits angiogenesis.* Circ Res, 2002. **90**(6): p. 697-702.

153. Puto, L.A., et al., *p21-activated kinase 1 (PAK1) interacts with the Grb2 adapter protein to couple to growth factor signaling.* J Biol Chem, 2003. **278**(11): p. 9388-93.

154. Lu, W., et al., *Activation of Pak by membrane localization mediated by an SH3 domain from the adaptor protein Nck.* Curr Biol, 1997. **7**(2): p. 85-94.

155. Arias-Romero, L.E. and J. Chernoff, *A tale of two Paks.* Biol Cell, 2008. **100**(2): p. 97-108.

156. Bokoch, G.M., *Biology of the p21-activated kinases.* Annu Rev Biochem, 2003. **72**: p. 743-81.

157. Sanders, L.C., et al., *Inhibition of myosin light chain kinase by p21-activated kinase.* Science, 1999. **283**(5410): p. 2083-5.

158. Zang, M., C. Hayne, and Z. Luo, *Interaction between active Pak1 and Raf-1 is necessary for phosphorylation and activation of Raf-1.* J Biol Chem, 2002. **277**(6): p. 4395-405.

159. Frost, J.A., et al., *Cross-cascade activation of ERKs and ternary complex factors by Rho family proteins.* EMBO J, 1997. **16**(21): p. 6426-38.

160. Xiao, G.H., et al., *p21-activated kinase links Rac/Cdc42 signaling to merlin.* J Biol Chem, 2002. **277**(2): p. 883-6.

161. Scheffzek, K., M.R. Ahmadian, and A. Wittinghofer, *GTPase-activating proteins: helping hands to complement an active site.* Trends Biochem Sci, 1998. **23**(7): p. 257-62.

162. Ahmadian, M.R., et al., *Individual rate constants for the interaction of Ras proteins with GTPase-activating proteins determined by fluorescence spectroscopy.* Biochemistry, 1997. **36**(15): p. 4535-41.

163. Ahmadian, M.R., et al., *Confirmation of the arginine-finger hypothesis for the GAP-stimulated GTP-hydrolysis reaction of Ras.* Nat Struct Biol, 1997. **4**(9): p. 686-9.

164. Scheffzek, K., et al., *Structural analysis of the GAP-related domain from neurofibromin and its implications.* EMBO J, 1998. **17**(15): p. 4313-27.

165. Ahmadian, M.R., et al., *Aluminum fluoride associates with the small guanine nucleotide binding proteins.* FEBS Lett, 1997. **408**(3): p. 315-8.

166. Wey, M., et al., *Kinetic mechanisms of mutation-dependent Harvey Ras activation and their relevance for the development of Costello syndrome.* Biochemistry, 2013. **52**(47): p. 8465-79.

167. Schubbert, S., K. Shannon, and G. Bollag, *Hyperactive Ras in developmental disorders and cancer.* Nat Rev Cancer, 2007. **7**(4): p. 295-308.

168. Hunter, J.C., et al., *Biochemical and Structural Analysis of Common Cancer-Associated KRAS Mutations.* Mol Cancer Res, 2015. **13**(9): p. 1325-35.

169. Bos, J.L., H. Rehmann, and A. Wittinghofer, *GEFs and GAPs: critical elements in the control of small G proteins.* Cell, 2007. **129**(5): p. 865-77.

170. DerMardirossian, C. and G.M. Bokoch, *GDIs: central regulatory molecules in Rho GTPase activation.* Trends Cell Biol, 2005. **15**(7): p. 356-63.

171. Fukumoto, Y., et al., *Molecular cloning and characterization of a novel type of regulatory protein (GDI) for the rho proteins, ras p21-like small GTP-binding proteins.* Oncogene, 1990. **5**(9): p. 1321-8.

172. Leonard, D., et al., *The identification and characterization of a GDP-dissociation inhibitor (GDI) for the CDC42Hs protein.* J Biol Chem, 1992. **267**(32): p. 22860-8.

173. Lelias, J.M., et al., *cDNA cloning of a human mRNA preferentially expressed in hematopoietic cells and with homology to a GDP-dissociation inhibitor for the rho GTP-binding proteins.* Proc Natl Acad Sci U S A, 1993. **90**(4): p. 1479-83.

174. Scherle, P., T. Behrens, and L.M. Staudt, *Ly-GDI, a GDP-dissociation inhibitor of the RhoA GTP-binding protein, is expressed preferentially in lymphocytes.* Proc Natl Acad Sci U S A, 1993. **90**(16): p. 7568-72.

175. Platko, J.V., et al., *A single residue can modify target-binding affinity and activity of the functional domain of the Rho-subfamily GDP dissociation inhibitors.* Proc Natl Acad Sci U S A, 1995. **92**(7): p. 2974-8.

176. Gorvel, J.P., et al., *Differential properties of D4/LyGDI versus RhoGDI: phosphorylation and rho GTPase selectivity.* FEBS Lett, 1998. **422**(2): p. 269-73.

177. Brunet, N., A. Morin, and B. Olofsson, *RhoGDI-3 regulates RhoG and targets this protein to the Golgi complex through its unique N-terminal domain.* Traffic, 2002. **3**(5): p. 342-57.

178. Hoffman, G.R., N. Nassar, and R.A. Cerione, *Structure of the Rho family GTP-binding protein Cdc42 in complex with the multifunctional regulator RhoGDI.* Cell, 2000. **100**(3): p. 345-56.

179. Scheffzek, K., et al., *The Rac-RhoGDI complex and the structural basis for the regulation of Rho proteins by RhoGDI.* Nat Struct Biol, 2000. **7**(2): p. 122-6.

180. Grizot, S., et al., *Crystal structure of the Rac1-RhoGDI complex involved in nadph oxidase activation.* Biochemistry, 2001. **40**(34): p. 10007-13.

181. Boulter, E., et al., *Regulation of Rho GTPase crosstalk, degradation and activity by RhoGDI1.* Nat Cell Biol, 2010. **12**(5): p. 477-83.

182. Rolli-Derkinderen, M., et al., *Phosphorylation of serine 188 protects RhoA from ubiquitin/proteasome-mediated degradation in vascular smooth muscle cells.* Circ Res, 2005. **96**(11): p. 1152-60.

183. Wright, L.P. and M.R. Philips, *Thematic review series: lipid posttranslational modifications. CAAX modification and membrane targeting of Ras.* J Lipid Res, 2006. **47**(5): p. 883-91.

184. Fu, H.W. and P.J. Casey, *Enzymology and biology of CaaX protein prenylation.* Recent Prog Horm Res, 1999. **54**: p. 315-42; discussion 342-3.

185. Seabra, M.C., et al., *Protein farnesyltransferase and geranylgeranyltransferase share a common alpha subunit.* Cell, 1991. **65**(3): p. 429-34.

186. Boyartchuk, V.L., M.N. Ashby, and J. Rine, *Modulation of Ras and a-factor function by carboxyl-terminal proteolysis.* Science, 1997. **275**(5307): p. 1796-800.

187. Freije, J.M., et al., *Identification and chromosomal location of two human genes encoding enzymes potentially involved in proteolytic maturation of farnesylated proteins.* Genomics, 1999. **58**(3): p. 270-80.

188. Otto, J.C., et al., *Cloning and characterization of a mammalian prenyl protein-specific protease.* J Biol Chem, 1999. **274**(13): p. 8379-82.

189. Clarke, S., et al., *Posttranslational modification of the Ha-ras oncogene protein: evidence for a third class of protein carboxyl methyltransferases.* Proc Natl Acad Sci U S A, 1988. **85**(13): p. 4643-7.

190. Gutierrez, L., et al., *Post-translational processing of p21ras is two-step and involves carboxyl-methylation and carboxy-terminal proteolysis.* EMBO J, 1989. **8**(4): p. 1093-8.

191. Hrycyna, C.A., et al., *The Saccharomyces cerevisiae STE14 gene encodes a methyltransferase that mediates C-terminal methylation of a-factor and RAS proteins.* EMBO J, 1991. **10**(7): p. 1699-709.

192. Pillinger, M.H., et al., *Characterization of a plasma membrane-associated prenylcysteine-directed alpha carboxyl methyltransferase in human neutrophils.* J Biol Chem, 1994. **269**(2): p. 1486-92.

193. Hancock, J.F., K. Cadwallader, and C.J. Marshall, *Methylation and proteolysis are essential for efficient membrane binding of prenylated p21K-ras(B).* EMBO J, 1991. **10**(3): p. 641-6.

194. Ahearn, I., M. Zhou, and M.R. Philips, *Posttranslational Modifications of RAS Proteins.* Cold Spring Harb Perspect Med, 2018. **8**(11).

195. Bhattacharyya, R.P., et al., *Domains, motifs, and scaffolds: the role of modular interactions in the evolution and wiring of cell signaling circuits.* Annu Rev Biochem, 2006. **75**: p. 655-80.

196. Brown, M.D. and D.B. Sacks, *Protein scaffolds in MAP kinase signalling.* Cell Signal, 2009. **21**(4): p. 462-9.

197. Zeke, A., et al., *Scaffolds: interaction platforms for cellular signalling circuits.* Trends Cell Biol, 2009. **19**(8): p. 364-74.

198. Langeberg, L.K. and J.D. Scott, *Signalling scaffolds and local organization of cellular behaviour.* Nat Rev Mol Cell Biol, 2015. **16**(4): p. 232-44.

199. Heinrich, R., B.G. Neel, and T.A. Rapoport, *Mathematical models of protein kinase signal transduction.* Mol Cell, 2002. **9**(5): p. 957-70.

200. Garrington, T.P. and G.L. Johnson, *Organization and regulation of mitogen-activated protein kinase signaling pathways.* Curr Opin Cell Biol, 1999. **11**(2): p. 211-8.

201. Meister, M., et al., *Mitogen-Activated Protein (MAP) Kinase Scaffolding Proteins: A Recount.* Int J Mol Sci, 2013. **14**(3): p. 4854-84.

202. Casar, B. and P. Crespo, *ERK Signals: Scaffolding Scaffolds?* Front Cell Dev Biol, 2016. **4**: p. 49.

203. Dard, N. and M. Peter, *Scaffold proteins in MAP kinase signaling: more than simple passive activating platforms.* Bioessays, 2006. **28**(2): p. 146-56.

204. Abel, A.M., et al., *IQGAP1: insights into the function of a molecular puppeteer.* Mol Immunol, 2015. **65**(2): p. 336-49.

205. Choi, S. and R.A. Anderson, *IQGAP1 is a phosphoinositide effector and kinase scaffold.* Adv Biol Regul, 2016. **60**: p. 29-35.

206. Hedman, A.C., J.M. Smith, and D.B. Sacks, *The biology of IQGAP proteins: beyond the cytoskeleton.* EMBO Rep, 2015. **16**(4): p. 427-46.

207. Smith, J.M., A.C. Hedman, and D.B. Sacks, *IQGAPs choreograph cellular signaling from the membrane to the nucleus.* Trends Cell Biol, 2015. **25**(3): p. 171-84.

208. Watanabe, T., S. Wang, and K. Kaibuchi, *IQGAPs as Key Regulators of Actin-cytoskeleton Dynamics.* Cell Struct Funct, 2015. **40**(2): p. 69-77.

209. White, C.D., M.D. Brown, and D.B. Sacks, *IQGAPs in cancer: a family of scaffold proteins underlying tumorigenesis.* FEBS Lett, 2009. **583**(12): p. 1817-24.

210. Fukata, M., et al., *Rac1 and Cdc42 capture microtubules through IQGAP1 and CLIP-170.* Cell, 2002. **109**(7): p. 873-85.

211. Johnson, M., M. Sharma, and B.R. Henderson, *IQGAP1 regulation and roles in cancer.* Cell Signal, 2009. **21**(10): p. 1471-8.

212. Mateer, S.C., et al., *Actin filament binding by a monomeric IQGAP1 fragment with a single calponin homology domain.* Cell Motil Cytoskeleton, 2004. **58**(4): p. 231-41.

213. Roy, M., Z. Li, and D.B. Sacks, *IQGAP1 binds ERK2 and modulates its activity.* J Biol Chem, 2004. **279**(17): p. 17329-37.

214. Grohmanova, K., et al., *Phosphorylation of IQGAP1 modulates its binding to Cdc42, revealing a new type of rho-GTPase regulator.* J Biol Chem, 2004. **279**(47): p. 48495-504.

215. Kurella, V.B., et al., *Crystal structure of the GTPase-activating protein-related domain from IQGAP1.* J Biol Chem, 2009. **284**(22): p. 14857-65.

216. Li, Z., et al., *IQGAP1 promotes neurite outgrowth in a phosphorylation-dependent manner.* J Biol Chem, 2005. **280**(14): p. 13871-8.

217. Nouri, K., et al., *IQGAP1 Interaction with RHO Family Proteins Revisited: KINETIC AND EQUILIBRIUM EVIDENCE FOR MULTIPLE DISTINCT BINDING SITES.* J Biol Chem, 2016. **291**(51): p. 26364-26376.

218. Owen, D., et al., *The IQGAP1-Rac1 and IQGAP1-Cdc42 interactions: interfaces differ between the complexes.* J Biol Chem, 2008. **283**(3): p. 1692-704.

219. Jaiswal, M., et al., *Biochemical assays to characterize Rho GTPases.* Methods Mol Biol, 2012. **827**: p. 37-58.

220. Abdul-Manan, N., et al., *Structure of Cdc42 in complex with the GTPase-binding domain of the 'Wiskott-Aldrich syndrome' protein.* Nature, 1999. **399**(6734): p. 379-83.

221. Hemsath, L., et al., *An electrostatic steering mechanism of Cdc42 recognition by Wiskott-Aldrich syndrome proteins.* Mol Cell, 2005. **20**(2): p. 313-24.

222. Kuhn, S., et al., *The structure of FMNL2-Cdc42 yields insights into the mechanism of lamellipodia and filopodia formation.* Nat Commun, 2015. **6**: p. 7088.

223. Fukata, M., et al., *Cdc42 and Rac1 regulate the interaction of IQGAP1 with beta-catenin.* J Biol Chem, 1999. **274**(37): p. 26044-50.

224. Kuroda, S., et al., *Cdc42, Rac1, and their effector IQGAP1 as molecular switches for cadherin-mediated cell-cell adhesion.* Biochem Biophys Res Commun, 1999. **262**(1): p. 1-6.

225. Gremer, L., et al., *Fluoride complexes of oncogenic Ras mutants to study the Ras-RasGap interaction.* Biol Chem, 2008. **389**(9): p. 1163-71.

226. Flex, E., et al., *Activating mutations in RRAS underlie a phenotype within the RASopathy spectrum and contribute to leukaemogenesis.* Hum Mol Genet, 2014. **23**(16): p. 4315-27.

227. Aoki, Y., et al., *Gain-of-function mutations in RIT1 cause Noonan syndrome, a RAS/MAPK pathway syndrome.* Am J Hum Genet, 2013. **93**(1): p. 173-80.

228. Bekhouche, B., et al., *A toxic palmitoylation of Cdc42 enhances NF-kappaB signaling and drives a severe autoinflammatory syndrome.* J Allergy Clin Immunol, 2020.

229. Seeland, I., et al., *The actin remodeling protein cofilin is crucial for thymic alphabeta but not gammadelta T-cell development.* PLoS Biol, 2018. **16**(7): p. e2005380.

230. Li, W., et al., *Defective thymic output in WAS patients is associated with abnormal actin organization.* Sci Rep, 2017. **7**(1): p. 11978.

231. Dasouki, M., et al., *Deficient T Cell Receptor Excision Circles (TRECs) in autosomal recessive hyper IgE syndrome caused by DOCK8 mutation: implications for pathogenesis and potential detection by newborn screening.* Clin Immunol, 2011. **141**(2): p. 128-32.

232. Caye, A., et al., *Juvenile myelomonocytic leukemia displays mutations in components of the RAS pathway and the PRC2 network.* Nat Genet, 2015. **47**(11): p. 1334-40.

233. Hsu, A.P., et al., *Dominant activating RAC2 mutation with lymphopenia, immunodeficiency, and cytoskeletal defects.* Blood, 2019. **133**(18): p. 1977-1988.

234. Martinelli, S., et al., *Functional Dysregulation of CDC42 Causes Diverse Developmental Phenotypes.* Am J Hum Genet, 2018. **102**(2): p. 309-320.

235. Kaduwal, S., et al., *Sur8/Shoc2 promotes cell motility and metastasis through activation of Ras-PI3K signaling.* Oncotarget, 2015. **6**(32): p. 33091-105.

236. Holly, S.P., M.K. Larson, and L.V. Parise, *The unique N-terminus of R-ras is required for Rac activation and precise regulation of cell migration.* Mol Biol Cell, 2005. **16**(5): p. 2458-69.

237. Capri, Y., et al., *Activating Mutations of RRAS2 Are a Rare Cause of Noonan Syndrome.* Am J Hum Genet, 2019. **104**(6): p. 1223-1232.

238. Altmuller, F., et al., *Genotype and phenotype spectrum of NRAS germline variants.* Eur J Hum Genet, 2017. **25**(7): p. 823-831.

239. Scheffzek, K., et al., *The Ras-RasGAP complex: structural basis for GTPase activation and its loss in oncogenic Ras mutants.* Science, 1997. **277**(5324): p. 333-8.

240. Rodriguez-Viciana, P., et al., *A phosphatase holoenzyme comprised of Shoc2/Sur8 and the catalytic subunit of PP1 functions as an M-Ras effector to modulate Raf activity.* Mol Cell, 2006. **22**(2): p. 217-30.

241. Young, L.C., et al., *SHOC2-MRAS-PP1 complex positively regulates RAF activity and contributes to Noonan syndrome pathogenesis.* Proc Natl Acad Sci U S A, 2018. **115**(45): p. E10576-E10585.

242. Chen, P.C., et al., *Activation of multiple signaling pathways causes developmental defects in mice with a Noonan syndrome-associated Sos1 mutation.* J Clin Invest, 2010. **120**(12): p. 4353-65.

243. Wu, X., et al., *MEK-ERK pathway modulation ameliorates disease phenotypes in a mouse model of Noonan syndrome associated with the Raf1(L613V) mutation.* J Clin Invest, 2011. **121**(3): p. 1009-25.

244. Nakamura, T., et al., *Mediating ERK 1/2 signaling rescues congenital heart defects in a mouse model of Noonan syndrome.* J Clin Invest, 2007. **117**(8): p. 2123-32.

245. Nussinov, R., et al., *Calmodulin and IQGAP1 activation of PI3Kalpha and Akt in KRAS, HRAS and NRAS-driven cancers.* Biochim Biophys Acta Mol Basis Dis, 2018. **1864**(6 Pt B): p. 2304-2314.

246. Ren, J.G., Z. Li, and D.B. Sacks, *IQGAP1 modulates activation of B-Raf.* Proc Natl Acad Sci U S A, 2007. **104**(25): p. 10465-9.

247. Roy, M., Z. Li, and D.B. Sacks, *IQGAP1 is a scaffold for mitogen-activated protein kinase signaling.* Mol Cell Biol, 2005. **25**(18): p. 7940-52.

248. Papke, B. and C.J. Der, *Drugging RAS: Know the enemy.* Science, 2017. **355**(6330): p. 1158-1163.

249. Stalnecker, C.A. and C.J. Der, *RAS, wanted dead or alive: Advances in targeting RAS mutant cancers.* Sci Signal, 2020. **13**(624).

250. LeCour, L., Jr., et al., *The Structural Basis for Cdc42-Induced Dimerization of IQGAPs.* Structure, 2016. **24**(9): p. 1499-508.

251. Ozdemir, E.S., et al., *Unraveling the molecular mechanism of interactions of the Rho GTPases Cdc42 and Rac1 with the scaffolding protein IQGAP2.* J Biol Chem, 2018. **293**(10): p. 3685-3699.

252. Bhattacharya, M., et al., *IQGAP1-dependent scaffold suppresses RhoA and inhibits airway smooth muscle contraction.* J Clin Invest, 2014. **124**(11): p. 4895-8.

253. Casteel, D.E., et al., *Rho isoform-specific interaction with IQGAP1 promotes breast cancer cell proliferation and migration.* J Biol Chem, 2012. **287**(45): p. 38367-78.

254. Bustelo, X.R. and M. Barbacid, *Tyrosine phosphorylation of the vav proto-oncogene product in activated B cells.* Science, 1992. **256**(5060): p. 1196-9.

255. Bustelo, X.R., J.A. Ledbetter, and M. Barbacid, *Product of vav proto-oncogene defines a new class of tyrosine protein kinase substrates.* Nature, 1992. **356**(6364): p. 68-71.

256. Turner, M. and D.D. Billadeau, *VAV proteins as signal integrators for multi-subunit immune-recognition receptors.* Nat Rev Immunol, 2002. **2**(7): p. 476-86.

257. Movilla, N. and X.R. Bustelo, *Biological and regulatory properties of Vav-3, a new member of the Vav family of oncoproteins.* Mol Cell Biol, 1999. **19**(11): p. 7870-85.

258. Chang, K.H., et al., *Vav3 collaborates with p190-BCR-ABL in lymphoid progenitor leukemogenesis, proliferation, and survival.* Blood, 2012. **120**(4): p. 800-11.

259. Cilloni, D. and G. Saglio, *Molecular pathways: BCR-ABL.* Clin Cancer Res, 2012. **18**(4): p. 930-7.

260. Thomas, E.K., et al., *Rac GTPases as key regulators of p210-BCR-ABL-dependent leukemogenesis.* Leukemia, 2008. **22**(5): p. 898-904.

261. Schurmann, A., et al., *p21-activated kinase 1 phosphorylates the death agonist bad and protects cells from apoptosis.* Mol Cell Biol, 2000. **20**(2): p. 453-61.

262. Llorca, O., et al., *Global conformational rearrangements during the activation of the GDP/GTP exchange factor Vav3.* EMBO J, 2005. **24**(7): p. 1330-40.

Acknowledgement

Firstly, I would like to express my sincere gratitude to my advisor Reza Ahmadian for giving me fantastic support, guidance and motivation during my whole academic time. You helped me to grow up as a scientist and I greatly appreciate the continuous confidence you had for my decisions and work.

I would like to express my thanks to my co-supervisor Prof. Lutz Schmitt for his guidance during the time of my Ph.D. studies. Besides my advisor, I want to thank Jürgen Scheller and Roland Piekorz. Both of you accompanied me on my scientific journey, gave useful advices, helped me with challenges that I had, and shared your huge knowledge with me.

Special thanks go to Marco Tartaglia, Martin Zenker, Jordan Orange, Nico Nassar, and He´le`ne Cavé. You made it possible for me to collaborate with many groups from all over the world and I would like to thank you for the opportunity to participate in such interesting projects.

I also want to thank all members of the institute of Biochemistry and Molecular Biology II for the valuable discussions and the funny moments we spent together. Special thanks go to my group members of the last years. We had a very special time with a lot of work but more important with a fantastic team spirit.

Außerdem möchte ich noch Petra Opree, Fereshteh Kamrani und nicht zu vergessen Ilse Meyer danken. Ihr habt mir meinen Alltag, wo ihr nur konntet, erleichtert. Mit euch zusammenzuarbeiten hat mir immer größte Freude bereitet.

Bei so vielen Namen darf natürlich einer nicht fehlen. Marcel und ich waren von Tag 1 ein unschlagbares Team, haben sämtliche Praktika zusammen durchgestanden, Bachelor- und Masterarbeit zusammen gemeistert und schlussendlich auch unsere Doktorarbeit. Wir haben unfassbar viele besondere Momente geteilt und ich konnte in guten, wie in schwierigen Zeiten immer auf dich zählen. Ich danke dir!

Ich möchte natürlich auch noch meinen Freunden danken. Ihr habt es möglich gemacht, dass ich während meiner Doktorarbeit nicht meinen Kopf verloren habe. Danke, dass es euch gibt und ihr mich in Allem unterstützt!

Selbstverständlich danke ich ganz besonders meiner Familie, die mich mein ganzes Leben lang unterstützt und immer an mich geglaubt haben. Wer ich heute bin und was ich erreicht habe, ist im Wesentlichen euch zu verdanken!

Und am meisten möchte ich Sabrina, der wichtigsten Person in meinem Leben, danken. So viel Unterstützung, Zuspruch, Geduld, Toleranz und Liebe kann man normalerweise nicht von einem Menschen verlangen. Du hältst immer zu mir und bist immer für mich da. Dafür danke ich dir aus tiefstem Herzen!

Eidesstattliche Erklärung

Ich versichere an Eides Statt, dass die Dissertation von mir selbstständig und ohne unzulässige fremde Hilfe unter Beachtung der „Grundsatze zur Sicherung guter wissenschaftlicher Praxis an der Heinrich-Heine-Universität Düsseldorf“ erstellt worden ist.

Es wurden keinerlei andere Quellen und Hilfsmittel, außer den angegebenen, benutzt. Zitate aus anderen Arbeiten wurden kenntlich gemacht. Diese Dissertation wurde in der vorgelegten oder einer ähnlichen Form noch bei keiner anderen Institution eingereicht und es wurden bisher keine erfolglosen Promotionsversuche von mir unternommen.

Oliver Krumbach

Düsseldorf, Mai 2020